Universidade de Aveiro Departamento de Eletrónica, Telecomunicações e Informática
2016

José Fernando Fachada Rosado

Locomoção Bípede Adaptativa a partir de uma Única Demonstração Usando Primitivas de Movimento

Adaptive Biped Locomotion from a Single Demonstration Using Motion Primitives

Universidade de Aveiro Departamento de Eletrónica, Telecomunicações e Informática
2016

José Fernando Fachada Rosado

Adaptive Biped Locomotion from a Single Demonstration Using Motion Primitives

Dissertação apresentada à Universidade de Aveiro para cumprimento dos requisitos necessários à obtenção do grau de Doutor em Eng. Electrotécnica, realizada sob a orientação científica do Doutor Filipe Miguel Teixeira Pereira da Silva, Professor Auxiliar do Departamento de Eletrónica, Telecomunicações e Informática da Universidade de Aveiro e do Doutor Vítor Manuel Ferreira dos Santos, Professor Associado do Departamento de Engenharia Mecânica da Universidade de Aveiro

Dedico este trabalho aos meus pais, José Rosado e Laurinda Rosado, à minha mulher Sandra e aos meus filhos Jorge e Célia.

o júri

presidente

Prof. Doutor João Lemos Pinto
Professor Catedrático da Universidade de Aveiro

vogais

Prof. Doutor José António Tenreiro Machado
Professor Coordenador com Agregação do Instituto Politécnico do Porto

Prof. Doutora Cristina Manuela Peixoto Santos
Professora Auxiliar da Universidade do Minho

Prof. Doutor Jorge Manuel Mateus Martins
Professor Auxiliar do Instituto Superior Técnico, Universidade de Lisboa

Prof. Doutor José Nuno Panelas Nunes Lau
Professor Auxiliar da Universidade de Aveiro

Prof. Doutor Filipe Miguel Teixeira Pereira da Silva
Professor Auxiliar da Universidade de Aveiro (**orientador**)

Acknowledgements

Starting with the academic side I would like to start thanking my supervisors: a very big special thanks to Professor Doctor Filipe Silva for all is support, guidance, help and teaching in many new areas to me. Also thanks for all the time he dedicated in help me through this work, for receiving me at his home in many meetings that were crucial to development of this work; a very special thanks to Professor Doctor Vítor Santos for all the continuous motivation he give to me and for all the work he had in reviewing this document on such a little time.

I would also like to thank Professor Doctor António Amaro for letting us use the motion lab at the ESSUA and all the knowledge he has given in the subject of human locomotion. Also, from the ESSUA, a thanks to Mário Rodrigues for all the teaching he give me in working with the VICON system, helping in solve some of the issues and helping in the all the preparation of the experiments conducted at the motion lab.

I would also like to thank Jorge Almeida for helping me on the first contact with the VICON Nexus software and to João Valente and Marcelo for being the test subjects in the motion capture performed.

Finally thanks to IEETA and IPC for supporting the registrations and other expenses in the conferences I attend.

As for the non-academic side of my life, I would like of course for starting to thank to my beloved parents José Rosado and Laurinda Rosado. Without their continuous support, without the sacrifices they made so I could study on a town away from home and have my “licenciatura”, neither the following steps (including this) could have been possible.

Last but certainly not least, I would like to thank my beloved wife, Sandra, for her continuous support.

palavras-chave

Locomoção bípede, demonstração única, primitivas de movimento, aprendizagem por imitação, comportamento adaptativo, generalização de movimentos.

resumo

Este trabalho aborda o problema de capacidade de imitação da locomoção humana através da utilização de trajetórias de baixo nível codificadas com primitivas de movimento e utilizá-las para depois generalizar para novas situações, partindo apenas de uma demonstração única. Assim, nesta linha de pensamento, os principais objetivos deste trabalho são dois: o primeiro é analisar, extrair e codificar demonstrações efetuadas por um humano, obtidas por um sistema de captura de movimento de forma a modelar tarefas de locomoção bípede. Contudo, esta transferência não está limitada à simples reprodução desses movimentos, requerendo uma evolução das capacidades para adaptação a novas situações, assim como lidar com perturbações inesperadas. Assim, o segundo objetivo é o desenvolvimento e avaliação de uma estrutura de controlo com capacidade de modelação das ações, de tal forma que a demonstração única apreendida possa ser modificada para o robô se adaptar a diversas situações, tendo em conta a sua dinâmica e o ambiente onde está inserido.

A ideia por detrás desta abordagem é resolver o problema da generalização a partir de uma demonstração única, combinando para isso duas estruturas básicas. A primeira consiste num sistema gerador de padrões baseado em primitivas de movimento utilizando sistemas dinâmicos (DS). Esta abordagem de codificação de movimentos possui propriedades desejáveis que a torna ideal para geração de trajetórias, tais como a possibilidade de modificar determinados parâmetros em tempo real, tais como a amplitude ou a frequência do ciclo do movimento e robustez a pequenas perturbações. A segunda estrutura, que está embebida na anterior, é composta por um conjunto de osciladores acoplados em fase que organizam as ações de unidades funcionais de forma coordenada. Mudanças em determinadas condições, como o instante de contacto ou impactos com o solo, levam a modelos com múltiplas fases. Assim, em vez de forçar o movimento do robô a situações pré-determinadas de forma temporal, o gerador de padrões de movimento proposto explora a transição entre diferentes fases que surgem da interação do robô com o ambiente, despoletadas por eventos sensoriais. A abordagem proposta é testada numa estrutura de simulação dinâmica, sendo que várias experiências são efetuadas para avaliar os métodos e o desempenho dos mesmos.

Keywords

Biped locomotion, single demonstration, motion primitives, imitation learning, adaptative behaviour, motion generalization.

Abstract

This work addresses the problem of learning to imitate human locomotion actions through low-level trajectories encoded with motion primitives and generalizing them to new situations from a single demonstration. In this line of thought, the main objectives of this work are twofold: The first is to analyze, extract and encode human demonstrations taken from motion capture data in order to model biped locomotion tasks. However, transferring motion skills from humans to robots is not limited to the simple reproduction, but requires the evaluation of their ability to adapt to new situations, as well as to deal with unexpected disturbances. Therefore, the second objective is to develop and evaluate a control framework for action shaping such that the single-demonstration can be modulated to varying situations, taking into account the dynamics of the robot and its environment.

The idea behind the approach is to address the problem of generalization from a single-demonstration by combining two basic structures. The first structure is a pattern generator system consisting of movement primitives learned and modelled by dynamical systems (DS). This encoding approach possesses desirable properties that make them well-suited for trajectory generation, namely the possibility to change parameters online such as the amplitude and the frequency of the limit cycle and the intrinsic robustness against small perturbations. The second structure, which is embedded in the previous one, consists of coupled phase oscillators that organize actions into functional coordinated units. The changing contact conditions plus the associated impacts with the ground lead to models with multiple phases. Instead of forcing the robot's motion into a predefined fixed timing, the proposed pattern generator explores transition between phases that emerge from the interaction of the robot system with the environment, triggered by sensor-driven events. The proposed approach is tested in a dynamics simulation framework and several experiments are conducted to validate the methods and to assess the performance of a humanoid robot.

Contents

List of Figures

List of Tables

List of Abbreviations

2D	2 Dimensions
3D	3 Dimensions
AI	Artificial Intelligence
AIBO	Artificial Intelligence Robot
API	Application Programming Interface
ASIMO	Advanced Step in Innovative Mobility
AU	Adaptive Unit
BABIL	Behavior Acquisition via Bayesian Inference and Learning
CCD	Charged-Coupled Device
CNS	Central Nervous System
CoG	Center of Gravity
CoM	Center of Mass
CoP	Center of Pressure
CPG	Central Pattern Generator
CPU	Central Processor Unit
Cr-KR	Cost-regularized Kernel regression
CSV	Comma Separated Values
DARwIn-OP	Dynamic Anthropomorphic Robot with Intelligence–Open Platform
DC	Direct Current
DLL	Dynamic Link Library
DoF	Degree of Freedom
DMP	Dynamic Movement Primitives
DS	Dynamical Systems
EMG	ElectroMyoGraphy
ESSUA	Escola Superior de Saúde da Universidade de Aveiro
F_c	Foot clearance

FK	Forward Kinematics
FIRA	Federation of International Robot-soccer Association
GMM	Gaussian Mixture Models
GRF	Ground Reaction Forces
H_h	Hip height
HMM	Hidden Markov Models
HOAP	Humanoid for Open Architecture Platform
HRP	Humanoid Robotics Project
IDE	Integrated Development Environment
IK	Inverse Kinematics
KAIST	Korea Advanced Institute of Science and Technology
KHR	KAIST Humanoid Robot
LfD	Learning from Demonstration
LIPM	Linear Inverted Pendulum Model
LWR	Locally Weighted Regression
MDS	Multi-Dimensional Scaling
MSE	Mean Square Error
OPTI	OPTimization Interface
PCA	Principal Component Analysis
PGRL	Policy Gradient Reinforcement Learning
PHUA	Projecto Humanoide da Universidade de Aveiro
PID	Proportional-Integral-Derivative
PP	Primitive Points
QRIO	Quest for cuRIOsity
RFWR	Receptive Field Weighted Regression
RL	Reinforcement Learning
RMP	Reaction Mass Pendulum
RNN	Recurrent Neural Networks
RoboCup	Robot Soccer World Cup
ROS	Robot Operating System

SARSA	State-Action-Reward-State-Action
S_l	Step Length
SMA	Shape Memory Alloys
V-REP	Virtual Robot Experimentation Platform
WABIAN	WAseda BIpedal humANoid
WABOT-1	WAseda ROBot 1
WBC	Whole Body Coordination
ZMP	Zero Moment Point

Chapter 1
Introduction

Over the recent years, the interest in robotic systems dedicated to complex tasks has increased remarkably influenced by the use of state of the art supporting technologies, the demand for innovative solutions and the search for new areas of potential application (Bekey et al., 2008; Siciliano & Khatib, 2007). Thereby, the field of robotics is rapidly expanding into human environments and particularly engaged in its new challenges: interacting, exploring, and working with humans. In line with this, the new generation of robots will increasingly touch people and their lives, which permits to foresee an important step forward and a significant socio-economic impact in the forthcoming years. Additionally, with the world moving towards a society of longevity, robots are expected to play an important role in medical care, welfare, services and work at home.

Current research trends are devoted to the development of integrated systems relying on rich perceptual and motor capabilities, supporting crucial requisites such as safety, autonomy, mobility and efficiency when performing a wide variety of tasks in real-world environments. In particular, there is a considerable effort centred on the development of humanoid robots with human-like forms and movements (Adams et al., 2000; Atkeson et al., 2000; Bekey et al., 2008; Solis & Takanishi, 2010), but not necessarily with the ability to walk on two legs. Clearly, the field of humanoid robotics can be divided into two main categories: upper-bodies and whole-body robots. On the one hand, upper-body humanoid robots can be seen as the extension of industrial manipulators in the sense that they are fixed to a support base. The research focuses

mainly on the integration of intelligence and motor control for advanced manipulation tasks. The seminal work of Brooks (Brooks et al., 1999), within the Cog project, gave rise to an upper-body humanoid robot inspired by the biological and cognitive sciences to study human-like behaviours. Subsequently, many other projects with similar objectives have been initiated. On the other hand, whole-body humanoid robots have legs to move in real-world environments which pose additional challenging problems, namely in terms of balance and stability. In this context, among the missing key elements is the ability to develop control architectures that can deal with a rich repertoire of movements, variable speeds, constraints and, most importantly, uncertainty in the real-world environment in a fast and reactive manner.

Biped locomotion is one of the most important and challenging control problems in humanoid robotics. Typical aspects that make the control of legged locomotion a challenging problem are the nonlinear, highly coupled, multivariable and unstable nature of its dynamics and also the complexity of models and even their absence for cases of mechanical imperfections which may not be modelled. Likewise, there are inherent characteristics of biped locomotion playing a key role in control, namely the absence of fixed points in the inertial frame, the unilateral degree-of-freedom established between the foot and the ground, the discrete changes in the dynamics as the system switches between single and double-support phases and the subjective performance evaluation. Given the complexity of the problem, there is an increasing need to move away from robots that are pre-programmed explicitly towards those endowed with the ability to extract information from the environment, learn about it and, hypothetically, develop predictions. Seen from another perspective, biped robots require not just predetermined plans for a single execution path, but instead, policies describing online response under varying conditions.

This thesis is dedicated to the problem of biped locomotion in humanoid robots, giving rise to the following question: which are the strong reasons to pursue this research area? Among others, the following main reasons can be invoked: first, the surprising number of new humanoid robots appearing on the specialized literature (an overview is provided in Chapter 2) proves that they can have flexible mobility at a practical level. Second, the world of our everyday activities is largely designed for biped

locomotion. While a humanoid form is not necessarily the optimal one for every task, robots that are prepared to function in human environments tend naturally to have similar physical characteristics. Third, humanoids may prove to be the ideal robot design from the viewpoint of the human-robot interaction (*i.e.*, more accepting), leading to further potential of application. However, in order to properly work in the environment of humans, this new generation of robots should have a human-like behaviour in terms of motion skills, as well as advanced adaptation, learning and communication capabilities. Fourth, humanoid robotics research is, consensually, considered as a key area for promoting the adoption of biological principles in the design and development of autonomous robots. Creating robots inspired by biological principles may help share and refine the understanding of their own natural capabilities, providing an excellent test-bed for hypothesis and biological models.

In the past years, the main efforts in biped humanoid robots were aimed at addressing the various aspects of robot control, namely motion, contacts, constraints and obstacles. In order to pursue this line of research, significant efforts have been conducted through a close and systematic collaboration of multidisciplinary research teams whose knowledge encompasses a wide range of crucial areas, including electronics, mechanical, computer engineering, biomechanics and computational intelligence. While much progress has been made, numerous problems still remain in building human-like robots able to mimic the action, perception and cognition abilities of their biological counterparts. In this context, nature has always been a source of inspiration for the robotics community in terms of morphologies, modes of locomotion and/or control mechanisms. Biological systems provide working examples and conceptual proofs that strongly benefit the design of autonomous robots exhibiting efficiency, adaptability, robustness and versatility.

1.1 Motivation and Objectives

Humans excel in terms of learning and adaptation of locomotion patterns to accommodate the demands of a complex world. The continuous modulations of the coordination dynamics within and between legs are accomplished effortlessly such that

humans tend to underestimate their own capabilities. Indeed, the strength of human locomotion lies in the integrated capabilities for encoding, storing and accessing information about the world, developing and adapting internal models, learning from multiple sources using different mechanisms, predicting and anticipating in both space and time, among others.

Humanoid robots already have sophisticated control architectures and computational power for processing and reasoning. The Humanoid Project at the University of Aveiro (PHUA) represents a long-term multidisciplinary research effort whose main objective is the development of highly integrated humanoid platforms based on standard components and open software (Santos & Silva, 2006; Silva & Santos, 2007; Santos et al., 2012). Fig. 1.1 illustrates the latest full-body humanoid platform with a total of 25 active degrees-of-freedom (DoF), about 65 cm height and 6 kg weight.

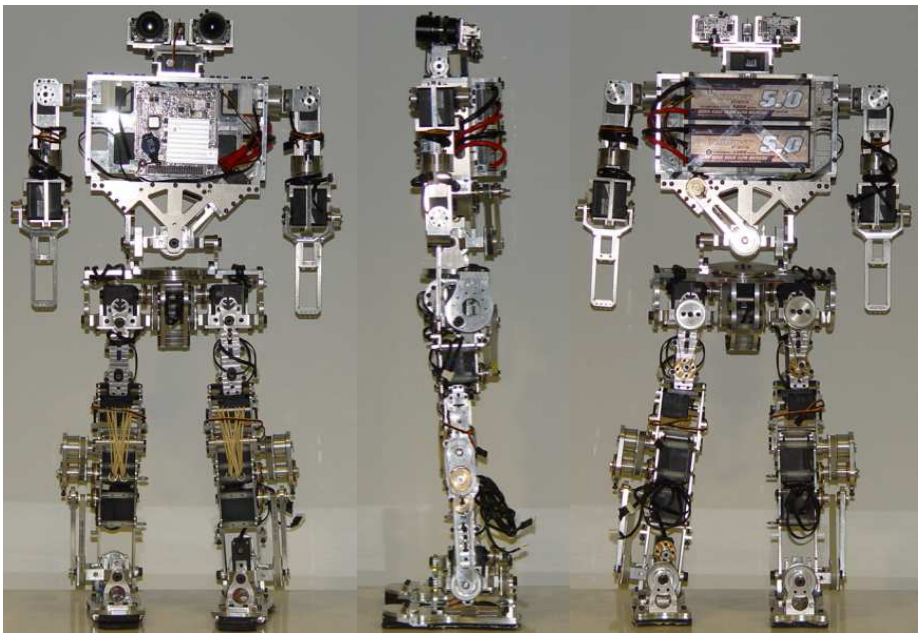

Fig. 1.1: Front, side and back views of the PHUA robot with 25-DoF, 65 cm height and 6 kg weight .

The PhD thesis was developed in the scope of current studies in multisensory perception, biped locomotion, autonomous navigation and learning methods. In particular, this work focuses on learning to imitate human locomotion actions through low-level motion trajectories encoded with motion primitives and on generalizing them to new and, often, unexpected circumstances. The main interest lies in learning

from a single-demonstration that can be modulated to varying situations, taking into account the dynamics of the robot and its environment. The first objective of this work is to encode human demonstrations and model locomotion tasks. This implies to extract motion primitives from human demonstrations by solving the so-called motion retargeting problem, dealing with mapping actions from a demonstrator to an imitator. In general, it is difficult to directly use captured motion data because the kinematics and dynamics of humanoid robots differ significantly from those of humans.

Transferring motion skills from humans to robots is not limited to the simple reproduction, but requires the evaluation of their ability to adapt to new situations, as well as to deal with unexpected disturbances. Therefore, the second central objective is to develop and evaluate a control framework for action shaping and automatization. The idea behind the approach is to address the problem of generalization from a single-demonstration by combining two basic structures. The first structure is a pattern generator system consisting of movement primitives learned and modelled by dynamical systems (DS). This encoding approach possesses desirable properties that make them well-suited for trajectory generation, namely the possibility to change parameters online such as the amplitude and the frequency of the limit cycle and the intrinsic robustness against small perturbations. The second structure, which is embedded in the previous one, consists of coupled phase oscillators that organize actions into functional coordinated units. The changing contact conditions plus the associated impacts with the ground lead to models with multiple phases. Instead of forcing the robot's motion into a predefined fixed timing, the proposed pattern generator explores transition between phases that emerge from the interaction of the robot system with the environment, for example, triggered by sensor-driven events.

At any of the deployment phases, the applicability of the proposed concepts is demonstrated by numerical simulations performed in V-REP, Virtual Robot Experimentation Platform (Rohmer et al., 2013). Several experiments are conducted in order to validate the methods and to assess the performance of the humanoid robot.

1.2 Main Assumptions

For the purpose of pursuing the main goals of the work, two deployment phases will be considered. The strategy that will be used is, firstly, to learn the locomotion task in an offline phase after transferring the demonstrated data to the humanoid robot by adding balance constraints. The biped locomotion task is difficult to learn from multiple demonstrations, because of the high variability of the task execution, even when the same subject provides the demonstrations. Therefore, this work addresses the important concept of generalization from a single "average" demonstration, focusing on steady-state walking on flat ground surfaces. In order to comply with a dynamic environment, the demonstration example is encoded by combining both discrete and rhythmic Dynamic Movement Primitives (DMP), as proposed by Ijspeert (Ijspeert et al., 2002a; Ijspeert et al., 2013) and Schaal (Schaal et al., 2003).

When applied to biped locomotion, DMP are, typically, learned in joint space, as reported by Nakanishi (Nakanishi et al., 2004a) and Morimoto (Morimoto et al., 2008). However, exploring the generalization and adaptation of learned primitives by modulation of their control parameters becomes difficult when the demonstrated trajectories are available in the joint space. This occurs because a change in the primitive's parameters does not correspond to a meaningful effect on the current behaviour. Unlike the above mentioned works, the use of DMPs learned in task-space has been applied by Pastor (Pastor et al., 2009) and Ude (Ude et al., 2010), but limited to the specific domain of robot manipulation. The main difficulty may arise in multi-body systems with a large number of DoFs since calculating the inverse kinematics is required. Supported by the development of efficient algorithms for whole-body coordination (Choi et al., 2007) as well as advances in designing robots that can learn such kinematic models by themselves (Hoffmann et al., 2009), the solution adopted here is based on DMPs learned in task-space and directly relate their parameters to task variables, such as step length, hip height, foot clearance and forward velocity.

In a second phase, such low-level representation of movement trajectories will be used by the robot online, in autonomous manner, accommodating novel constraints and goals by adjusting a few open parameters of the learned model. This will generate

new movements which fulfil task-specific features, while maintaining the overall style of the demonstration. Therefore, this work assumes the existence of a reliable vision system that contributes for planning locomotion movements towards adaptive behaviour. Vision will support important behaviours such as gait cycle modulation, navigation and obstacle avoidance. For example, when stepping over an obstacle, the vision system will provide accurate information about the properties of the obstacle and surrounding environment that can be used to pre-plan subtle gait adjustments guiding the foot placement.

1.3 Original Contributions

This thesis contributes with a particular view into the problem of adaptive locomotion from a single-demonstration by addressing some aspects that, in the specific context of biped robots, have not received much attention before. The main contributions of this work are the following:

- The human demonstrations are extracted from "robot-like" walking gaits on a flat surface. A "robot-like" walking gait means that the human stance foot will be constrained to remain in flat contact with the ground, forcing the "bent-knee" at all times in contrast with the typical straight-legged style. Two advantages can be envisioned: first, less effort should be required for transferring the kinematic data from the human to the robot. Second, it allows extracting directly the time course of the centre-of-pressure (CoP) that may be used for balance purposes.
- Most existing works concentrate on frameworks able to select movement primitives from a library based on the current task context. Instead, this work addresses the important concept of generalization from a single demonstration. Given the stringent balance constraints specific to biped locomotion tasks, the generalization to new situations gains a particular interest. This is not a big departure from the existing literature, but rather a refocusing of the attention to the specific application of biped locomotion.
- The DMP formulation is extended and refined in this thesis at different levels. The first extension occurs by including coupling terms among the x-, y- and z-

coordinates of the DMP defined in task-space. Second, rhythmic DMP to generate rhythmic locomotion are combined with discrete DMP to adapt the motion primitives to a constantly changing goal (e.g., precise foot placement). The transition process is autonomously adapted based on visual feedback. Third, it is demonstrated how the DMP formulation can be incorporated to existing balancing algorithms based on the zero moment point (ZMP) criterion.

- A clear separation is assumed from the classical control that forces the robot's motion to follow a predefined fixed timing (time-based) into a more event-based control. The changing contact conditions, plus the associated impacts with the ground, lead to models with multiple phases. Instead of forcing the robot's motion into a predefined fixed timing, the proposed pattern generator explores transition between phases that emerge from the interaction of the robot system with the environment, for example, triggered by sensor-driver events.

1.4 Document Structure

Although the chapters in this thesis are partially built upon results of the preceding chapters, most of them can be read independently. A description of the structure of the thesis follows below:

Chapter 2 reviews different aspects of human and biped robot locomotion. First, an overview over the human locomotion biological aspects is done including an analysis of the most relevant terms of human anatomy. To conclude the human locomotion discussion, an overview of the two main model theories about the human locomotion is presented. Then an overview across the evolution and research done in biped locomotion is discussed. The chapter ends with an overview of the two most common methodologies that have been used by researchers in control of biped robots locomotion.

Chapter 3 provides a survey on the main techniques used to learning and optimizing applied to robotics, including learning from demonstrations and reinforcement learning. The survey provides an overview of techniques and applications, but with particular focus on the specific challenges of biped locomotion.

Chapter 4 discusses the neurophysiological evidences of movement pattern primitives that have been found to be present in many animals and, with a great possibility, in humans. Based on this concept, a methodology known as Dynamic Movement Primitives (DMP) is implemented and evaluated for motion representation based on demonstrations from a human teacher. In particular, the study focuses on the properties of discrete and rhythmic movement primitives from the viewpoint of adaptation and generalization.

Chapter 5 presents one of the contributions of this work, by presenting a locomotion mode called as "robot-like" walking mode and used in several motion capture experiments. First, some concepts related to the human gait cycle are presented. Then, a brief description of the motion capture system and the experiments performed are given. The remainder of the chapter compares the normal human gait with the "robot-like" gait, both in terms of kinematics and dynamics data acquired with a VICON system and a force platform, respectively.

Chapter 6 discusses the methodologies used to transfer the single-demonstration as described in Chapter 5 to the humanoid robot. It is assumed an offline phase during which the skill transfer relies on (*i*) spatiotemporal scaling such that human and robot scale uniformly in all dimensions and, thereby, maintain their proportions, (ii) the application of a reduced model such that the dynamics of a humanoid robot are projected at its CoM and (iii) an algorithm that influences only a small number of variables that are sufficient for the core task (i.e., motion of the lower-limbs), leaving the rest of the degrees-of-freedom free to accomplish additional tasks (i.e., balance maintenance based on the ZMP criterion).

Chapter 7 presents the control framework developed to address the problem of generalization from a single-demonstration by combining two basic structures. The first structure is the pattern generator system consisting of discrete and rhythmic movement primitives as described in Chapter 4. The second structure consists of coupled phase oscillators that organize actions into coordinated units. This framework provides the possibility to generalize and create adaptive behaviour to different situations in real world environments. Several simulations are performed to assess the validity of the proposed concepts.

Chapter 8 concludes the thesis with a discussion on the results achieved and with a reflection on the future work.

Chapter 2
Biped Locomotion in Humans and Robots

The development of humanoid systems that are able to approximate the motion skills, level of safety, energy efficiency and power autonomy of the human being has been the inspiration of the robotic community for many years. Despite of the growing number of humanoid systems, there is still a significant gap between the current physical capacities and performances of the most advanced humanoid robots and humans. In order to adopt control concepts found in nature, it is well worth understanding the mechanisms that make normal walking in humans such an efficient form of two-legged locomotion. This chapter will review the nature of the human walking cycle, the associated anatomical characteristics and some basic biological control mechanisms. Then, the major challenges related with the design and the control of bipedal robots is emphasized. Finally, this chapter reviews some of the planning and control approaches found in the literature for developing biped walking humanoids.

2.1 Biological Aspects of Human Locomotion

Human locomotion is the result of a complex coupling between the neural and body dynamics. Accordingly, the understanding of many fundamental aspects of locomotion control implies the investigation of the neural circuits involved, as well as the body it controls. It is possible to decompose the general organization of the human locomotion into a simple cascade, namely brain activates muscles, muscles move skeleton and

skeleton performs work on external world. However, such a unidirectional framework fails to incorporate essential dynamic properties that emerge from feedback operating among and within levels. One key challenge in the current study of locomotion is to determine how each individual component within a locomotor system is implemented, while at the same time gaining insight on how they interplay and function collectively as an integrated whole.

2.1.1 The Human Control Loop

The problem of motor coordination of complex multi-joint movements has been recognized as very difficult to understand in biological, as well as to synthesize in artificial systems. The high degree of redundancy of such movements and the complexity of their dynamics make it difficult to achieve a robust solution. However, biological systems are able to move with remarkable elegance while interacting with the terrain in a highly energy-efficient way during walking or running. In particular, human walking is a prominent example of how to generate smooth motion by the interplay of appropriate biomechanics and adaptive neural control. It has been suggested that the coordination of this complex process involves a hierarchical organization of levels. Recently, theories of motor hierarchies have become more specific and have been applied to all levels of the motor system (Wolpert & Kawato, 1998; Arbib et al., 2000; Hamilton & Wolpert, 2002).

The majority of these theories recognize four levels in the vertebrate motor system hierarchy: the spinal cord, the brain stem, the motor cortex, and the association cortex. It also contains two side loops: the basal ganglia and the cerebellum, which interact with the hierarchy through connections with the thalamus. The higher-order areas concern with more global tasks regarding action, such as deciding when to act, devising an appropriate sequence of actions, and coordinating the activity of many limbs. They do not have to program the exact force and velocity of individual muscles, or coordinate movements with changes in posture. These low-level tasks are performed by the lower levels of the hierarchy. At the same time, the lower levels (*e.g.*, interactions between muscles and the spinal cord) are largely autonomous, while the higher level control (*e.g.*, cortical) arises only point wise as needed. This distributed and

hierarchical organization requires a control architecture formed by several nested sensori–motor loops combining rapid preflexes with multimodal sensory feedback and feedforward motor patterns. Additionally, the cycle period available to coordinate all these loops can be rather short, namely at a maximal walking speed. In humans, the slow feedback is compensated by a powerful brain function: prediction. The neurological basis of prediction is not yet well understood, even though there is an important body of evidence suggesting that prediction plays a fundamental role in many processes, such as learning, behaviour, motor control, perception (multi and cross-modal perception), among others. Fig. 2.1 depicts a simplified control loop relating cerebral motor cortex and cerebellum in supervising the spinal cord controlling the musculoskeletal system.

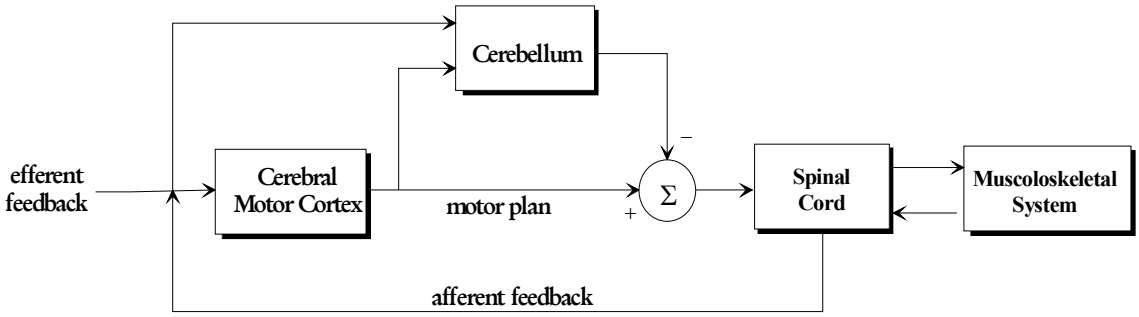

Fig. 2.1: Simplified human control loop relating motor cortex and cerebellum in supervising the spinal cord that controls the musculoskeletal system. The distributed organization combines rapid mechanical preflexes with multimodal sensory feedback and feedforward motor patterns.

Locomotion is initiated and modulated by supraspinal descending pathways. Some of these are direct pathways between the motor cortex and the spinal cord, such as the pathway from the vestibular nuclei and the cerebellum to the spinal neurons, and the corticospinal tracts that play an important role in visuomotor coordination, namely the accurate foot placement in uneven terrains. The postural problem involves an important role of the cerebellum for behaviourally successful locomotion, while the corticospinal pathway plays a role for the visually-guided modification of the locomotion cycle. Instead, other pathways are relayed by the centres in the brainstem, such as the reticularspinal tract that integrates information from the motor system to coordinate automatic movements of locomotion and posture, facilitating and inhibiting voluntary movement. Feedforward pathways are driven by specialized

circuits distributed throughout the spinal cord, called central pattern generators (CPGs).

CPGs generate the rhythmic oscillations that drive motor neurons of limb and body muscles in animals as diverse as lampreys, birds, insects, cats, and rats (Orlovski et al., 1999). Although CPGs may not require sensory feedback for their basic oscillatory behaviour, such feedback is essential for shaping and coordinating the neural activity with the actual mechanical movements. Sensory feedback is especially important in animals with upright posture, because the limbs play an important role in supporting the body in addition to locomotion.

A recent study have not only confirmed the presence of the CPG for human locomotion, but also confirmed its robustness and adaptability to different gait patterns and different walking contexts (Choi & Bastian, 2007). The distributed and cooperative nature of the feedback is what makes locomotion behaviours so robust in uncertain environments. Studied from a general perspective, motor output is constantly modified by both mechanical and neural feedback (Gandevia & Burke, 1994):

- Locomotor appendages and body segments not only exert forces on the external world, but also sense the forces they exert. The main sensory feedback to the CPGs is provided by sensory receptors in joints and muscles. A set of neurosensory devices measure the magnitudes and dynamics of force and length changes in the musculoskeletal system throughout each cycle of locomotion. In addition, viscoelastic behaviour of the musculoskeletal system itself provides a form of non-neural feedback that can operate almost without delay. Such viscoelastic behaviour produces responses to disturbances before the fastest neural reflexes. This preflexive mechanical feedback provides an additional component that functions in parallel with reflexive neural feedback and feedforward control from motor circuits to coordinate neural activity with mechanical activity;
- Neural feedback from sensors during locomotion takes three general forms. First, the input from directional sensors such as eyes, ears, and noses influences the overall speed and direction of locomotion, guiding toward a specific destination or avoiding obstacles. Second, specialized equilibrium organs, such

> as the inner ears, function to maintain specified body orientation during locomotion. Third, rapid feedback from mechanosensory cells, can tune cyclic motor patterns on a cycle-by-cycle basis, either by modulating cells within CPGs or by activating motor circuits that operate in parallel with pattern generating networks. The muscles and tendons of vertebrates are replete with diverse arrays of mechanoreceptors that monitor body kinematics and force production during locomotion. By integrating information across an array of sensors, a rich source of information is available for tuning motor output to changes of the internal and external environment within or between locomotor cycles.

Sensory feedback reflexes and mechanical preflexes are complimentary pathways that provide feedback from the environment. Rapid feedback from both neuronal and mechanical pathways is integrated with guidance from eyes, ears, noses, and equilibrium organs to direct an animal toward a desired locale or stabilize it in the face of an environmental perturbation. Current studies of motor control address the dynamic coupling among CPGs, sensory feedback, mechanical preflexes and the environment. Such integration may provide a global view of motor control and will likely redefine the roles of the individual components.

2.1.2 Normal Human Locomotion

Over the past decades, the advances in the area of gait science have produced a precise description of normal human locomotion. This includes an array of terms and concepts related to gait analysis, phases of walking connected to kinematic or kinetic events, basic principles of normal walking and the postural control function based on reflexes and supra-spinal high-level actions from the motor cortex. This section presents selected work related to these topics.

Basic Anatomical Terms

The anatomical terms describe the relations between different parts of the body and they are based on what is called the anatomical position, shown in Fig. 2.2. In this position, the subject is standing upright, with the arms by the sides of the body, the

palms forward and the feet together. Relative to the centre of the body, six terms are used to describe the directions as follows:

- **Superior** or **cranial** – toward the head end of the body;
- **Inferior** or **caudal** – away from the head;
- **Anterior** or **ventral** – front side of the body;
- **Posterior** or **dorsal** – back side of the body;
- **Left** and **right** – they refer of course to the left and right side of the body.

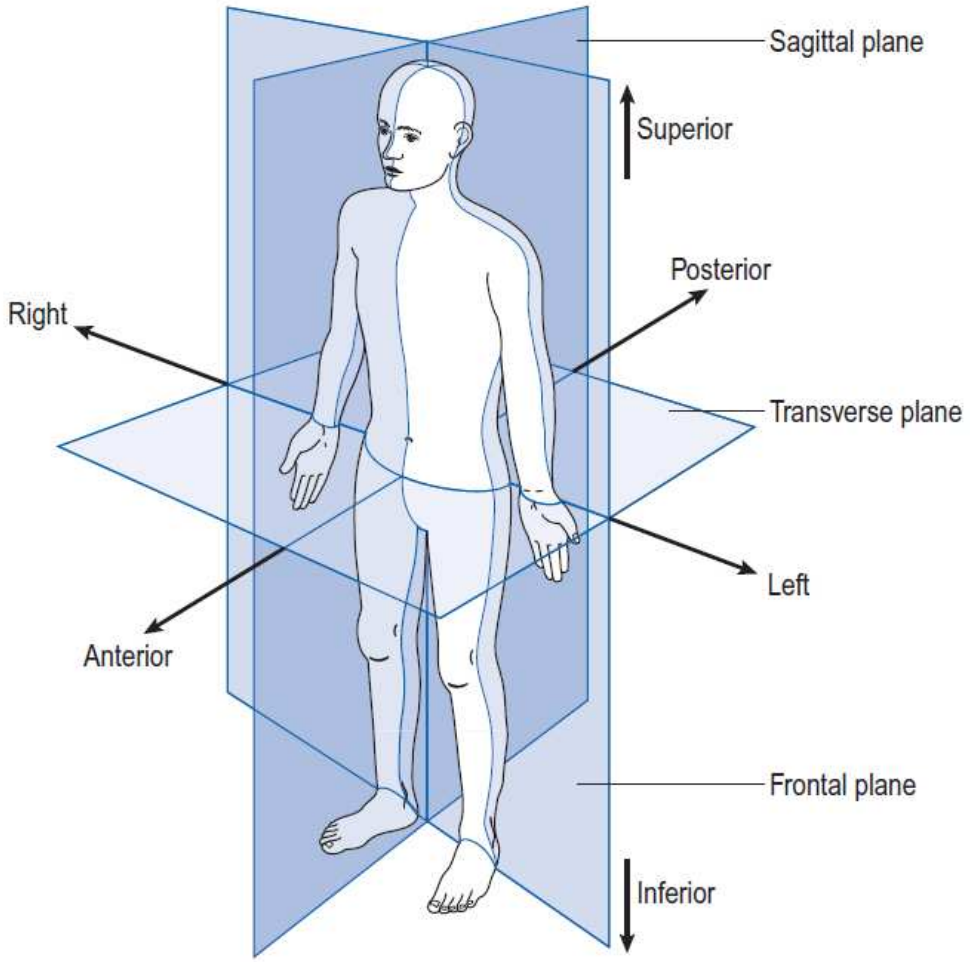

Fig. 2.2: The anatomical position, showing the three reference planes and the six fundamental directions (from Whittle, 2007a).

Three planes are defined as follows:

- **Sagittal** or **lateral plane** – a vertical plane running from the back to the front and divides the whole body into the left and right sides;

- **Frontal** or **coronal plane** – a vertical plane that divides the body into the front (anterior) and back (posterior) sections;
- **Transverse** or **axial plane** – a horizontal plane that divides the body into the upper and lower parts.

Most of the joints present on the human body can only move in one or two of these three planes. The directions of these motions for the hip, knee, ankle, foot and toes can be seen in Fig. 2.3. Although there's not a single designation, they are commonly designed as:

- **Flexion** and **extension** – are the movements that are performed in the sagittal plane;
- **Abduction** and **adduction** – these movements are performed on the frontal plane;
- **Internal** and **external rotation** – they take place on the transverse plane.

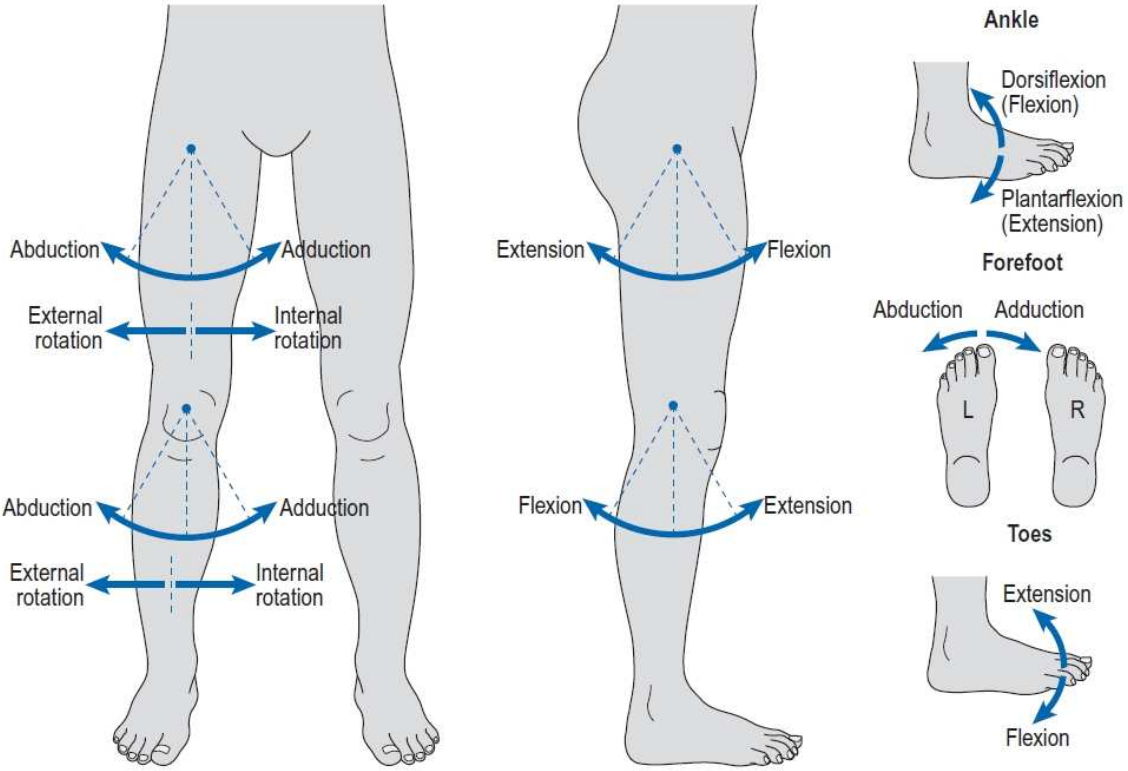

Fig. 2.3: Movements performed on the hip, knee, ankle, foot and toes joints (from Whittle, 2007b).

Morphological Adaptations in the Musculoskeletal System

The human musculoskeletal system presents a combination of complex anatomical characteristics to cope with the dynamics of balancing an upright trunk, while efficiently moving the body forward. As far as the muscles is concerned, current evidence points to the variety of functions in locomotion where muscles serves as motors, brakes, stiffness regulators and stores of energy. During locomotion, the amplitudes, frequencies and phases of the signals sent to the multiple muscles must be well coordinated, with many muscles per joint and several muscles acting on more than one joint. This coordination extends from the different joints and limbs to the antagonist muscles which combine periods of co-activation for modulating the joint's stiffness with periods of alternation for actuating the joint. This human musculoskeletal system's ability to control force and position simultaneously is the key to versatile interaction with our surroundings.

There were also interesting morphological adaptations in the human skeleton, found within the pelvis and lower limbs, that make it able to cope with the dynamics of balancing an upright trunk, while efficiently moving the body forward, as described in Lewin (Lewin, 2004) and Harcourt-Smith (Harcourt-Smith, 2007):

- The human pelvis has particular features that greatly facilitate support of the upright trunk. First, it places the trunk's centre of gravity closer to the hip joint. Second, the contraction of the gluteus muscles, positioned at the side of the pelvis, tilt the trunk toward the leg in contact with the ground, providing greater balance and stability.
- Humans have an inward sloping angle of the thigh (valgus knee angle) resulting in the knee being placed closer to the midline of the body than the femoral head articulated to the pelvis. This greatly reduces the lateral movements of the body's centre of gravity, leading to a more efficient and energy saving walking.
- The human knee has the ability to "lock" when full extended during the stance phase which greatly facilitates upright walking by keeping the leg straight and enabling the efficient transfer of weight between legs during the double-support phase.

- The talar articular surface of tibia is oriented perpendicular to the long axis of the bone, allowing a more efficient weight-transfer through to the foot.
- The shape of the human foot is particularly specialized for the requirements of biped locomotion with its arches. The combination of short and straight toes with a relatively long tarsus results in a more efficient propulsion lever during the stance phase. Second, the longitudinal arching combined with the locking morphology of the calcaneo-cuboid joint allows acting either as an efficient shock absorber or a rigid structure during weight-transfer to the ground.

Away from the adaptations of the pelvis and the lower limbs, the curves of the spinal column are also particularly relevant. Humans use less muscular effort to stand/walk upright and support more weight with a curved spine than if it were straight (curves increase resistance to axial compression). Most of the aforementioned characteristics of biped locomotion relate to two major factors: balancing the body as a whole and keeping the downward transmission of force as close to the midline of the body as possible. The minimization of the mediolateral swaying of the body during walking acts to stabilize the body over the supporting leg and to reduce energy expenditure.

Divisions of the Gait Cycle

The gait cycle is defined as the period of time between any two identical events in the walking cycle. Although any event can be selected as the onset of the gait cycle, initial contact of one foot is normally used as the starting event. The human walking cycle is characterized by two distinct phases: the stance phase, when the foot is in contact with the ground, and the swing phase, when it is off the ground in forward motion. The stance phase begins with heel strike as the foot hits the ground. The knee is fully extended and the foot dorsiflexion makes the heel strike the ground before the rest of the foot. Then, the plantar flexion occurs and, typically, force is transmitted to the ground along its lateral border. The point when the body is directly over the weight-bearing foot is known as the midstance phase.

The body then carries its forward momentum over the leg, at which point force moves medially to the ball of the foot (where the toes join with the rest of the foot).

At this point, strong muscular contraction of the plantar-flexors results in the ball of the foot pushing against the ground and, eventually, lifting away from it as the body continues to move forward. This action finishes with a final push-off of the big toe known as toe-off. The leg is now off the ground and in the swing phase, with the knee and hip both bent so as to keep the leg off the ground as it swings forward to make the next heel-strike.

On the one hand, double-support is the period of time when both feet are on the ground, occurring twice in the gait cycle at the beginning and end of stance phase. Generally, in normal walking, the two periods of double-limb support represent 25 percent of the gait cycle, decreasing the value as velocity increases. On the other hand, single-support is the period of time when only one foot is in contact with the ground (equal to the swing phase of the other limb). A complete description of the functional tasks and phases of gait is provided in Section 5.1.

2.1.3 Control Mechanisms of Biped Walking

The distinctive feature of human locomotion, compared with other bipedal animals, is the well recognizable straight-legged style: humans walk while keeping the legs almost straight (Alexander, 1992). At its most fundamental level, human locomotion appears to be a simple process: by applying forces on the external environment and, through the Newton's law, reaction forces are generated which move the body forward in the opposite direction. The spatiotemporal dynamics of locomotion are complicated, but understandable on the basis of a few common principles, including mechanisms of energy exchange and the use of force for propulsion, stability and manoeuvrability. There are essentially two major theories in human walking that have dominated over the last five decades: the inverted pendulum analogy and the six determinants of gait. In the following, these two complementary theories are discussed.

Inverted Pendulum Analogy

Two basic mechanisms have been proposed to explain the different patterns of time-variant forces measured during walking and running (Alexander & Vernon, 1975; Cavagna & Kaneko, 1977). When walking, the human body's centre of mass (CoM)

travels up and down during each step, reaching its lowest point when both feet are on the ground and rising to its highest point while it jumps over a straight supporting leg (Fig. 2.4). This vertical CoM movement enables humans to save energy through a pendulum-like mechanism, where the kinetic and gravitational potential energies are exchanged cyclically. While humans CoM moves up they slow down and when it moves down they speed up, thus passively converting gravitational potential energy to forward kinetic energy and back again. Kinetic energy in the first half of the stance phase is transformed into gravitational potential energy, which is partially recovered as the body falls forward and downward in the second half of the stance phase.

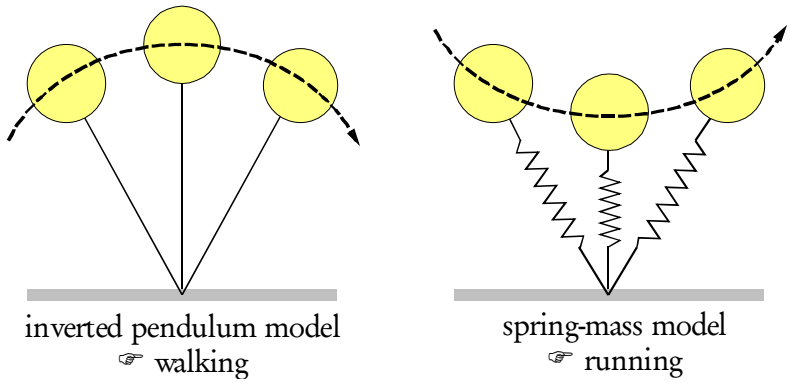

Fig. 2.4: Two basic models for legged locomotion: in walking (left), the centre of mass travels over a rigid leg, analogously to an inverted pendulum. In running (right), the leg acts as a spring, compressing during the braking phase and recoiling during the propulsive phase.

This pendulum-like mode of walking, which is a consequence of the straightness of our legs, reduces the mechanical work that our muscles must supply to raise and accelerate the CoM. On the other hand, while walking straight, the line of action of our body's weight passes close to the leg joints, and little tension is needed in the muscles to prevent the joints from collapsing under the load. Hence, another possibly more important consequence of our straight-legged style of walking is that it enables us to support our weight without the need for large forces in our leg muscles, thereby reducing the effective energy cost. In order to travel faster, humans change to a running gait that is similar to bouncing on a pogo stick (Fig. 2.4). Like a simple spring-mass system, the kinetic and gravitational potential energies are temporarily stored as elastic energy in muscles, tendons, and ligaments during the braking phase (as a leg strikes the

ground), being nearly all recovered during the propulsive second half of the stance phase. Remarkably, these basic mechanisms of energy conservation have been demonstrated in a wide variety of animals that differ in leg number, posture, body shape, body mass, or skeleton type, including humans, kangaroos, dogs, lizards, crabs, and cockroaches. The inverted pendulum model is a simple model for human walking and a study of its weakness and strengths can be found in a work of McGrath *et al.* (McGrath et al., 2015). More recently other extensions of the inverted pendulum have been proposed that include springers, telescopic actuators, dampers and additional joints and segments (Srinivasan, 2011; Pratt et al., 2012; Hong et al., 2013; Kim & Park, 2011).

Time-variant forces and energy exchange in the lateral direction (non-propulsive) could be equally important. Lateral forces may enhance both the passive stability and active manoeuvrability of locomotion, or other criteria that become apparent in natural environments. By pushing laterally, legs create a more robust gait that can be passively self-stabilizing as the animal changes speed or moves over uneven terrains (Kubow & Full, 1999). Forces generated orthogonal to the direction of motion may also contribute to the overall stability of locomotion, because the movement of animals and the natural environments through which they must navigate are complex and variable. Forces lateral to the direction of movement are often larger than one might expect for efficient locomotion, but they may enhance stability, and their modulation seems essential for active manoeuvres.

Determinants of Gait

Several studies have pointed out to other characteristics of the human gait, referring namely to optimizations performed during the gait cycle to minimize the excursions of the center of gravity and the energy expenditure. These optimizations, often called the "determinants of gait" were first presented by Saunders et al. (SAUNDERS et al., 1953). These determinants of gait have been accepted for a long time (about 40 years) as important to the reduction of energy expenditure. Only later (Della Croce et al., 2001; Gard & Childress, 1996) it was suggested that even though they exist, they play little or even no part in reducing energy expenditure, while Kerrigan (Kerrigan, 2003)

suggested that only one of the determinants (the fifth) significantly reduces the vertical excursion of the centre of mass and Baker (Baker et al., 2004) rejected the notion that energy is conserved by restricting the vertical movements and proposed that energy is mainly conserved by an exchange between potential and kinetic energy. Nevertheless, since these determinants are present in the human gait, a list of those determinants is provided:

- **Pelvic Rotation**: increases step length; increases radius for the arcs of the hip thus smoothing the arcuate trajectories of the CoM; helps regulate angular momentum in vertical direction.

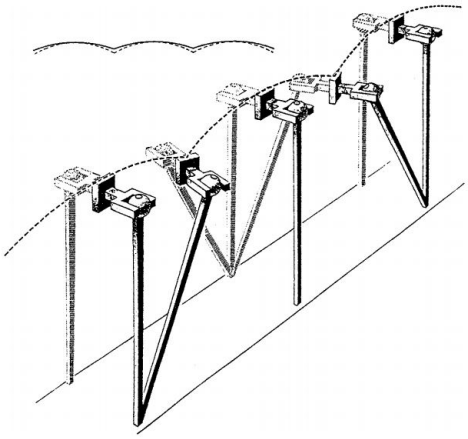

Fig. 2.5: Schematic figure used to illustrate the pelvic rotation (from Medved, 2000).

- **Pelvic tilt**: augment knee extension and Achilles tendon energy storage; helps regulate angular momentum in anterior-posterior direction.

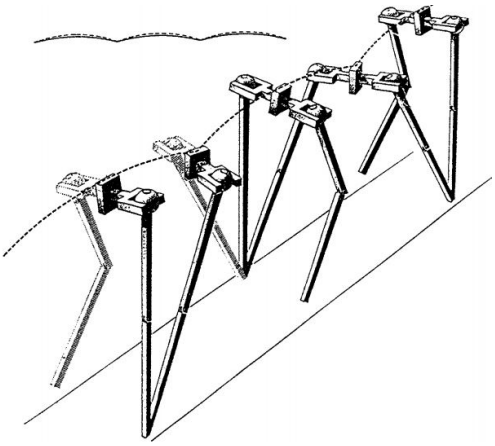

Fig. 2.6: Schematic figure used to illustrate the pelvic tilt (from Medved, 2000).

- **Knee flexion** (early support phase): shock absorption; helps regulate angular momentum in medio-lateral direction.

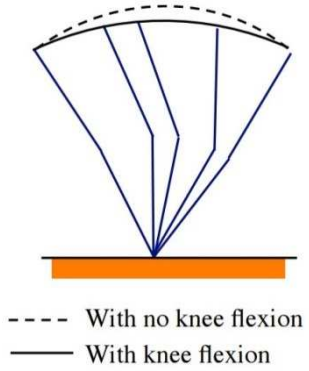

Fig. 2.7: Double-pendulum model in the sagittal plane used to illustrate the contribution of knee flexion to the vertical displacement of the CoM during stance (from Robinovitch, 2007).

- **Controlled plantarflexion**: depresses ascending limb of arcuate trajectory; absorbs shock of forefoot collision; helps regulate angular momentum in medio-lateral direction.

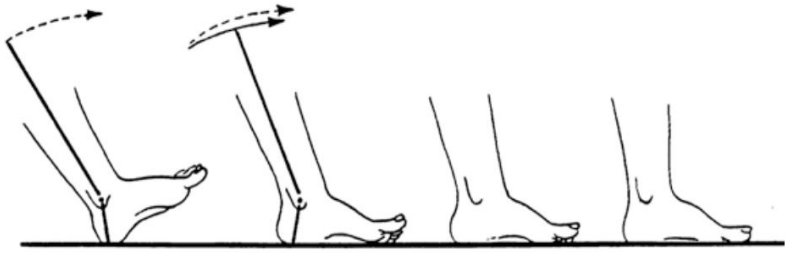

Fig. 2.8: Anatomical diagram of foot used to illustrate controlled plantarflexion during early stance (from Robinovitch, 2007).

- **Powered plantar flexion**: elevates descending limb; helps regulate angular momentum in mediolateral direction; decreases impact of adjacent leg.

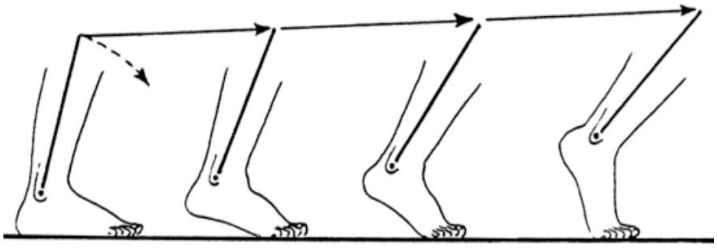

Fig. 2.9: Anatomical diagram of foot used to illustrate powered plantarflexion during late stance (from Robinovitch, 2007).

- **Lateral displacement of the pelvis**: with respect to a sagittal plane, the knees are medial to the hips; the effect of adducted posture of lower extremities is the reduction of total lateral displacement (~4.5 cm).

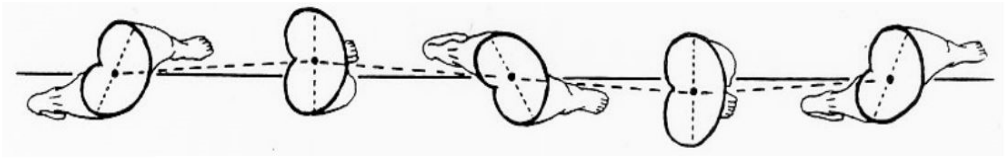

Fig. 2.10: Anatomical diagram of the lower-limbs used to illustrate lateral displacement of the pelvis(from Robinovitch, 2007).

2.2 Biped Locomotion in Humanoid Robots

The world has witnessed an impressive progress in legged robots during the last decades, from animal-like hopping robots and passive mechanisms to walking humanoid robots and small-size commercial platforms for research and entertainment. The continuous progress in robotics technology and the promoting activities of humanoid-robots soccer competitions, organized by RoboCup, FIRA and others, have strengthened the academic involvement. The next sections describe the common paradigms in robot design, examples of some prominent biped robots developed throughout the world and the inherent characteristics of biped locomotion that make its control an open challenging problem.

2.2.1 Paradigms in Robot Design

A retrospective analysis shows that there has long been a dichotomy in styles used in designing and implementing biped robots. On the one side, an increasing number of studies support the idea that the structure and mechanical characteristics of the robot body (*i.e.*, morphology) play a crucial role in behaviour generation and control. The morphology determines the kinematics and dynamics of the robot, and thereby the possible repertoire of behaviours, as well as affects the control required for these behaviours.

The relevance of this idea has become apparent with the pioneering work of Tad McGeer (McGeer, 1990) who built self-stabilizing passive mechanisms which could

dynamically walk with no sensing, actuation or feedback. This can be done by mechanical structures that execute the necessary step motions by using pendulum legs and passive interaction of gravity and inertia when, for example, walking down a slope. Although cannot be used as a complete walking algorithm for a humanoid robot, it is useful to combine elements of passive walking into the motion patterns thinking on the energy conservation that can be achieved with it.

Since McGeer, many other researchers have been demonstrating how well-designed morphologies can lead to reduction in control requirements and improved efficiency (Anderson et al., 2005; Collins & Ruina, 2005; Hobbelen & Wisse, 2007). The recent trend of passive walking research is influenced by concepts such as control on level ground (actuation), more joints and links (*e.g.*, upper-body with torso and arms, knees and ankles) and 3D stability focused on real-robot experiments. For important recent work refers to Wisse et al. (2007), Narukawa et al. (2008), Wang et al. (2009), Iida & Tedrake (2010).

Despite dynamic walking robots can produce economical human-like gaits, they tend to have poor versatility (*e.g.*, able to walk at various speeds on different terrains). As result, many articles about biped locomotion fall in on the other extreme of the spectrum: the full-active bipedal walking robots. From the viewpoint of robotics, numerous approaches for active biped locomotion control have been developed with their own solutions to the problems of pattern generation, postural control and coordination among DoFs.

2.2.2 Examples of Actively Controlled Bipeds

The world's first full-scale anthropomorphic robot, WABOT-1, was built in 1973 at Waseda University (Kato et al., 1974). Since then, the history of biped walking humanoids research has attracted the attention of a growing community, both from the industry and the academia. The impressive designs and skills of Honda's P2, P3 and ASIMO robots represent a landmark research work (Hirai et al., 1998; Sakagami et al., 2002). The QRIO prototypes were targeted to develop robotics systems for entertainment by following up the success of AIBO robot (Nagasaka et al., 2004). Although this project is not being pursued, the robots' natural motions when operating

in groups and when interacting with humans make their skills remarkably similar to human skills.

The HRP project involves efforts from the industry and the academia focusing on the potential of real-world applications for humanoids (Akachi et al., 2005; Hirukawa et al., 2004; Kaneko et al., 2004). At the same time, several small-size valuable commercial platforms have also appeared suitable for research and education purposes, such as the HOAP robots developed by Fujitsu (Fujitsu, 2003), the NAO robot developed by Aldebaran Robotics (Gouaillier et al., 2009) and the DARwIn-OP open platform developed at Virginia Tech (Muecke et al., 2006).

The involvement of several universities in long-term research programs was the key to breakthroughs and promoting innovative design and applications. The activities at the University of Tokyo with a number of humanoid robots (Nishiwaki et al., 2005), at the Waseda University with the WABIAN series robots (Ogura et al., 2006), the Johnnie designed by the TUM group in Germany (Lohmeier et al., 2004) and the KHR series robots from KAIST in Korea (Park et al., 2004; Park et al., 2007) are examples of humanoid robots focusing on biped locomotion research. At the same time, several easy-to-design humanoid platforms have been described in the literature, namely mechatronics details and technical solutions useful to others replicate (see, for example, Behnke & Stückler, 2008; Furuta et al., 2001; Kim et al., 2004; Santos & Silva, 2006; Yamasaki et al., 2001). Some of the most prominent representatives of actively controlled humanoid robots are shown in Fig. 2.11.

More recently, evidence of how human brains generate the wide variety of human behaviours has been revealed by neuroscience and psychological studies. Despite the increased understating of the human brain mechanisms, the replication of similar mechanisms into artificial devices is slower. The RobotCub project (Sandini et al., 2004; Tsagarakis et al., 2009) and the Computational Brain project (Cheng et al., 2007a, 2007b) have focused on psychology and neuroscience research as a guide for cognition in developing, respectively, the child-like iCub and the human-sized CBi humanoid robots.

Fig. 2.11: Examples of humanoids robots developed throughout the world: WABOT-1, ASIMO and QRIO (top from left to right); HRP, HOAP and NAO (bottom from left to right).

2.2.3 Inherent Characteristics of Biped Locomotion

The control of bipedal walking is a challenging problem not currently solvable by classical control theory. Some of the characteristics that make it difficult are the nonlinear dynamics, the multivariable dynamics and the unstable nature of the dynamics (*i.e.*, most biped robots will fall down without control). A bipedal walking robot is a multi-body system with a large number of degrees-of-freedom (typically 12 of more joints in their lower limbs) possessing highly-coupled nonlinear dynamics. The mathematical model of the system is very complex and it is described by nonlinear high order differential equations. Thus, the tools for linear systems typically cannot be applied to bipeds, except in special cases. Several strategies can be used to solve these potential problems, such as to simplify the dynamical model, to ignore the effects of friction and flexibility and to minimize the impacts with the ground.

In addition to these properties, some inherent characteristics of biped walking play a key role in control, namely the limited foot/ground interaction, the discrete changes in the dynamics (time-varying dynamics) and the subjective performance evaluation. First, the absence of fixed points in the inertia frame makes the system under-actuated. The DoF established between the foot and the ground is unilateral and the moment applied around the foot must be limited to avoid the complete rotation around the heel or toes. Because the robot's foot can only push on the ground (but not pull on it), control is limited and, in many circumstances, little can be done to prevent falling but to be caught by the next support foot. The absence of an actuator at the contact point requires the conversion from the internal forces generated by each joint actuator to the external reaction forces through the interaction with the environment. More concretely, the control of legged robots requires the manipulation of the contact point (or the point of action of the total external forces) and the force acting at that point. A property of human-like walking results from the high centre of gravity (CoG) with a small contact area to the ground. As result, balance maintenance is a central concern in order to engage useful tasks, from standing upright posture to motion goals. The most well-known stability measure to enhance trajectory-tracking controllers and to analyse their stability is the so-called ZMP-criterion proposed by Vukabrotovic and colleagues (Vukobratovic & Juricic, 1969; Vukobratović & Borovac, 2004).

Second, there is a change on the system's dynamics during the walking cycle as the system changes between single-support phase and double-support phase (*i.e.*, the system is supported by one foot or by both). This is an advantage that allows biped robots to walk in environments not accessible to wheel-based mobile platforms, such as climbing stairs. However, the changing contact conditions at the feet plus impacts at heel strike, which cause jump in the velocities, lead to models with multiple phases. As result, bipedal robots have characteristics of both continuous and discrete systems, making control design and analysis more difficult. Third, successful walking results in transporting the body section from one point to another safely and efficiently, even though the exact trajectories are not strictly important. Performance is usually defined in terms of efficiency, locomotion smoothness, maximum speed and robustness in rough terrains rather than typical notions such as trajectory tracking and disturbance

rejection. Therefore, it is difficult to define a cost function as required by automatic control learning and synthesis techniques. The problems mentioned before contribute to difficult the development of a simple and robust control system for biped robots.

Another recurrent problem in bipedal robots is how to design a controller that generates closed-loop motions, such as walking, running, or balancing, that are periodic and stable. Due to the complex dynamics associated with bipedal robots, the inherent under actuation and the changing contact conditions with the ground, the problem is far from being solved and there are just a few examples of algorithms developed using this approach. A good example is BIPER, a robot built by Miura and Shimoyama at Tokyo University (Miura & Shimoyama, 1984) that walked with straight legs. The small joint angle excursions were appropriate to linear control synthesis methods.

Other linearization approaches are commonly adopted to reduce the nonlinear dynamics into a linear one and facilitating the application of linear multivariable control methods (Gubina et al., 1974; Golliday, C. & Hemami, 1977; Mita et al., 1984). In the same line of thought, RABBIT is a biped robot aimed at the fundamental research of modelling and control of a class of nonlinear, hybrid systems that arise in the study of legged locomotion (Chevallereau et al., 2003; Westervelt et al., 2007). New paradigms, concepts and algorithms have been explored to deal with the problem of truly dynamic walking (the robot has no feet). In this work, authors present a systematic approach for achieving asymptotically stable motions that includes topics from mathematical modelling of walking gaits to theoretical control analysis and feedback synthesis.

2.3 Control Approaches in Biped Robots

In this section, the most important control approaches used in developing bipedal robots are discussed. This is a vast and complex task which can only be fulfilled in a limited fashion given the growing community of researchers working in the field. However, it seems reasonable to include in this study model-based and model-free approaches, each with their own advantages and limitations.

2.3.1 ZMP Based Approaches

Starting from the work of Vukobratovic and Juricic (Vukobratovic & Juricic, 1969), a considerable research effort has been dedicated to motion generation, stabilization and improvement using model-based approaches. The majority of the walking control systems (*e.g.*, Honda humanoid robots) use modulated feedback of pre-programmed joint trajectories. The desired motions can be calculated in advance using some form of pattern generator formulation (*e.g.*, parameterized curves, optimization of some metric) or capturing human motions by taking recordings (*e.g.*, walking, climbing stairs, etc). Then, an accurate dynamic model is used to compute dynamically admissible joint trajectories offline. These planned trajectories are then played back during walking and modified online through feedback, according to a simple control law (ZMP-based), in order to maintain stability. The trajectory modulation can be done online, while the robot walks, by measuring the ground reaction forces and/or the body orientation, and by comparing with the predicted forces and orientations.

The more advanced humanoid robots look extremely good when walking based on an important idea: using demonstrations of human walking. However, in general, the ZMP-criterion constrains the stance foot to remain in flat contact with the ground at all times and leaves less freedom for optimizing performance. As result, only slow motions can be achieved in a stable manner, while the walking gait is limited in terms of efficiency, natural appearance and disturbance handling (trajectories are rigidly tracked using typically high gain position servos). Furthermore, in spite of the remarkably human-like and convincing demonstrations, this approach places additional demands to allow locomotion across difficult terrains where no previous example is available. Fig. 2.12 illustrates the control problem if the ground reaction varies, as well as two common approaches used in practical robots to solve this question: ground reaction control and target ZMP control.

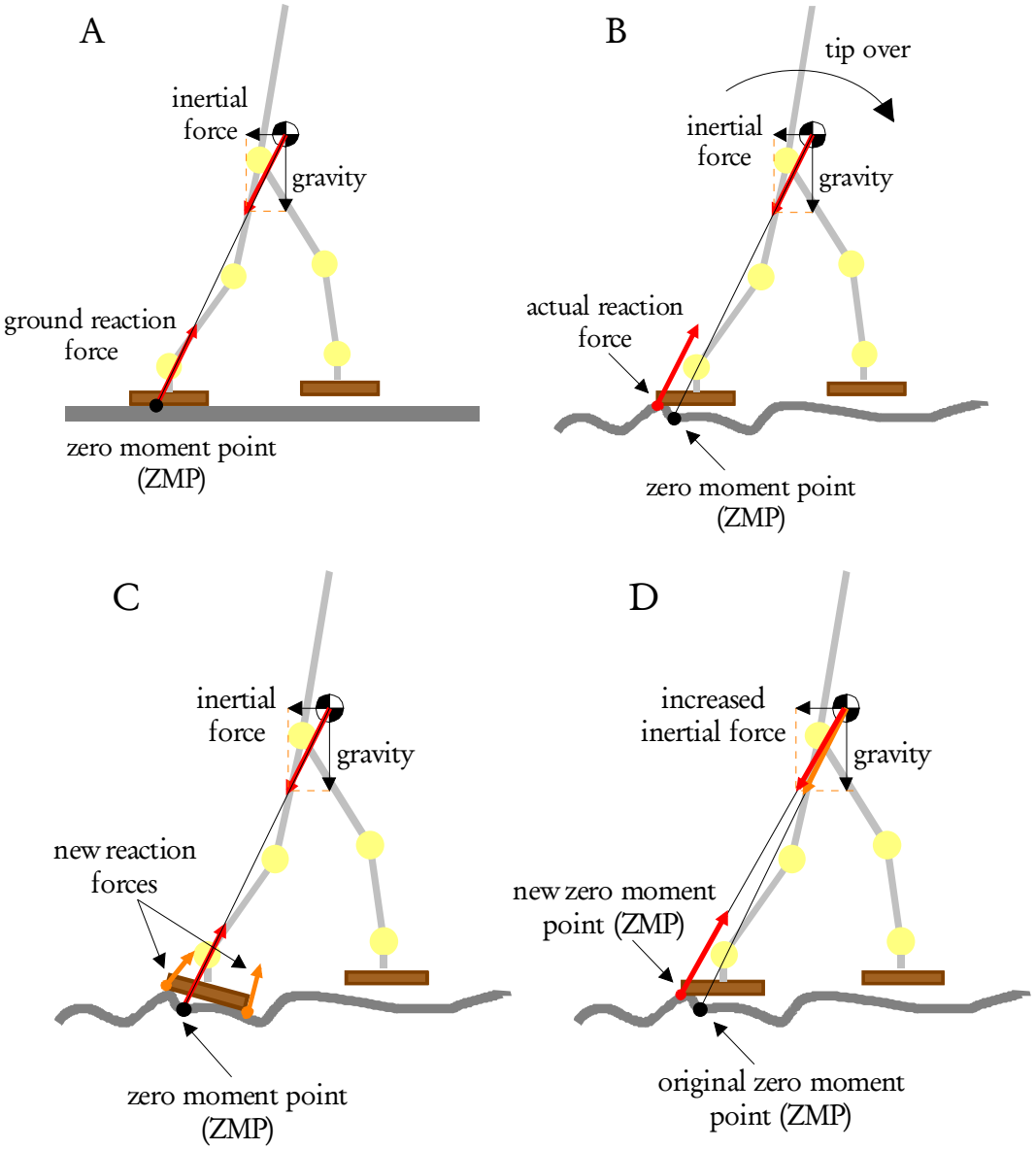

Fig. 2.12: Fundamental problem of stability in biped locomotion: (A) in flat surface the ZMP must by inside the supporting area and, typically, the ground reaction force and the total force acting at the CoM are colinear; (B) in irregular terrains the misalignment may lead to tip over; (C) the ground reaction control approach accommodates the ground reaction force by distributing the force between the heel and the toe so that the resultant force may pass through the ZMP; (D) the target ZMP control approach accelerates the upper torso to increase the inertial force so that the resultant force may pass through the ZMP.

Besides their several drawbacks, considerable results have been achieved by using Zero-Moment Point (ZMP) considerations to ensure stability. Examples include joint control strategies (Sano & Furusho, 1990; Stephens, 2007), whole-body motion control (Choi et al., 2007; Kajita & Kanehiro, 2003; Sugihar et al., 2002a), optimal control

policies (Muico et al., 2009; Zhou & Meng, 2003), predictive control (Ibanez et al., 2014) and reflex-based control (Huang & Nakamura, 2005). A more dynamic form of walking is now being attempted in humanoid robots that use the upper-body, or additional degrees-of-freedom, to control the vertical component of their centre of gravity. This form of walking is referred as "straight leg walking" and it is easily observable as the robot does not need to adopt the typical "crouched gait". Two examples are the highly integrated humanoids WABIAN-2 (Ogura et al., 2006) and JOHNNIE (Pfeiffer, 2007) developed at Waseda University and Technical University of Munich, respectively.

It should be noted, however, that other research groups use time-invariant control schemes based on heuristics, simple feedback rules and simple physical models. Examples include Timmy at Harvard (Dunn & Howe, 1996), Meltran at Tsukuba Lab (Kajita & Kobayashi, 1987) and the Spring-Flamingo developed at MIT Leg Lab (Pratt et al., 2001). Instead of pre-computing joint trajectories (time-dependent algorithms), simple feedback rules are used online to control the robots what, typically, improves the robustness against disturbances. The exploration of the specific characteristics of biped walking (or natural dynamics) is another key factor to closely relate the planning and motion control problem.

2.3.2 Bio-inspired Central Pattern Generators

Supported by neurophysiological evidences and robot models, an increasing number of researchers are adopting model-free approaches for the control of biped locomotion in humanoid robots. An example gaining an increased acceptance is the bioinspired approach based on the design of central pattern generators (CPGs). As stated in section 2.1.1, central pattern generators are neural circuitry located in the spinal cord which can generate low level rhythmic patterns without sensory or central input. The phase relation among these oscillatory components must be well synchronized so as to generate an adequate locomotion pattern, such as the biped gait. In vertebrates, the locomotion system is organized such that the spinal CPGs are responsible for producing the basic rhythmic patterns, while the higher-level centres (*i.e.*, motor cortex, cerebellum and basal ganglia) are responsible for modulating these patterns

according to environmental conditions. Sensory feedback plays also an important role in shaping the rhythm patterns, providing the opportunity to obtain entrainment between the CPG and the mechanical body. Grillner (Grillner, 1985) and Pearson (Pearson, 1993) have significant studies concerning the locomotion of vertebrates controlled by central pattern generators. Since the seminal work of Taga (Taga, 1995b, 1995a), different CPG-models have been studied being capable of producing rich behaviours through modulation of their parameters.

Properties of CPG Models

As an alternative to methods based on pre-recorded reference trajectories (*e.g.*, ZMP-based) or heuristic control laws, CPG models present several interesting properties, such as the distributed control architecture, the ability to deal with redundancies and the fast control loops. These properties, when transferred to mathematical models, make CPGs useful build blocks for locomotion controllers in robots:

- It reduces time delays in the motor control loop since rhythms are coordinated with mechanical movements using short feedback loops directly through the spinal cord.
- It significantly reduces the dimensionality of the descending control signals and, as consequence, the necessary bandwidth between the higher level centres and the spinal cord. Indeed, the control signals do not need to specify muscle activity, but only modulate CPG activity.
- The system rapidly returns to its normal rhythmic limit cycle behaviour after transient perturbations of the state variables, providing robustness against perturbations.
- CPG models typically produce smooth modulations of the produced trajectories even when the control parameters are abruptly changed (the differential equations typically act as first or second order filters). This property is useful for doing online trajectory generation that avoids possible damage in motors and gearboxes due to abrupt changes of motor commands.

Therefore, a properly implemented CPG model reduces the dimensionality of the control problem such that higher level controllers (or learning algorithms) do not need to directly produce multidimensional motor commands, but only higher level control signals about task goals, desired direction of movement and speed. In this context, it seems clear that the CPG models should be more effective when used with distributed control implementations (*i.e.*, the layered architecture mentioned previously), being interesting for modular robots.

Three different types of CPG models are implemented in most robots, including connectionist models (Arena, 2000; Lu et al., 2005), vector maps (Okada et al., 2002) or systems of coupled oscillators (Matsuoka, 1985; Williamson, 1998; Kimura et al., 1999; Crespi et al., 2006; Ijspeert et al., 2007). In a few cases, spiking neural network models have also been used (Lewis, 2002). All significant implementations involve a set of coupled differential equations that are numerically integrated and solved on a given processor. At the same time, several aspects must be taken in consideration when designing and implementing the CPG model, such as: (1) the general architecture of the CPG, including the type and number of oscillators or neurons. In a real robot, it also involves choosing between position control, where the outputs of the CPG are desired joint angles provided to a feedback controller, and torque control where the outputs directly control the torque produced by the motors; (2) the type and topology of couplings that determine the conditions for phase-coupling among oscillators; (3) the selection of the waveforms that determine which trajectories will be performed by each joint angle during a cycle; and (4) the influence of the input signals and of the feedback signals. Input signals will define how control parameters can modulate important quantities such as the frequency, amplitude, phase lags (*e.g.*, for gait transition), or waveforms (*e.g.*, for independently adjusting swing and stance phases). Feedback signals will define how feedback from the body will affect the activity of the CPG, for example, accelerating or decelerating it depending on environmental conditions. A major difficulty in designing CPGs is that the above design aspects are all strongly interconnected.

CPG Models for Biped Locomotion

Most of the previous works centred on the application of CPG models for biped locomotion is limited to simulation studies. Only a few experimental applications can be found on the literature largely due to hardware limitations, difficulty in parameter tuning and large modelling errors between simulations and experiments. Thus, more than an exhaustive review of the literature, this subsection aims to provide a brief overview of the principal issues and proposed solutions with emphasis, whenever possible, to experimental applications with real robots. Interesting overviews of CPG-controlled biped locomotion were provided by Ijspeert (Ijspeert, 2008) and, more recently, by Matos and Santos (Matos & Santos, 2014).

Bay and Hemami (Bay & Hemami, 1987) co-authored the first article found on the IEEE explore database that relates the use of CPGs to biped locomotion control. Using a set of van der Pol oscillators, the authors constructed a CPG model that could be used to generate the angles for the lower limb over a single step walking cycle. By using computer simulations, they fit the parameters so that the oscillators generate the correct angles for a walk and jump test, and the reproduced values exhibited coordinated motions quite similar to human walking and jumping. It should be noticed that only the angles of the hips and knees were taken into account (*i.e.*, the ankle joint was not considered). At the same time, undesired knees bends and unusually large angular displacements were found before the system reaches a steady state. Later, Miyakoshi *et al.* (1998) simulated a 3D model with 11-DoF and 8-links using three neural oscillators. The several simulations showed the possibility to achieve a stable biped motion even in the presence of perturbations.

Tsuchiya and Aoi (Aoi et al., 2004a) proposed a locomotion control system based on nonlinear oscillators which generate the commanded trajectories of the joints as function of the phase oscillators and a low-level control system at the individual joints. The oscillators tune the oscillatory phases through mutual interactions and feedback signals from touch sensors. Using both simulations and a real robot, they showed that the proposed control system is able to produce adaptive walking patterns under environment change conditions by setting the locomotion period. Later, the same

authors added a turning control system that works by changing the duty ratios of the leg motion generators (Aoi et al., 2004b). Experimental results showed that the robot is able to successfully turn around corners using a CCD camera.

Nakanishi (Nakanishi & Morimoto, 2004) proposed a framework for learning biped locomotion using dynamical movement primitives based on non-linear oscillators. Their ultimate goal was to establish control design principles in order to achieve natural human-like locomotion. In this article, the trajectories are learned from demonstrations based on data captured from a human walking, while the frequencies of the learned trajectories are adjusted automatically by an adaptation algorithm based on phase resetting and entrainment of the coupled oscillators. The role of phase resetting in terms of biped walking robustness both against external perturbations and environmental changes was tested in the same paper. Numerical and experimental results demonstrated the effectiveness of the proposed control algorithm and the frequency adaptation algorithm.

Matsubara (Matsubara et al., 2005b) addressed the problem related with sensory feedback and they proposed an efficient learning framework for CPG-based biped locomotion controller using a policy gradient method. It is worth noting that the CPG controller was used at the hip joints, while the knees were controlled by a state machine. Numerical simulations showed that an appropriate sensory feedback controller could be acquired. The implementation of these concepts on a physical robot showed that the learning controller works appropriately on a real world environment, although, occasional the robot could not start walking or fall off after a couple of steps.

Endo (Endo et al., 2005) attempted to achieve 3D biped locomotion using a neural oscillator with a full-body humanoid robot QRIO. In order to simplify the oscillator connections and feedback pathways, authors proposed the allocation of the neural oscillators in a task space coordinate system, instead of the traditional way in which each joint has a neural oscillator allocated. In this way, they were able to reduce the number of open parameters in the neural oscillator, while making it much easier to design effective feedback pathways to generate a stable limit cycle. As result, they showed how straight walking with different velocities can be achieved, both in

simulation and in experiments with a real robot. The robustness against external perturbations and environmental changes was demonstrated.

Komatsu and Usui (Komatsu & Usui, 2005) also make use of a CPG in their experiments with walking and running motions. They proposed a hybrid CPG method to perform adaptive dynamic motions by combining CPG models with a force control system that controls the acting reaction forces in the vertical and horizontal directions. Simulation and experimental studies showed that the robot was able to walk and run in horizontal floor and slopes, reaching speeds up to 1.6m/s (the motion is only done in 2D).

2.4 Final Remarks

While research efforts in the last years have produced some impressive progress, the goal of a robot with human-like abilities seems to be far away in the future. In particular, biped locomotion is a key research topic in humanoid robotics that is still far from being maturely solved. Based on a thorough review on biomechanics and robotics literature, this chapter highlighted a few research lines that seem to be relevant in framing the future of humanoid robotics. Recent advances in integrative and comparative study of animal locomotion have revealed several general principles (for reviews see Dickinson et al., 2000; Donkelaar, 2001). The generality of these mechanisms, observed in different modes of the human locomotion, is just beginning to be explored by the robotics community. For example, the mechanisms of non-steady locomotion, including starting, stopping, and turning, are emerging areas of interest as well. In nature, unlike in the laboratory, straight-line, steady-speed locomotion is the exception rather than the rule.

There are some active areas of research in humanoid robotics that constitute a relevant background for this work. Two emerging paradigms appeared in last years with great influence on the research focus: modular motor control and robot learning. There are strong evidences that basic building blocks of pattern generators co-exist at the spinal level and they are used by the CNS to create movements. CPGs, motion primitives and related concepts, such as muscle synergies, force fields, and motor

schemas, are seen as elementary modular controllers that produce specific movements under the control of a few open control parameters. Neurophysiological models and experiments have shown that very rich behaviours can be generated, being capable of modulating speed, direction, and types of gaits depending on descending control signals. However, the link with other motor behaviours such as scratching, standing up, kicking, sitting down, laying down, reaching or manipulation, remains to be decoded in animals and implemented in robots.

Learning is another active branch of robotics with different bio-inspired mechanisms like those implementing reinforcement (Matsubara et al., 2006; Nakamura et al., 2007; Peters & Schaal, 2008) or imitation learning schemes (Billard, 2001; Mataric, 2002; Nakanishi et al., 2004a; Schaal, 1999). Researchers in humanoid robotics have been aware that complex sensorimotor skills can most likely only be acquired through learning methods. Otherwise, it is too complicated to solve problems arising from high-dimensional and highly nonlinear perception-action spaces. In the same line of thought, embodiment implies to change the paradigm from the human-like outer shape to more human-like principles in perception and locomotion (Anderson, 2003; Lungarella et al., 2003; Pfeiffer, 2007).

Chapter 3
Learning in Biped Locomotion

Humans evolve and learn from different situations occurring in everyday life, being able to predict the effects of their actions in the environment and, in this way, react accordingly. Inspired by biology, several research projects are underway to develop machines endowed with cognitive abilities and that can learn the same way humans do. This chapter provides a perspective of two techniques that have been widely used in the robotics field and that sometimes are commonly used together: learning from demonstration and learning by trial and feedback. First, an overview over the challenges for robot learning is provided. Then, the concept of Learning from Demonstration (LfD) is presented together with some examples of application in biped locomotion. Finally, an overview on reinforcement leaning (RL) is provided, followed by some examples of its use to the specific problem of biped locomotion.

3.1 Challenges for Robot Learning

Applying learning to the problem of biped locomotion is difficult due to the many DoFs, the high-dimensional state-action space and the demanding balance constraints. Two additional obstacles need to be considered. First, there is the lack of computational tools for rapid learning of new behaviours allowing the robot to adapt to the environment. Experience on a real physical system is tedious to obtain, expensive and often hard to reproduce, but it usually cannot be replaced by learning in

simulations alone since small modeling errors can accumulate to a substantially different behavior.

The second obstacle is the lack of ability to handle incomplete knowledge of the environment due to uncertainties and ambiguities in perception systems. Looking again at the humans, it is clear that imitation is a fundamental mechanism for rapid learning which can be observed throughout life. For example, while children routinely learn new skills by imitating their parents (*e.g.*, opening a door, throwing a ball, tying their shoes), adults continue to learn (improve) by imitating skilled instructors (*e.g.*, playing tennis).

3.1.1 Trajectory Representation

The choice of the representation for the trajectory or encoding a trajectory is a central issue. Among the simplest representations, simple storing of large time-indexed vectors is one of the options (Kawamura & Fukao, 1994). Other approaches have included function approximators, such as neural networks (Maass et al., 2002; Zegers & Sundareshan, 2003) and recurrent neural networks (RNN) (Paine & Tani, 2004; Tani & Ito, 2003). More compact representations can be constructed by using interpolation algorithms such as spline fitting and only storing key viapoints (Schaal, 1999). More recently, Bayesian Networks (Grimes et al., 2007), Gaussian Mixture Models (GMM) (Calinon et al., 2007) or, hidden Markov models (HMM) (Inamura et al., 2004), have been used. Probabilistic models have also been used with knowledge-based systems (Hersch et al., 2008).

Due to their cyclic nature, encoding of rhythmic motions requires particular types of encoding. Different approaches have been used as cyclically reading vectors, cyclic vector fields (Li & Horowitz, 1999; Okada et al., 2002), and encoding trajectories into the limit cycle behaviour of nonlinear oscillators (Nishii, 1998; Ijspeert et al., 2002b). In some representations hierarchical structures in which a trajectory is encoded as a superposition and/or sequence of simpler trajectories are used (Mussa-Ivaldi, 1997; Tsuji et al., 2002; Rohrer & Hogan, 2003; Drumwright et al., 2004). These approaches are generally inspired in the concept of motion primitives found in vertebrate motor

control (Schaal, 1999; Matarić, 1998), and these are interesting ways of making the encoding of multiple trajectories with a compact representation.

Depending on the type of representation chosen, the usage of learning algorithms could be or not necessary. For example, no learning algorithm is needed when time-indexed vectors (Kawamura & Fukao, 1994) are used. If the representations are based on spline-fitting they typically can use well-established fitting algorithms (Miyamoto et al., 1996), which are the via-points used by these algorithms that can be assigned by the user or automatically. In cases where the parameters of chosen representation are linear, regression methods can be sufficient (Maass et al., 2002; Ijspeert et al., 2002b) with the advantage of fast learning. In other cases, gradient-descent algorithms have been extensively used, in particularly for neural networks, as for example in variants of the backpropagation algorithm (Simard & Le Cun, 1992). In alternative, evolutionary algorithms can also be used for instantiating the network's parameters with a cost function describing the desired trajectories given (Ijspeert et al., 1999). However, gradient descent and evolutionary algorithms are both typically slow.

3.1.2 Adaptation by Modulation

Besides correctly reproducing a learned trajectory, there is a high interest in adapting it to new conditions, *i.e.*, modulate the learned trajectory. The modulations can be simple, like repeating these trajectories and varying the speed or the amplitude, or can be more complex, in which there can be time/space dependence in order to avoid an obstacle, for example. In other cases, other modulations may be necessary when, for example, the robot is subjected to external perturbations, and it should be noticed that some representations are more suitable than others for dealing with perturbations.

In many situations, reproducing the learned trajectories at different speeds and/or different amplitudes can be obtained by using simple scaling laws, like with time-indexed vector representations (Kawamura & Fukao, 1994) or using dynamic optimization methods, like in representations using spline fitting and via-points (Miyamoto et al., 1996). There exists, however, the disadvantage that the control policy is time dependent, which makes them highly sensitive when unforeseen perturbations in the environment disrupt the normal time flow. This problem is not present in neural

networks, that can be trained to generalize and produce a range of different motions from a fixed set of training examples, without requiring explicit time indexing (Zegers & Sundareshan, 2003).

In human-like movements some specific features cannot be accounted for by simply using scaling. Encapsulation of these features can be done by optimization criteria, such as minimum variance of end position (Harris & Wolpert, 1998) or minimum torque change (Kawato, 1996). Other options include dynamical systems designed to replicate human movements and to generate new movements by modulating attractor points (Bullock & Grossberg, 1989), as well as the methods that synthetize a trajectory from a given set of learned motions (Ude et al., 2008; Mezger et al., 2005).

By using coupled nonlinear oscillators (Righetti et al., 2006), reproduction and modulation of trajectories is also possible. Adaptive frequency oscillators were used to learn separate frequency components from the demonstrated trajectory and then added to recreate the signal. However, this system can only be modulated in speed and amplitude. Besides this, after suffering a perturbation, the return to the limit cycle regime is relatively slow because the time the system needs to converge to the right phase lags between the multiple oscillators that are used to encode a specific one-dimensional signal. At the same time, when applied to complex signals or when scaling into multi-dimensionality, the number of oscillators grows quickly, leading to a complex system structure.

One of the most complex problems is dealing with perturbations when performing a trajectory with a robot in the presence of obstacles and/or external forces. For example, a reaching movement and hitting an obstacle with a limb requires a different trajectory modulation during a walking sequence. There are some situations in which the trajectories might not need to be modulated if the natures of the perturbations are small and/or short. At the same time, whenever the robot is provided with an on-line tracking controller (*e.g.* a PID feedback controller), the feedback control loop could be enough to overcome the perturbation. However, large perturbations require on-line modulations of the desired trajectories to prevent risks like falling (in the case of a biped robot) or damage. Some approaches have been used like a criterion to modulate the learned trajectories (Hersch et al., 2008) or encoding desired trajectories in terms of

vector fields, *e.g.* velocity fields (Li & Horowitz, 1999), or potential fields (Khatib, 1986). The vector fields essentially represent an attractor landscape, with the desired trajectory as attractor trajectory and so offering the opportunity to introduce repulsive forces for avoiding obstacles.

3.1.3 Learning Paradigms

The dependence on robots that must be carefully programmed and calibrated before use and thereafter whenever the task changes does not seem acceptable for robots that have to coexist and cooperate with humans in real-world environments subject to uncertainty. Therefore, there is an increasing need to go beyond robots that are pre-programmed explicitly towards those that learn and adapt to natural and dynamic environments using approaches typically observed in animals. The general concept of machine learning refers usually to the changes in a given system that automatically learn to recognize complex patterns, to link perception, reasoning and action processes, to make intelligent decisions and to predict situations that it may encounter. Machine learning can be achieved at different levels of complexity, much like different scientific fields investigate learning processes in biological systems. Nonetheless, three learning paradigms are considered in the machine learning literature: supervised, unsupervised and reinforcement learning.

Supervised learning is the task of inferring a function from a supervised set of training examples consisting of an input object and a desired output value. It has been successfully applied in machine learning, statistical pattern recognition, and artificial neural networks (*e.g.*, classification and prediction tasks). Unsupervised learning is about understanding the world by mapping or clustering given data according to some principles, where there is no explicit teaching signal. Reinforcement Learning (RL) is between the two since learning occurs by means of the reward signal with possible delays. Many neurophysiological evidences exist pointing to that different brain structures are specialized in different learning paradigms, namely the cerebellum in supervised learning, the basal ganglia in reinforcement learning and the cerebral cortex in unsupervised learning (Houk & Wise, 1995; Doya, 2000).

3.2 Learning from Demonstration (LfD)

In order to properly function in a real world, the gait of humanoid robots must be able to constantly and quickly adapt to new situations. Programming robots to perform such actions and that take into account the robot's complex dynamics is a challenging and complex problem. Essentially, traditional approaches will require highly accurate and prior knowledge of the robot's dynamics and the environment in order to create complex control algorithms able of generating a stable dynamic motion. Given the complexity of the problem, there is an increasing need to move away from robots that are pre-programmed explicitly towards those endowed with the ability to extract information from the environment, learn about it and, hypothetically, develop predictions.

3.2.1 Computational Approaches Taxonomy

A considerable research effort has been dedicated to the use of human demonstrations as input for teaching robots to perform from simple movements to complex skills. In particular, robot learning from demonstration is a powerful approach promoting movements that look natural and predictable and also powerful mechanism for social learning that has received a great deal of interest from researchers in the fields of both animal behaviour and child development. At least two perspectives can arise from the task of imitation learning and social interaction: (1) an engineering perspective, in which a robot that could imitate the actions of a human would provide a simple and effective means for the human to specify a task to the robot and for the robot to acquire new skills without any additional programming, and (2) a computer science perspective, where imitation provides a means for biasing interaction and constraining the search space for learning.

In this context, the field of learning from demonstration (LfD) has explored computational tools for robot programming that relies on example executions of a task, typically provided by a human teacher (Argall et al., 2009; Billard et al., 2008). The survey provided by Argall et al. (Argall et al., 2009) provides a good classification of the correspondence between the recorded mapping (relation between the teacher

execution and the recorded execution) and the embodiment mapping (relation between the recorded execution and the learner), reproduced here in Fig. 3.1. Broadly speaking, the recording mapping will refer to whether the exact states/actions experienced by the teacher during the demonstration are recorded into the dataset in a direct form or there is a need for a mapping function; As for the embodiment mapping, it refers to the fact that whether the states/actions recorded in the dataset will relate directly to those the learner will execute, or if some kind of transformation/mapping function is needed. Based on this classification and the description provided in Chapter 5 and Chapter 6, the work presented in this text could be classified as imitation with a direct recorded mapping.

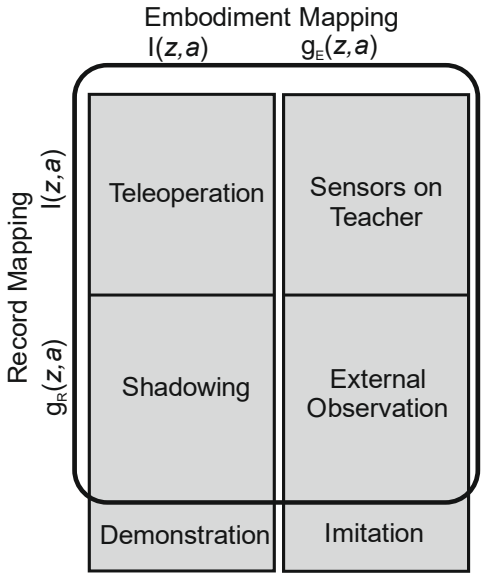

Fig. 3.1: Intersection between the recording and embodiment mappings. I(*z*,*a*) means there is a direct relation between the teacher execution and the recording in the recording mapping or a direct relation between the recorded execution and the learner action in the embodiment mapping. If the relation is not direct, it is represented by *g* function (adapted from Argall et al., 2009).

Based on the embodiment mapping, the data acquisition can be divided into two main categories as follows:

- Demonstration: the mapping is direct since the demonstration is performed directly on the actual robot learner;
- Imitation: the mapping is not direct since the demonstration is performed on a platform other than the robot learner.

At the same time, the way the data is recorded in any of these classification modes can be further divided according to the following approaches (see Fig. 3.2):

- Teleoperation: the teacher operates the robot, be it in a direct form (the robot actuators must be able to operate in a compliance mode), or through a joystick. In either way, the recording mapping is directly related to the actions performed by the teacher. As an example, consider a human manipulating a robot arm directly to perform a reaching task, while the robot records the joint states during the entire demonstration (a good example is the experiment B performed in Ude et al., 2010);
- Shadowing: the robot learner records the execution using its own sensors and attempts to match or mimic the teacher motion as it is executed by the teacher.
- Sensors on teacher: sensors placed on the teacher are used to record the examples performed by him/her. An example is the case of marker systems placed on the body of the teacher, like the VICON system;
- External observation: the sensors used to record the performed task are external to the executing body (teacher) and may or not be located on the robot learner.

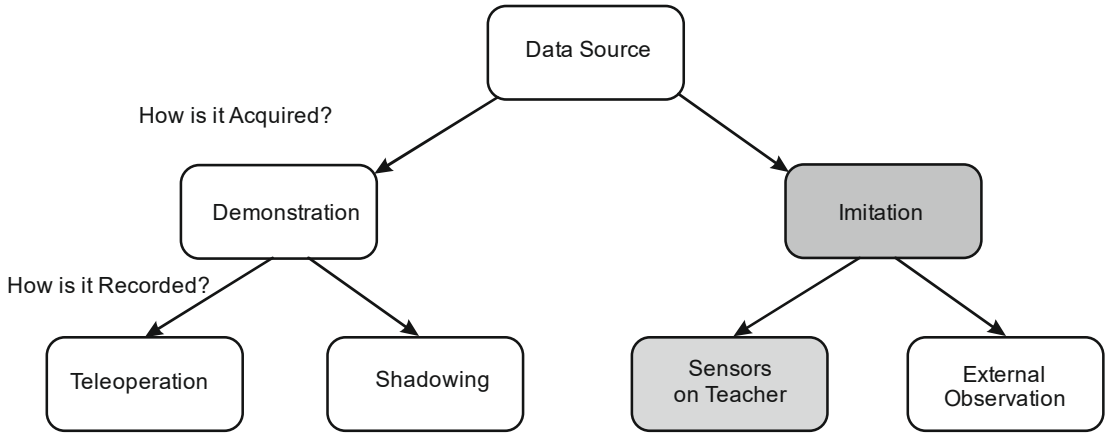

Fig. 3.2: Classification of the approaches used for building the demonstration dataset. Shadowed regions represent the approach followed in this work (adapted from Argall et al., 2009).

Once a given dataset has been recorded, several approaches for deriving a policy from demonstration data can be envisioned. Fig. 3.3 presents a diagram introducing how these policies can be classified:

- Mapping Function: here the policy learning calculates a function with the goal to approximate the state to action mapping. Typically, the policy is then used to reproduce the teacher actions and generalize to new similar actions based on statistical techniques which are used to compute this mapping function;
- System Model: the world is modelled as a state transition model, where actions are chosen and lead to a change on the current state to a new state. The policy is derived in order to maximize a reward based on the actions taken;
- Plans: here the desired robot behaviour is represented as a plan that represents the policy as a sequence of actions that lead from an initial state to a final goal.

The first two options can further be divided based on which statistical techniques are used to create the mapping function or how the reward function is defined. In the first case, classification techniques generally group similar inputs into classes that will lead to similar actions as output. Several classification techniques exist like Gaussian mixture models (GMMs), Bayesian networks, and hidden Markov models (HMM). On the other hand, regression techniques, *e.g.*, locally weighted regression (LWR) and receptive field weighted regression (RFWR) map input states to output actions that can be derived by combining input actions. As for the reward function, this one can either be defined by the user or learned by the system itself by exploration (typically Reinforcement Learning and inverse Reinforcement Learning methods are used).

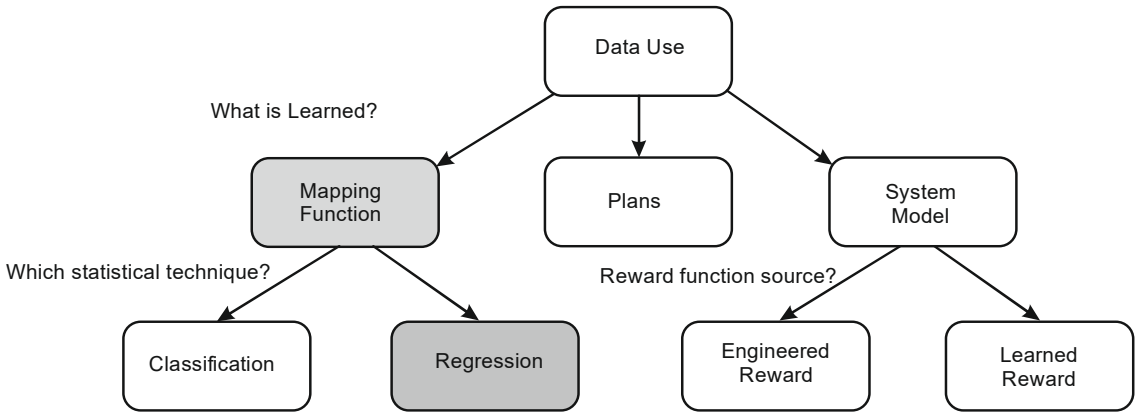

Fig. 3.3: Classification of the approaches to learn a policy from a demonstration dataset. Shadowed regions represent the approach used in this work (adapted from Argall et al., 2009).

The shadowed blocks in Fig. 3.2 and Fig. 3.3 highlight the approach followed in this work in order to capture demonstration data and to define the policy. However, since the work described in this text is not limited to imitation of the movement performed by the teacher, but more a generalization from a single demonstration to new situations, classifying this work as an imitation would be very limiting.

3.2.2 LfD in Robotics

LfD presents however several challenges (Breazeal & Scassellati, 2002) and problems. However, robot learning from human demonstrations is a promising direction of research, followed both in simulation and on real robots (Kormushev et al., 2011; Kulic et al., 2012; Chalodhorn et al., 2010; Nakanishi et al., 2004b; Lee et al., 2010) with a wide variety of approaches for encoding human demonstrations and modelling locomotion tasks. One of the problems that LfD faces is the motion retargeting (this problem only occurs in cases that are classified as Imitation in Fig. 3.1). Some use methods like getting the Cartesian coordinates of the demonstrator and then applying IK to the robot model to obtain the joint angles (Kulic et al., 2012). Others use a kinematic mapping transformation based on the relationships between the robot and human bodies (Chalodhorn & Rao, 2010; Chalodhorn et al., 2005); this transformation is then passed by a PCA analysis, creating a low dimensional space of eigenposes.

Dynamic Bayesian networks (Cole et al., 2007) are used to imitate human 3D poses learned using a human performer with a code coloured body suit and a probabilistic dynamic balance model to find stable motions without the previous requirement of the robot's dynamics properties, and here various IK techniques are used to perform the motion retarget. Schemes based on colours had been used before (Riley et al., 2003), although it had been combined with a full body inverse kinematics (IK) methodology incorporating a kinematic model of the teacher.

One of problems in LfD when using humanoids is the ability to perform the imitation while keeping the balance, a problem that can be solved by using a balance controller based on the inverted pendulum model, combined with a tracking controller that computes the joint torques and minimizes the difference from desired inputs, as well as the error from desired joint accelerations to track the motion capture data,

considering exact full-body dynamics (Yamane & Hodgins, 2009). The most recent approaches to policy representation well suited for robot learning from demonstration are based on probabilistic models (*e.g.*, Hidden Markov Models) (Calinon et al., 2007; Asfour et al., 2008; Calinon et al., 2010) and dynamic movement primitives (DMPs) (Gams et al., 2009; Ijspeert et al., 2013, 2002a; Kober & Peters, 2011a). Motion capture from human dancers using markers was transferred to the upper body of a HRP1 with IK and motion primitives (Nakaoka et al., 2005); the upper and lower body motions were modified in order to satisfy the ZMP criteria.

Most imitation works are typically done with off-line processing, but an online framework imitation method inspired on computer animation studies and a developed humanoid-normalized model to solve the motion retargeting problem, achieving a good success in transferring a large range of motion from human demonstrator to humanoid has been used (Montecillo et al., 2010); this model uses a combination of Cartesian positions, joint angles and virtual planes that define the human posture. In order to keep stability, a CoM anticipation model is used to keep the stability in single support phases. In other example of online motion transfer (Dariush et al., 2009, 2008a), the proposed retargeting framework relies on human motion descriptors obtained from a marker-less vision algorithm combined with an online self-collision avoidance and optimization algorithm and kinematic constraints; the methodology is applied to a ASIMO robot, but only for upper body imitation without any balancing method proposed. In another study (Dariush et al., 2008b), the authors used a learning approach to generate knowledge about a number of human postures, then during the motion retargeting head and torso motion was monitored so that the template closest to the ones learned was assigned.

Most systems for LfD are either based on marker less vision systems or marker-based, but not both, as in (Do et al., 2008), where a system for motion imitation based on a master motor map (a model that provides a reference kinematic model by defining the maximum number of DoF) that is capable of incorporate various human motion capture techniques. The output of the model is then transformed to the structure of a ARMAR-IIIb robot using a nonlinear optimization technique with the goal focused on the end effector position on the task space. For the imitation task, a Cartesian control

approach in which a set control points are connected with virtual springs to markers approach is defined in (Ott et al., 2008), and then Hidden Markov Models are used for motion recognition and generation. In many imitation frameworks, kinematics scaling is used in order to accomplish the imitation tasks, but generally this requires the use of an extra balance control and exact end-effector position is not always guaranteed, so sometimes IK methodology is used after a scaling process has been performed (Sophie Sakka et al., 2014). The imitation problem can also be formulated as an optimization problem (Suleiman et al., 2008; Ruchanurucks et al., 2006) with constraints defined by the joint limitations of the robot. On the first, the joint motion was scaled into the humanoid robot's joints and then the objective function tries to minimize the difference between the angular values of the humanoid robot and those of the virtual actor; on the second, in order to increase the convergence speed, they parametrized the motion with B-splines.

Surprisingly, very few texts can be found on the literature about the subject relating LfD and biped locomotion and even although some use biped robots, they are not entirely related to biped locomotion subject itself. Using low dimensional spaces helps to reduce the complexity of the LfD on a framework that allows a humanoid to learn bipedal locomotion (Chalodhorn & Rao, 2010), combined with eigenposes and working as an offline motion planner. Dimension reduction represents an important role in the LfD, since it allows circumvent intractability due to very high-dimensional state and control spaces.

Combined together with the use of dynamic Bayesian models (Grimes & Rao, 2009) allows for building a framework (Fig. 3.4) that provides the possibility of a humanoid robot to learn new behaviours from a human teacher through imitation and exploratory learning. A kinematic mapping that includes the scaling of the human foot and the ZMP trajectories and a dynamic mapping that modifies the humanoid pelvis motion in order to assure movement stability provide the generation of a dynamically whole body motions is used on a humanoid robot (Kim et al., 2009) with data converted from human motion capture.

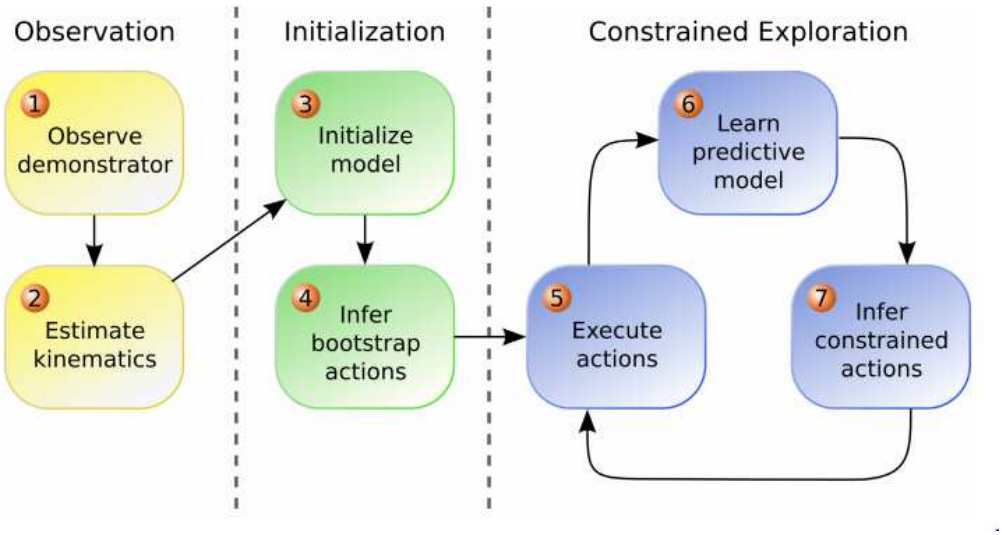

Fig. 3.4: The BABIL imitation learning framework proposed by Grimes (image from article Grimes & Rao, 2009).

Other studies (Shon et al., 2005) have used machine learning for human motion imitation after a low dimensional latent space that mapped from robot to human motion and vice-versa had been generated, and an intensive training was required using pairs from both motion modes so a stable motion could be achieved.

3.3 Learning by Trial-and-Feedback

In humans, learning plays an important role in balance stabilization, gait generation and modulation of new behaviours and actions. Some actions are learned anew throughout life likely based on a process of trial-and-feedback in which the subject interacts with its environment. Specifically, the human being has a direct sensorimotor connection to its environment that, when exercised, produces a wealth of information about cause and effect, about the consequences of actions and about what to do in order to achieve goals. For example, when learning to drive a car, humans are acutely aware of how the environment responds to what he/she is doing in order to influence what happens through his/her own behaviour. In the same line of thought, the goal of building robots that can adapt to their environment and learn from their experience has attracted many researchers.

Reinforcement learning is a powerful method to develop goal-directed action strategies (Sutton & Barto, 1998) where the system learns behavioural reactions controlled by reward in a trial and error process. The development of the field of cognitive neuroscience led to an increased interest in the brain mechanisms involved in the processing of rewards and punishments. As result, the computational study and application of reinforcement learning has expanded to diverse disciplines such as control theory, artificial intelligence and neuroscience. Particularly important have been some contributions that helped to establish and develop its relationship to the theory of optimal control and dynamic programming.

At the most fundamental level, reinforcement learning is different from supervised learning. Learning from examples provided by an external supervisor is an important kind of learning, but alone it is not adequate for learning from interaction. In many problems, it is impractical to obtain examples of desired behaviours that are both correct and representative of all the situations in which the system will act. The importance of learning will increase as robots move away from level ground into more unstructured and unknown environments, being able to learn from its own experience by taking uncertainty into account.

3.3.1 Formulation of a RL Problem

More than a powerful method, reinforcement learning is best defined by characterizing a learning problem that can be formulated as follows: an agent (*e.g.*, robot learner) interacts with the environment to achieve a goal formalized in terms of a special reward signal passing from the environment to the agent. Such an agent is able to sense the state of the environment and to take actions that affect its state within a formulation that includes the following three aspects: sensation, action and goal (see Fig. 3.5).

The key idea behind RL is learning what to do (*i.e.*, how to map situations to actions) in order to maximize a numerical reward signal. Instead of telling which actions to take, as in most forms of machine learning, the learner has to discover which actions yield the most reward by trying them. The agent prefers actions that it has tried in the past and found to be effective in producing rewards, but it has also to explore new actions in order to make better action selection in the future. Over many trials,

the robot learns the value of all states (in terms of reward proximity) and how to get to higher-valued states to reach the goal. In resume, one can say that trial-and-error search and delayed reward are two important and distinctive characteristics of reinforcement learning.

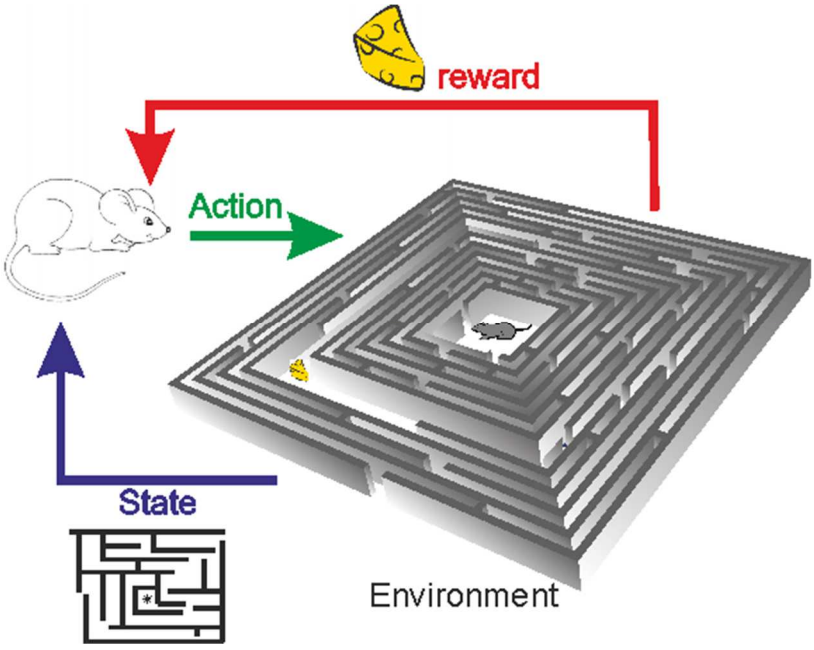

Fig. 3.5: An illustration representing the RL problem and its components: agent (the mouse) performs actions (chooses a path) on the environment (the maze) which in turn lead to a change on the state (actual position in the maze) and receives a reward (positive if it find the cheese, negative if it not finds the cheese).

Besides the agent and the environment, other sub-elements of reinforcement learning can be identified (Sutton & Barto, 1998):

- The *policy*, the core of an RL agent, defines the learning agent's way of behaving at a given time. Roughly speaking, a *policy* is a mapping from perceived states of the environment to actions to be taken when in those states. In some cases, the policy may be a simple function or lookup table (in general stochastic), whereas in others it may involve extensive computation, such as a search process.
- The *reward* function defines the goal and it represents the way of communicating to the agent what it wants it to achieve. In other words, it maps each perceived state (state-action pair) of the environment to a single number – the reward – indicating the intrinsic desirability of that state. The objective is to

maximize the total *reward* the agent receives in the long run. In practice, the use of a reward signal to formalize the idea of a goal proved to be flexible and widely applicable.

- The *value function* specifies what is good in the long run. The *value* of a state is the total amount of *reward* an agent can expect to accumulate over the future, starting from that state. Most importantly, whereas *rewards* determine the immediate, intrinsic desirability of environmental states, *values* indicate the long-term desirability of states after taking into account the states that are likely to follow and the *rewards* available in those states. It is worth noting that value functions are not strictly necessary to solve reinforcement learning problems. For example, search methods such as genetic algorithms, genetic programming, simulated annealing and other optimization methods have also been used.
- The *model* of the environment is the final element of a typical reinforcement learning system. Some reinforcement learning systems learn by trial-and-error and, simultaneously, learn a model of the environment that it is used for planning (*i.e.*, considering possible future situations before they are actually experienced).

The general framework described above is flexible and can be applied to many different problems in many different ways. In order to obtain the best policy for a specific task, several methods of reinforcement learning exist, namely, dynamic programming, Q-learning, SARSA and expected SARSA, and policy gradient methods (a more detailed information can be found in (Sutton & Barto, 1998; Kaelbling et al., 1996; Andrew Bagnell, 2014). The application of RL to robotics problems is challenging because sensors, such as cameras, deliver high-dimensional input that does not define a state in a way suitable for most tasks. Furthermore, several actions are to be learnt in different contexts with different reward types being given.

3.3.2 RL in Biped Walking Robots

Salatian *et al.* (Salatian et al., 1997) used reinforcement learning together with a neural network mechanism to modify the gait of a biped robot walking on a sloping surface,

without *a prior* knowledge of its inclination. The knee less biped robot, called SD-2, has a total of nine links and eight joints (4 DoF per leg). Each step is divided into eight static configurations, called primitive points (PP), and each PP is decomposed into a large number of set points with duration of 28ms. Additionally, the robot has two force sensors in each foot, one in the toes and the other in the heel, that allow computing the Centre of Gravity (CoG). The system is controlled by a neural controller composed by a memory that stores previous learned gaits, an adaptive unit (AU) responsible for modifying the joint trajectories and a sensor unit. The AU consists of a set of four neurons for each joint, giving a total of 24 neurons (both top hip joints are controlled by the same signal). The difference between the forces exerted at the toe and the heel generate the reinforcement signal that trains the neural network. The robot is stable, as long as this difference equals the ideal force balance obtained by recording it when the robot walks on a level surface and the gait is optimal. Authors conducted several training and experimental trials with several unknown slopes, demonstrating that it is possible for a biped robot to walk adaptively on unknown terrains using the neural network approach with unsupervised reinforcement learning.

Sato *et al.* (Sato et al., 2002) proposed a reinforcement learning method for a central pattern generator controller that generates rhythmic movements. Given that standard RL methods, such as temporal difference learning, Q-learning and actor critic methods are not suitable for training the CPG, authors proposed a new method called CPG-actor-critic. This method was applied to a planar model that started to walk after about 5800 trials. Although working properly, the learning process was rather unstable and it was necessary to fine tune the weights of the mutual connections among the CPG neurons that compose the controller with only the sensory feedback connections adjusted by RL.

Morimoto e*t al.* (Morimoto et al., 2004, 2005) used RL together with a Poincaré map in a simulation study with a planar five link robot. By using Poincaré maps, the robot was able to properly place the swing leg, while keeping the stability. In several articles published later, Matsubara and Morimoto (Matsubara et al., 2005b, 2005a, 2006) applied the policy gradient method combined with CPGs to a real robot with a U-shape foot (no ankle joint). The CPG controller only affects the hip joints, while the

knee joints are controlled by a state machine (Fig. 3.6). This strategy allowed for the simplification of the RL process, since the number of states and action spaces is lower.

Lee and Oh (Lee & Oh, 2007) defined initially a stable biped walk pattern based on a third order polynomial generator for the ankle and the hip joints. They were able to simulate a stable walking pattern in the sagittal plane by using both ZMP to decide on stability and reinforcement learning to get the proper boundary condition and the velocity of the walking pattern. In a different context, Tomoyuki *et al.* (Tomoyuki et al., 2009) proposed the use of reinforcement learning to increase the energy efficiency of biped walking generated by a CPG controller. With this in mind, authors introduced torque-free periods in the hip joint of the swinging leg. During these periods the controller does not generate any input to the hip joint. Since the initial and final instants dependent in some way of the walking environment, authors used reinforcement learning to acquire the suited values in an online fashion.

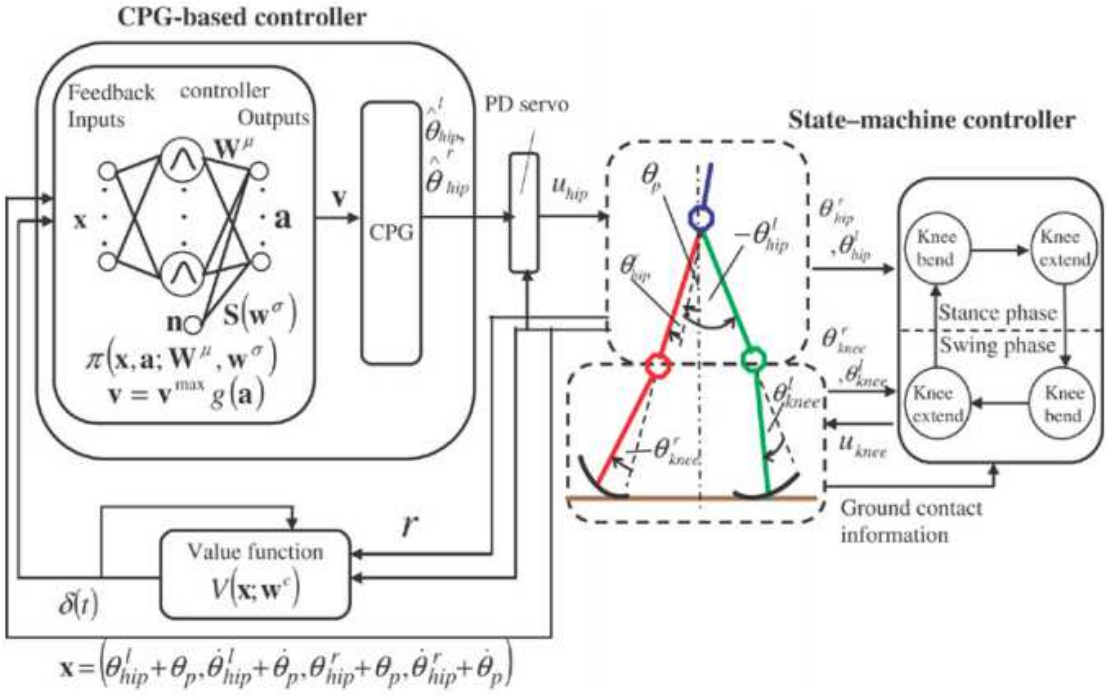

Fig. 3.6: Proposed control architecture for a 5-link biped robot that combines CPG and a policy gradient RL function (image from Matsubara et al., 2005b, 2005a, 2006).

Reinforcement learning has also been used by Li *et al.* (Li et al., 2011) to control the gait patterns and enhance the walking speed of a biped robot. Firstly, they use Policy

Gradient Reinforcement Learning (PGRL) to control the gait of the robot using as reward function the velocity achieved by the robot. After 10 iterations, the velocity increased from an initial velocity of 30.6 mm/s to 113.9mm/s, but the percentage of robot's falls reached a very high value (60%). In order to reduce this, the reward function was modified to take in account the stability of the robot, using a Zero Moment Point (ZMP) desired trajectory. With this new reward function, a speed of 130mm/s was achieved after 16 iterations with a decrease on the falling down percentage to around 42.5%. Secondly, the combination of linear polynomial interpolation in the motion generator with a fuzzy logic controller allowed the robot to adjust the walking speed and direction when following a straight line.

3.4 Final Remarks

This chapter reviewed two widely used approaches in robot learning. On the one hand, methods in which a robot obtains some or all of its training data from human demonstrations have gained widespread interest in recent years. Learning from Demonstration (LfD), also referred to as Imitation Learning and Programming by Demonstration, has become a central topic in robotics attracting researchers from different areas such as robot control, machine learning and human-robot interaction (see Argall et al., 2009; Billard et al., 2008) for surveys about imitation learning for robotics). On the other hand, the use of reinforcement learning is providing a conceptual framework for departing from the manual "hard coding" of behaviours.

Reinforcement learning algorithms allow a robot to carry out behaviours that maximize whatever it has been programmed as reward in a similar way as the dopaminergic system does in animals. Inspired by the brain's dopamine-based reward system (Khamassi, 2005), the mechanisms involved may be associated with models based on the basal ganglia to endow a robot with a motivational system and action-selection capabilities. However, applying reinforcement learning to high dimensional movement systems like humanoid robots remains an open problem. Peters *et al.* (Peters et al., 2003) pointed out the concepts and problems of traditional and novel reinforcement learning approaches in terms of their applicability to humanoid motor

control. Several new RL algorithms have been proposed in order to reduce the computation time, such as Policy Gradient methods (Peters & Schaal, 2006; Koval, 2011; Peters & Schaal, 2008) or Cr-KR methodology (Kober & Peters, 2013).

In any case, learning from a teacher or by practice, a suitable choice of the representation (or encoding) of movement trajectories is a central problem. On the one hand, when talking about human trajectories demonstrations whose variables evolve over time, a system for encoding them should possess some important properties, such as compactness of representation and ease of use (i.e., modulation for related new tasks). On the other hand, before any reward-based algorithm can be applied for solving real-world problems in robotics, an appropriate policy representation needs to be devised.

Chapter 4
Encoding Demonstration Trajectories with Dynamic Movement Primitives

This work follows a promising perspective in neurosciences: the modular approach to movement generation in which movements result from the combination of a set of motion primitives. This chapter gives an overview about the concept of motion primitives from a neurobiological perspective and its application in robotic systems as well. An evolution of this concept, known as Dynamic Movement Primitives (DMP) is then discussed, as well as the main advantages and properties of this formulation. Two case studies are performed, the first one based on simulated data and the second one based on human motion capture data. This study allowed gaining insight about the implementation of DMP and how to take advantage of its properties.

4.1 Modular Approaches to Movement Generation

4.1.1 Neurophysiological Evidences in Animals

The notion of a gradually increasing and changing set of primitives as a means to use a very high DoF actuation space is attractive. This concept is supported by evidences of the existence of muscle synergies and force-field primitives in the spinal cord that act like motion primitives. For example, experiments in frogs showed that the combination of muscle synergies were able to account for most movement patterns produced by the animal and that these can be activated from the spinal cord (Tresch et

al., 1999). More precisely, by stimulating certain areas of the spinal cord, they observed that the limb was moved in the direction of the same target posture (equilibrium point), independently of the initial position of the limb. They called the set of vectors corresponding to the directions obtained by the stimulation Force Fields. Similar results were shown by a combination of force fields (Giszter et al., 1993).

Recent neurobiological ideas and experiments have refined current understanding of the spinal cord system in generating many neural activity patterns that would generate certain motion behaviours. Besides the CPGs, additional modular motor circuits called primitives are present in different behaviours of rats and frogs (Bizzi et al., 1991; Giszter et al., 1993). Experiments on decerebrated and spinalized animals indicate that, like CPGs, many of these motor primitives are implemented at a low level in the vertebrate central nervous system, namely in the brainstem and the spinal cord (Whelan, 1996; Stein & Smith, 1997; Bizzi et al., 2000; Tresch et al., 2002; Grillner, 2006). These studies show different observations of the same phenomenon: the existence of motion primitives in the spinal cord that are combined to produce movement.

A common hypothesis of human behaviour is that the CNS uses internal representations of the sensorimotor system and the environment to select the next action to perform. An inverse dynamic model is then required to find the activation commands to be the muscles in order to fulfil the desired task. According to some authors, motor primitives provide the CNS with built-in links between muscles and movement direction that could help finding the muscle commands generating the desired trajectory (Georgopoulos, 1996; Mussa-Ivaldi & Bizzi, 2000). From this biological perspective, animal motor control is based on motion primitives and complex movements are generated by combining a finite set of these simpler elementary movements (Thoroughman & Shadmehr, 2000; Tresch et al., 2002; Schaal, 2002; Todorov, 2004; Flash & Hochner, 2005). Indeed, the existence of motion primitives seems to be, so far, the best possibility to explain how autonomous systems cope with the complexity of motor control and learning.

4.1.2 Discrete and Rhythmic Movements

In motor control, rhythmic and discrete movements are frequently considered separately. By looking at the human motion, one can roughly say that the act of walking is an example of rhythmic movement, while the act of picking, for example, a bottle of water is a discrete movement. However, this is a simplified view since the movements performed by humans are finite and, at any instant, a simple obstacle may lead to a trajectory change. Hogan and Sternad (Hogan & Sternad, 2007) classify both movements as follows: a discrete movement is defined as a movement which occurs between two postures, where posture stands for a non-zero interval of time where no movement has occurred. Instead, rhythmic movements are categorized in several subsets, going from strictly periodic movements to movements with recurrent patterns. However, authors point out that these two definitions are not exclusive, such as: (1) rhythmic movements occur in between postures and, in this sense, enter in the definition of discrete; and (2) discrete movements can be repeated in order to become periodic.

Neurophysiological evidences also provide a simplified view of movement generation in which the potential differences between discrete and rhythmic movements are not related to sensory feedback or muscle interaction, but can be explained by the spinal processes underlying them and the higher-level commands needed to activate these same processes. In experiments using chemical stimulations of neurons in the spinal cord of the frog, Saltiel *et al.* (Saltiel et al., 1998) found out that the areas of activation of the discrete and the rhythmic movements for a given orientation are topographically close. According to these findings, the difference between discrete and rhythmic movements at the spinal level can be due to differences in the topology of the network and not distinct pathways.

In this context, Degallier and Ijspeert (Degallier & Ijspeert, 2010) defined four possible structures for the generation of discrete and rhythmic movements that provide basic grounds for reflection on the possible differences between them. They distinguish between two phases for a movement generation: the planning phase and the execution phase. Planning is the process required to choose the features of the movement, while

execution is the process responsible for the spatial-temporal activation of the muscles that generate the correspondent limbs' trajectories. The four structures mentioned above are as follows:

- Two/Two: discrete and rhythmic movements are generated through two totally different processes, both at the planning and the execution phases;
- One/Two: the planning process is common to both movements, while their generation depends on different structures;
- One/One: both the planning process and the generation process is common in both types of movements;
- Two/One: the planning process is different for each movement, but the generator is common.

For each of these structures, Degallier and Ijspeert (Degallier & Ijspeert, 2010) proposed several interesting mathematical models to generate discrete and rhythmic movements. The models are based on a powerful tool for studying qualitative time courses for a system as well as the interconnections between its parts.

4.1.3 Motion Primitives in Robotics

From a robotics point of view, the idea of using motor primitives for constructing controllers for complex motor skills is appealing and is attracting a growing number of researchers (Mussa-Ivaldi, 1997; Ijspeert et al., 2003; Todorov et al., 2005; Schaal & Schweighofer, 2005). The difficulty lies in identifying motion primitives that can constitute a full set of representative movements for all required tasks. Simple systems have been demonstrated for robot arms in the past (Matarić, 1998) and force-field primitives have been used for reactive robot obstacle avoidance (Khatib, 1986). However, a full set of motion primitives that can perform a range of tasks similar to humans has yet to be demonstrated.

Konczak (Konczak, 2005) discusses the notions of reflexes and motion primitives and their evolution in time. Motion primitives are already present at the birth time (and even previously). From initial reflexes to controlled motions, the functionality of motion primitives is being integrated with later maturing of supra-spinal motor centres

to give rise to more complex motor behaviours and to rich interactions with the environment. Minh Tuan *et al.* (Tuan et al., 2010) deal with the problem of generating realistic human like reach movements from a small set of movements primitives. To accomplish this task, authors use two database sets, one obtained numerically and other from recording human movements, from which the primitives are extracted by applying Principal Component Analysis (PCA).

The first attempt to use these primitives to generate realistic reaching movements proved to be too slow. Subsequently, another method was used with much better results by constraining the trajectory in the operational space and by satisfying a minimum jerk criterion. Another example of the use of motor primitives comes from Kober and Peters (Kober & Peters, 2011b). Here, the authors use motor primitives together with a reinforcement learning algorithm to train a robot arm to perform a "ball-in-a-cup" game. The proposed methodology starts with the application of LfD followed by a reinforcement learning method to improve the task execution.

A few articles report the definition and composition of complex movements, using basic primitives, for the motion of bipedal humanoid robots (Denk & Schmidt, 2003; Schaal et al., 2005; Borovac et al., 2011). Denk and Schmidt (Denk & Schmidt, 2003) present a systematic approach to generate a database of walking primitives allowing step length adaptation, changes in the direction and stepping over obstacles. They use ZMP and friction conditions for ensuring postural stability of a biped robot and they validate the trajectories in simulation. Schaal and their colleagues (Schaal et al., 2005) discuss a framework for modular motor control based on the theory of dynamic movement primitives (DMP). DMP are a formulation of movement primitives with autonomous nonlinear differential equations, whose time evolution creates smooth kinematic control policies. A novel reinforcement learning technique based on natural stochastic policy gradients allows a general approach of improving DMPs by trial and error learning with respect to almost arbitrary optimization criteria. The different elements of the DMP are demonstrated in simulation, involving learning biped walking from demonstration and self-improvement of the movement patterns towards energy efficiency.

4.2 Dynamic Movement Primitives

Dynamic Movement Primitives (DMPs) appeared as a powerful tool for motion representation based on demonstrations from a human teacher. This encoding approach possesses desirable properties that make them well-suited for trajectory generation, such as the possibility to change parameters online and the intrinsic robustness against small perturbations. The basic idea behind Dynamic Movement Primitives (DMP) is to use an analytically well-understood dynamical system with convenient stability properties and modulate it with nonlinear terms such that it achieves a desired point or limit cycle attractor. The approach was originally proposed by Ijspeert et al. (Ijspeert et al., 2002a) and, since then, other mathematical variants have been proposed (Ijspeert et al., 2013).

4.2.1 Mathematical Formulation

Discrete primitives can be defined as the counterpart of human reaching movements. The method allows reaching a target by modulating a set of damped spring models which can be written in the first-order notation as follows (generally designated as transformation system):

$$\begin{aligned} \tau \dot{z} &= \alpha_z \left[\beta_z \left(g - y \right) - z \right] + f \\ \tau \dot{y} &= z \end{aligned} \tag{4.1}$$

where τ is a time constant, α_z and β_z are positive constants, y is the current position, f is the forcing term and g is the goal of the movement. The essence of the methodology is to transform well-understood simple attractor systems with the help of a learnable forcing function term into a desired attractor system. If the forcing term f is zero, the equations represent a second order linear system with $(y, z) = (g, 0)$ as a point attractor. The term f allows fitting the DMP to a specific trajectory and is defined as:

$$f(t) = \frac{\sum_{i=1}^{N} \psi_i(x)\omega_i}{\sum_{i=1}^{N} \psi_i(x)} x(g - y_0)$$
$$\psi_i = \exp\left(-\frac{1}{2\sigma_i^2}(x - c_i)^2\right) \tag{4.2}$$

Here, y_0 is the initial state $y(t=0)$, τ_i and c_i are constants that determine, respectively, the width and the centres of the basis functions, x is a state variable that converges monotonically to zero, indicating that the goal g has been reached and allowing the system to become time independent. Accordingly, the canonical system is given by:

$$\tau \dot{x} = -\alpha_x x, \tag{4.3}$$

In the same way, discrete movement primitives where related to discrete tasks, rhythmic movement primitives are related with periodic movements, like walking and running. The formulation of rhythmic primitives is similar to the discrete ones in equation (4.1), differing only on the canonical system and the forcing term that are defined by the following equations:

$$\tau \dot{\phi} = \Omega$$
$$f(\phi, r) = \frac{\sum_{i=1}^{N} \psi_i \omega_i}{\sum_{i=1}^{N} \psi_i} r \tag{4.4}$$
$$\psi_i = exp(-h_i(cos(\phi - c_i) - 1))$$

where r is the amplitude, Ω is the frequency of the oscillation and the g term on the transformation system acts as a baseline for the oscillation.

4.2.2 Learning from Recorded Trajectories

The DMP formulation provides an easy way to learn from demonstration examples (or learning from observed behaviour). The learning process is composed by two phases: determining the high level parameters (g, y_0, τ and r) and then learn the weights, ω_i, parameters of the forcing term. These high level parameters have different meanings depending on if they are from the discrete system or they are from the rhythmic system.

For discrete systems, the parameter g is the position at the end of the movement (hence, the name "goal" previously mentioned) and the parameter y_0 defines the start point of the movement. It should be noticed that on a sequence of discrete movements, the goal of the previous movement will become the start point of the next movement and so on. Finally, τ specifies the duration of the movement.

For rhythmic systems, the parameter g allows setting the baseline of the oscillation, being given by:

$$0.5 \times \left(min(y_{demo}) + max(y_{demo}) \right) \tag{4.5}$$

where $y_{(demo)}$ is a demonstration signal. As for y_0, it can be used to adjust the starting point of the oscillation, if it is different from 0. τ should be set equal to the period of the oscillation and r is the amplitude of the signal.

Learning the weight parameters ω_i can be performed using any of the many available learning algorithms such as, for example, RL. Other simple method is using locally weighted regression (LWR). In this case, the input to the learning algorithm is the demonstration trajectory defined by the triplets of position, velocity and acceleration: $y_{(demo)}$, $\dot{y}_{(demo)}$ and $\ddot{y}_{(demo)}$. Re-arranging equation (4.1) and equating y to $y_{(demo)}$, z to $\tau \dot{y}_{(demo)}$ and $\dot{z}$ to $\tau \ddot{y}_{(demo)}$, the following equation can be derived:

$$f_{target} = \tau^2 \ddot{y}_{demo} - \alpha_z [\beta_z (g - y_{demo}) - \tau \dot{y}_{demo}] \tag{4.6}$$

LWR finds, for each kernel function, ψ_i, the weight vector ω_i that minimizes the following quadratic error criterion:

$$J_i = \sum_{k=1}^{P} \psi_i(k) \left(f_{target}(k) - \omega_i \zeta(k) \right)^2, \tag{4.7}$$

where k represents an index associated to the discrete time steps and $\zeta(k) = x(k)(g - y_0)$ for the discrete DMP and $\zeta(k) = r$ for the rhythmic DMP. This is a weighted linear regression problem that can be solved using a batch or an incremental regression. The batch solution is given by:

$$\omega_i = \frac{z^T \Upsilon_i f_{target}}{z^T \Upsilon_i z}, \tag{4.8}$$

where:

$$z = \begin{pmatrix} \zeta(1) \\ \zeta(2) \\ \cdots \\ \zeta(P) \end{pmatrix} \quad \Upsilon_i = \begin{pmatrix} \psi_i(1) & & & 0 \\ & \psi_i(2) & & \\ & & \cdots & \\ 0 & & & \psi_i(P) \end{pmatrix} \quad f_{target} = \begin{pmatrix} f_{target}(1) \\ f_{target}(2) \\ \cdots \\ f_{target}(P) \end{pmatrix} \tag{4.9}$$

As for the incremental solution, it can be derived using recursive least squares with a forgetting factor λ. Given the target data $f_{(target)}$, the update of the weights ω_i is performed for each time-step k as follows:

$$\begin{aligned} \omega_i^{k+1} &= \omega_i^k + \psi_i P_i^{k+1} \zeta e^k \\ P_i^{k+1} &= \frac{1}{\lambda}\left(P_i^k - \frac{P_i^{k^2} \zeta^2}{\frac{\lambda}{\psi_i} + P_i^k \zeta^2} \right) \\ e^k &= f_{target}^k - \omega_i^k \zeta \end{aligned} \tag{4.10}$$

On the one hand, when the forgetting factor λ is one, batch and incremental learning regressions provide identical weights ω_i. On the other hand, when the forgetting factor is less than one, the differences appear since the incremental regression tends to forget older data and give more weight to recent ones. An example of batch regression learning is given in Fig. 4.1 for a periodic signal based on the sum of sinusoidal functions.

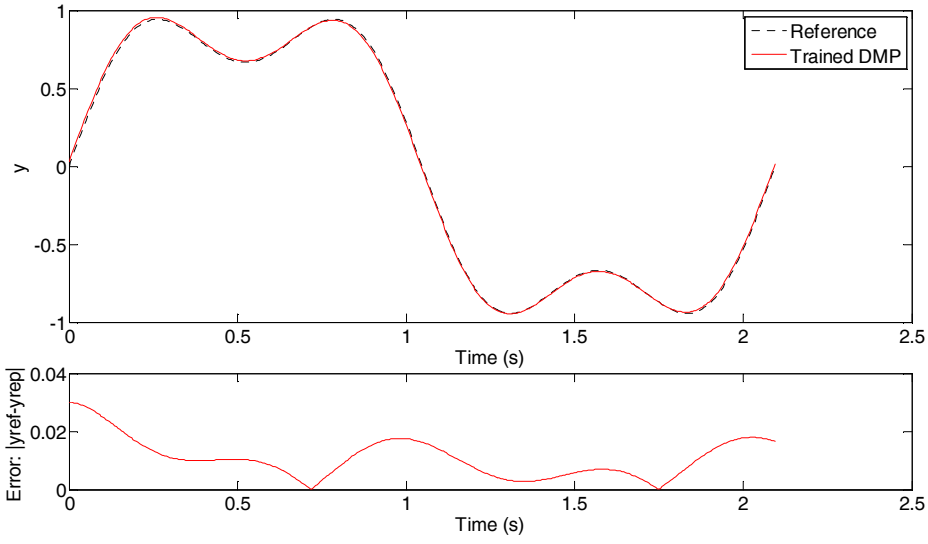

Fig. 4.1: An example of batch learning for a periodic signal; top: learned signal superimposed with the reference signal ($y_{demo} = sin(\omega t) + \frac{1}{3} sin(3\omega t)$); bottom: error signal.

4.2.3 Extension to Multiple Degrees of Freedom

The literature refers to three essential approaches for extending DMP to multiple DoF (Gams et al., 2009; Taga et al., 1991; Perk & Slotine, 2006). The most direct solution would be to define, for each DoF, its own complete set of dynamic equations (Fig. 4.2, left top). However, this would leave a situation where there is no coordination at all among the several DoF, which is not desirable. The second solution would be to have coupling terms between the several DoF (Fig. 4.2, bottom). These terms could be used on the canonical system whenever a phase difference between DoFs is desirable during rhythmic movements, such as locomotion systems. The drawback is that, generally, it is rather complex to fine tune the coupling terms for synchronization, stability analysis and dealing with the transient behaviour before the system phase-locks.

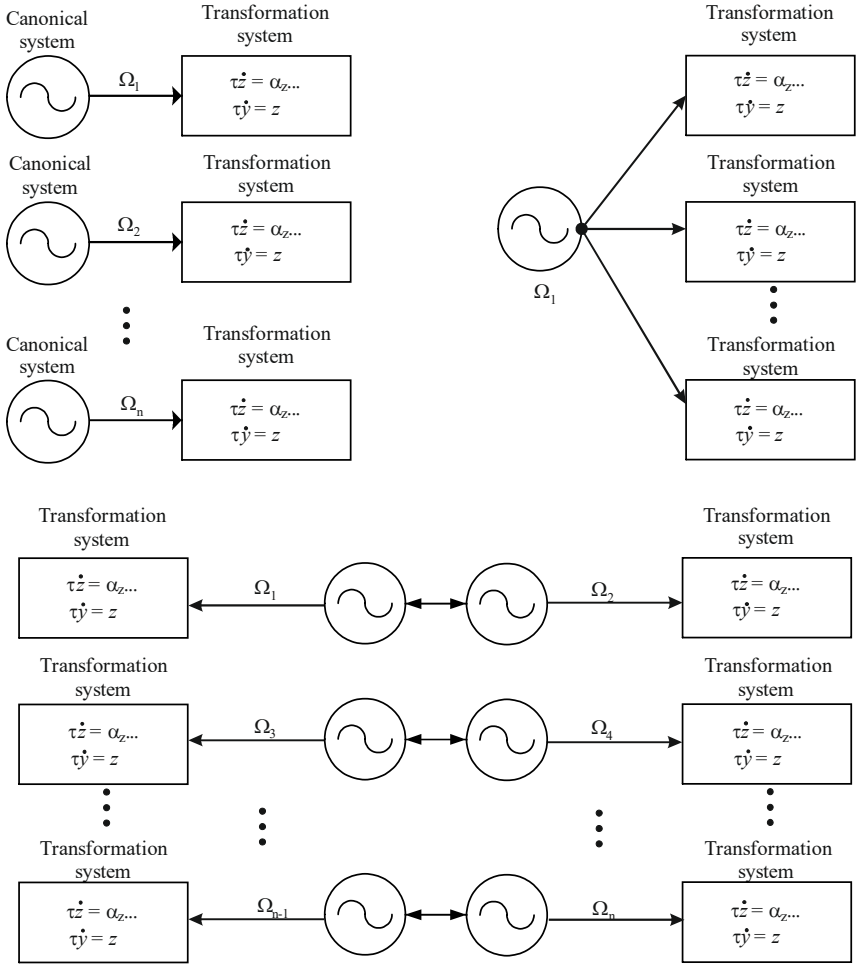

Fig. 4.2: Three most common approaches to multiple DoF extension of DMP: one complete system for each DoF (left top); only one oscillator (canonical system) for all DoF (right top); coupling between several DoF (bottom).

The third approach is to share the canonical system between all DoF, while providing a transformation system for each one (Fig. 4.2, right top). This, in turn, enforces that each DoF has its own set of forcing terms. By using this topology, the canonical system works as a clock to all DoF, providing a coupling between them. However a more adequate typology to a humanoid robot would be a combination of the second and the third approaches. In this case, each limb would have its own canonical system, allowing each DoF of that limb be synchronized. Furthermore, a coupling term between the canonical system of each limb would allow a phase difference to be set to a fixed value (e.g., out of phase would be the adequate phase difference between the two legs when walking on an environment without irregularities).

4.2.4 Properties of the DMP

Creating a good policy representation is not a trivial problem due to a number of challenges posed by high requirements from a robotic system. DMPs offer several useful properties, such as:

- Compactness of representation: the policy should use very compact encoding, despite the high DoF of the robot. DMP formulation only requires a transformation system for each DoF and generally something like twenty to fifty weights parameters are sufficient to encode the learning trajectory with low error.
- Smoothness: the policy representation needs to encode smooth continuous trajectories without sudden accelerations or jerks.
- Time independence: this is the property of the policy not to depend on precise time or position, in order to cope with unforeseen perturbations. Time independence is present by the use of the canonical system. This will allow influence of the temporal evolution of the system, without affecting the spatial pattern created by the transformation system.

- Invariance property: the policy should be an invariant representation of the task (e.g., rotation invariant, scaling invariant, position invariant) allowing generalization to similar movement tasks. This allows a learned signal to keep the time and spatial aspect, even if some high level parameters are changed such as the goal (g), the amplitude (r) or the timescale (τ). Fig. 4.3 shows an example of when these parameters suffer a modification using the example signal from Fig. 4.1. Here, it can be observed that a change of the timescale and the amplitude parameters around 2.2s results on a change of the frequency and amplitude of the signal to the double. At around 4.2 s a change on the goal parameter[1] is performed. Finally, at 6.3 s the timescale signal is modified again, resulting on another duplication of the frequency of the signal. As can be observed on any of these modifications, the signal keeps its aspect and similarity with the original one. Thus invariance properties are useful when generalizing the signal to new situations where it is required a change on original learned primitive. However, there are some situations where this property is a disadvantage (see Section 4.4.4).

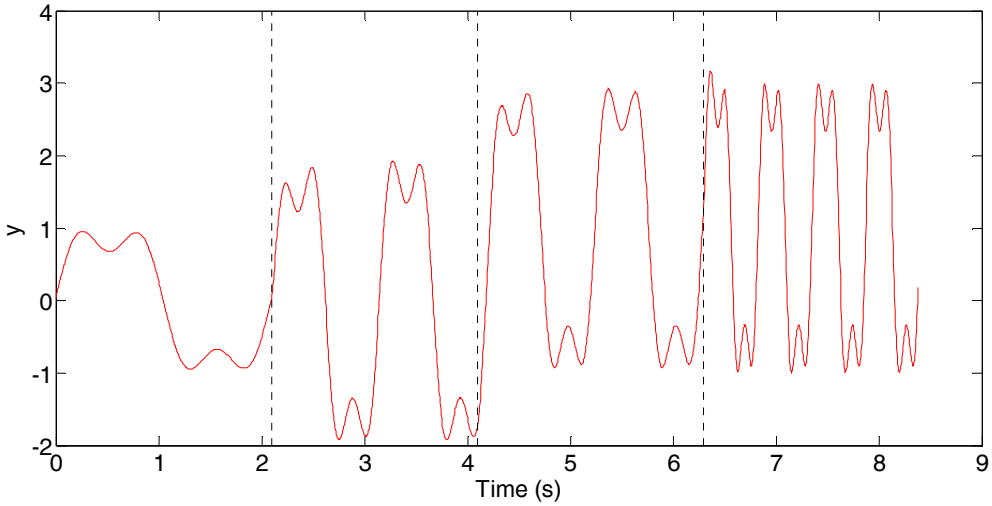

Fig. 4.3: Example of invariance properties of the DMP, when changing some of the high level order parameters.

[1] Remember that a change on the goal parameter (g) on a rhythmic signal will result on a change of the baseline of the oscillation.

- Robustness to disturbances: the output of the transformation system is inherently robust against perturbations (e.g., external perturbations). Even when a perturbation occurs, the system will resume smoothly to the learned trajectory, as it can be observed in Fig. 4.4. Here, at around 2.1s the system was subject to a perturbation that ended around 5s. It can be clearly observed that the system resumes smoothly the learned trajectory, as expected from a second order system. It should be noticed that the output given by the system is the desired trajectory and not the real trajectory. So some kind of feedback should be added so that the output trajectory of the generated trajectory can be modified, in order to reduce the error.

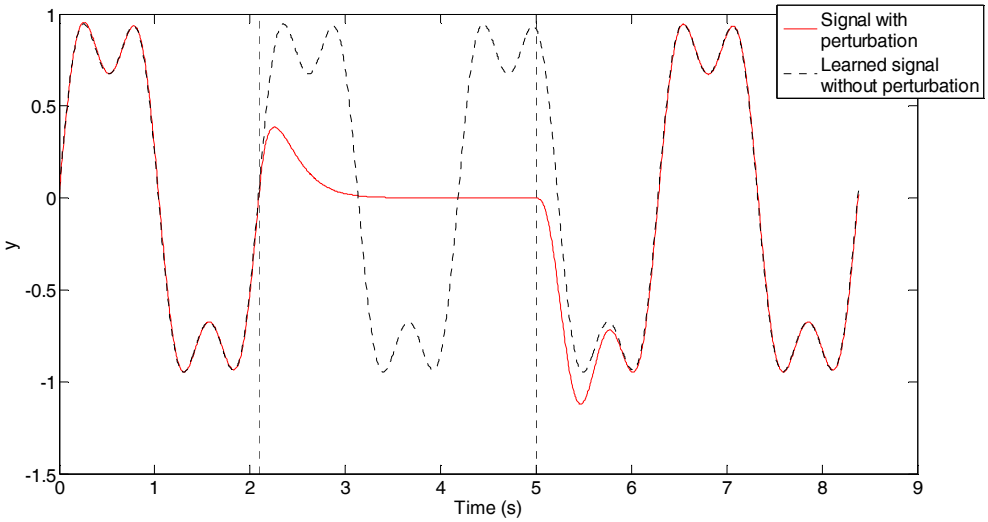

Fig. 4.4: Output of the transformation system when subjected to a perturbation.

4.2.5 Modulation of Learned Trajectories

It is desirable that the system is not only able to correctly reproduce the learned trajectory, but also to adapt the trajectory to new situations. Using the DMP formulation, this can be done essentially in three different ways: first, the modulation may occur by changing the high level parameters associated with the speed of the system such as the frequency of the oscillator or the timescale, while other parameters (amplitude and baseline) can be associated with the position at rest of a component of

the robot or the amplitude of a certain movement (like for example the step length on a biped robot).

It is possible that, in certain situations, modulation of the high order parameters is not enough for the robot to adapt and a change in the learned signal by modifying the weight vector (low-level parameters) is required. An appropriate learning methodology should be carefully chosen, since there is the risk that the learning process takes an undesired high time to converge. An alternative for trajectory modulation requires incorporating coupling terms to implement closed-loop perception-acting systems. The possibility of adding coupling terms, allows the implementation of systems with coupling between the phase oscillators of different degrees-of-freedom. Coupling terms can be present both on the transformation system, used for obstacle avoidance (Hoffmann et al., 2009), or on the canonical system forcing this system to phase lock with an external oscillator (Sternad et al., 1996; Matthews et al., 1991) or even frequency modulation at a specific phase relationship (Nakanishi et al., 2004a; Pongas et al., 2005).

4.3 Case Study 1: Invariance Property with Simulated Data

The invariance property of DMPs is useful for generalizing movements that are not confined to the region of the learned primitive. In fact, the parameters that determine the particular shape of the trajectory of a DMP are insensitive towards movement translation and spatial and temporal scaling. However, the adaptation of DMPs to new situations becomes difficult when they are defined in joint space, because their parameters (e.g., goal) are not related to variables meaningful for the task. Alternatively, learning in task space is the solution followed to assure that a change in DMP's parameters maintains desirable properties for a given task. In this work, it was implemented a DMP for every DoF that should learn its own forcing function, although all share the same canonical system. In particular, the variables involved to define each DMP are the positions of the elbow and end-effector in Cartesian space (six-dimensional DMP).

In order to evaluate the generalization performance from a single demonstration, two specific tasks (or two classes of DMPs) are considered: discrete straight point-to-point movements and periodic circular paths. As result, the inverse kinematics algorithm is simplified: two degrees-of-freedom completely describe the elbow when the position of the shoulder is known (the elbow lies on the surface of a sphere centered at the shoulder). Similarly, the wrist can only lie on the surface of a sphere centered at the elbow. Although other solutions could be used, these restrictions allow maintaining the consistency between the study performed with synthesized and motion capture data.

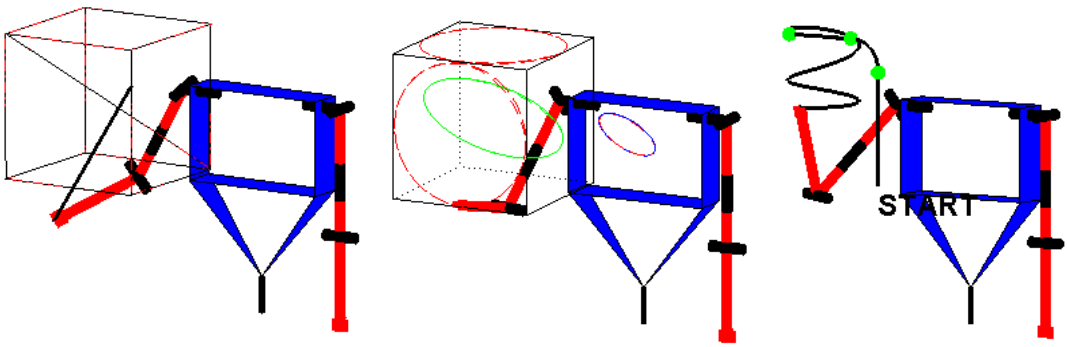

Fig. 4.5: Generalization from single demonstration; left) the DMP was modulated using "random" line (bold black) and then used to reproduce the edges and a diagonal on the cube; center) the DMP was modulated using a random circle (red and blue dashed) and then used to reproduce the other circles on two faces and inside the cube; right) the modulated DMPs on the other examples were used together to perform a complex movement.

In our first experiment with simulated data (Fig. 4.5, left), a discrete DMP is trained using the trajectory specified by the black bold line. Once the weights have been learned, a test is performed in this DMP to see how well it scales to reproduce the movements over the edges of a cube figure and a diagonal (black dashed lines), by simply adjusting the start and the goal point. The resulting trajectory is depicted by the red dashed lines. From the visual results it can be seen that the DMP can reproduce the intended trajectory.

Table 4-1 shows the error between the intended trajectory (created with the pseudo-inverse method) and the reproduced trajectory. It can be seen that the error for the Elbow trajectory is considerably higher. This can be explained by the invariance properties of the DMP and the lower Elbow error on the diagonal confirms this, since

the movement used to modulate the DMP was a diagonal. Next, the same kind of test was performed on rhythmic movements (Fig. 4.5, center). Here, a small circle (red and blue line) was used to modulate the primitive. This primitive was then used to perform a new set of circles on two faces and inside the cube (red and green circles). Here can by simply adjusting 2 parameters of the DMP (amplitude and baseline of the oscillation) a circle can be reproduced anywhere on the work space of the robot, even though it does not lie on the same plane as the movement used to modulate the DMP.

	Movement Direction			
	X-axis	**Y-axis**	**Z-axis**	**Diagonal**
Elbow error	28.1±27.9	33.9±25.8	72.0±64.8	16.2±11.7
Wrist error	0.20±0.15	0.18±0.15	0.17±0.14	0.34±0.25

Table 4-1: Trajectory errors for the cube once a "random" movement is learnt (MSE$\times 10^{-3}$ and standard deviation).

4.4 Case Study 2: Reproduction and Generalization with Captured Data

As said in previously, DMP possess the ability to learn from observed behaviour. In order to collect data to train the DMP, a set of movements using a Kinect sensor was captured. This section and the following ones will present a set of tasks performed in order to capture this data using the Kinect, process it, study it and use it on DMP training and generalization. The Kinect sensor provides a 640×480 depth image, at 30 frames per second, for the skeleton-based pose estimation with depth resolution of a few centimetres. The human skeleton estimated from the depth image includes a total of 20 body joints that will be the input for our approach. This captured data consists of a set of Cartesian points in the 3D volume for each human pose, which will be called raw-data hereinafter. Several studies have assessed the accuracy of the depth reconstruction and joint positions from the Kinect pose estimation, including comparisons with ground truth motion capture data (Khoshelham & Elberink, 2012; Smisek et al., 2011; Obdrzálek et al., 2012). In general, these studies highlight the potential of the Kinect skeleton in controlled body postures whenever self-occlusions are avoided.

In the experiments a single Kinect camera positioned at about 3 meters from the human subject to capture the whole body standing upright was used. In this study the attention is dedicated to the upper limbs, including the shoulder, elbow and wrist joints of both right and left arms. In order to ensure the most convenient acquisition conditions, the human subject was asked to prevent lower trunk movements and to perform controlled scapular motions. Precautions were also taken to avoid occlusions of the upper limb parts.

Besides the accuracy and robustness of the skeletal poses, a critical element is the stability of the estimated frame-to-frame body geometry. A characteristic of the human body skeletonization with the Kinect sensor is that the limb lengths are not kept constant through the entire sequence and differ between the two arms. The variations of the limb lengths, from frame-to-frame, for a static posture and a reaching arm movement were evaluated. In the static case, the mean value rounds 268 mm for the arm and 233 mm for the forearm, while the standard deviation is around 3.65 mm and 1.51 mm, respectively. These measures are significantly different during the execution of a reaching movement: a mean of 265 mm for the arm and 216 mm for the forearm with a standard deviation of 15.9 mm and 8.8 mm, respectively.

4.4.1 Constrained-Based Motion Filtering

The pose correction method aims to convert the motion of a source human subject into a new motion, while satisfying a given set of kinematic constraints. These kinematic constraints are formulated in order to assure a kinematic model with constant limb lengths. The proposed method, applied to each individual frame, can be divided into two main steps:

- Static calibration: the first step is a static calibration of the arms, prior to each data collection, to define the reference model of the subject anthropometry. Concretely, the human subject was told to hold his arms full extended aligned with the trunk (fundamental standing position), while several frames are acquired. A distance vector among consecutive joints (shoulder-elbow and elbow-wrist) is calculated as the mean value taken over all these frames for both arms. It should be pointed out that this arm calibration is the basis for the joint-

angle calculations: all joints angles are defined as zero degrees at this calibration posture.

- Pose correction: the basic problem is to find the closest configuration $X = (x_1, x_2, ..., x_n) \in \Re^{(3\times n)}$, with $(x_1, ..., x_n) \in \Re^3$, to the measurements that are observed over time $\hat{X}$, such that the distance between consecutive points (*i.e.*, link lengths) remains constant.

In line with this, the standard form of the optimization problem defines a minimization problem as follows:

$$\min_x \sum_{i=1}^{n} \left\| X - \hat{X} \right\| \tag{4.11}$$

where $\|\bullet\|$ is an appropriate matrix norm which measures goodness of fit. Here the Euclidean norm was admitted as a measure of closeness. The goal is to minimize the objective function (4.11) by selecting a value of X that satisfies all equality quadratic constraints defined by:

$$\|x_i - x_{i+1}\| = d_{i,i+1} \tag{4.12}$$

where the left part is the Euclidean distance between two consecutive points and the right part is the link lengths in the reference model.

Since the main goal is to generate large sets of human motion data for robotic imitation, all the computations at this point where performed offline using the Matlab environment. The constrained minimization problem was solved with the OPTI toolbox that can solve this problem of optimizing a quadratic function of several variables subject to quadratic constraints. In this context, the execution time is around 15 seconds per frame on an Intel Core2 Duo CPU T9400 @ 2,53GHz. The comparison of the human skeletons obtained with the Kinect raw-data and those after the pose correction are illustrated in Fig. 4.6. Different poses are represented for a movement sequence involving both the right and the left arm. Table 4-2 presents some statistical measurements applied for quantifying the error between the Kinect raw-data and the filtered data after the pose correction.

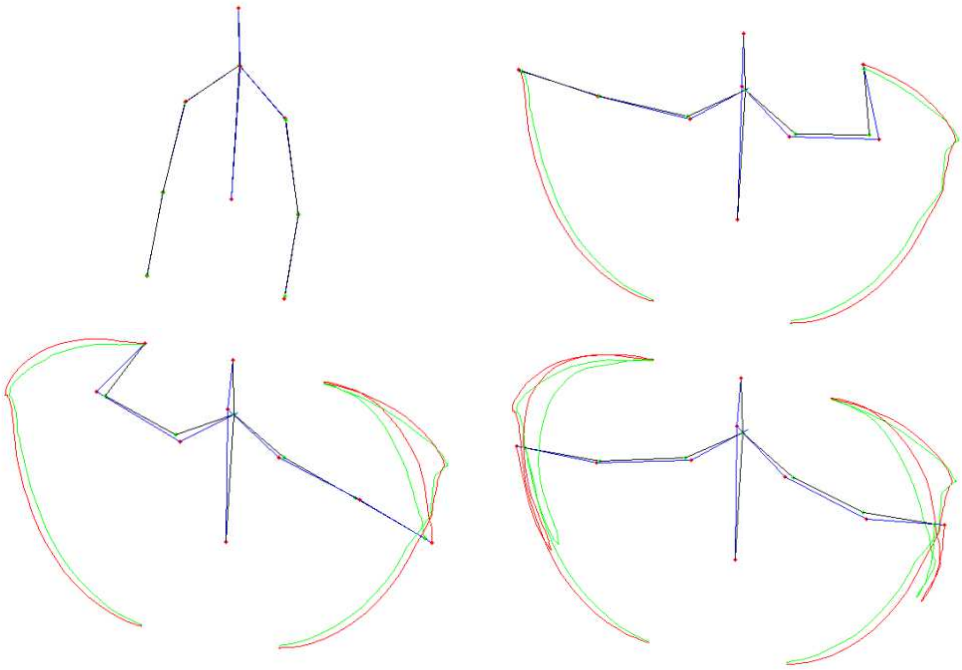

Fig. 4.6: Overlap of the human skeletons extracted from the Kinect raw-data (green points and black lines) and those after the constraint-based optimization (red points and blue lines) at different frames (green and red lines represent the end-effectors' paths).

Joint	Minimum error (mm)	Maximum error (mm)	Mean error (mm)	Standard deviation
Left Shoulder	0.5	25.7	15.1	7.0
Left Elbow	8.6	89.5	31.7	14.7
Left Wrist	5.2	75.2	30.9	16.0
Right Shoulder	0.8	56.0	21.8	13.5
Right Elbow	2.4	86.5	27.2	14.7
Right Wrist	4.2	82.6	25.0	18.6

Table 4-2: Error quantification between the Kinect raw-data and the filtered data.

4.4.2 Kinematic Mapping

One of the main issues in using motion capture data for training robots is to convert the 3D joint positions into joint angles relative to a robot model. In this context, the human skeleton is replaced by two 4 DoF robot arms of the same dimensions. Then, an inverse kinematics algorithm generates the corresponding joint angles of the robot

for each pose. The problem is decomposed into a per-frame inverse kinematics algorithm, followed by motion filtering and interpolation.

The filtered movement data is the input for the inverse kinematics module in which the human arms are modeled as two independent 4-dof serial chains consisting of a 3-DoF shoulder (rotations joints with intersecting axis) and a 1-DoF elbow joint (Fig. 4.7). The implementation of the inverse kinematics follows some basic assumptions. First, the robot model was defined to match the anthropometric measures of the human subject, avoiding the retargeting problem (*i.e.*, compensate for body differences).

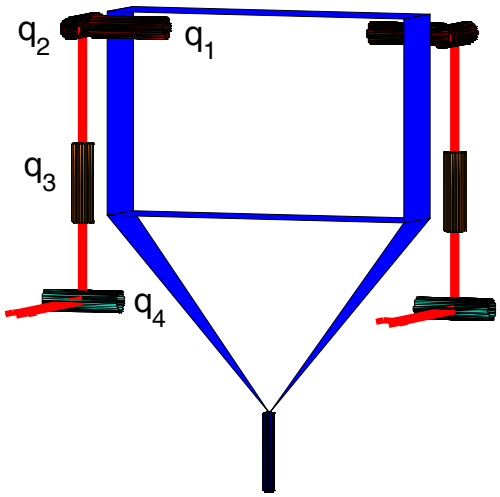

Fig. 4.7: Kinematics model of the two manipulator arms: both arms comprise 4-DoF. The joint variables q_1, q_2 and q_3 represent the spherical glenohumeral joint, while the joint variable q_4 represents the elbow joint.

Second, the perturbations in the movement data caused by the movement of the subject's shoulder are ignored. Concretely, it was considered that all joint positions are uniformly affected by the perturbations and the shoulders are at the origin of the reference system with fixed coordinate frames. Third, the inverse kinematics considers mechanical constraints on the joints, such as physical limits both on the range of joint motions (*e.g.*, the elbow cannot invert the motion when full-stretched) and on the maximum joint velocities.

Given the 3D positions of the shoulder, elbow and wrist, the inverse kinematics algorithm is simplified: two degrees-of-freedom completely describe the elbow when

the position of the shoulder is known (the elbow lies on the surface of a sphere centred at the shoulder). Similarly, the wrist can only lie on the surface of a sphere centred at the elbow. Thus, the configuration of the arm is completely represented by four variables (the joint angles). Attention was devoted to avoid discontinuous jumps near ±180º associated with the use of inverse tangent functions.

Additionally, the implemented algorithm includes a validation test since there may be motions where the robot's joints are not able to approximate the human pose in a reasonable way due to physical limitations. The proposed strategy to properly cope with the joint velocity limits is to slowing down the task-space trajectory whenever the limits are encountered. Thus, whenever the generated joint velocities violate the limits of the joint actuators, the trajectory is scaled in time by an appropriate constant that simultaneously assures tracking of the desired arm path and the fulfilment of the velocity constraints.

The frame rate of the Kinect sensor and high frequency components in the movement data imposed a post-processing stage to refine results. The exact procedure combines basic interpolation and smoothing techniques. On the one hand, the joint-angle trajectories are filtered using a moving average algorithm to smooth out short-term fluctuations based on predefined trail onset and termination times. On the other hand, the strategy adopted to provide a more detailed description of the action performed by the human subject is to use spline interpolation over the set of observations to satisfy the requirements of differentiability. To evaluate the different steps of post-processing, a measure based on jerk, the third time derivative of position, was used to quantify smoothness at the level of the joint-angles trajectories. Concretely, the particular jerk metric used to quantify movement smoothness is the integrated squared jerk (Platz et al., 1994) defined by:

$$\eta_{isj} = \int_{t1}^{t2} \dddot{x}(t)dt \tag{4.13}$$

A comparison of movement smoothness measures among the original signal (after pose correction), the moving average filtered signal, the cubic spline interpolation and the fifth-order spline interpolation was performed (Fig. 4.8). The exact procedure to be

followed depends on the ultimate goal. Anyway, the previous considerations may be of importance in determining what strategies are appropriate to the problem in hand.

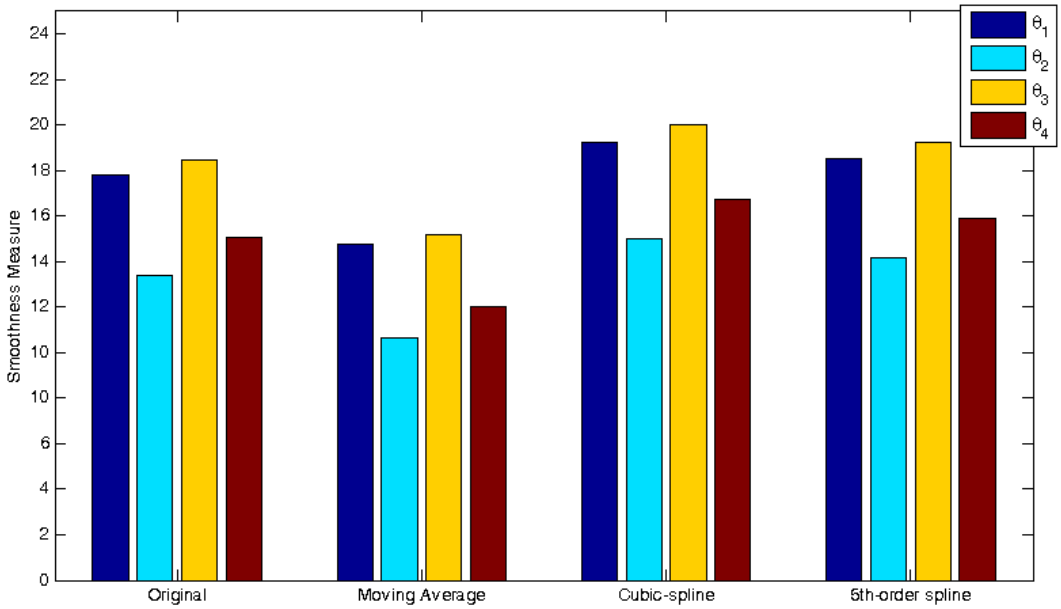

Fig. 4.8: Comparison of the smoothness measure for different motion post-processing methods applied on the joint-angle trajectories (for graphical presentation, a log was applied to results from (4.13) before plotting).

4.4.3 Example A: Imitation Task

Several real-time movements executed by a human subject were captured using the Kinect sensor to provide validation for our algorithms. One movement consisting of discrete sequence of upper-limb was chosen. Fig. 4.10 compares the positions of the right and left wrists as seen by the filtered data and the robot simulation. The consistency between the two curves suggests the efficacy of the human motion reconstruction algorithm proposed.

For this particular movement, the difference between the motion capture data (after pose correction) and the gestures replicated by the robot are quantified using the Euclidean distance. The time courses of the error measure for the elbow and wrist of the left and right arm are shown in Fig. 4.9.

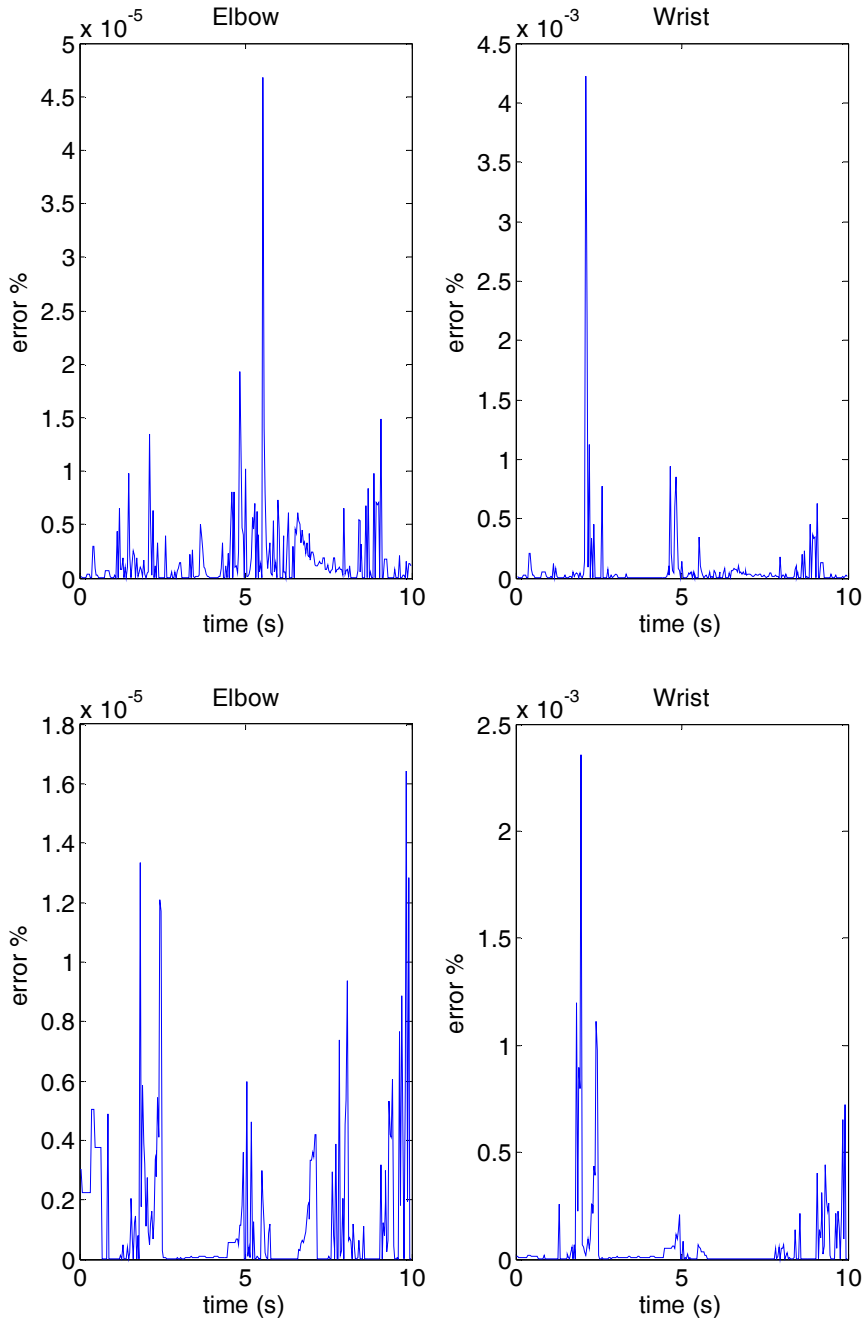

Fig. 4.9: Difference between the motion capture data and the gestures replicated by the robot for the left arm (top) and the right arm (bottom).

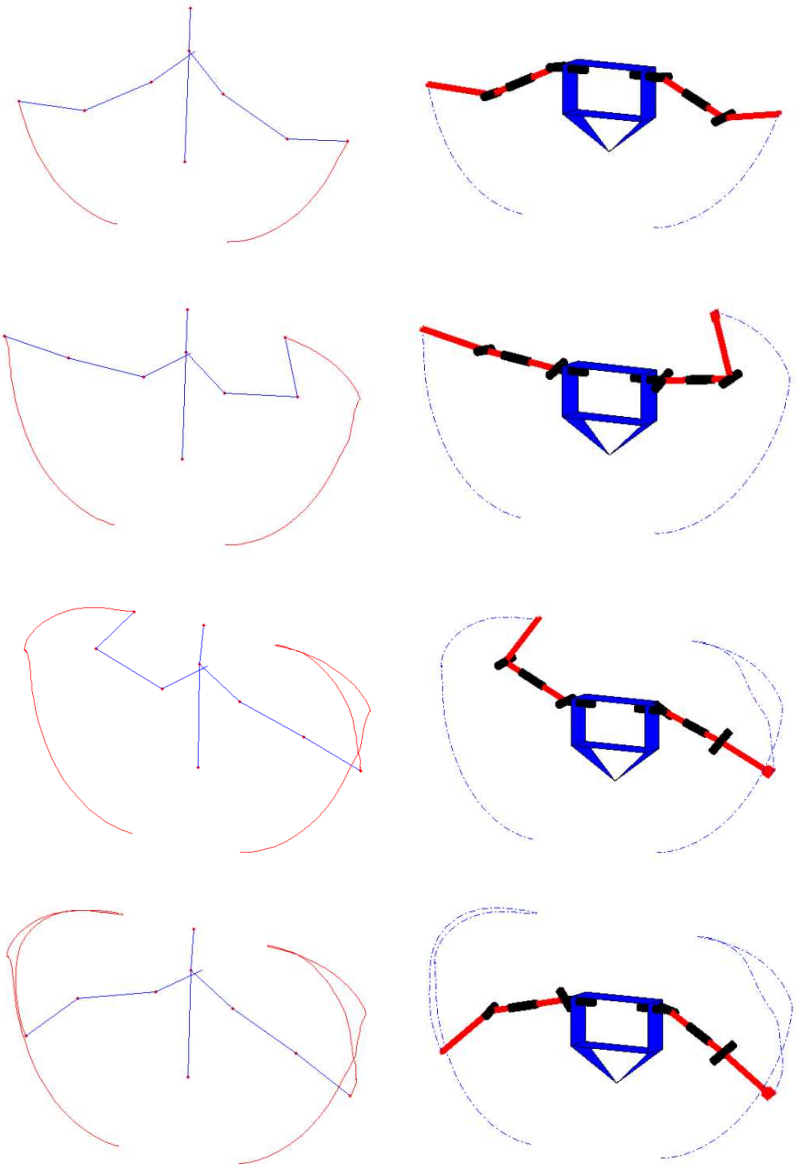

Fig. 4.10: Comparison of the motion capture data (left) with the corresponding gestures replicated by the robot (the end-effector path is represented in both cases).

4.4.4 Example B: Generalization of a Reaching Task

The purpose of this section is to clarify the nature of the generalization performance from single demonstrations provided by human motion capture data. The main focus is placed on a three-dimensional reaching task involving the coordination of four joint angles (using the same 4-DoF robot model). The reaching dataset allowed maintaining a common set of actions throughout the experiments, while at the same time varying the movement kinematics required to achieve those actions.

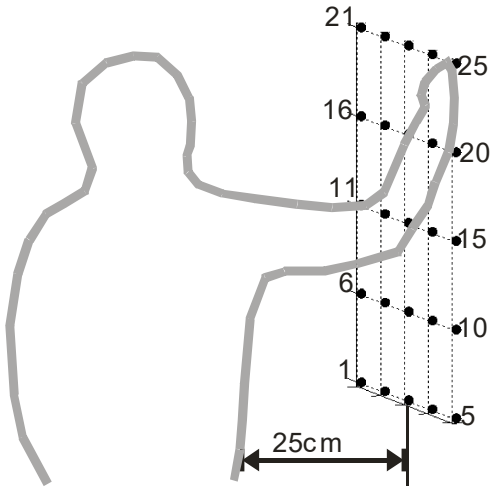

Fig. 4.11: Illustration of the reaching task defined by a grid of 25 target points.

Several reaching movements executed by a human subject were captured using the Kinect sensor. More specifically, reaching trajectories towards a total of 25 targets located on a vertical plane in front of the subject were recorded (see Fig. 4.11). The points were spaced by 10 cm on a 40 by 40 cm grid. The subject is instructed to perform each trial as follows: "After the 'go' signal, move the hand in one continuous motion to the designated target at a comfortable speed, while being as accurate as possible. Try to keep the speed consistent across all trials." Prior to each experiment, the subject was asked to assume the same starting position. All the captured data was subject to a motion filter restriction (see 4.4.1) before the joint angles were computed.

Multidimensional scaling (MDS) is used for exploring the similarity measures among the complete set of reaching movements. For visualization purposes, the analysis is performed in a 3D representation space using a 25×25 similarity matrix, in which each cell represents the Euclidean distance between a pair of movements evaluated along a reference time. The MDS visualization in Fig. 4.12 helps to find apparent clusters present in the data. MDS constructs a configuration of points in the three dimensional space from information about inter-point distances in high dimensional space. This new geometrical configuration of points preserves the proximities of the high dimensional space and, further, it facilitates the perception and interpretation of the data's underlying structure. The proximity among items measures their similarities and

it is a distance measure (more similarity means smaller distances). In this study, the metric used to define the distance matrix is the Euclidean distance metric.

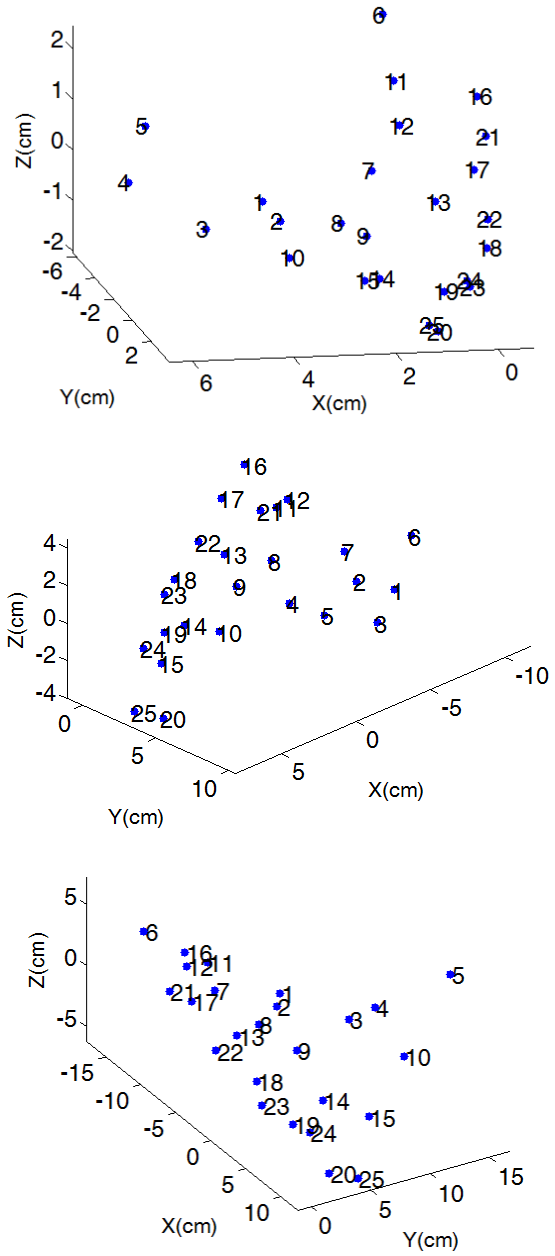

Fig. 4.12: MDS visualization of the Euclidean distances among the reaching movements (top: for the elbow; center: for the end-effector; bottom: global distances).

At the same time, performing PCA on the set of the 25 movements (both on the joint variations and on the task space variations) shows that more than 98% of the total variation of the data could be explained using only 3 principal components, meaning that the movements are probably built up in a modular way. In these experiments, the

generalization performance involves a metric that evaluates the accuracy of the reproduction in terms of spatial information using the mean-square-error (MSE) that compares the path followed by the elbow and the endpoint of the robot model.

In this study, the DMP approach was tested trying to answer the following questions: (1) Can the coordination of motions obtained from primitives fitted to one particular reaching movement be used to generalize to other target points (*i.e.*, its parameters are fixed and only the goals change)? (2) How well the motion primitives fit to new situations when they are learnt in joint space or, alternatively, in task space? (3) Can the problem be posed by selecting the single demonstration as a spatial clustering one based on the visual interpretation of the MDS?

In order to address the first question, the motion primitives are fitted to the target point 13. To address the second question, the original recorded reaching movements are fitted by the DMPs learnt in both the joint and task space. Fig. 4.13 depicts the results of the root-mean-square error between the original recorded and the reproduced movements expressed in terms of the spheres' radii. One simple observation is that a significant difference exists when the targets are located above or below the original target. Further, these results are in agreement with the MDS representation once they reflect the proximities (smaller distances) around the target point 13 (points 1, 2, 8, 9 and 22).

Then, these DMPs are used to reproduce the movement to the original target, point 13. Consistent with expectations and previous results with simulated data, it was found that learning the DMPs in the task space is rather advantageous, as it can be observed in Fig. 4.13. Also the maximum error (111.6×10^{-3} for the joint space versus 58.7×10^{-3} for the task space) and the mean error (76.5×10^{-3} for the joint space versus 39.37×10^{-3} for the task space) confirm these results.

Based on the fact that closer points on the MDS graphic to the movement used to modulate the DMP had a minor error, a question arises: would a point on the MDS graphic with more points closer to it be used to modulate a DMP that lead to a lower error on the generalization movement? To test this hypothesis, point 12 was selected to modulate the DMP. The results of this test (Fig. 4.14, left) are in line with what was expected and it can be seen that the errors in general are lower. Computation of the

mean global error for the joint space case (48.47×10^{-3}) and the task space case (33.48×10^{-3}) confirm this expectation. At the same time, a DMP modulated to point 19 (Fig. 4.14, right) shows smaller errors on points that are closer (14, 15, 18, 20, 23).

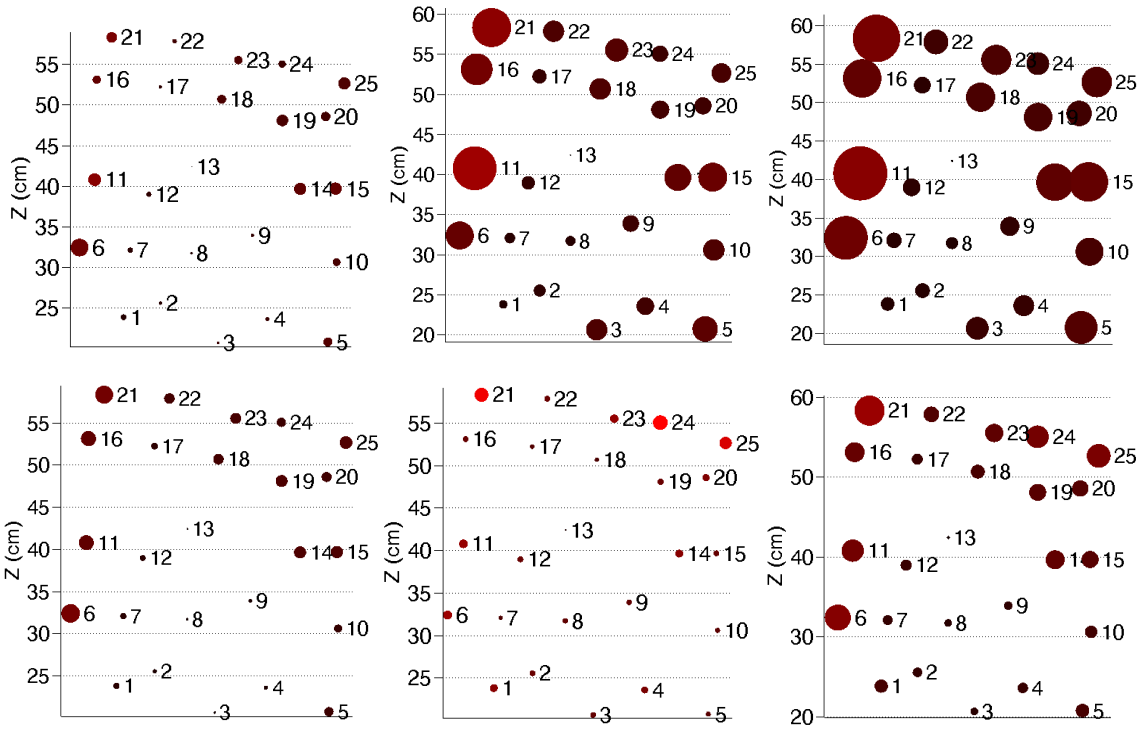

Fig. 4.13: Error between the recorded movements and the those reproduced by the robot when fixing the parameters of the motion primitives once fitted to the target point 13 (left: elbow error; centre: end-effector error; right: total error). The DMPs are learnt in the joint-space (top) and in the task-space (bottom). The minimum and maximum total errors (MSE$\times10^{-3}$) are the following: **8.4**±4.9 and **111.6**±72.3 (joint space); **7.1**±3.3 and **58.7**±39.3 (task-space).

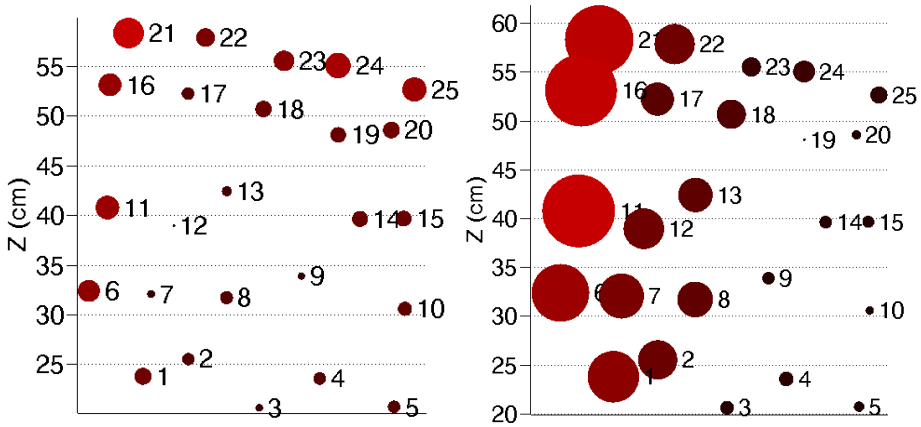

Fig. 4.14: Error between the recorded movements and the movements reproduced by the robot when fixing the parameters of the motion primitives once fitted to the target point 12 (left) and target point 19 (right).

4.5 Final Remarks

Inspired by recent neurophysiological evidences, a new representation paradigm is shedding light on the organization of sensory-motor structures in biological systems. This research direction posits that human behavior is composed of motor primitive units, called motion primitives (Thoroughman & Shadmehr, 2000; Tresch et al., 2002; Schaal, 2002; Todorov, 2004; Flash & Hochner, 2005), explaining how such elementary primitives can be sequenced and superimposed to accomplish more complex movement tasks.

Proposed by Ijspeert et al. (Ijspeert et al., 2002a), dynamic movement primitives are defined by analytically well-understood dynamical systems with convenient stability properties. By modulating them with nonlinear terms, it is possible to achieve a desired point or limit cycle attractor. Dynamic movement primitives (DMP) present several properties that make them very attractive in robot systems, namely for biped locomotion. Perhaps the most important of the properties is the ability to be modulated with a demonstration signal, making them very useful in the context of robot learning by demonstration.

When applied to biped locomotion, dynamic movement primitives are, typically, learned in joint space, as reported by Nakanishi *et al.*(Nakanishi et al., 2004a) and Morimoto *et al.* (Morimoto et al., 2008). However, exploring the generalization and adaptation of learned primitives by modulation of their control parameters becomes difficult when the demonstrated trajectories are available in the joint space. This occurs because a change in the primitive's parameters does not correspond to a meaningful effect on the current behaviour. Unlike the above mentioned works, the use of DMPs learned in task-space has been applied by Pastor *et al.* (Pastor et al., 2009) and Ude *et al.* (Ude et al., 2010), but limited to the specific domain of robot manipulation.

The hypothesis is that successful results can be achieved by using DMPs learned in Cartesian space. The main difficulty arises in multi-body systems with a large number of DOFs since calculating the inverse kinematics is required. Supported by the development of efficient algorithms for whole-body coordination (Choi et al., 2007) as well as advances in designing robots that can learn such kinematic models by

themselves (Hoffmann et al., 2010), the solution adopted here is based on DMPs learned in task-space and directly relate their parameters to task variables. This allows generating new motions which fulfil task-specific features, while maintaining the overall style of the demonstration.

Chapter 5
Human Motion Capture

The preceding chapter described the mathematical tools that will be used to encode human demonstrations based on the concept of motion primitives. This chapter aims to present the study that led to the extraction of the single-demonstration to be transferred into the humanoid robot. Firstly, the acquisition of human demonstrations using a VICON gold-standard motion capture system is addressed. Normal walking in humans, assuming no pathological issues affecting the gait, is compared with a "robot-like" walking mode in which the subject's feet remain in flat contact with the ground, forcing the bent-knee at all times. Secondly, the analysis of the kinematics and dynamics data acquired from the motion capture system and the force platform, respectively, will be addressed for both locomotion modes (normal and "robot-like" walking). In line with this, a comparative study of the different phases of the gait and the associated events is performed.

5.1 Normal Walking in Humans

The human gait cycle can be described as the sequence of movements that occurs between two consecutive contacts of the same foot with the ground (DeLisa, 1998). Therefore, it can be considered that the walking cycle starts with the first heel contact of the left (or right) foot and ends with the next heel contact with the ground of the left (or right) foot. According to Whittle (Whittle, 2007b), the gait cycle consists of seven periods associated with the following events: initial contact, opposite toe off, heel

rise, opposite initial contact, toe off, feet adjacent and tibia vertical. The complete cycle is composed of two phases: the stance phase, occurring when the foot is on the ground, and the swing phase, occurring when the foot is moving in the air. The first one is composed of four of the seven mentioned periods and lasts from the initial contact to toe off. It can be subdivided into loading response, mid-stance, terminal stance and pre-swing. The second phase is composed of three of the seven mentioned periods, lasting from the toe off till the next initial contact. It can be subdivided into initial swing, mid-swing and terminal swing. The events, phases and sub-phases are depicted in Fig. 5.1.

During the walking cycle, it is also possible to identify two different periods: the single and the double support periods. The former corresponds to the moment in which only one foot is in contact with the ground and the other leg is in the swing phase. The latter occurs between the initial contact of the right/left foot and the toe-off of the left/right foot, *i.e.*, the period in which both feet are in contact with the ground. For each cycle, there are two periods of double support and a period of single support. During normal walking, the stance phase lasts about 60% of the gait cycle, with each double support period lasting about 10%, and the swing phase lasts about 40%.

During human walking, foot placement is typically quantified by spatial and temporal measures in a global reference frame. Examples of these measures are the step length and step width as shown in Fig. 5.2. These measures quantify foot placement in relation to the other foot without accounting for body position. However, foot placement closely relates to movements of the body and can also be quantified in a body reference frame which, in turn, may prove physiologically more relevant (Townsend, 1985). In the stance phase, the body centre of mass is propelled within the limits related to foot placement. Similarly, at the end of the swing phase, precise placement of the foot relative to the body establishes a new base of support at each step that determines the dynamic stability during walking.

In this study, the foot placement is also defined in a body reference frame as the calculation of foot position relative to body position during walking (*i.e.*, independent of the other foot). In a body reference frame, the step length is calculated as the anterior distance between the leading foot center-of-mass (reflecting foot position) and pelvis

center-of-mass (reflecting body position) at initial-contact. Whereas in a global reference frame, the step length is calculated as the anterior distance between the leading and trailing foot without accounting for the body position.

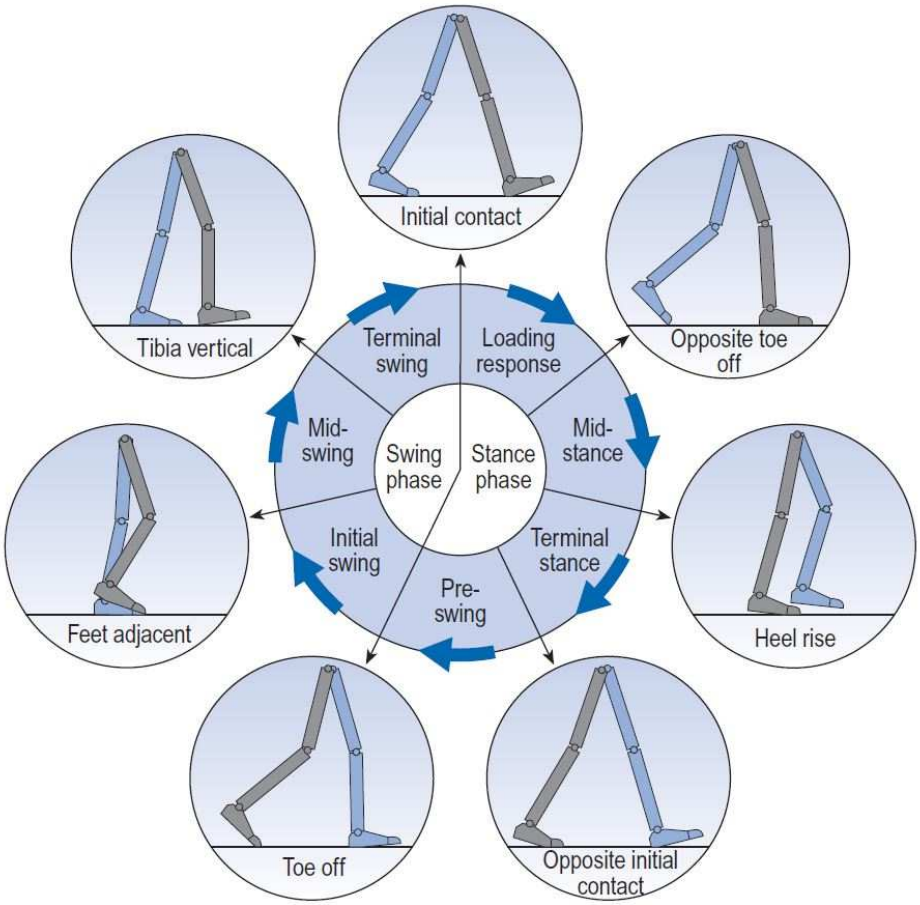

Fig. 5.1: Events, periods, phases and sub-phases during normal walking cycle (from Whittle, 2007b).

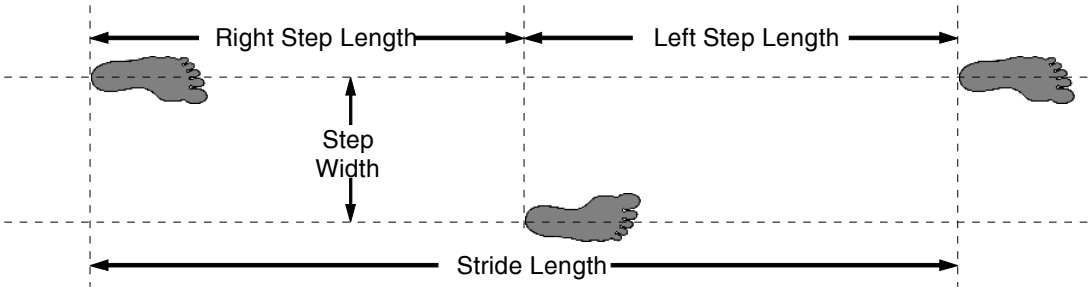

Fig. 5.2: Terms used to describe foot placement on the ground.

In this study, the foot placement is also defined in a body reference frame as the calculation of foot position relative to body position during walking (*i.e.*, independent

of the other foot). In a body reference frame, the step length is calculated as the anterior distance between the leading foot center-of-mass (reflecting foot position) and pelvis center-of-mass (reflecting body position) at initial-contact. Whereas in a global reference frame, the step length is calculated as the anterior distance between the leading and trailing foot without accounting for the body position.

Other parameters that define the human gait are the cadence (C), cycle time (T_c) and forward velocity (V_f). The cadence can simply be defined as the number of steps per minute. Inversely, the cycle time, also known as the stride time, is given by:

$$T_c = 120 / C \tag{5.1}$$

The simplest definition of the forward velocity is the distance covered by the entire body in a given time. While the instantaneous speed varies along the whole walking cycle, the average forward velocity is given by:

$$\bar{V}_f = \frac{S_l \times C}{60} \tag{5.2}$$

Age (years)	***C* (steps/min)**	T_c **(s)**	**Stride length** $2 \times S_l$ **(m)**	**Forward velocity** V_f **(m/s)**
13 – 14	103 – 150	0.8 – 1.17	0.99 – 1.55	0.90 – 1.62
15 – 17	100 – 144	0.83 – 1.20	1.03 – 1.57	0.92 – 1.64
18 – 49	98 – 138	0.87 – 1.22	1.06 – 1.58	0.94 – 1.66
50 – 64	97 – 137	0.88 – 1.24	1.04 – 1.56	0.91 – 1.63
65 – 80	96 – 136	0.88 – 1.25	0.94 – 1.46	0.80 – 1.52

Table 5-1: Typical gait cycle values for female subjects (Whittle, 2007a).

Age (years)	**C (steps/min)**	T_c **(s)**	**Stride length** $2 \times S_l$ **(m)**	**Forward velocity** V_f **(m/s)**
13 – 14	100 – 149	0.81 – 1.20	1.06 – 1.64	0.95 – 1.67
15 – 17	96 – 142	0.85 – 1.25	1.15 – 1.75	1.03 – 1.75
18 – 49	91 – 135	0.89 – 1.32	1.25 – 1.85	1.10 – 1.82
50 – 64	82 – 126	0.95 – 1.46	1.22 – 1.82	0.96 – 1.68
65 – 80	81 – 125	0.96 – 1.48	1.11 – 1.71	0.81 – 1.61

Table 5-2: Typical gait cycle for male subjects (Whittle, 2007a).

Table 5-1 and Table 5-2 show the normal ranges for the cadence, cycle time and forward velocity for both female and male subjects, respectively, at different ages.

5.2 Human Motion Capture: Experimental Protocol

This section describes the experimental measurements of motion capture data to extract human demonstrations of normal and "robot-like" walking on a flat surface. A "robot-like" walking gait means that the human stance foot is constrained to remain in flat contact with the ground, forcing the "bent-knee" at all times. This is the typical configuration adopted by most humanoid robots, since the straight-leg style of human walking requires an articulated foot.

5.2.1 Participants and Procedures

Motion capture was performed in a human gait analysis laboratory equipped with a gold-standard VICON optoelectronic system (Vicon Systems, 2015), two HD video cameras, two force platforms and up to thirty non-invasive surface electromyography (EMGs) sensors. Three-dimensional kinematics data was collected at 100 Hz using a VICON system composed of 8 infrared cameras with 2.0 Mpixel resolution. A standard full-body marker set was attached to the following landmarks of the subject: head, shoulders, elbows, wrists, hands, pelvis, hip, knees, ankles and feet (as shown in Fig. 5.3). All captured signals are synchronized with appropriated hardware and those of interest were extracted with the VICON Nexus software, version 1.8.5. More details about the VICON system are provided in Appendix B.

Four normal young adults, suffering from no known abnormalities, participated in the recording sessions having been granted some practical trials. Some subjects found "robot-like" walking uncomfortable and a training period was crucial before a subject have been selected to participate in the study. The subjects were asked to walk in a straight line at a freely, but constant, chosen speed (his "natural speed"). The experimental protocol assumed desirable to provide normal visual input during the trials and to measure gait over a sufficient number of steps to ensure consistent time-series analysis and statistical measures. In order to measure kinematics during many cycles of motion in the limited sensing volume, the subject is asked to start walking a few meters ahead so as to achieve a steady speed (steady-state walking) when entering the recording area with full-marker visibility.

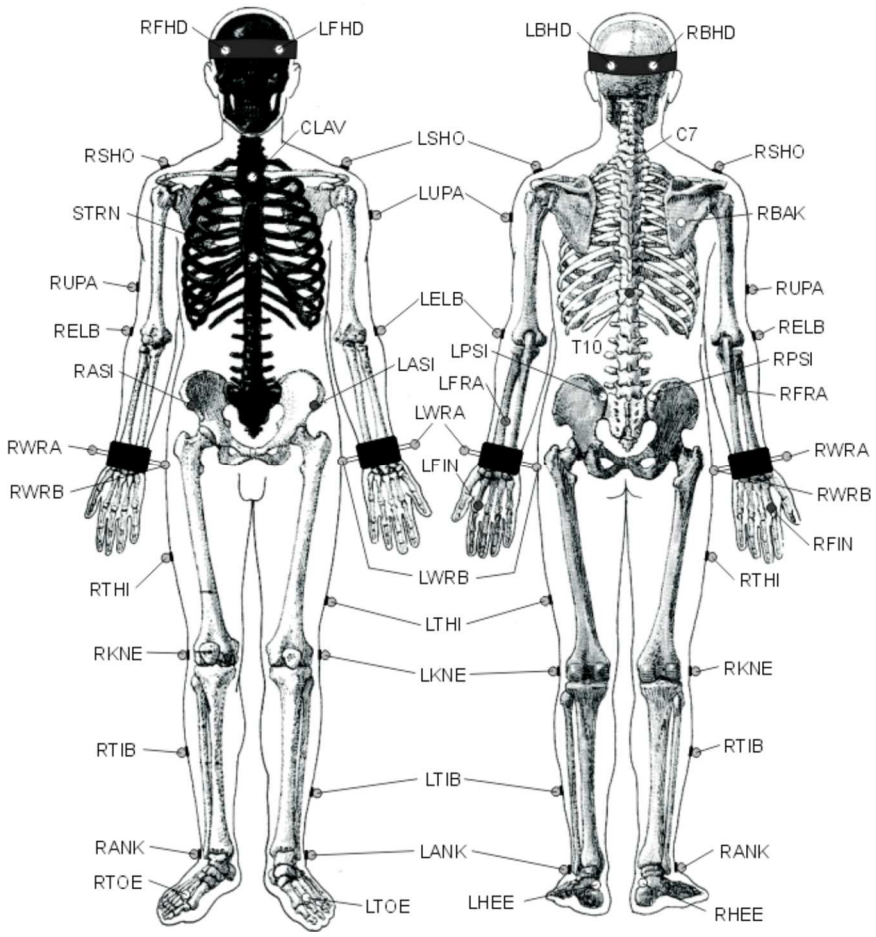

Fig. 5.3: VICON's markers disposition and abbreviated names.

In order to perform a comparative analysis, human demonstrations were extracted both from normal and "robot-like" walking gaits on a flat surface. The "robot-like" gait means that the human stance foot is constrained to remain in flat contact with the ground, forcing the "bent-knee" during the entire cycle in contrast with the typical straight-legged style. Consequently, the typical heel-strike and foot-off events are not found in the corresponding gait patterns. In terms of skill transfer, two advantages can be envisioned by the "robot-like" gait. First, less effort should be required for transferring the kinematic data from the human to the robot. Second, it allows extracting directly the time courses of the centre-of-pressure.

In addition to capturing human locomotion in flat ground (the fundamental mode of locomotion in this study), additional experiments included walking upstairs/downstairs, walking in sloped surfaces, walking in irregular terrains or

overcoming obstacles (see Fig. 5.4). Their main purpose is to provide examples that can help to define adaptation strategies for similar situations in the humanoid robot.

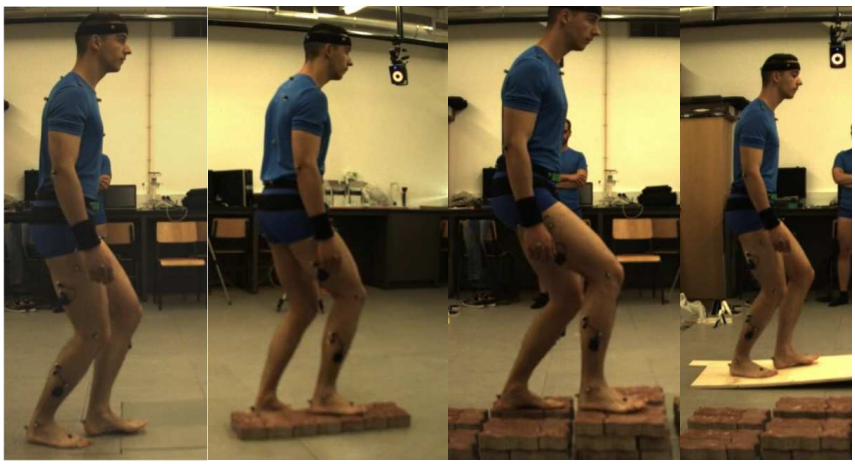

Fig. 5.4: Experiments performed in different situations using the "robot-like" walking mode. From left to right: walking in level surface, walking through a path with small steps of increasing complexity and walking on a sloped ground.

5.2.2 Spatial-Temporal Normalization

In all trials the participants were asked to walk in straight line by selecting, preferably, the foot placement along a specific direction aligned with an axis of the VICON's coordinate reference frame. Even so, working inside a limited working volume requires precise localization of the standard planes to ensure comparability of previously obtained datasets both during the same or different acquisitions. In line with this, an initial effort was dedicated to spatial normalization, *i.e.*, placing the data into a common coordinate system before the gait description and analysis. The approach used for extracting the longitudinal plane involves collecting gait data for a number of strides so that the unknown model parameters are estimated from the markers placed at the participant's hip section.

At the same time, considering the availability of a fixed gait lab with a limited sensing volume, the elimination of transient phases resulting from changes in walking direction that occur when the participant approaches those limits was also required. In order to perform the analysis and compare the normal with the "robot-like" parameters, the gait cycle is defined as the time window between two successive heel strikes of the right foot (*i.e.*, the initial instant of time corresponds to the right foot

heel strike). Each individual cycle was extracted from the time-series using an index based on the kinematic trajectories of the ankle, heel and toe markers, aiming to automatically detect this event.

5.3 Kinematics Gait Description and Analysis

Kinematic data were analysed off-line with customized software written in Matlab (Mathworks, MA). Space calibration was oriented so that the Y-axis is aligned with the walking direction, while the X- and Z-axis are transversal and vertical to that direction, respectively. Accordingly, the motion planes are defined as follows: sagittal plane (YZ), frontal plane (XZ) and horizontal plane (XY). The analysis method involves collecting data for a number of strides, time-normalizing the data from each stride to a standard length (100%) and then averaging the data across strides. This approach seeks to examine the nature of gait patterns exhibited during both normal and "robot-like" strides. For that purpose, the kinematics data of one representative participant is analysed, including spatial and temporal gait parameters. The subject's height is 1.85 m and the body mass 76 kg.

First, typical parameters are calculated from the kinematic data, including the average values of cadence (C), forward velocity (V_f), step length (S_l) and step width (S_w). The variability found from stride to stride is computed using the standard deviation. The subject walked with an average cadence of 120.2±7.8 (101.8±9.2) steps/min and an average forward velocity of 0.50±0.1 (1.0±0.2) m/s for the "robot-like" (normal) walking mode. Lateral and fore-aft foot placement in gait were systematically measured to obtain an average stride length (two consecutive steps) of 50.3±7.8 (118.7±13.7) cm and an average step width of 7.3±2.4 (6.7±2.0) cm. In agreement with typical values found in literature (Perry, 1992), the step length decreased significantly, as well as the forward velocity when comparing the "robot-like" with the normal gait pattern. In the same line of evidences (Bauby & Kuo, 2000), the lateral variability associated with the two walking modes exceeds that of the fore-aft direction.

Second, the analysis of the human "robot-like" walking pattern is dedicated to gait trajectories directly related to kinematic parameters, such as step length, hip height and

foot clearance. The next graphics depict the time history plots of averaged single-stride gait characteristics (black line) for both normal (top) and "robot-like" walking (bottom). Here, the variability is represented by the full range over the several trials (gray region). Fig. 5.5 represents the mean trajectory of the right heel marker along the direction of the movement (Y-axis) obtained by centring the range of values on zero. The significant limitations imposed by the "robot-like" walking mode are clearly illustrated.

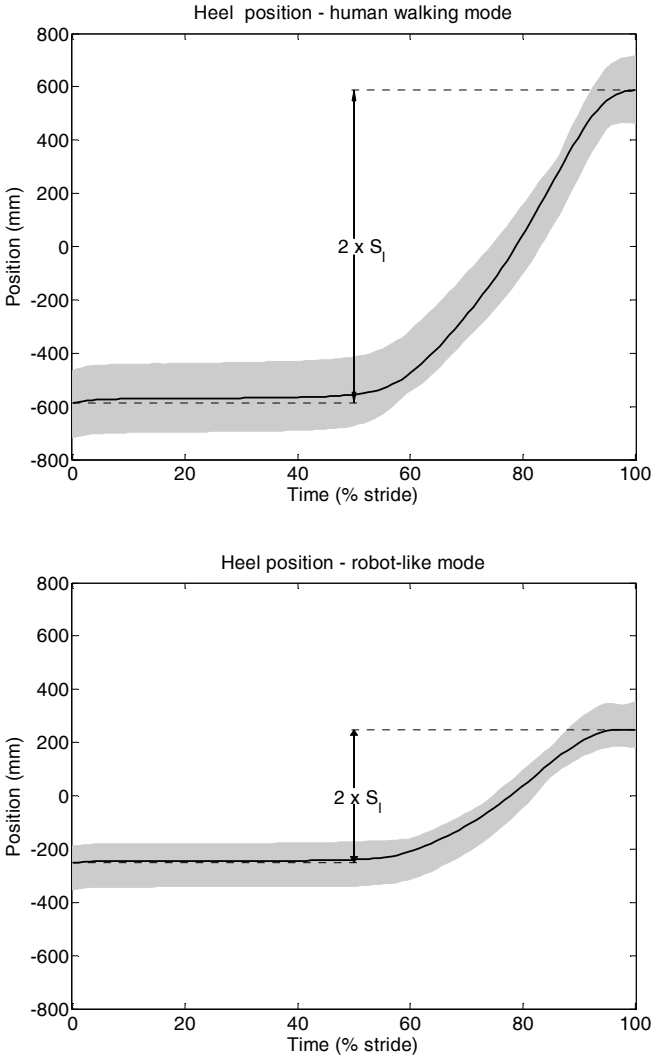

Fig. 5.5: Heel *y* position (direction of the movement) for normal (top) and "robot-like" walking mode (bottom): the solid line shows the average trajectories, while the grey region shows full range of trajectories overall several trials.

At the same time, the vertical displacement of the right heel marker, shown in Fig. 5.6, allows for estimating that the swing leg motion is characterized by a mean foot

clearance of about 21.1±6.9 cm and 13.4±4.7 cm for the normal and "robot-like" modes, respectively. Besides a minor displacement during the first half of the stance phase, the other important difference is that, in the "robot-like" mode, the influence of the swing leg retraction phenomenon is not apparent (*i.e.*, motion just prior to ground contact).

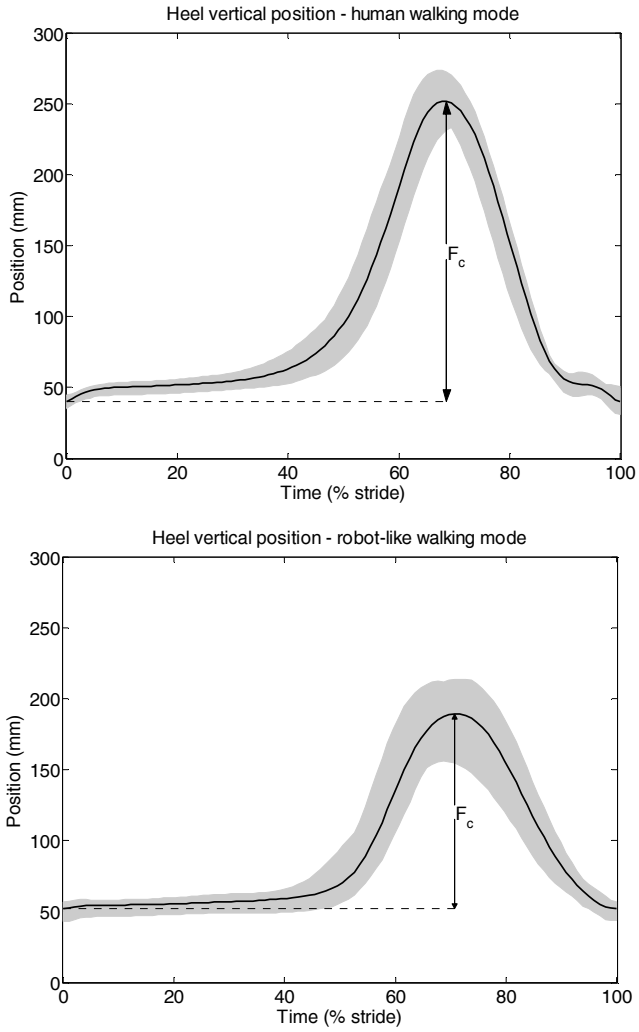

Fig. 5.6: Heel vertical position for both human walking mode (top) and "robot-like" walking mode (bottom): the solid line shows the average trajectories, while the grey region shows full range of trajectories overall several trials.

The vertical displacement of the centre-of-mass (CoM) is an important factor that influences energy expenditure. The pendulum-like mode of walking, which is a consequence of the straightness of our legs, reduces the mechanical work that our muscles must supply to raise and accelerate the CoM. Fig. 5.7 illustrates the vertical displacement of the pelvis section in percentage of maximum height derived from the

standard anatomical position. The typical mean values of hip height are 97.9±0.8% for normal walking and 88.3±0.5% for "robot-like" walking. Although the shape remains similar, the "robot-like" mode of walking reduces not only the mean hip height, but decreases also the mean peak-to-peak oscillation from 2% to 1.5%.

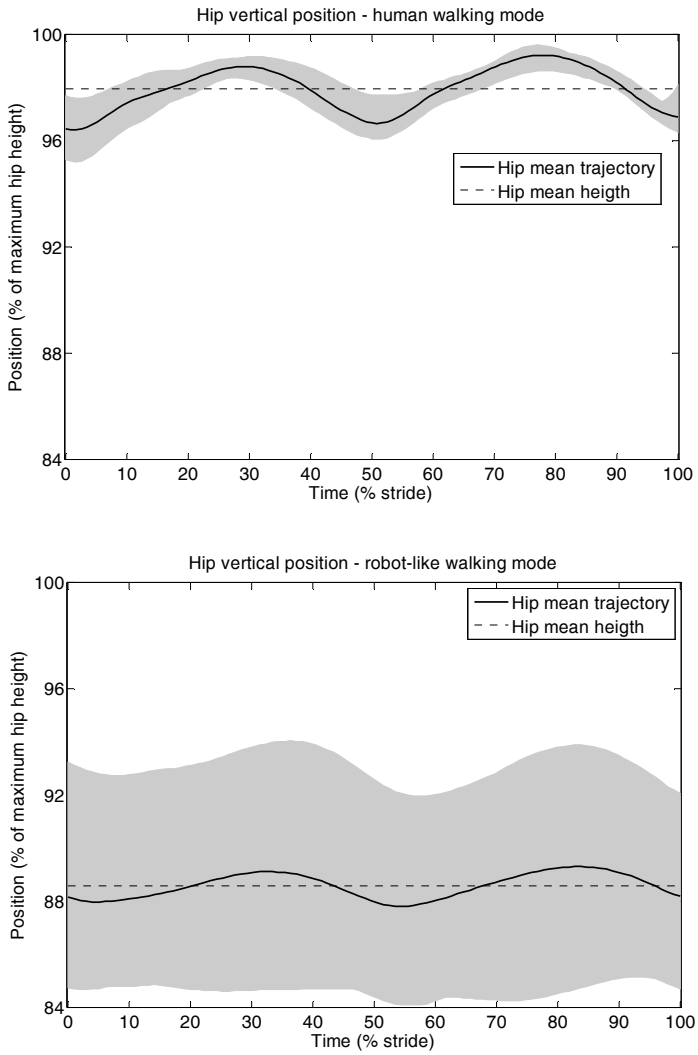

Fig. 5.7: Hip height for both walking modes, show in % of the hip height when standing. Solid line shows the average hip trajectory from several steps; dashed line is the average hip height; grey region shows the full range overall several trials.

A comparison between walking modes regarding pelvic kinematics is performed by using the VICON's markers placed at the hip section. On the one hand, Fig. 5.8 depicts the results obtained for pelvic rotation after averaging the values taken from several steps re-scaled to the same time duration (the average time cycle for each walking

mode). From the graphics, it can be observed that, even though the pelvic rotation still occurs in the "robot-like" mode, the amplitude of the rotation is much lower than that observed during the normal walking mode (about 2.5 times lower).

On the other hand, pelvic tilt is also present in both walking modes as illustrated in Fig. 5.9. Although the range of values is not very different, it can been seen that, when the foot is standing, there seems to be a kind of a "pause" on the tilt for the "robot-like" mode, since the variation of the values is small at these moments (from 0 to 10% of the stride, and 50% to 60% of the stride).

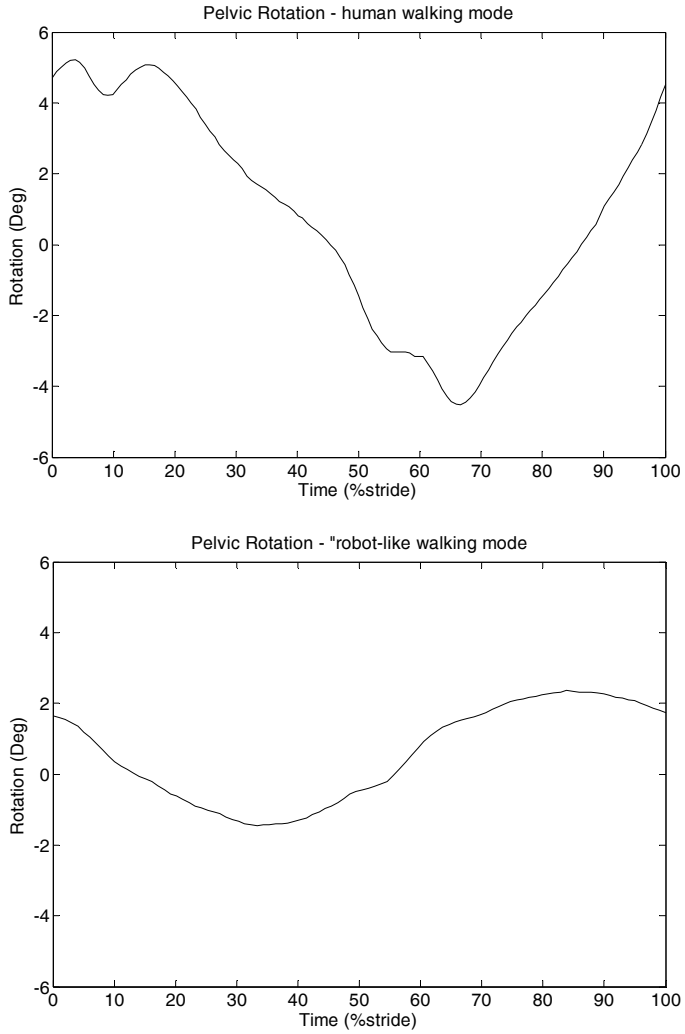

Fig. 5.8: Pelvic rotation for both human and "robot-like" walking modes (plot shows the average values taken from several steps).

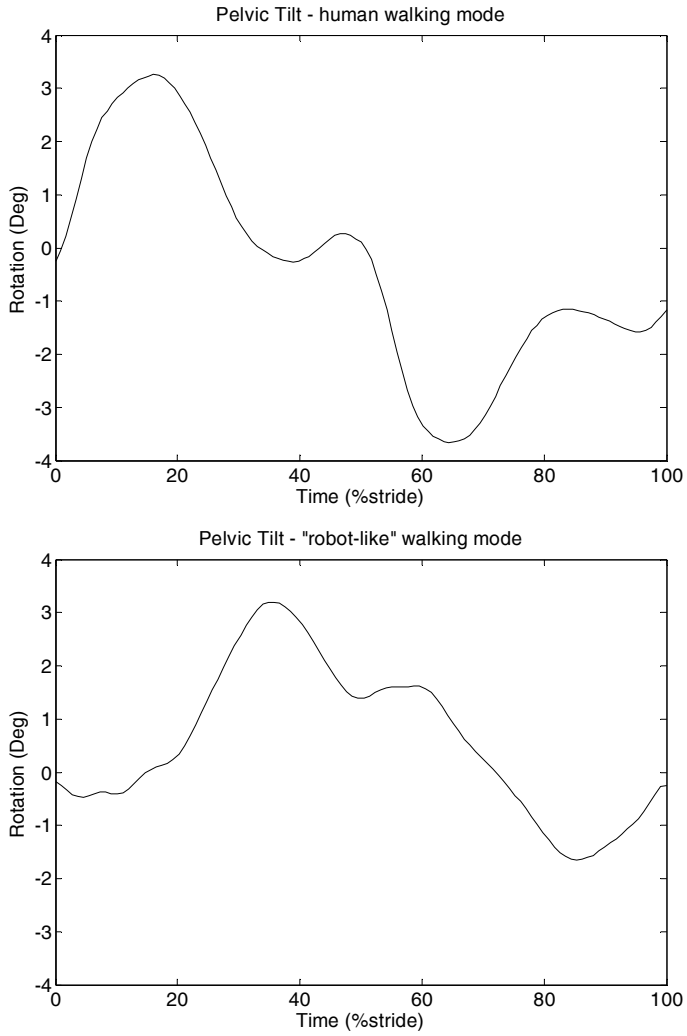

Fig. 5.9: Pelvic tilt for both human walking mode and "robot-like" walking mode (plot shows average values taken from several steps).

At last, this study includes the trunk kinematics analysis aiming to understand the role of trunk during walking (the rotation of the thoracic region in the horizontal plane is disregarded). The orientation of the trunk is estimated using the markers placed on the pelvis (markers LASI, LPSI, RASI, RPSI) and on the shoulders (markers RSHO and LSHO). The kinematic study during walking demonstrates a general inclination of the trunk in the sagittal plane that changes considerably from trial to trial (between 10 and 25 degrees) with small amplitude of oscillation (< 5 degrees), without showing a well-defined pattern. In contrast, in the lateral plane, a similar pattern of the flexion on each side per cycle can be observed (see Fig. 5.10): after the middle of the double

support phase, where it reached its maximum, there is a bending towards the side of the new swing leg, reaching the aligned position at ankles crossing.

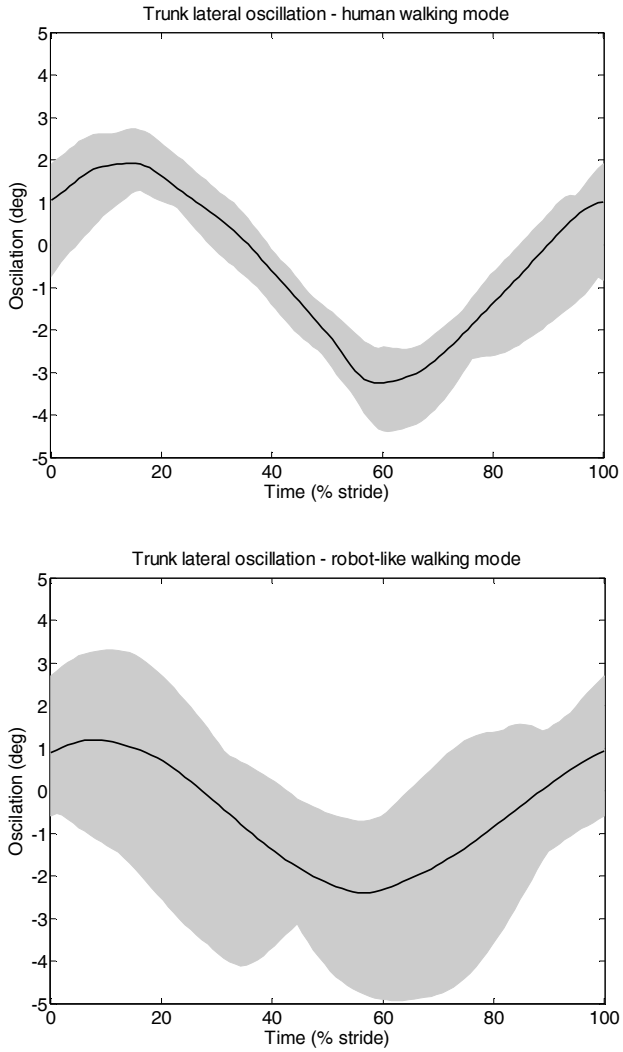

Fig. 5.10: Lateral trunk oscillation for both walking modes. Solid line shows the average oscillation value taken from several steps and grey region shows the full range overall several trials.

An anatomical description of the movement, regardless of the walking mode, is provided by the stick diagram in the plane of the movement (see Fig. 5.11). Each body segment is represented by a straight line and the different segments are joined together, providing their spatial orientation at any point in time. This plot is repeated at equal intervals of time to provide a pictorial description of the movement. As expected, some determinants of gait that can be clearly observed during normal walking (top diagram) are not present during "robot-like" walking (bottom diagram), such as the controlled

plantarflexion and the powered plantar flexion. Table 5-3 summarizes and compares all the parameters mentioned before.

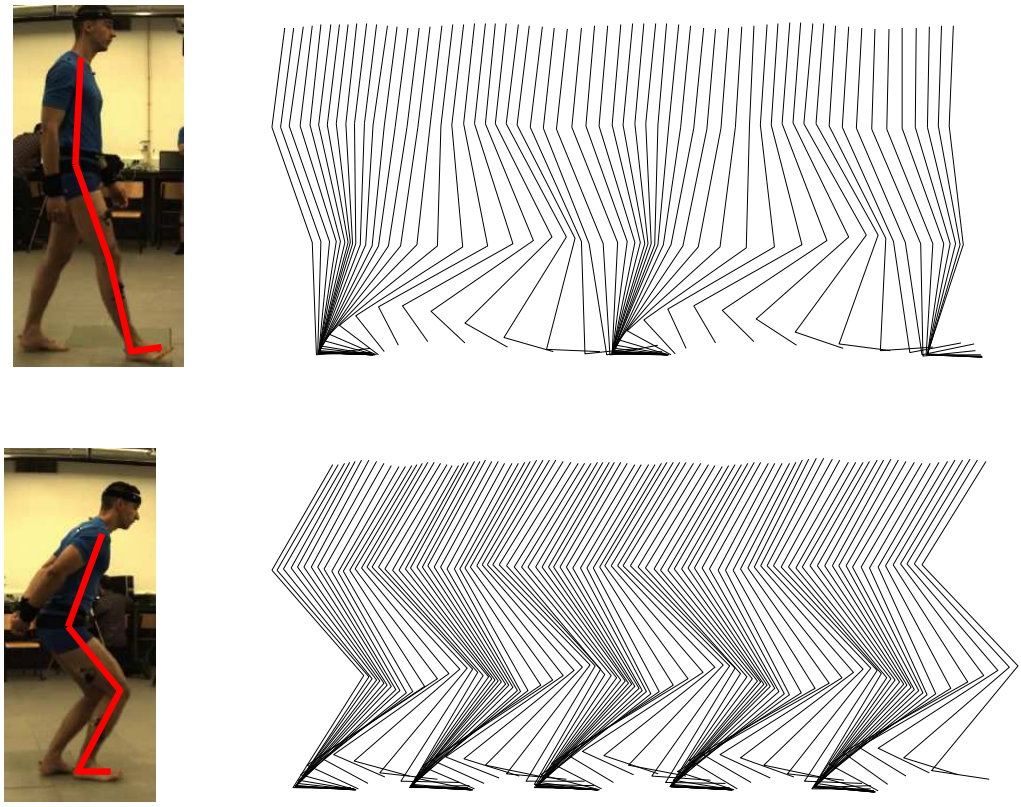

Fig. 5.11: Stick diagram on the plane of movement using the segments depicted in left side. Human natural gait on top and "robot-like" gait on bottom, with arms movements restricted.

	Normal walking	"Robot-like" walking	Difference
Cadence, C (steps/m)	101.8±9.2	120.2±7.8	+18.1%
Time of cycle, T_c (s)	1.2±0.1	1.00±0.06	-16.7%
Stride length, $2\times S_l$ (cm)	118.7±13.7	50.3±7.8	-57.6%
Foot Clearance, F_c (cm)	21.1±6.9	13.4±4.7	-36.5%
Hip Height, H_h (cm)	105.5±0.9	95.7±0.5	-9.3%
Forward Velocity, V_f (m/s)	1.0±0.2	0.50±0.09	-50%
Step Width, S_w (cm)	6.68±2.0	7.29±2.4	+9.1%
Double Support, DS (% T_c)	20.9	20.4	-2.4%
Stance Phase, SP (% T_c)	58.6	62.1	+6.0%

Table 5-3: Comparison between the several parameters of both walking modes. All values taken from the average of several cycles, except the last two rows taken from a cycle. The last column is the ratio between the previous columns.

5.4 Whole-Body Dynamics from the Force Platform

As mentioned before, human motion analysis lab comprises two force platforms (see Fig. 5.19). These platforms provide the total force applied by the ground surface on the foot, without additional information about its distribution across the contact surface (from the heel to the forefoot). The electrical output signals that come from the force platforms are processed by the VICON Nexus software to produce the three-dimensional description of the single equivalent force and moment applied to the surface (*i.e.*, the three components of force and moment in the vertical, lateral and fore–aft directions) and its point of application usually called the centre-of-pressure.

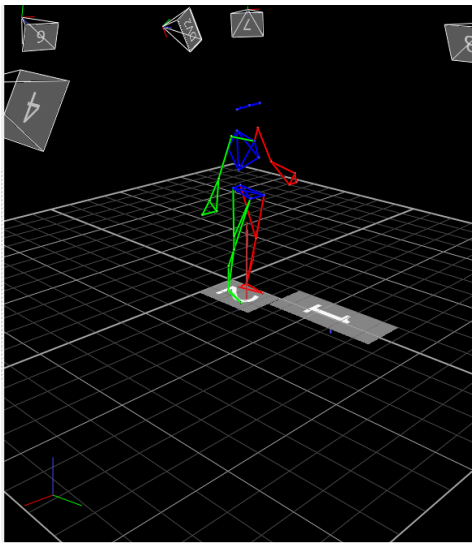

Fig. 5.12: Localization of the two force platforms available at the human motion analysis laboratory.

5.4.1 Ground Reaction Forces

A very interesting signal is the ground reaction force, represented in Fig. 5.13 for both walking modes and both feet. Starting with what is common, notice that both feet present the typical heel strike transient (present at the beginning on both graphs for right foot and around 550 ms for “robot-like” walking mode and 650 ms for human walking mode for left foot), even though for the “robot-like” mode there is no real heel strike, since the foot will completely hit the ground. Still on this event, also notice that the transient has higher values at the “robot-like” walking mode, which can be

explained by the fact that the entire foot hits the ground at once (instead of only the heel), causing a higher transient.

This can also explain the fact the "robot-like" walking mode has higher values of reaction forces; since the entire foot is placed at once on the ground, there is an immediate transfer of all the weight to that foot. Another curious difference is the weight transition between feet: while in the human walking mode this transfer is done at once (notice the reaction forces drops almost instantly when the foot is leaving the ground), on the "robot-like" walking mode there is first a reduction on the reaction force to a lower value, where it keeps stable during a while, and then finally the weight is all transferred to the other foot.

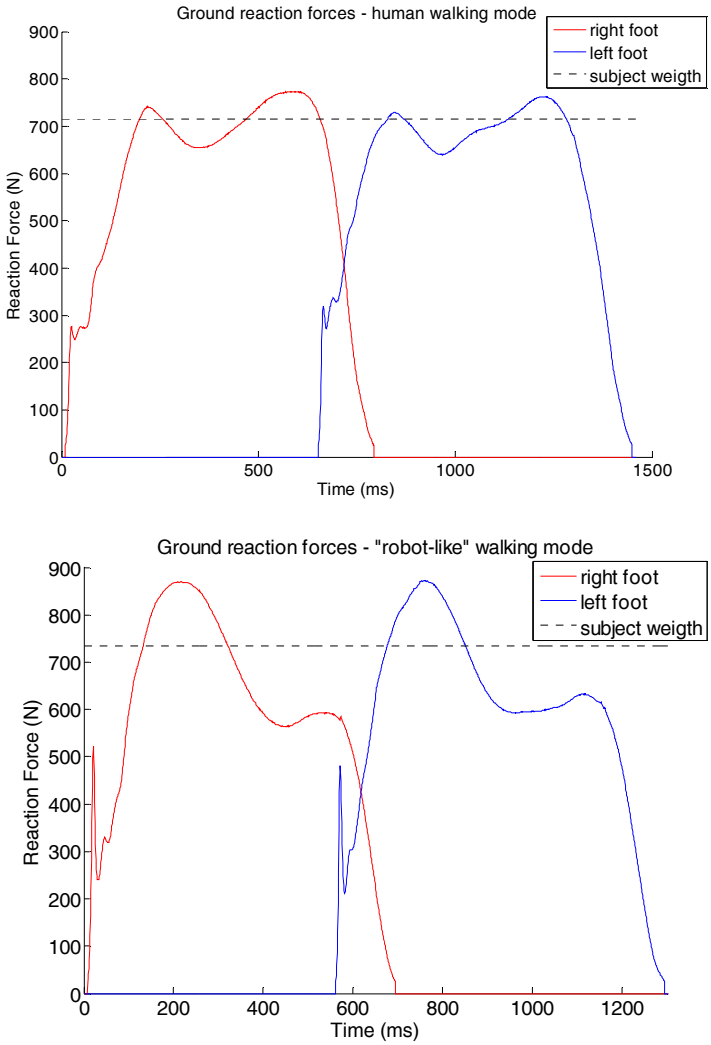

Fig. 5.13: Ground normal reaction force for both walking modes and both feet.

The lateral and fore-aft reaction forces also show important information of the movement. These signals are represented in Fig. 5.14 and Fig. 5.15 for right foot, and over the complete time the foot is on the ground. Marked on the graphic with black dashed lines are key events in the following order: initial contact of the foot, opposite toe off, heel rise of the foot, opposite foot initial contact and finally the toe off. Starting with the normal walking mode (see Fig. 5.14), one can note that at the initial contact (first black dashed line) the lateral ground reaction points to the inner side of the body. This tells us that the body is still tilted to the left foot side, but before the opposite toe off, the body starts to tilt to the other side. Just at the moment of the left foot toe off (second black dashed line), this force is zero and then it increases, showing the body inclination to the right side. A little after the heel rise (third black dashed line) and before the opposite initial contact (fourth blacked dashed line), the body starts to incline to the other side, preparing for the weight transfer to the other foot, and this reaction force becomes near null before the toe off. For the fore-aft reaction force, a braking effect can be observed from the initial contact, with a little reduction of the braking effect, to the moment of the opposite toe off. Then, the acceleration effect appears with a zero value on this force corresponding to the heel rise moment and the peak of this force just a little after the opposite initial contact to then quickly reduce to zero at the toe off event.

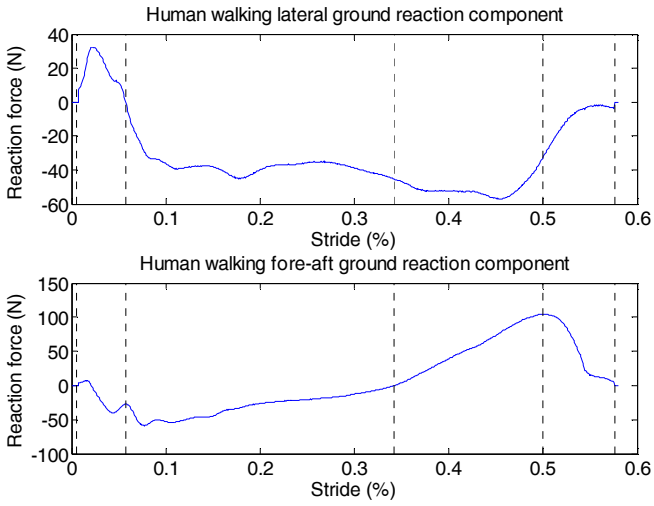

Fig. 5.14: Lateral and fore-aft ground reaction forces in one of the feet for human walking mode. Black dashed lines represent important events by the following order: initial contact, opposite toe off, heel rise, opposite initial contact and toe off.

For the “robot-like” walking mode (see Fig. 5.15), these signals reveal some interesting facts. Starting with the lateral component, just as in the human walking mode at the initial contact, the reaction component points to the inner side of the body, but the event of the opposite toe off only happens much later when the reaction force has already passed the zero value and is pointing to the outside of the body. This reveals that the body has already a big inclination to the right foot side when it leaves the double support phase. Also curious is the fact the body will only start to incline to the other side after the opposite initial contact (fourth blacked dashed line), even though there was a lateral oscillation between the opposite toe off (second black dashed line) and the heel rise (third blacked dashed line), given by the increase followed by a decrease on this reaction component.

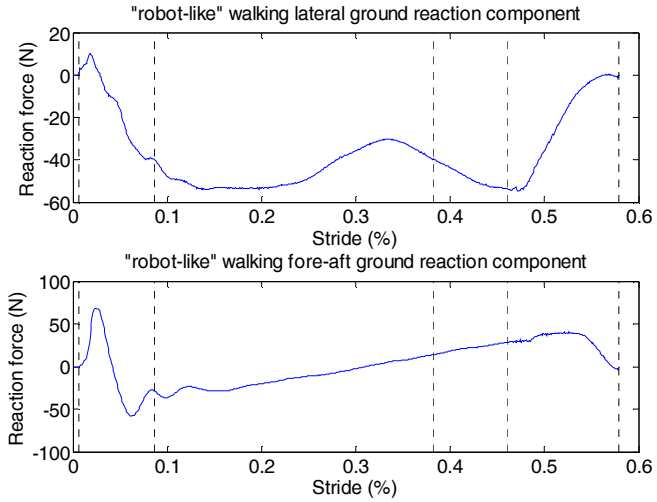

Fig. 5.15: Lateral and fore-aft ground reaction forces in one of the feet for “robot-like” walking mode. Black dashed lines represent important events by the following order: initial contact, opposite toe off, heel rise, opposite initial contact and toe off.

The fore-aft component reveals that instead of a braking effect after the initial contact, there is acceleration, as if the body had a need to keep propelling itself to the front. Only then there is a braking effect with a small acceleration peek at the event of the opposite toe off. When the heel rise happens, the reaction force is already on the direction of the movement (as if there is a need to propel the body before the heel rise) and the opposite initial contact occurs much before the second maximum value of this force. What can also be seen is that this maximum is lower than the one on the human

walking mode; this could explain the fact that instead of braking at the initial contact, there is still a need for acceleration of the body.

5.4.2 Centre of Pressure Pattern

The centre-of-pressure is defined as a representation of the path of the vertical component of the resultant ground-reaction force. When measured from a force platform, the CoP is defined as the projection on the ground plane of the centroid of the vertical force distribution acting on the plantar surface of the foot. In this sense, the CoP is the instantaneous point of application of the resultant foot-ground reaction vector. In reality, the total force is made up of innumerable small force vectors that are spread out across a finite area on the surface of the platform. Knowledge of the CoP trajectory during stance allows for appropriate calculations of balance control during gait. Additionally, the CoP velocity and the time spent in each foot region (*e.g.*, rear-, mid-, fore-foot and toes) can be calculated to provide comparative baseline data.

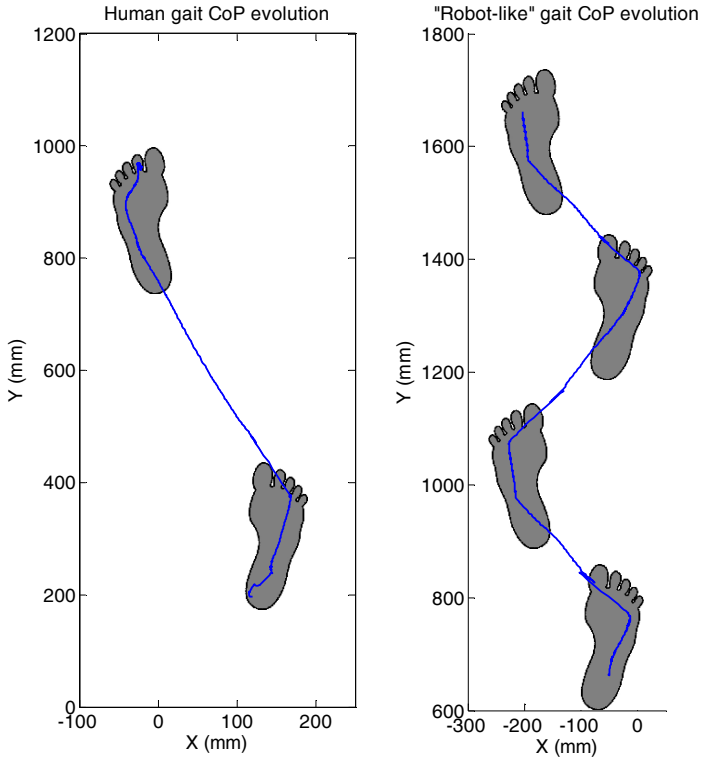

Fig. 5.16: Displacement of the CoP for both normal and modified "robot-like" gait conditions. Footprints represent the stance foot locations obtained from the positions of the subject's foot markers with respect to the force platform reference frame. It was found that the step-to-step variability is more pronounced for the lateral part of the midfoot.

The purpose is to compute the CoP for each stance limb using the ground reaction forces and moments collected from the two force plates and the software supplied by the manufacturer. Fig. 5.16 shows the displacement of the CoP for the normal and the modified gait conditions. These results lead to some observations: first, the footprint patterns of the right and left legs reveal a symmetrical pattern, corresponding to the symmetry in the spatio-temporal variables of gait. Second, it is clear, in comparison, that the step length and walking base are smaller in the "robot-like gait". Third, the transition of the CoP from one foot to the other is faster and jerkier in "robot-like" gait.

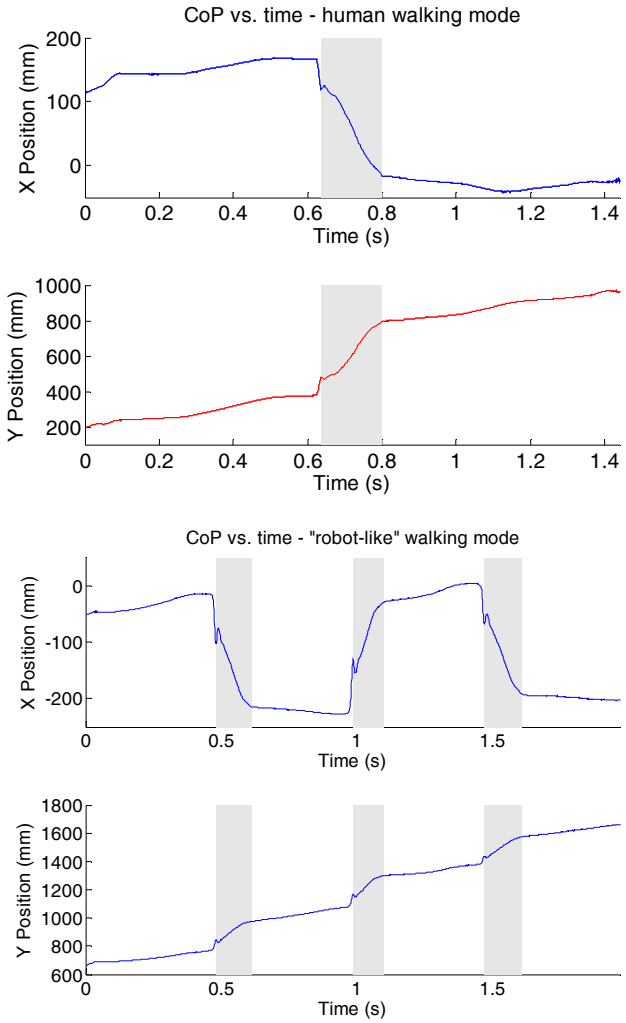

Fig. 5.17: Variation of the CoP over time for both walking modes. Grey shaded regions represent the phases of double support.

Fig. 5.17 shows the variation of both the lateral and sagittal CoP for both walking modes over time. The double support areas are marked by the grey shaded areas, where it can clearly be seen that the CoP quickly moves to the front and to the other foot. Notice that, while in human walking mode and in the single support phase, the CoP keeps moving in the direction of the movement along the foot (even if slower than when in the double support phase), in the "robot-like" walking mode the CoP stays most of the time in the same place, only moving on the final phase of the single support phase. At the same time, it should be noted that the beginning of each double support phase is marked by a "retraction" of the evolution of the lateral CoP. The spatial visualization of the CoP and the ground reaction forces for the right foot are presented in Fig. 5.18.

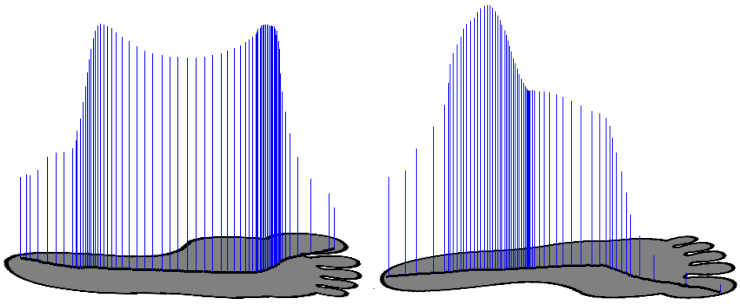

Fig. 5.18: Foot outline, centre-of-pressure and sagittal plane representation of the ground reaction force vector for both human walking mode (left) and "robot-like" walking mode (right).

A careful observation of these results shows some interesting results: first, it is noticeable that, during normal walking mode, the CoP starts near the heel, travels to the front of the foot and ends at the thumb toe. The spacing between two successive samples (vectors) gives an idea about the time the CoP lies in each specific area. In line with this, it can observed that it quickly moves from the heel, stays for some more time just a little bit after the heel, then evolves in a constant speed until it reaches the start of the toes, where it stays for a little bit longer and finally quick moves to the edge of the thumb toe. In the case of the "robot-like" mode, it can be seen that the CoP starts at the heel, but quickly moves to the middle of the foot and then to the thumb toe. What can be seen is that it stays much longer at the middle of the foot, than at the edges, from where it quickly moves away. Table 5-4 summarizes these results by

showing the percentage of time of the stance phase in which the CoP stays in a specific regions of the foot divided into rear-, mid- and fore-foot sections of equal size.

	Normal walking	"Robot-like" walking
Rear-foot section	32.0%	38.2%
Mid-foot section	24.0%	54.4%
Fore-foot section	44.0%	7.4%

Table 5-4: Mean values of the percentage of time spent by the CoP in each foot region during the stance phase of normal and "robot-like" gaits. The rear-, mid- and fore-foot regions are defined by dividing equally the plantar outline in three sections.

5.5 Gait Cycle Phases and Events

Section 5.1 presented the most common gait terminology used in the literature and in this section, some of these parameters in both normal human walking and the "robot-like" walking data will be analysed, starting with the gait cycle events, phases and sub-phases. Fig. 5.19 shows the heel and toe markers for both feet on segments of human natural walking for a little more than a whole step performed by the right foot. For simplicity, the initial contact (performed by the heel strike of the right foot) was placed at the moment $t = 0\,s$, and black dashed lines mark some of the key events. The complete cycle is comprised between this first initial contact (marked with the first black dashed line at $t = 0\,s$) and the second initial contact marked with the last black dashed line (at $t = 1.28\,s$), giving a total of $1.28\,s$ for the cycle time for this example. At $t = 0.14\,s$ occurs the opposite toe off, marked also by a black dashed line. At this instant, the loading response sub phase ends, corresponding also to an end of the double support. Based on this value and the cycle value, the double support shows a duration of 10.9%, a little higher than the standard value of 10%. By looking to the graph, it is not very clear to determine where the next sub phase (mid-stance) ends. This would be at the event corresponding to the right heel rise, which places it somewhere near the $0.3\,s$.

The terminal stance sub phase will then start, ending at the heel strike (initial contact) of the opposite foot (left foot), marked with a black dashed line at $t = 0.62\,s$. The next sub phase (pre-swing) starts here together with the second double support

stage, and both end at the right foot toe off marked with the fourth black dashed line at $t = 0.75\,s$, which gives a duration of 10% for this second double support stage. This event will also mark the end of the stance phase with 58.6% duration of the cycle gait near the standard value of 60%.

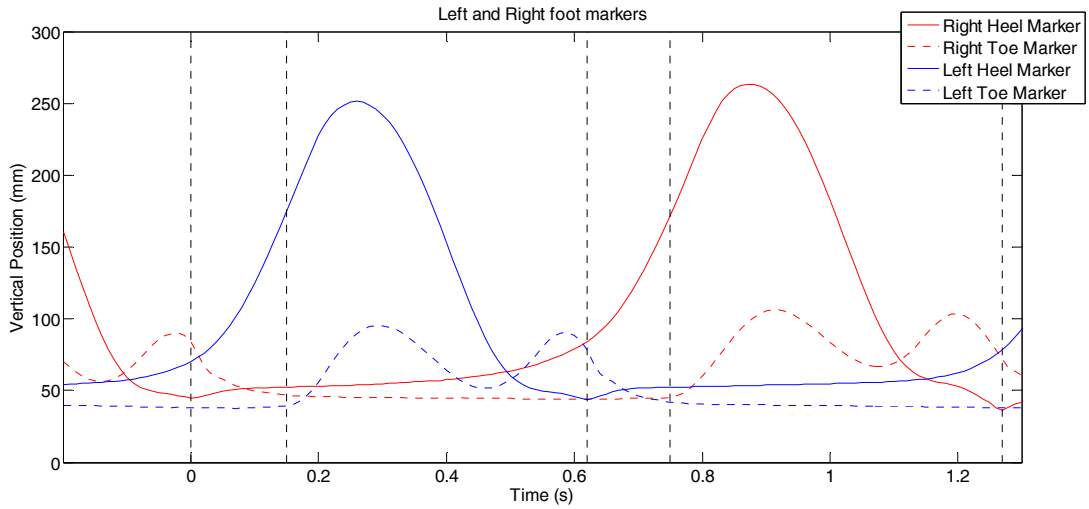

Fig. 5.19: Segment of human walking mode for a little more than a single step, with the vertical position of both feet heel and toe markers. Vertical black dashed lines mark key moments. For purpose of representation, the time starts at the first heel strike.

The swing phase, composed of the initial swing and composed of the sub phases mentioned above will then start and end with the initial contact of the right foot marked at the end of the cycle with the last black dashed line at $t = 1.28\,s$, giving it 41.4% of the gait cycle. All the values are near the standard values for human walking and it should be noticed that the little differences are most likely due to the selection of this step cycle; had another cycle been chosen, most likely there would be some small variation on these values.

As for the other gait parameters, first an average of the cycle time is computed using all the gait cycles captured. The value obtained was $1.2 \pm 0.1s$ which agrees with the values in Table 5-2. This value was used to normalize all steps to the same duration and get the other values. So, the cadence is then given using the formula of equation (5.1), resulting in a value of 101.8 ± 9.2 steps/min clearly inside the standard values. The step length was already presented in section 5.2.2, so the speed can be computed giving a

value of 1.0 ± 0.2 m/s, a little below the standard values, result of a step length also lower than the standard. Finally, the walking base value is 66.8 ± 19.8 mm.

Concerning the data given from the "robot-like" walking mode and in the same way that was done to the human walking mode, Fig. 5.20 shows a plot of the markers placed in the foot for a complete gait cycle. Before starting the analysis of the numerical data given by this figure, notice the following: one of the premises for "robot-like" gait was to walk with the feet always parallel to the ground. This restriction would result on a landing of the entire foot at the same time on the ground and on the lifting of the entire foot from the ground at the same time. This is of course totally anti-natural to the classic human gait: humans without any gait issues first land the heel, and then the rest of the foot "slowly" descends until all the foot is in contact with the ground, and on the rising movement the heel is also the first to rise and the toes will rise later.

It appears that none of the subjects was able to fully perform the intended "robot-like" gait. A closer look at the plot in Fig. 5.20 shows that on the landing phase the subject is able to land the entire foot almost at the same moment. However, on the rising phase, it is clear that the heel rises first and the toe only rises about 100 milliseconds later. It is possible that with an extensive training an almost perfect "robot-like" walking mode could be achieved, but all subjects referred that the effort required to walk like this was intensive and very tiring.

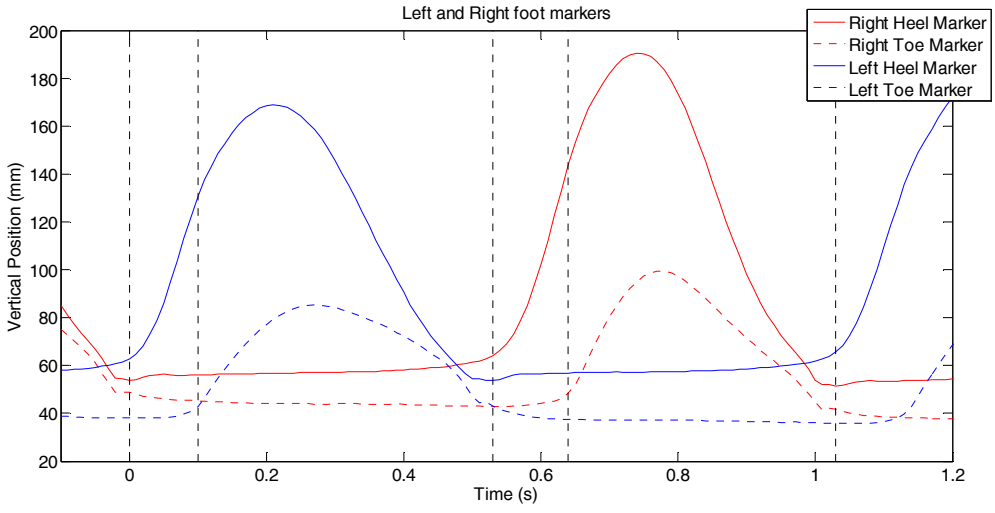

Fig. 5.20: Segment of "robot-like" walking mode for a little more than a single step, with the vertical position of both feet heel and toe markers. Vertical black dashed lines mark key moments. For purpose of representation, the time starts at the first heel strike.

The noticeable difference is that the cycle time (time that goes from the first till the last black dashed lines) is lower than that of the normal walking mode; in this cycle example, the value is $1.03\,s$, but the average value taken from all cycles is around 1.00 ± 0.06 s. Since the movement is not the same as a human gait, it makes no sense to mention all the events, periods, phases and sub phases that are present on the human movement. There are however some similarities with the human movement, like the terminal stance and pre-swing sub phases, for example. There are also a stance phase and a swing phase and of course two double support and one single support period. The first double support period starts at $t = 0\,s$ and ends on the second black dashed line in Fig. 5.20, that is at $t = 0.1\,s$. This corresponds to 9.7% of the whole cycle, which is smaller than the double support in human walking mode.

The second double support is comprised between the third and fourth black dashed lines in Fig. 5.20, starting at $t = 0.53\,s$ and ending at $t = 0.64\,s$, giving it a duration that is 10.7% of the whole cycle. These results show that even with a capture frame rate of 100fps, the precision is not high. As for the stance phase, the duration goes from the first right foot contact with the ground at $t = 0\,s$, until the toe off at $t = 0.64\,s$, giving a duration of 62.1% of the cycle time, slightly higher than the human locomotion and a corresponding 37.9% for the swing phase.

5.6 Final Remarks

In this chapter, a detailed analysis of both normal human gait and a "robot-like" gait was performed. Humans walk with their legs kept straight (when compared with typical humanoids walking) and the thighs bent inward so that the knees are almost directly under the body, rather than out to the side. This type of gait greatly facilitates upright walking during the stance phase, enabling the efficient transfer of weight between legs during the double-support phase. Instead, a "robot-like" walking gait means that the human stance foot is constrained to remain in flat contact with the ground, forcing the "bent-knee" at all times in contrast with the typical straight-legged style. This is the typical configuration adopted by most humanoid robots, since the straight-leg style of human walking requires an articulated foot.

The analysis of the kinematics data reveals significant differences in terms of typical parameters that characterize the gait pattern, such as the average value of cadence, time of cycle, stride length, foot clearance and forward velocity. In a similar way, data from the force platforms show significant changes during the gait cycle that help to gain a better understanding of the limitations imposed by the "robot-like" walking style. The analysis involved recording human gait data from a number of strides, time-normalizing the data from each stride to a standard length and averaging the data across strides. Symmetry is ensured by averaging over the corresponding data points of the left and the right legs. Accurate and efficient detection of gait events is also essential for the comparative analysis. Computational methods of event detection were developed relying on data from reflective markers placed on the heel, foot and toe through multiple frames.

This study provides evidence of the main differences between normal and robot-like walking modes. However, the ultimate purpose of this study is to extract the single demonstration, from the "robot-like" walking pattern, to be transferred to the humanoid robot. The idea is to simplify the motion retargeting problem by recording human motion data that resembles the typical gait pattern of humanoid robots.

Chapter 6
Human-to-Humanoid Motion Transfer

After gaining a deeper insight on the limitations imposed by the "robot-like" human gait, the extracted single-demonstration will be transferred to the humanoid robot, which means addressing the "motion retargeting" problem (also referred as "correspondence problem"). To attain this objective, motion transfer from humans to humanoids must respect the kinematics and dynamics differences between the two. This chapter describes the methodologies used to transfer the single-demonstration, extracted in the preceding chapter, to the humanoid robot. First, an overview of the proposed approach that is divided into an offline and an online phase is provided. In the offline phase, the motion transfer relies on spatiotemporal scaling such that human and robot scale uniformly in all dimensions and, thereby, maintain their proportions. Then, an inverted-pendulum model relating the CoP and the CoG is described such that the dynamics of the humanoid robot are projected at its CoG. Finally, a CoG-Jacobian algorithm influencing only a small number of variables that are sufficient for the main task is discussed.

6.1 Overview of the Approach

The main challenge for motion transfer from human beings to humanoid robots is balance. When human joint motion is directly applied to the robot, the humanoid robot may or may not maintain equilibrium. Therefore, the joint trajectories obtained from the human motion need to be modified such that the humanoid balance is

maintained throughout the complete motion to be imitated. Numerous research works have been carried out to map offline human motion to humanoid motion. Pollard *et al.* (Pollard et al., 2002) used a kinematic joint velocity filtering approach for the upper body motion imitation. Later, the approach was associated to motion primitives to include balance management (Nakaoka et al., 2003) and extended to whole body offline imitation. Many other offline approaches were carried in human to humanoid motion imitation by optimization (Suleiman et al., 2008; Do et al., 2008), by control (Kim et al., 2009) or by machine learning using hidden Markov models (Ott et al., 2008). The motivation for the approach proposed in this chapter results, in part, from the fact that the human demonstrations are extracted using the "robot-like" gait style in which the stance foot will be constrained to remain in flat contact with the ground. Fig. 6.1 illustrates the hybrid approach based on two deployment phases that are described in the next subsections.

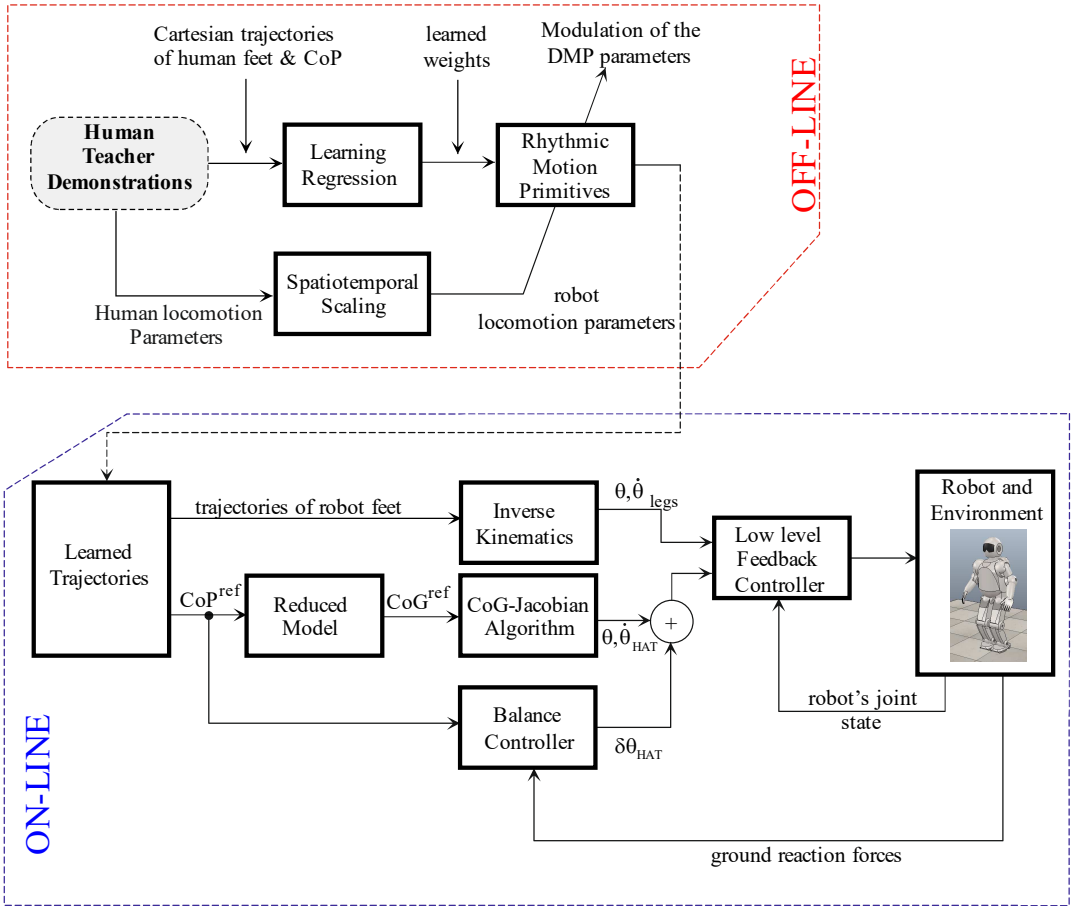

Fig. 6.1: Overview of the approach for transferring the single-demonstration from the human teacher to the humanoid robot. The Asti humanoid model is available in the V-REP simulation libraries.

6.1.1 Off-line Phase

In the first phase, the strategy that will be used is to learn offline the human teacher demonstrations, including the Cartesian coordinates of the feet and the CoP. More specifically, the idea is to learn and encode the periodic human movements with nonlinear dynamical systems and modulate them through the filtered locomotion parameters derived from spatiotemporal scaling rules. For that purpose, a set of parameters that describe the main characteristics of the locomotion in task space are extracted from the human data. These parameters are related with the movement of the lower limbs such as the step length, the hip height, the foot clearance and the forward velocity. This modulation is possible because the DMP are learned in task-space and directly relate their parameters to these task variables. As a result, the proposed encoding allows for a wide variety of human-robot geometries.

The humanoid robot used in this work is the Asti model shown in Fig. 6.2. The Asti has a height of 1.28 m, weighs 73 kg and it comprises a total of 20 rotational joints. Of these, the 6-DoFs per leg are distributed as follows: 2-DoF in the foot, 1-DoF in the knee and 3-DoF in the hip. The upper trunk includes 2-DoF in each shoulder, 1-DoF in each elbow and 2-DoF in the neck/head.

As mentioned before, the offline phase is based on spatiotemporal scaling of a set of locomotion parameters that characterize the gait pattern extracted from human demonstrations, such that human and robot scale uniformly in all dimensions and, thereby, maintain their proportions. The idea of applying scaling rules is, for example, described by Hodgins and Pollard (Hodgins et al., 1997) for automatically adaptation of existing behaviours of an animated character to a new one with different limb lengths, masses and moments of inertia. Here, the robot motion is computed from the human motion based on the following spatiotemporal scaling rules applied to the locomotion parameters: (1) spatial scaling is expressed as the ratio between human and robot body height in the vertical direction and the direction of progression, (2) spatial scaling is expressed as the ratio between human and robot hip breadth in the side-ways direction, and (3) the robot has the same cadence (steps per minute) of the original human data.

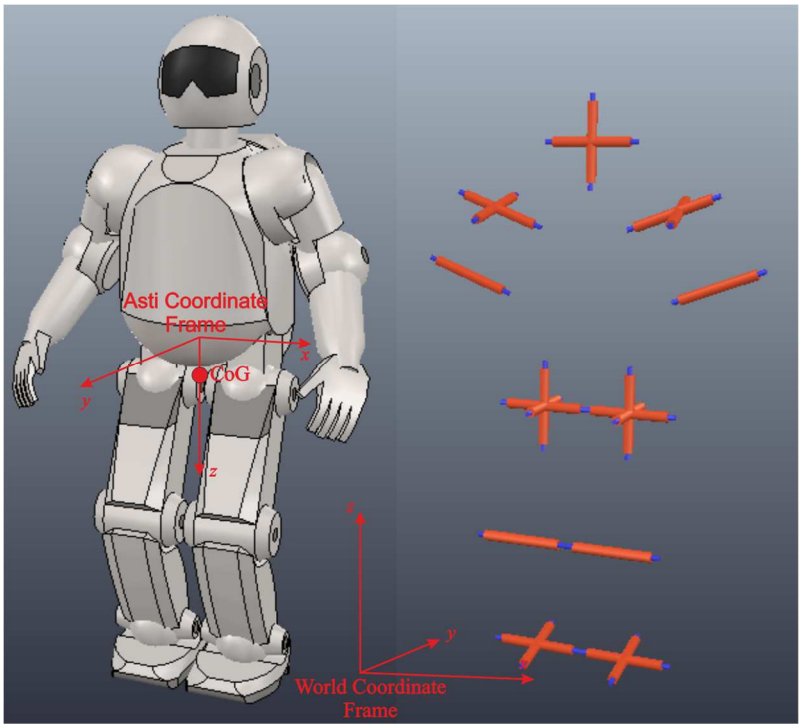

Fig. 6.2: Humanoid robot and coordinate systems in the V-REP simulation environment (left) and the joint kinematic layout of the robot model with the rotational joint axes (right).

When scaling the locomotion parameters, a similar mapping occurs in the rhythmic dynamical system since the DMP parameters are directly related to task variables. This allows generating new motions which fulfil task-specific features, while maintaining the overall style of the demonstration. The invariance property of the DMP is useful for transferring the locomotion skill when their properties are not just confined to a very local area of the original learned primitives. Specifically, it should be noted that a change of the DMP parameters creates, automatically, a rescaling of the entire movement. As a result, the limit cycle of the dynamic system represents a model of the learned model.

As mentioned before, the difference of the masses and moments of inertia will be solved in the second deployment phase. At this point, a comparison is made between human and robot mass distributions, assuming the bodies are divided into four sections: head, arms, trunk and legs. Fig. 6.3 shows the difference between robot data and the anthropometric data (Winter, 1990), when expressing the mass of each segment as a percentage of the total body mass. The most notable difference occurs at the trunk section where the Asti robot has a value far below what happens in the human case, as

opposed to what happens with the upper- and the lower-limbs. This gave rise to the decision of restricting the movement of the trunk section and the upper-limbs during the gait cycle. In line with this, the trunk section should remain in a static upright position, while the arms vertically aligned at the sides. This decision is related to two facts: the pelvic rotation during human walking shows reduced amplitude and the Asti robot is not provided with additional DoFs in the spine.

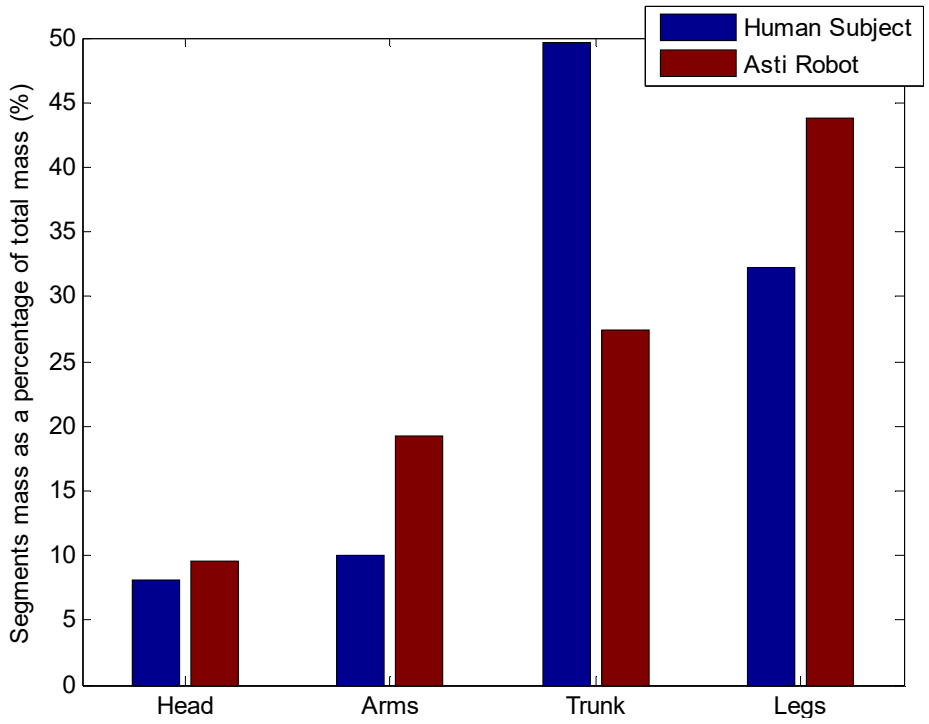

Fig. 6.3: Differences in the mass distribution between the human subject and the Asti robot as a percentage of the total mass.

6.1.2 On-line Phase

In the second phase, the learned trajectories of the robot's feet and the reference CoP will be used by the humanoid robot online, in autonomous manner, accommodating motion goals and balance constraints. On the one hand, the outputs of the DMP associated with the robot' feet are converted, through an inverse kinematics algorithm, to the desired joint trajectories used as reference input to a low-level feedback controller of the lower limbs. On the other hand, the reference CoP (stability criterion) is the input argument for a reduced model that allows computing the reference Cartesian trajectory for the robot's CoG. This reduced model (variation of the inverted

pendulum model) allows ignoring the movements of the individual limbs of the humanoid and, instead, to focus on two important points: the CoP and the CoG. In the scope of this work, the pressure point is modelled as moving along the foot by approximating the profile of the human teacher.

This implementation explores the concept of centroidal dynamics, following the same perspective already pursued by other authors when moving from the joint-trajectory based ZMP control of humanoids for direct CoM control using simple models, such as the Linear Inverted Pendulum Model (LIPM) proposed by Kajita et al. (Kajita et al., 2003). Such reduced models pave the way for the development of novel controllers that, otherwise, would be difficult to design by addressing the complex humanoid dynamics.

However, it is worth noting that, although these models are relevant at the planning stage, an approach based on a reduced model of the humanoid robot is not able to immediately provide full joint control. As soon as the main characteristics of the control approach are formulated in the reduced-dimensional space, the strategy needs to be mapped back into the full dynamic model of the humanoid. For example, a CoG-based control is only concerned with the regulation of the CoG motion. However, the final joint trajectories are subsequently obtained by imposing additional constraints.

Then, an inverse kinematics algorithm is implemented such as the CoG of the whole-body is related with the active joints through a Jacobian. The implementation follows the concept of robot kinematic control that consists of solving the motion control problem into two stages: first, the desired end-effector trajectories are transformed into the corresponding joint trajectories through inverse kinematics. Then, these joint trajectories constitute the reference inputs to some joint space control scheme. In line with this, the robot kinematics is handled outside the control loop allowing the problem of kinematic singularities and/or redundancy to be solved separately from the motion control problem.

6.2 CoM Trajectory from a Desired CoP

A number of inverted pendulum based models have allowed gaining a deeper insight into the dynamics of a humanoid robot. In general, these reduced humanoid models contain as an integral component the CoM, playing a key role in the analysis and control of the system. The centre-of-gravity (CoG) of a humanoid robot is, simultaneously, the effective location of the robot's total mass and, at the same time, the point through which the resultant gravity force acts. In other words, an enhanced understanding of the humanoid dynamics can be obtained simply by following the trajectory of its CoG and CoP.

By modelling walking with an inverted pendulum, the foot acts as the pivot point and the body's entire mass is represented, at the end of the pendulum, by a single point mass. According evidences with human motion measurements (Herr & Popovic, 2008), this model fails when assuming that the pressure exerted by the foot acts at a single fixed pivot point. This is because it incorrectly predicts the forces acting on the body's centre of mass unless the pressure point moves along the foot. In line with this, a number of progressively complex models are currently used for analysis and control (see Fig. 6.4).

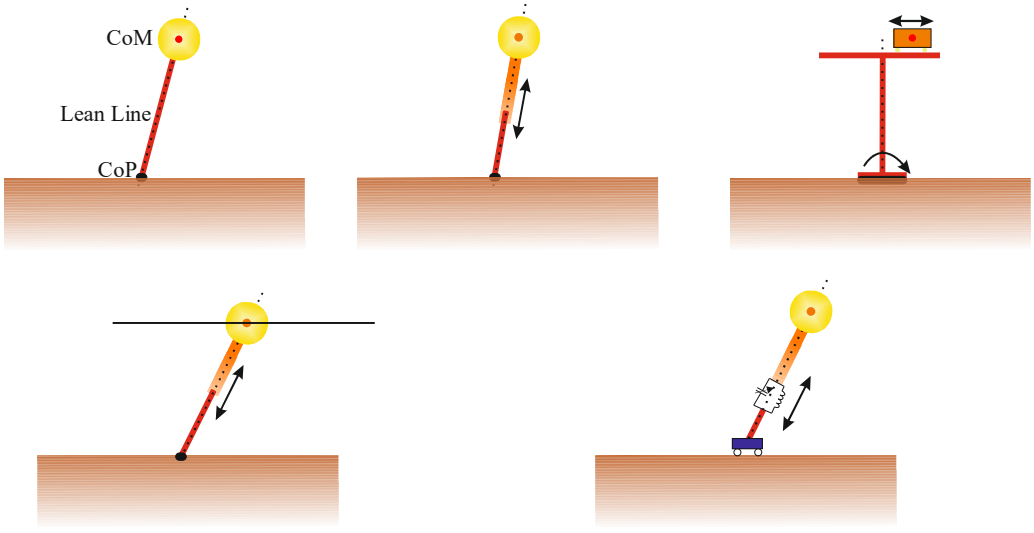

Fig. 6.4: Schematic representation of some reduced one-legged models used in human and humanoid balance and gait analysis. From top to bottom and from left to right: the rigid inverted pendulum, the telescopic inverted pendulum, the cart-table model, the linear inverted pendulum model (LIPM) and the variable impedance inverted pendulum.

The selection of an appropriate reduced model should take into account two aspects: the utility and the complexity of the adopted model. A key aspect is the physical effect that the model is intended to capture according its specific application domain. Anyway, there is more than one way to improve the simple "point mass" inverted pendulum, each with its unique pros and cons. The Cart-Table model and the inverted pendulum model are the most common reduced models used to approximate the robot dynamics. In this work, the humanoid robot is modelled based in the LIPM model. Often, this model is used in combination with desired foot trajectories. A trajectory for the centre of mass is generated so that the centre of pressure is always within the base of support.

In the scope of this work, the humanoid robot is modelled by an extension of the LIPM and the algorithm for applying it is as follows: first, foot placements are extracted from human demonstrations and the desired CoP trajectory is derived based on it, as well. Then, the CoG trajectory is calculated by the reduced model. Finally, inverse kinematics based on a CoG-Jacobian algorithm is used to find the joint angular trajectories.

The humanoid robot is subjected to both internal joint force/torque as well as external forces. The relationship between the CoP and the CoG is obtained by considering all the external forces acting on the humanoid system, which include the gravity force at the humanoid CoM, ground reaction forces (GRF) between the robot feet and the support surface and all the other interaction forces applied on the robot (*e.g.*, perturbation forces).

For a humanoid robot to be in an equilibrium state, the following equations must be held with the position of the total ground reaction force denoted by $[p_x, p_y]^T$ being underneath the foot supporting polygon:

$$\begin{aligned} p_x\left(M\ddot{z}_{COM}+Mg\right) &= \dot{L}_y + x_{COM}Mg + z_{COM}M\ddot{x}_{COM} \\ p_y\left(M\ddot{z}_{COM}+Mg\right) &= \dot{L}_x + y_{COM}Mg + z_{COM}M\ddot{y}_{COM} \end{aligned} \tag{6.1}$$

where M denotes weight of the humanoid robot, z_{COM} and $\ddot{z}_{COM}$ denote the vertical position and acceleration of the robot's CoM, z_{COM} and y_{COM} denote the position of the CoM in the x- and y-directions, respectively. L_x and L_y denote the rate of change

in the angular momentum at the CoM of the humanoid robot in the *x*- and *y*-directions, respectively. From these relations, the position of the CoP can be calculated as follows:

$$p_x = x_{COM} - \frac{z_{COM}}{g + \ddot{z}_{COM}} \ddot{x}_{COM}$$
$$p_y = y_{COM} - \frac{z_{COM}}{g + \ddot{z}_{COM}} \ddot{y}_{COM} \tag{6.2}$$

where the vertical displacement of the CoG, z_{COM}, is obtained by approximating the average data extracted from the VICON system by a sinusoidal function.

The next problem is to generate the trajectories of the CoG in the *x*- and *y*-coordinates. This is known as the inverse problem and it can be solved in two steps: first, by using a central difference approximation to discretize the second derivative of $\ddot{x}_{COM}$. Second, substituting the result in the above equation gives rise to the tridiagonal system that can be solved efficiently using the Thomas algorithm (Thomas, 1949).

6.3 Inverse Kinematics Based on the CoG-Jacobian

The preceding section described how the CoG trajectory can be planned from the desired CoP trajectory using a reduced inverted pendulum model. After this step, a computational method will be employed for relating the CoG of the whole-body with active joints by resorting to a differential mapping based on the Jacobian. More specifically, this work follows the ideas of Choi *et al*. (Choi et al., 2007) who proposed a method of real-time motion generation for humanoids with the motion-embedded CoG-Jacobian.

6.3.1 CoG-Jacobian

The Jacobian is one of the most important tools for characterizing complex robotic systems, such as humanoid robots. It is useful for developing inverse kinematics algorithms and designing control schemes. There are several works in the literature focused on the generation of whole-body motions for complex mechanisms such as humanoid robots (Choi et al., 2007; Kajita et al., 2003; Sugihara & Nakamura, 2002). A popular approach for motion planning has been to specify the task to be

accomplished by a given end-effector. Among these works, inverse kinematics algorithms which relate the whole body motion with the motion of the robot's centre of mass become popular.

In general terms, the kinematics of a humanoid robot with *n*-DoF can be expressed in terms of a nonlinear relationship between the joint vector $\boldsymbol{q}$ and the task vector $\boldsymbol{x}_G$, *i.e.*,

$$\boldsymbol{x}_G = f(\boldsymbol{q}) \tag{6.3}$$

A numerical approach to solve (6.3) can be pursued by resorting to the differential mapping, such that:

$$\dot{\boldsymbol{x}}_G = J_G(\boldsymbol{q})\dot{\boldsymbol{q}} \tag{6.4}$$

where $J_G(\boldsymbol{q}) = \partial f / \partial q$ is the CoG-Jacobian. The linearity in the configuration velocities is the important advantage of (6.4) over (6.3). This allows solving the differential kinematics by a suitable inversion of the Jacobian matrix:

$$\dot{\boldsymbol{q}} = J_G^{-1}(\boldsymbol{q})\dot{\boldsymbol{x}}_G \tag{6.5}$$

which can be integrated over time to give $\boldsymbol{q}$.

The CoG-Jacobian, for humanoid robots, was firstly proposed by Kagami *et al*. (Kagami et al., 2000) using a numerical algorithm. Later, an analytical formulation of the CoG-Jacobian was proposed by Sugihara *et al*. (Sugihara & Nakamura, 2002). The method needs considerable computation for solving an optimization problem. In line with this, Choi *et al*. (Choi et al., 2007) proposed a walking controller for improving the feasibility of a task.

6.3.2 Centre-of-Mass of the Robot System

The position of the CoM of the robot system, represented on the world coordinate frame, is the point *G* defined by the position vector *c*, given by:

$$\boldsymbol{c} = \boldsymbol{l}_o + \sum_{j=1}^{n} R_o {}^o\boldsymbol{c}_j \tag{6.6}$$

where n is the number of limbs, c is the position vector of CoM represented on the world coordinate system, and ${}^oc_j$ means the CoM position vector of the *j*th limb represented on the body centre coordinate frame. Differentiating both members of

(6.6) with respect to time, the conventional CoM Jacobian explained in (Sugihar et al., 2002b) is obtained as follows:

$$\dot{\boldsymbol{c}} = \dot{\boldsymbol{l}}_o + \boldsymbol{\omega}_o \times (\boldsymbol{c}_o - \boldsymbol{l}_o) \sum_{j=1}^{n} R_o \, {}^{o}J_{c_j} \dot{\boldsymbol{q}}_j \tag{6.7}$$

where ${}^{o}J_{c_j} \in \Re^{3\times n_j}$ is the CoM Jacobian matrix of the *j*th limb represented on the body centre coordinate frame, n_j is the number of active links of the *j*th limb, and hereafter, the relation $J_{c_j} \triangleq_o {}^{o}J_{c_j}$ will be used.

At this point, it is convenient to express the CoG-Jacobian matrix of each individual limb on the body centre frame. For the *j*th limb, this matrix can be expressed by:

$${}^{o}J_{c_j} \triangleq \sum_{k=1}^{n_j} \boldsymbol{\mu}_{j,k} \frac{\partial {}^{o}\boldsymbol{c}_{j,k}}{\partial \boldsymbol{q}_j} \tag{6.8}$$

where ${}^{o}\boldsymbol{c}_{j,k} \in \Re^3$ represents the position vector of the centre of mass of the *k*th link in *j*th limb represented on the body centre frame. The mass influence coefficient of the *k*th link in the *j*th limb is defined as

$$\boldsymbol{\mu}_{j,k} \triangleq \frac{m_{j,k}}{\sum_{i=1}^{n}\sum_{k=1}^{n} m_{j,k}} = \frac{\text{mass of } k\text{th link in } j\text{th limb}}{\text{total mass}} \tag{6.9}$$

where the CoM position of the *j*th limb represented on body centre frame is obtained as follows:

$${}^{o}\boldsymbol{c}_j = \sum_{k=1}^{n_j} \boldsymbol{\mu}_{j,k} \, {}^{o}\boldsymbol{c}_{j,k} \tag{6.10}$$

6.3.3 IK Solution with Embedded Motion

This subsection provides all the details of the kinematic resolution method of CoM Jacobian with embedded motion proposed by Choi *et al*. (Choi et al., 2007). In this work, it is assumed that the upper bodies is kept erect or slightly bend forward, while the arm movements are restricted. In this case, the humanoid robot has $n = 3$ limbs (two lower-limbs and an upper limb) and the stance leg is assumed as the base limb. Although the base limb can be any limb, it should be on the ground to support the

body. Each limb of a robot is hereafter considered as an independent limb. In general, the *j*th limb satisfies the relation

$$ {}^{o}\dot{\boldsymbol{y}}_j = {}^{o}J_j \dot{\boldsymbol{q}}_j \tag{6.11} $$

for $j = 1, 2, \ldots, n$, where ${}^{o}\dot{\boldsymbol{y}}_i \in \Re^6$ is the velocity of the end point of the *j*th limb, $\dot{\boldsymbol{q}}_j \in \Re^{n_j}$ is the joint velocity of the *j*th limb, ${}^{o}J_j \in \Re^{6\times n_j}$ is the usual Jacobian matrix of the *j*th limb, and n_j means the number of active links of the *j*th limb. The leading superscript ^{o} implies that the elements are represented on the body centre coordinate system which is fixed on the humanoid robot.

Compatibility Condition

The end-point position of the *j*th limb represented on the world coordinate is given by:

$$ \boldsymbol{l}_j = \boldsymbol{l}_o + R_o \, {}^{o}\boldsymbol{l}_j \tag{6.12} $$

where R_o is the rotation matrix of body centre frame with respect to world coordinate frame. Let us differentiate the aforementioned equation, then

$$ \begin{aligned} &\dot{\boldsymbol{l}}_j = \dot{\boldsymbol{l}}_o + \dot{R}_o \, {}^{o}\boldsymbol{l}_j + R_o \, {}^{o}\dot{\boldsymbol{l}}_j \leftarrow \dot{R}_o = [\boldsymbol{\omega}_o \times] R_o \\ &\dot{\boldsymbol{l}}_j = \dot{\boldsymbol{l}}_o + [\boldsymbol{\omega}_o \times] R_o \, {}^{o}\boldsymbol{l}_j + R_o \, {}^{o}\dot{\boldsymbol{l}}_j \leftarrow [\boldsymbol{a}\times]\boldsymbol{b} = -[\boldsymbol{b}\times]\boldsymbol{a} \\ &\dot{\boldsymbol{l}}_j = \dot{\boldsymbol{l}}_o - [R_o \, {}^{o}\boldsymbol{l}_j \times]\boldsymbol{\omega}_o + R_o \, {}^{o}\dot{\boldsymbol{l}}_j \end{aligned} \tag{6.13} $$

in which

$$ [\boldsymbol{a}\times] = \begin{bmatrix} 0 & -a_z & a_y \\ a_z & 0 & -a_x \\ -a_y & a_x & 0 \end{bmatrix} \tag{6.14} $$

By including the angular velocity, then the total velocity of the *j*th limb motion represented on the world coordinate is as follows:

$$ \begin{aligned} &\dot{\boldsymbol{l}}_j = \dot{\boldsymbol{l}}_o - [R_o \, {}^{o}\boldsymbol{l}_j \times]\boldsymbol{\omega}_o + R_o \, {}^{o}\dot{\boldsymbol{l}}_j \\ &\boldsymbol{\omega}_j = \boldsymbol{\omega}_o + R_o \, {}^{o}\boldsymbol{\omega}_j \end{aligned} \tag{6.15} $$

Therefore,

$$\begin{bmatrix} \dot{\boldsymbol{l}}_j \\ \boldsymbol{\omega}_j \end{bmatrix} = \begin{bmatrix} I_3 & -\left[R_o\, {}^o\boldsymbol{l}_j \times\right] \\ 0_3 & I_3 \end{bmatrix} \begin{bmatrix} \dot{\boldsymbol{l}}_o \\ \boldsymbol{\omega}_o \end{bmatrix} + \begin{bmatrix} R_o & 0_3 \\ 0_3 & R_o \end{bmatrix} \begin{bmatrix} {}^o\dot{\boldsymbol{l}}_j \\ {}^o\boldsymbol{\omega}_j \end{bmatrix} \tag{6.16}$$

in short

$$\begin{aligned} &\dot{\boldsymbol{y}}_j = Y_j^{-1}\dot{\boldsymbol{y}}_o + Y_o\, {}^o\dot{\boldsymbol{y}}_j \\ &\therefore \dot{\boldsymbol{y}}_j = Y_j^{-1}\dot{\boldsymbol{y}}_o + Y_o J_j \dot{\boldsymbol{q}}_j \leftarrow {}^o\dot{\boldsymbol{y}}_j = J_j\dot{\boldsymbol{q}}_j \end{aligned} \tag{6.17}$$

In our specific case, the body centre is floating, and consequently, the end point motion of the *j*th limb about the world coordinate system can be written by:

$$\dot{\boldsymbol{y}}_j = Y_j^{-1}\dot{\boldsymbol{y}}_o + Y_o\, {}^oJ_j\dot{\boldsymbol{q}}_j \leftarrow {}^o\dot{\boldsymbol{y}}_j = J_j\dot{\boldsymbol{q}}_j \tag{6.18}$$

where $\dot{\boldsymbol{y}}_o = \left[\dot{\boldsymbol{l}}_o^T ; \boldsymbol{\omega}_o^T\right] \in \Re^6$ is the velocity of the body centre represented on the world coordinate system, and

$$Y_j = \begin{bmatrix} I_3 & -\left[R_o\, {}^o\boldsymbol{l}_j \times\right] \\ 0_3 & I_3 \end{bmatrix} \text{ and } \mathrm{Y}_o = \begin{bmatrix} R_o & 0_3 \\ 0_3 & R_o \end{bmatrix} \tag{6.19}$$

where Y_j is a (6×6) matrix that relates the body centre velocity and the *j*th limb velocity, and I_3 and 0_3 are an (3×3) identity and zero matrix, respectively. $R_o\, {}^o\boldsymbol{l}_j$ is the position vector from the body centre to the end point of the *j*th limb represented on the world coordinate frame and [(•)×] is a skew-symmetric matrix for the cross product. Y_o is the transformation matrix, in which $R_o \in \Re^{3\times 3}$ is the orientation of the body centre represented on the world coordinate frame. Hereafter, the relation $J_j \triangleq Y_o\, {}^oJ_j$ will be used.

All the limbs in a robot should have the same body centre velocity. From (6.18), it can be seen that all the limbs should satisfy the compatibility condition, that is, the body centre velocity is the same and, accordingly, the *j*th limb and the *k*th limb should satisfy the following relation:

$$Y_j\left(\dot{\boldsymbol{y}}_j - {}^oJ_j\dot{\boldsymbol{q}}_j\right) = Y_k\left(\dot{\boldsymbol{y}}_k - J_k\dot{\boldsymbol{q}}_k\right) \tag{6.20}$$

From (6.20), the joint velocity of any limb can be represented by the joint velocity of the base limb and Cartesian motions of limbs. Actually, the base limb should be

chosen to be the support leg in single support phase or one of both legs in double support phase.

Expressing the base limb with the subscript 1, then the joint velocity of the *j*th limb is expressed as

$$\dot{\boldsymbol{q}}_j = J_j^+ \dot{\boldsymbol{y}}_j - J_j^+ Y_{j1} \left(\dot{\boldsymbol{y}}_1 - J_1 \dot{\boldsymbol{q}}_1 \right) \text{ for } j = 1, 2, \ldots, n \tag{6.21}$$

where J_j^+ means the Moore–Penrose pseudoinverse of J_j and

$$Y_{j1} \triangleq Y_j^{-1} Y_1 = \begin{bmatrix} I_3 & -\left[R_o \left({}^o\boldsymbol{l}_1 - {}^o\boldsymbol{l}_j \times \right) \right] \\ 0_3 & I_3 \end{bmatrix} \tag{6.22}$$

Based on the compatibility condition, the inverse kinematics of a humanoid robot can be solved by using the information of base limb like.

CoM-Jacobian with Embedded Motion

The motion of body centre frame can be obtained by using (6.18) for the base limb as:

$$\begin{aligned} \dot{\boldsymbol{y}}_o &= Y_1 \left\{ \dot{\boldsymbol{y}}_1 - J_1 \dot{\boldsymbol{q}}_1 \right\} \\ \begin{bmatrix} \dot{\boldsymbol{l}}_o \\ \boldsymbol{\omega}_o \end{bmatrix} &= \begin{bmatrix} I_3 & \left[R_o \, {}^o\boldsymbol{l}_1 \times \right] \\ 0_3 & I_3 \end{bmatrix} \left\{ \begin{bmatrix} \dot{\boldsymbol{l}}_1 \\ \boldsymbol{\omega}_1 \end{bmatrix} - \begin{bmatrix} J_{v_1} \\ J_{\omega_1} \end{bmatrix} \dot{\boldsymbol{q}}_1 \right\} \end{aligned} \tag{6.23}$$

where J_{v_1} and J_{ω_1} are the linear and angular velocity part of the base limb Jacobian J_1 expressed on the world coordinate frame, respectively. Now, if (6.21) is applied to (6.7) for all limbs except the base limb with subscript 1, the CoG motion is rearranged as follows:

$$\begin{aligned} \dot{\boldsymbol{c}} = {} & \dot{\boldsymbol{l}}_o + \boldsymbol{\omega}_o \times \left(\boldsymbol{c} - \boldsymbol{l}_o \right) + J_{c_1} \dot{\boldsymbol{q}}_1 \\ & + \sum_{j=2}^{n} J_{c_j} J_j^+ \left(\dot{\boldsymbol{y}}_j - Y_{j_1} \dot{\boldsymbol{y}}_1 \right) + \sum_{j=2}^{n} J_{c_j} J_j^+ Y_{j_1} J_1 \dot{\boldsymbol{q}}_1 \end{aligned} \tag{6.24}$$

It should be noted that when (6.23) is applied to (6.24), then the CoG motion is only related with the motion of base limb:

$$\begin{aligned} \dot{\boldsymbol{c}} = {} & \dot{\boldsymbol{l}}_1 + \boldsymbol{\omega}_1 \times \boldsymbol{l}_{c_1} - J_{v_1} \dot{\boldsymbol{q}}_1 + \boldsymbol{l}_{c_1} \times J_{\omega_1} \dot{\boldsymbol{q}}_1 + J_{c_1} \dot{\boldsymbol{q}}_1 \\ & + \sum_{j=2}^{n} J_{c_j} J_j^+ \left(\dot{\boldsymbol{y}}_j - Y_{j_1} \dot{\boldsymbol{y}}_1 \right) + \sum_{j=2}^{n} J_{c_j} J_j^+ Y_{j_1} J_1 \dot{\boldsymbol{q}}_1 \end{aligned} \tag{6.25}$$

where $\boldsymbol{l}_{c_1} = \boldsymbol{c} - \boldsymbol{l}_1$ Also, if the base limb has the face contact with the ground (the end point of base limb represented on world coordinate frame is fixed, $\dot{\boldsymbol{y}}_1 = 0$, namely, $\dot{\boldsymbol{l}}_1 = 0$, $\boldsymbol{\omega}_1 = 0$ then the CoM Jacobian matrix with fully specified embedded motions can be written like usual kinematic Jacobian of base limb

$$\dot{\boldsymbol{c}}_{fsem} = J_{fsem}\, \dot{\boldsymbol{q}}_1 \tag{6.26}$$

where

$$\dot{\boldsymbol{c}}_{fsem} \triangleq \dot{\boldsymbol{c}} - \sum_{j=2}^{n} J_{c_j} J_j^{+} \dot{\boldsymbol{y}}_j \tag{6.27}$$

$$J_{fsem} \triangleq -J_{v_1} + \boldsymbol{l}_{c_1} \times J_{\omega_1} + J_{c_1} + \sum_{j=2}^{n} J_{c_j} J_j^{+} Y_{j_1} J_1 \tag{6.28}$$

Here, if the CoM Jacobian with fully specified embedded motions is augmented with the orientation Jacobian of body center ($\boldsymbol{\omega}_o = -J_{\omega_1} \boldsymbol{q}_1$) and all desired Cartesian motions are embedded in (6.27), then the desired joint configurations of base limb (support limb) are resolved as

$$\dot{\boldsymbol{q}}_{1,d} = \begin{bmatrix} J_{fsem} \\ -J_{\omega_1} \end{bmatrix}^{+} \begin{bmatrix} \dot{\boldsymbol{c}}_{fsem,d} \\ \boldsymbol{\omega}_{0,d} \end{bmatrix} \tag{6.29}$$

where the subscript *d* means the desired motion and

$$\dot{\boldsymbol{c}}_{fsem,d} = \dot{\boldsymbol{c}}_d - \sum_{j=2}^{n} J_{c_j} J_j^{+} \dot{\boldsymbol{y}}_{j,d} \tag{6.30}$$

The CoM motion with fully specified embedded motions $\dot{\boldsymbol{c}}_{fsem,d}$ consists of two relations: a given desired CoG motion (the first term) described in the previous section and the relative effect of other limbs (the second term), in which all the given desired limb motions $\dot{\boldsymbol{y}}_{j,d}$ are embedded in the relation of CoM Jacobian. Therefore, the effect of the CoG movement generated by the given limb motion is compensated by the base limb. By solving (6.29), the desired joint motion of the base limb is obtained. The resulting base limb motion makes a humanoid robot balanced automatically during the movement of the all other limbs. With the desired joint motion of base limb, the desired joint motions of all other limbs can be obtained by (6.21) as follows:

$$\dot{\boldsymbol{q}}_{j,d} = J_j^{+}\left(\dot{\boldsymbol{y}}_{j,d} + Y_{j1}J_1\dot{\boldsymbol{q}}_{1,d}\right) \quad \text{for } j = 2,\ldots,n \tag{6.31}$$

The resulting motion follows the given desired motions, regardless of balancing motion by base limb. In other words, the suggested kinematic resolution method of CoM Jacobian with embedded motion offers the WBC function to the humanoid robot automatically, allowing various contexts and for various purposes.

6.4 Extracting the Single Demonstration

The key idea is to transfer a single demonstration from human captures performed with the VICON system into a single demonstration applied to the humanoid robot. The framework detailed in the preceding sections solves the motion retargeting problem for balance and locomotion. Fig. 6.5 illustrates the CoP recorded from the human subject when performing a "robot-like" gait (after applying the necessary scaling factor) that is used as input reference.

This plot represents the spatial evolution of the CoP with respect to the Asti reference frame, starting at the point marked with a green asterisk: the CoP quickly moves from the left foot to the right one. Then, the CoP moves over the supporting foot, but since the referential is located at the Asti coordinate frame, it seems that moves back. When the left foot reaches the ground, the CoP quickly moves in that direction, repeating an almost symmetrical form before finishing at the red cross. The movement will repeat periodically, so choosing a signal, as seen from this coordinates system, has an advantage that it can used to train for example a set of DMPs (one for each coordinate).

The inverse kinematics mapping algorithm described in Section 6.3 results in the joint angles trajectories needed to accomplish the specified task, including balance and stability. In order to evaluate the proposed approach, the joint angles are first transformed into the desired foot's trajectories (see Fig. 6.6). Then, these time courses are used for training rhythmic movement primitives aiming to evaluate the stable walking and generalization abilities. Fig. 6.7 shows a sequence of snapshots of the Asti walking with the single demonstration signal extracted from the VICON data.

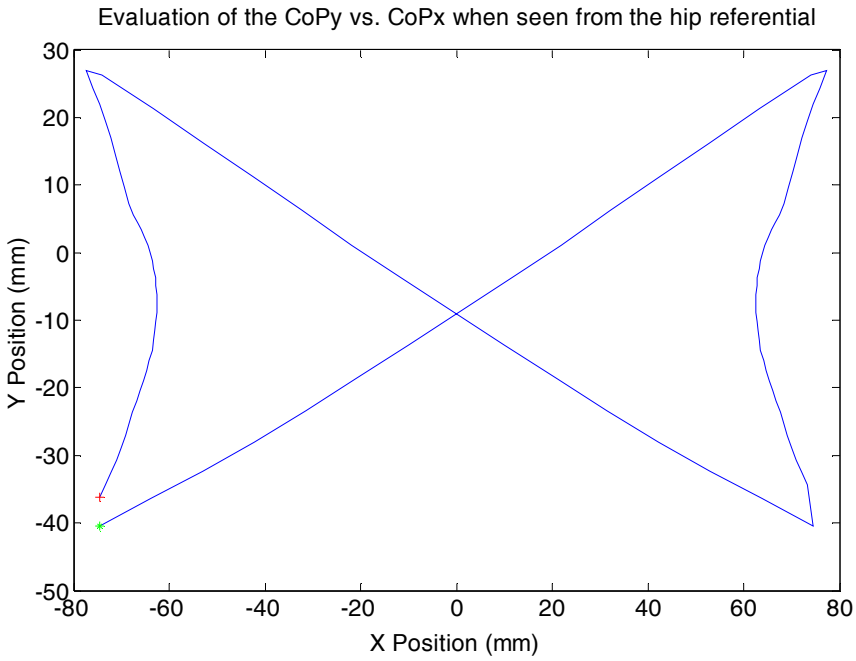

Fig. 6.5: Displacement of the CoP with respect to the Asti coordinate frame (the Y-axis points towards the movement direction) during a stride for the "robot-like" gait pattern.

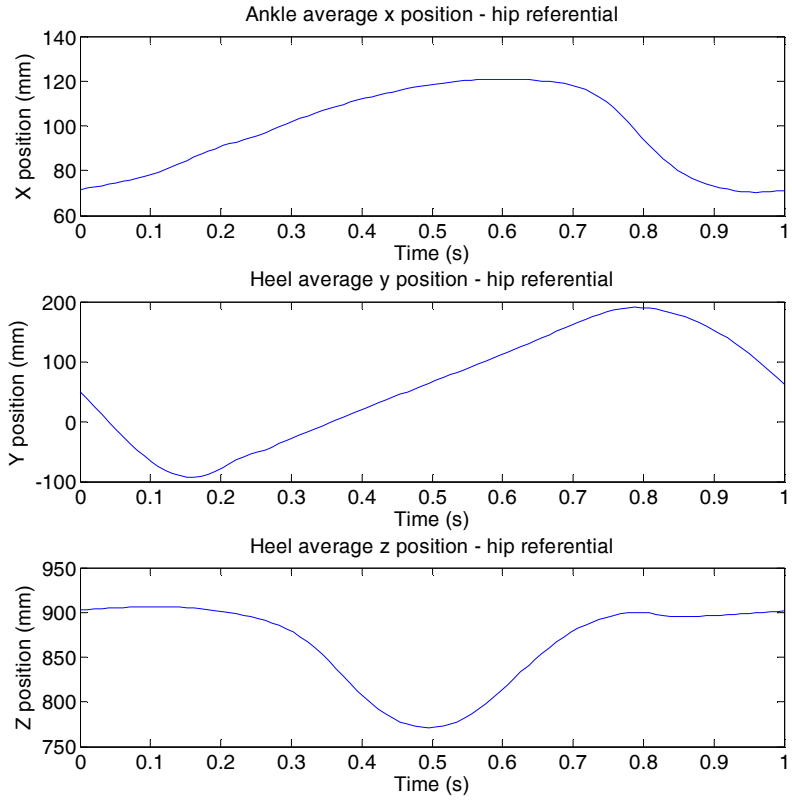

Fig. 6.6: Time courses of the *x*-, *y*- and *z*-coordinates of the robot's foot with respect to the Asti coordinate frame.

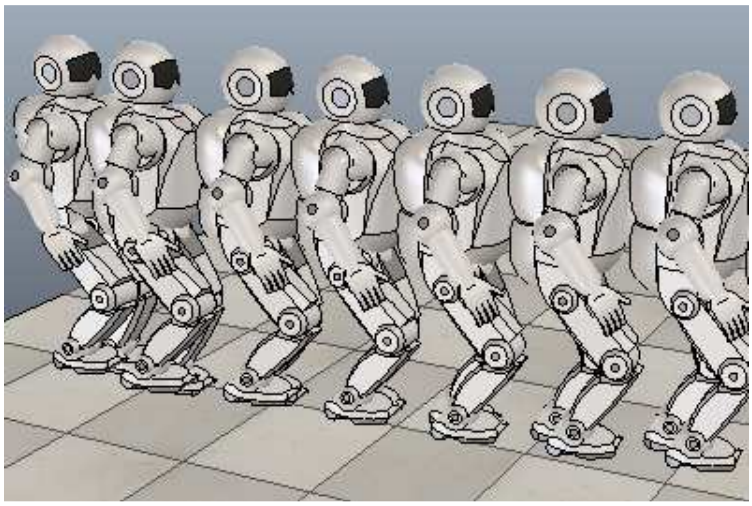

Fig. 6.7: Asti snapshots when walking with the single demonstration signal extracted from the VICON data.

The central objective of this work is to evaluate how the proposed framework based on DMP can be used to generalize and adapt this single demonstration by adjusting a few open control parameters of the learned model. More specifically, the applicability of the proposed control system will be demonstrated by numerical simulations, focusing on the adaptation of the robot's gait pattern to irregularities on the ground surface, stepping over and avoiding obstacles and, at the same time, on the tolerance to external perturbations. Having this in mind, two modifications are performed at the off-line phase by modulating the DMP parameters previously learned from the VICON data. Concretely, the forward velocity and the lateral motion are modified by trial and error aiming to improve balance and temporal symmetry of signal (this symmetry is present on the other components), because the dynamics of resulting walking gait appears to be quite inappropriate for generalization purposes. A smoothing process is also applied to all components.

After applying the online phase, the final single demonstration is superimposed with the trained DMP and the phases of double support in Fig. 6.8. The sequence of steps performed by the Asti when using the DMP trained with the single demonstration signal extracted from the VICON signal can be illustrated in Fig. 6.9.

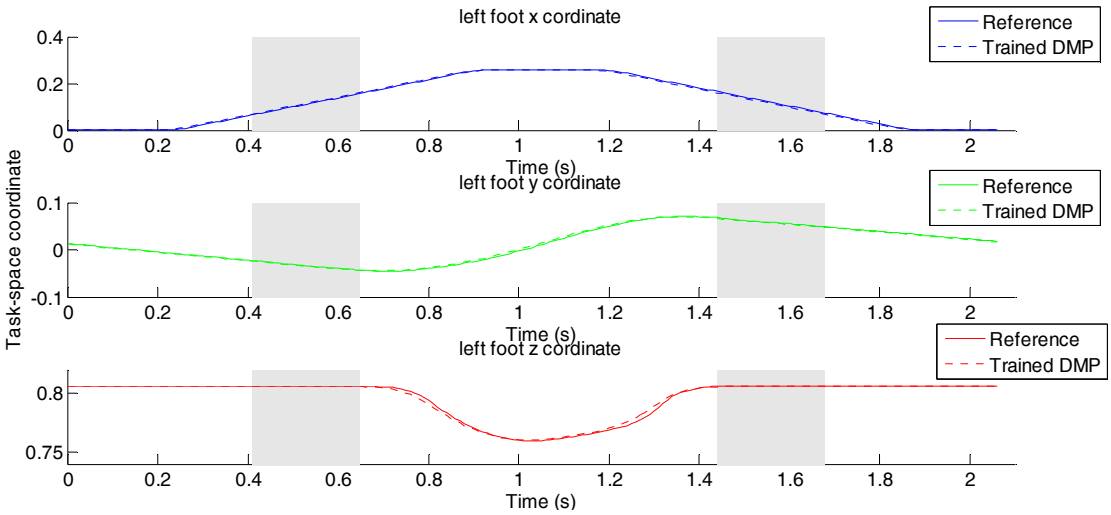

Fig. 6.8: Final single demonstration signal with the trained DMP superimposed and the double support phases represented by the grey shaded regions.

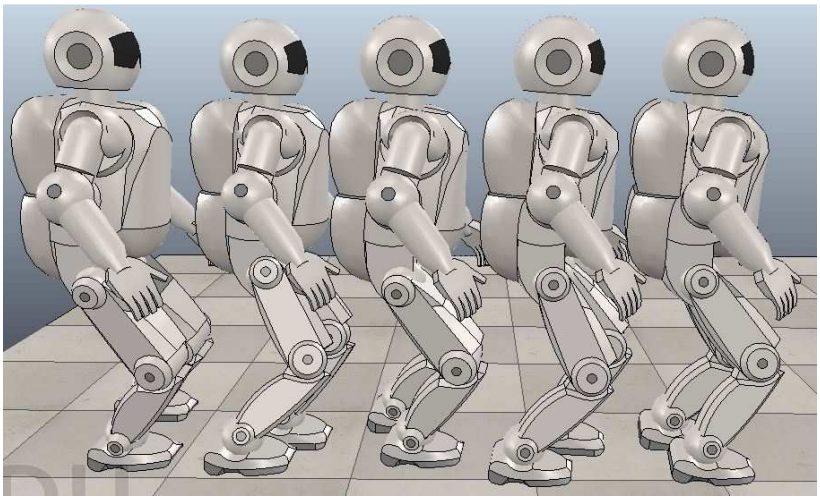

Fig. 6.9: Sequence of steps performed by the Asti when using the DMP trained with the single demonstration signal extracted from the VICON signal.

Finally, the invariance property of DMP is particularly useful when trying to generalize a learned primitive that is not confined to a very local area of the originally one. In line with this, several experiments were conducted in order to determine the range of locomotion parameters that could be used after training the DMP with the extracted single demonstration. Table 6-1 summarize these results, by keeping some of the parameters fixed and changing at least one parameter. It should be noticed that when changing some parameter, others may also be directly affected.

Fixed Parameters	Maximum S_l	Maximum V_f	Maximum C
C = 58 steps/m & F_C = 3.5 cm	20.68 cm	20.0 cm/s	--
C = 58 steps/m & F_C = 7 cm	21.09 cm	20.4 cm/s	--
S_l = 5 cm & F_C = 3.5 cm	--	6.5 cm/s	78.5 steps/min
S_l = 5 cm & 70% lat. oscillation	--	8.1 cm/s	97.08 steps/min

Table 6-1: Maximum values for step length, forward velocity and cadence obtained when changing the level parameters of the DMP trained with the single demonstration.

6.5 Final Remarks

Motion transfer from humans to humanoids must respect the kinematics and dynamics differences between the two. The motivation for the proposed novel approach results, in part, from the fact that the human demonstrations are extracted using the "robot-like" gait style in which the stance foot will be constrained to remain in flat contact with the ground. The approach proposed in this chapter is divided into an offline and an online phase. The first phase relies on spatiotemporal scaling of a set of locomotion parameters that characterize the gait pattern such that human and robot scale uniformly in all dimensions and, thereby, maintain their proportions. In the second phase, balance constraints are imposed through a reference COP used as input argument for a reduced model that allows computing the trajectory of the robot's centre of gravity (COG). After this step, a computational method relates the CoG of the whole-body with active joints by resorting to a differential mapping based on the Jacobian.

However, it is worth noting that whether such reduced models are valuable at the planning stage for obtaining the necessary single demonstration, the final implementation still needs to formulate control laws for the entire system. The actual joint trajectories are subsequently obtained by imposing additional constraints with the implementation of the balance controller. From a control perspective, the need for adaptability and stability in biped locomotion should be accomplished by combining both feedforward and feedback processes. The proposed control architecture allows

addressing the role of feedforward adaptation at the planning level without feedback control or, alternatively, a hybrid solution in which feedback can be important in compensating for disturbances common in legged systems subject, for example, to cyclic impacts with the ground.

Chapter 7
Adaptive Robot Biped Locomotion

In order to properly function in real-world environments, the gait of a humanoid robot must be able to adapt to new situations, as well as to deal with unexpected disturbances. A promising research direction to address these requirements is the modular generation of biped locomotion resulting from the combination of a set of basic primitives extracted from human demonstrations. In this chapter, a robot control framework that provides adaptive biped locomotion by combining the modulation of dynamic movement primitives (DMP) with rhythm and phase coordination is presented. Instead of selecting movement primitives from a library based on the current task context, the important concept of generalization from a single demonstration will be addressed.

One objective of this chapter is to present the prerequisites of the robot system upon which the control framework will be established. The second objective is to evaluate how the proposed framework can be used to generalize and adapt the single demonstration extracted in the preceding chapter by adjusting a few open control parameters of the learned model. The applicability of the proposed control architecture is demonstrated by numerical simulations, focusing on the adaptation of the robot's gait pattern to irregularities on the ground surface, stepping over and avoiding obstacles and, at the same time, on the tolerance to external perturbations.

7.1 Prerequisites and Research Context

The main hypothesis to verify at the end of this chapter is that a control system using modulation of a single-demonstration, encoded with DMP, can yield relevant adaptive capabilities for biped robots. For that purpose, the prerequisites and assumptions for the underlying humanoid robot system will be outlined. Then, the research context within which the study of adaptive biped locomotion occurs will be emphasized.

7.1.1 System Premises

This study makes important assumptions regarding the operation of both the perception and the actuation systems. The perception system consists of (*i*) a vision system providing reliable information about environmental conditions and changes, (*ii*) force sensors on both feet providing information about foot-ground contacts, weight distribution and estimates of the CoP location, and (*iii*) inertial sensors providing information about the orientation of the trunk section relative to the gravity vector.

This work assumes the existence of a reliable vision system that contributes for planning locomotion movements towards adaptive behaviour. Although the V-REP simulator provides vision sensors that allow extracting complex image information from a simulation scene, the implementation is based on the prior knowledge of the relative position and properties of the different elements in the environment in each instant of time. Additionally, uncertainty of measurements is expressed by additive noise characterized by a Gaussian distribution. In terms of perception system, vision will support important behaviours such as gait cycle modulation, navigation and obstacle avoidance. For example, when moving around or stepping over a perceived obstacle, the vision system will provide accurate information about the properties of the obstacle and surrounding environment that can be used to pre-plan subtle gait adjustments guiding the foot placement. In this context, an appealing feature of Cartesian trajectories is that they can be easily planned based on visuospatial information.

From the viewpoint of the actuation system, this work considers direct joint actuation driven by independent controllers. Thus, the humanoid robot is controlled using position control servo-loops based on low-level feedback units in a position control framework. This conventional motion control system considers the torque saturation assuming that each joint actuator has a limit value of torque available. This lays the groundwork for introducing the control framework that guided this research.

7.1.2 Adaptive Behavior: Study Context

The previous subsection discussed the prerequisites and the assumptions made throughout the work. This section clarifies the context of the study from the viewpoint of adaptive biped locomotion. In general, adaptive behaviours require the processing of a continuous flow of sensory information and their conversion into a sequence of actions. Adaptive behaviour can be established with closed-loop processes based on external (environment) and internal feedback, which express intent through behaviour in the environment and which evaluate the consequences of those behaviours to promote learning.

The basic structures guiding this research are the dynamic movement primitives and the coupled phase oscillators. Bearing this in mind, the aim of this research is to elucidate simple mechanisms and to suggest useful components to achieve adaptive walking, focusing on the modulation of motion primitives extracted from a single-demonstration. On the contrary, topics such as automated adaptation, robot learning or performance optimization are out of the scope of this research.

In this line of thought, adaptation may occur at two levels through trajectory modulation. On the one hand, high-level commands provide spatial adaptation guided by task specific goals and anticipatory information about the environment conditions. For example, adaptation can be induced by the need to change task specific parameters or to coordinate the activity of the limbs for synchronization or phase-locking. In general, these higher-level directives typically arise point wise as needed supported by proprioceptive and visual feedback. On the other hand, low-level sensory information provides temporal adaptation through phase and rhythm coordination. Modulating walking rhythm in response to sensory information (*e.g.*, swing-foot contact based on

ground reaction forces) is an important element to generate adaptive and robust walking.

It is worth note that all the simulations are performed by adjusting parameters of an encoding model learned from a single-demonstration without being able to change the learned model itself or incorporate a closed-loop postural control system. The resulting behaviour simply emerges from the DMPs modulation without any other interference or compensation from the postural control system. In this sense, the importance of the achieved results must be understood by comparing the range of parameters for which the humanoid robot restores the coordinated patterns (reach the goal) or the increased tolerance to external perturbations. Several experiments will be conducted to demonstrate: (*i*) the importance of spatial adaptation using DMP modulation; (*ii*) the role of changing between rhythmic and discrete DMP to allow precise foot placement and overcome terrain irregularities, and (*iii*) the role of phase and rhythm resetting for adaptive locomotion subject to perturbations.

7.2 Robot Control Framework

The approach followed in this work for controlling humanoid robots involves the use of single human demonstrations as input for teaching them to perform locomotion tasks. The low-level representation of the corresponding trajectories will be used by the robot online, in an autonomous manner, accommodating novel constraints and goals by adjusting a few open parameters of the learned model. This will generate new movements which fulfil task-specific features, while maintaining the overall style of the demonstration.

7.2.1 Control System

The global control system is depicted in Fig. 7.1. The typical scenario for the robot operation will be the following: the humanoid walks in an unknown environment, being confronted with novelty, change and uncertainty. The robot must carefully adapt its gait either guided by visual feedback or by sensory information provided by force sensors in the feet. Accordingly, the proposed control system can be seen as a

hybrid approach characterized by a homogeneous layout located between reactive and deliberative systems, that shows no conceptual break between the two layers.

The movement control system comprises two basic structures: the pattern formation system and the rhythm and phase generator system. The former is based on dynamic movement primitives (DMP) learned on task space, requiring an accurate modelling of the inverse kinematics. The latter consists of a set of coupled phase oscillators, embedded in the first one, providing adaptability through phase and rhythm coordination. Visual feedback will provide spatial adaptation guided by task specific goals and anticipatory information about the environment conditions. Gait modulation is achieved by appropriate changes of the DMP open parameters, namely amplitude, offset and frequency.

At the same time, the modulation based on the force sensors will provide temporal adaptation through phase and rhythm coordination. This will be associated to the coupled phase oscillators in each leg for more robust locomotion when dealing with unexpected disturbances. Bearing these assumptions in mind, the next subsections detail the most important subsystems, namely, the pattern generator based on DMP and rhythmic and phase coordination.

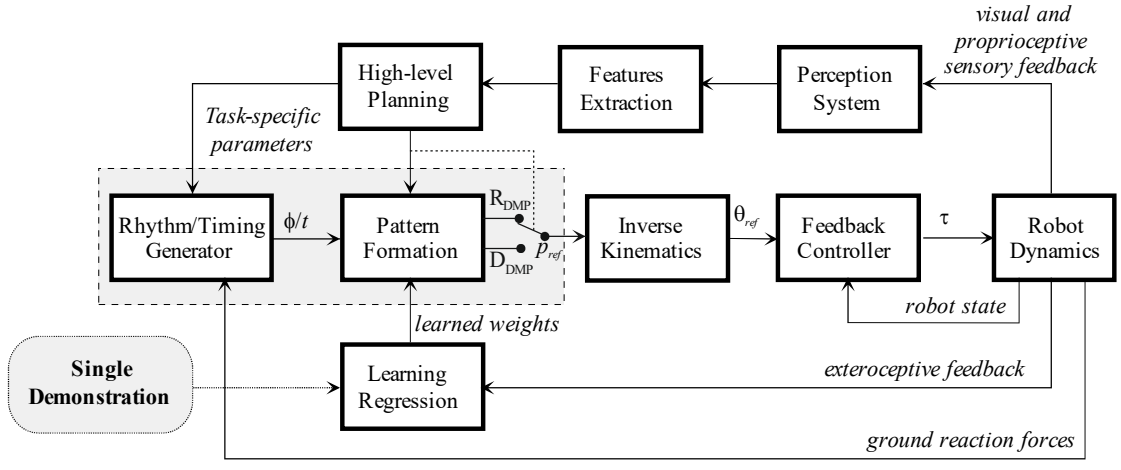

R_{DMP} - Rhythmic DMP
D_{DMP} - Discrete DMP

Fig. 7.1: Blocks diagram of the global control system.

7.2.2 Pattern Generation Based on DMP

As already mentioned, the problem of rhythmic pattern formation is addressed using dynamic movement primitives learned in task-space. An extensive study of DMP has already been presented in Chapter 4. The coordinate system is fixed to the hip section of the humanoid robot that serves as a reference frame where tasks are presented. The *y*-axis is aligned with the direction of movement, the *z*-axis is oriented downwards and the *x*-axis points towards the lateral side to form a direct system.

In line with this, a total of six DMP are learned to match the Cartesian trajectories of the lower extremities of both feet (end-effectors), using a single demonstration. Each DMP will correspond to a transformation system and all share the same canonical system. Therefore, the canonical system provides the temporal coupling among DoFs, the transformation system achieves the desired attractor dynamics for each individual DoF and the respective forcing terms modulate the shape of the produced trajectories. At the end, the outputs of the DMP are converted, through an inverse kinematics algorithm, to the desired joint trajectories used as reference input to a low-level feedback controller.

Our single demonstration signal obtained in Chapter 6 and a pre-programed reference signals are show in Fig. 7.2 (solid lines) together with the learned ones (dashed lines). The grey shaded regions show the phases of double-support. Once the complete desired movement is learned, new trajectories with similar characteristics can be generated, satisfying the desired stability conditions. These charts allow understanding the relationship between the DMP parameters (*i.e.*, amplitude and offset) and task specific parameters, such as step length S_l, hip height H_h, foot clearance F_c.

For example, the amplitudes of the DMP associated with the *y*- and *z*-coordinates are used to modify the step length and the foot clearance of the support leg (or swing leg), respectively, as identified in Fig. 7.2. In a similar way, the frequency parameter is used for speed-up or slow-down the motion, affecting the robot's forward velocity. It also should be noticed that the right foot signal can be defined from the left foot signal by defining a phase difference of 180 degree for between the canonical systems of each leg. All the experiments on the following sections where performed using both signals.

Rhythmic DMP offer the advantage of being periodic so the signal will repeat itself as long as the phase oscillator keeps on running. Also, the change of the high order parameters will easily relate to the gait parameters, like S_l, F_C and H_h when using them in the task space, and they can be changed online. The presence of a phase oscillator also allows the coupling between the oscillators of each leg, keeping them coordinated.

Despite all these advantages, it is harder (but not impossible at all) to use rhythmic DMP to do a precise foot placement and there are some situations where this can be necessary (see the examples provided in section 7.3). In this context it would be advantageous to use discrete primitives, since the high level parameters allow defining the start and end point of the movement (instead of the amplitude or baseline).

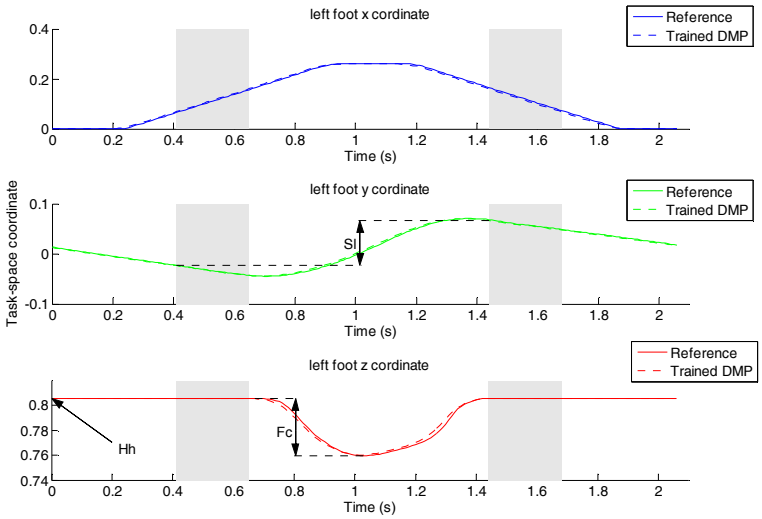

Fig. 7.2: Result of learning the single demonstration extracted in the preceding chapter for the left leg: the task is specified by the *x*, *y* and *z*-coordinates of the robot's foot in the reference frame. Reference signal (solid line) and trained signal (dashed line) are superimposed. Grey shaded regions show double-support phases.

However, three questions arise: *(i)* which signal is used to train the discrete DMP? *(ii)* How to change between rhythmic and discrete DMP? *(iii)* When to change between rhythmic and discrete DMP? As for the first question, there's no apparent reason preventing the use of the same signal that was used for the rhythmic DMP. In fact the use of this signal, as long as there's a mechanism that keeps the discrete and the rhythmic DMP synchronized, has the advantage to allow switching between them without creating abrupt transitions. However, the signal should not be used in the

same way it is used to train the rhythmic, *i.e.*, the starting point and end point for the discrete DMP would not be the same as the one defined for the rhythmic DMP. Instead, and since the objective of the use of a discrete DMP (that has no need to be periodic, there so, the start and end point don't have to be the same) is to create a mechanism for precise foot placement, the start point for the *y*-axis discrete DMP should be the start of the first DS phase (somewhere around the $0.5\,s$ in the signal present on the top of Fig. 7.2) and the end point at the start the second DS phase (around $1.5\,s$). Since at the start of the first DS phase the foot is on the ground, a precise knowledge of the current position of the foot is known(notice that the signal keeps on decreasing until $0.8\,s$ because the hip is moving forward, and not the foot that is moving). Also, because the start of the second DS phase defines when the foot hits the ground, this allows us to define where to place the foot in relation to the previous foot position and discount the fact the hip is moving (remember that these signals are seen from a referential placed on the hip).

Now, another question arises: what about the rest of the signal defined in the intervals between $0\,s$ and $0.5\,s$ and between $1.5\,s$ and $2.1\,s$? In this case, and since the signals are intended to be periodic anyway, there is no problem to create a DMP that starts at the $1.5\,s$ and keeps on going beyond the $2.1\,s$, but replicating the signal that goes from $0\,s$ until the $0.5\,s$. The only care that should be taken is the correct choice of the DMP output point in the correct time. A similar procedure can be applied to the *x*-axis DMP. As for the *z*-axis DMP, the main points of interest are the F_C and the H_h (which ultimately will define the *z* position of foot); so here the DMP should also be divided in two, but one starting at $0\,s$ and ending at the middle of the cycle ($\approx 1.05\,s$) and the other starting at the end of the first and ending at the end of the cycle. This way the start point and end point of each one will allow for adjusting the F_c and H_h values. This choice for the discrete DMP increases the number of DMP, but since encoding the DMP is a simple task, the complexity is still low.

As for the second question, and since the discrete DMPs are trained with the same signal as the rhythmic DMPs, the change between one and another will simply be done by passing to the output controller the returned signal of the selected DMP. As long as

they are kept in synchrony, there will be no abrupt transitions on the movement. Remember that the rhythmic and discrete DMP timings are defined by the canonical system expressed by equations (4.3) and (4.4), respectively.

For the final question, the answer lies simply on the environment. For example, if a robot is walking on a flat surface and is suddenly faced with some irregularities on its path (like the one found in Fig. 7.4), a change from rhythmic DMP to discrete DMP will allow it to define the precise placement of the foot (be it between the irregularities, or on the top of them).

7.2.3 Rhythmic and Phase Coordination

DMP exhibit a desirable property in the context of robot learning from demonstration; the system does not depend on an explicit time variable, giving them the ability to handle spatial and temporal perturbations. This property makes them attractive in order to create smooth kinematics control policies that can robustly replicate and adapt demonstrations. However, functional locomotion requires continuous modulation of coordination within (intra-limb coordination) and between (inter-limb coordination) legs to flexibly accommodate demands of real-word environments. For that purpose, one canonical system per leg and multiple transformation systems associated with the x-, y- and z-coordinates of the robot's end-effectors are adopted.

Intra-limb coordination results from planning trajectories in the Cartesian space, constraining the leg to act as one unit. Adaptation of inter-limb parameters is also essential to restore the symmetry of the gait cycle in order to reduce the likelihood of becoming unstable. For example, whenever one leg is constrained by external perturbations, compensatory reactions in the other legs are expected such as to restore the phase relationship among them. In particular, phase coordination between legs is provided by two separate canonical oscillators coupled such that the left and the right limbs move 180 degrees out-of-phase. Finally, rhythm modulation is achieved by phase resetting the nonlinear oscillators based on foot-contact information (a kinematic event) that depends on force sensors placed on the feet.

As a result, the dynamics of the phase oscillators for the left and the right leg, are modified according to:

$$\begin{aligned}\tau\dot{\varphi}_{left} &= \Omega - K_{\varphi}\sin\left(\varphi_{left} - \varphi_{right} - \pi\right) \\ &\quad -\left(\varphi_{left} - \varphi^{contact}\right)\delta\left(t - t_{left}^{contact} - \Delta t\right) \\ \tau\dot{\varphi}_{right} &= \Omega - K_{\varphi}\sin\left(\varphi_{right} - \varphi_{left} - \pi\right) \\ &\quad -\left(\varphi_{rightt} - \varphi^{contact}\right)\delta\left(t - t_{rightt}^{contact} - \Delta t\right)\end{aligned} \tag{7.1}$$

where K_{ϕ} is the coupling strength parameter ($K_{\phi} > 0$), ϕ^{contac} is the phase value to be reset when the foot touches the ground, $\delta(\cdot)$ is the Dirac's delta function, $t_i^{contact}$ (i = left, right) is the time when the foot touches the ground and Δt is a factor used to study the influence of delays in both sensory information and motor control.

7.3 Spatial Adaptation to Ground Irregularities

This section is dedicated to the evaluation simple strategies to achieve spatial adaptation using DMP modulation. The simplicity of the control architecture is here illustrated by examples in which the step length changes to adapt to the environment, the foot clearance increases to overcome an obstacle, the hip height is reduced to promote stability or the baseline of the oscillation is changed to define the foot lateral placement. In all the experiments, it is assumed that visual feedback provides information about the location (distance) and dimensions of the objects placed on the environment that the robot can use to modify its behaviour. Once again, it should be noted that all experiments performed hereinafter will use the same set of model and control unit parameters.

7.3.1 Adaptation to Ground Irregularities

Biped walking in irregular terrains depends on prediction about when the swing foot touches the ground. The adaptation can be performed on the fly using an estimate of the overall motion's duration or, instead, the system should react based on sensory information such as foot-contact events. In any case, the robot's behaviour needs to be modified online and the global shape of the learned movement needs to be adapted during the execution so that the robot can maintain its postural stability.

In this first experiment, the phase and rhythm resetting is disabled by the high-level directives when the humanoid robot, walking over a level surface, finds a small step of 2 cm high used to approximate irregularities of the environments. Here, the learned DMP parameters are modulated online to properly incorporate the sensory information from the force sensors mounted on the robot feet. More concretely, the dynamic event corresponds to foot-contact information at the instant of impact of the swing foot with the ground. Fig. 7.3 and Fig. 7.4 illustrate several snapshots of the robot walking response without DMP modulation and with the adjustments of the DMP parameters, respectively.

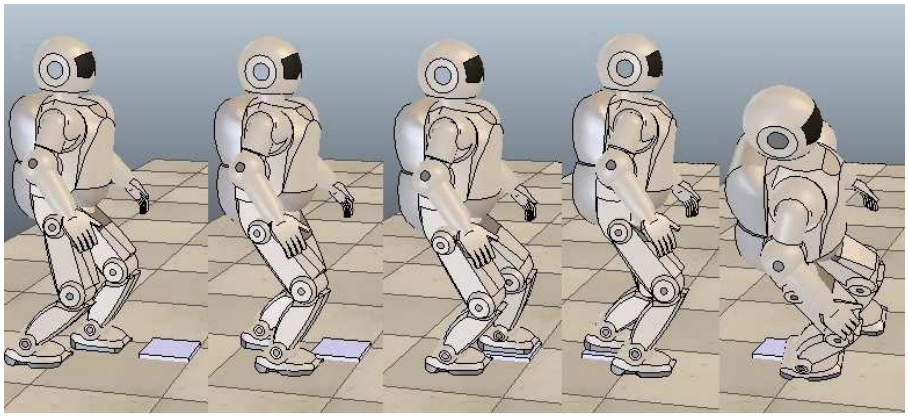

Fig. 7.3: Snapshots of the robot's response when walking on a level surface and it finds a small step 2 cm high. Without DMP modulation, balance is disturbed and the robot falls down.

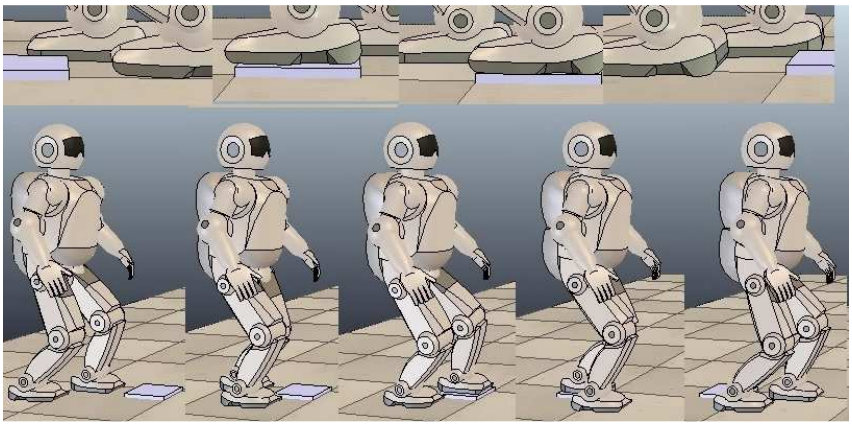

Fig. 7.4: Snapshots of the robot's response when walking on a level surface and it finds a small step 2 cm high (detail of foot placement provided on the top of the figure). With DMP modulation, the robot tolerates the irregularity.

It was found that using the locomotion pattern as defined by the learned DMP without any modulation, the robot tolerates step irregularities up to 0.5 cm height. Here, the proposed strategy is to change the baseline in the z-coordinate which corresponds to the hip height. When the left foot hits the irregularity, if nothing is done, the hip will keep on rising. This will make the right foot rise before full transfer of the weight to the left foot is complete.

Since the hip height is higher, this has also another effect: when the right foot ends its movement on the next step, the foot is not in touch with the ground (hip is higher, movement extension of the leg has not been modified); At this time, the robot starts to transfer the weight to this foot, but the foot is not in contact with the ground to support it, and so the robot will fall. When the baseline is reset to the current value and the amplitude set to zero, the rising of the hip is prevented, avoiding this phenomenon.

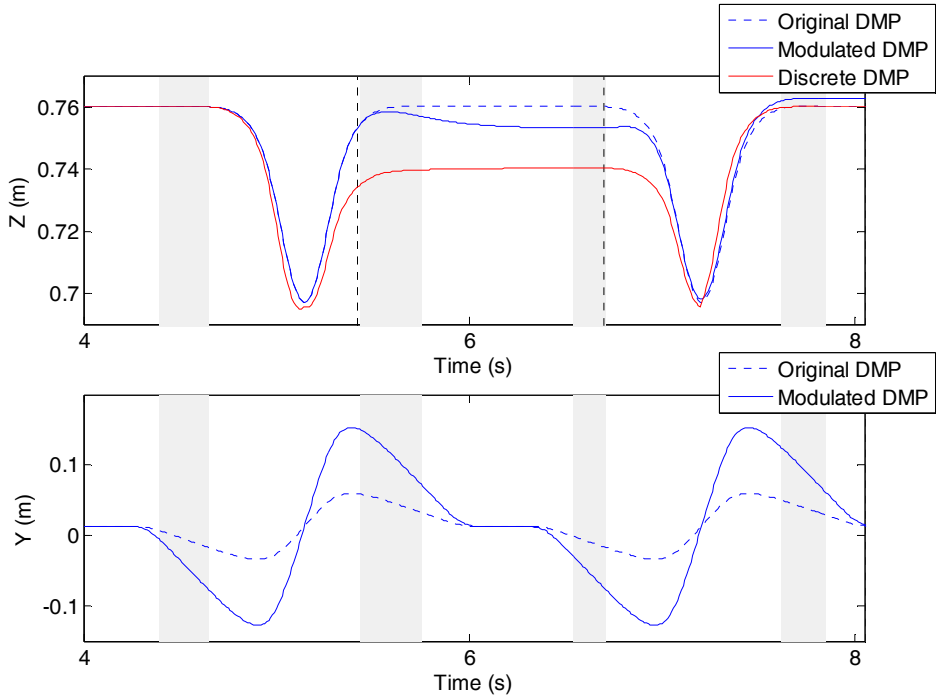

Fig. 7.5: The response of the dynamical system is highlighted in the top plot after the instant of foot-contact (black dashed line at $t = 5.4\,s$). The grey shaded regions show phases of double-support, being clear an increase in the specific stride according to the adopted strategy. The dashed line represents the original DMP without modification. The red line represents the use of a discrete DMP instead of the rhythmic for the *z*-axis.

Since DMP tends to smooth the movement, it can be seen in Fig. 7.5 that the DMP still rises a little after the foot contact (solid blue line, at $\approx 5.4\ s$), but then it slowly decays to the expected value, when the foot is already stable on the ground. This compensatory reaction allows the robot to keep stability, returning to the original movement after a short period of time marked in the plot by a vertical dashed-line (at $t = 6.7\ s$).

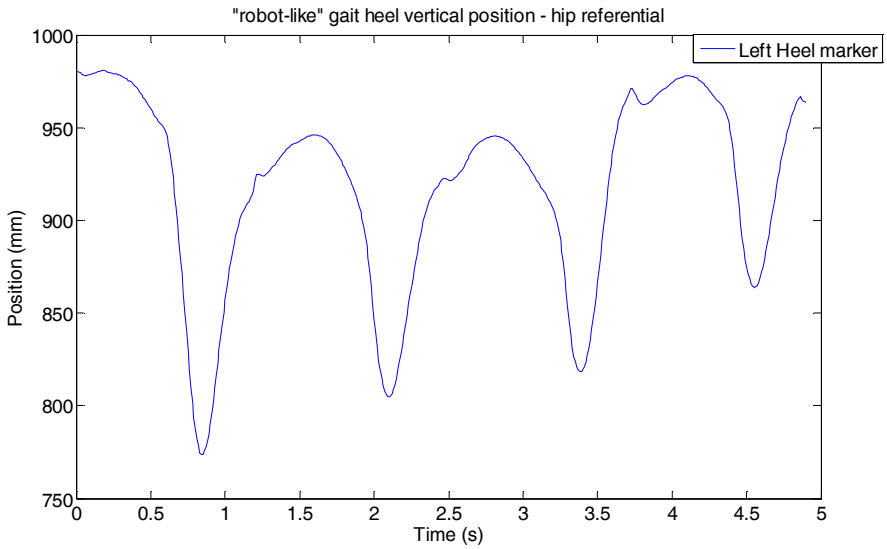

Fig. 7.6: Vertical LHEE marker position taken from a referential placed at the hip, when walking in "robot-like" mode over an irregularity placed on the path.

Looking at the heel trajectory (see Fig. 7.6) captured with the VICON system for the "robot-like" gait when overcoming an obstacle (situation similar to the one presented here), confirming that the devised strategy is consistent with what is performed by the human subject. In fact, at the beginning, the hip height is around 990 mm ($t = 0\ s$) and between $t \simeq 1\ s$ and $t = 3.5\ s$ the height is reduced to around 940 mm. This corresponds to two steps taken over an obstacle placed on the left foot path with a height of 50 mm. Finally at $t = 3.6\ s$ the hip height is resumed to the original value.

It should also be noticed that the step length is modified by changing the amplitude of the DMP on the direction of the movement (see Fig. 7.5, bottom). This change is based on the assumption that the visual feedback provides the robot constant information about the irregularity position and distance from the foot. The robot has also information about the maximum step length it can perform, and based on the

distance from the irregularity, it adjusts the step length so that on the next step the foot will land on the top of the irregularity. Also, typically decisions that involve changes on the step length are performed on the double support phase to promote stability of the robot.

7.3.2 Combining Discrete and Rhythmic Primitives

As mentioned before, one problem of biped gait generation has been, so far, the development of performant locomotion according to specifications. For example, it is possible to generate rhythmic locomotion, but it is difficult to achieve precise foot placement when working in a real world environment. This subsection discusses the solution to overcome this problem by combining rhythmic and discrete DMPs.

In line with this, the previous experiment is repeated, but the robot behaviour results from combining discrete and rhythmic primitives. Instead of modulating the rhythmic DMPs, an initial switch from rhythmic to discrete is performed, followed by the return to the rhythmic state after having overcoming the irregularity. This switch is represented by the red line in Fig. 7.5, showing the response of the dynamical system with the exchange from the rhythmic to the discrete primitives and back again to the rhythmic one.

Notice that in this case, since the final hip height can be controlled, the value for the hip is now lower than the one given by the modulated rhythmic. This promotes a better stability to the movement, since the hip height can now be reduced in the amount equal to the obstacle height. Several experiments where performed, finding that by using the change to discrete DMP instead of the simply modulating the rhythmic, the maximum height for the irregularity could be increased from 2.5 cm up to 5 cm. An example of the robot overcoming a 5 cm tall irregularity is shown in Fig. 7.7. A few more experiments performed found that the other dimensions of the irregularity could be reduced down to 11 cm $\times$ 6 cm (for reference, the Asti foot size is 16 cm $\times$ 22 cm).

Based on the possibility of changing between rhythmic and discrete DMPs for allowing precise foot (and hip height) placement, a more complex scenario was built involving two irregularities with different heights. Fig. 7.8 shows a sequence of

snapshots, where the trajectory performed by the robot is visible. On the right top of the first 4 snapshots, a detailed frontal view of the foot placement for that snapshot is visible. In the same image, on the two first frontal view of the foot, it is clear that the right foot is not aligned with the irregularity ahead, and so a correction will be necessary.

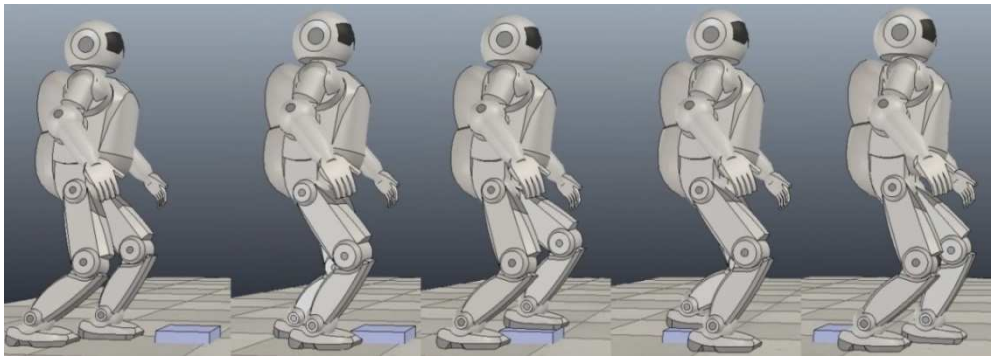

Fig. 7.7: Snapshots of the robot's response when walking on a level surface and it finds a small step 5 cm high on the path that could disturb its balance.

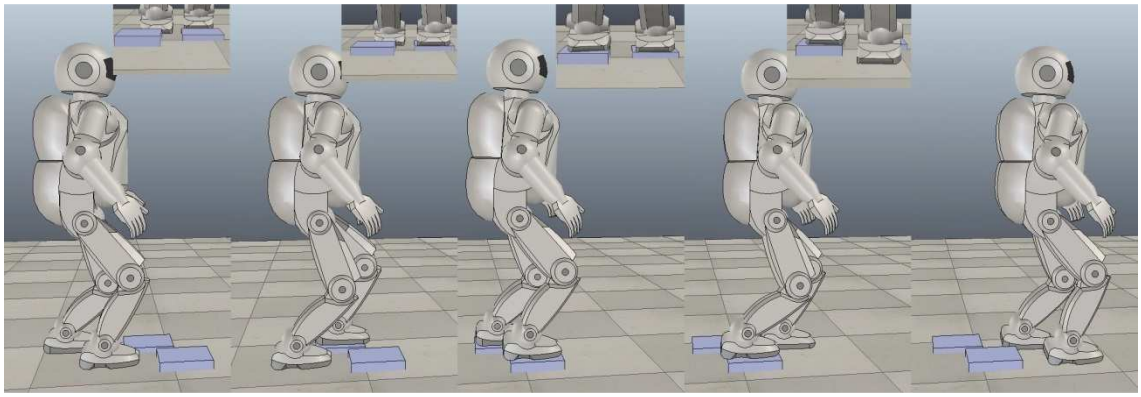

Fig. 7.8: Snapshots of the robot's response when walking on a level surface and it finds 2 irregularities with different heights on the path of each foot. On the top right corner there's a detail frontal view of the foot placement.

Due to the complexity of this path, the robot performs many changes in all the DMP so each one will be detailed independently. Fig. 7.9 shows the time evolution of the DMP related with the *z*-axis where the key events are marked with black dashed lines:

- At $0.47\,s$ (first of the black dashed lines), the hip height is reduced. This is done since it will allow for a bigger foot clearance and it will increase the stability;

- At $2.7\,s$ the foot clearance is increased in order to give some room that will allow the foot be placed on top of the first irregularity. Also, this is only done at this moment to give some time for the system to react to the first change described above;
- At $5.15\,s$ the left foot is now starting descending to the irregularity, so the rhythmic is replaced by a discrete DMP that has been synchronized with the DMP from the beginning. The goal parameter of this discrete DMP has been adjusted as the previous hip height minus the height of the obstacle. As already explained, this will prevent the rise of the hip before the transfer of the weight and balance to the left foot is concluded. If this was not done, the right foot would start to rise with the weight of the robot still on it and the robot would lose its balance;
- At $5.75\,s$ the weight is now all on the left foot, but there is another irregularity to overcome by the right foot. So, at this moment the goal of the discrete DMP associated with the left foot is adjusted to raise the hip so that the right foot can be placed on the top of the irregularity on its path;

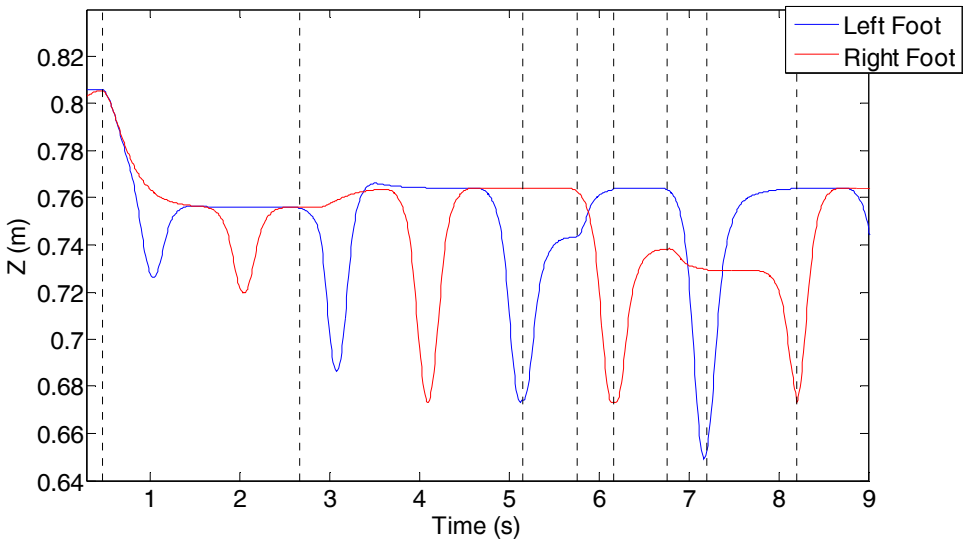

Fig. 7.9: Output of the dynamical system for both feet and the *z*-axis. For simplicity, the original DMP is not shown. Black dashed lines mark key events.

- Since now there is also an irregularity on the path of the right foot, at $6.16\,s$ the DMP associated with the right foot is commuted from rhythmic to discrete.

This discrete DMP has the goal parameter defined as the result given by the current hip height for left foot minus the difference of heights between the irregularities;

- At $6.76\,s$ two important and connected changes happen: since this is the moment the left foot "leaves" its irregularity, the hip height must be decreased, or else when the left leg "fully extends", it will not be touching the ground when the weight transfer starts, making the robot lose the balance and fall; by lowering the hip height this is avoided, but has a side effect that is the left foot hitting the irregularity that is about to leave; to avoid this the foot clearance of the left foot is also increased at this moment;
- At $7.2\,s$, the foot clearance of the left foot is resumed to the previous values;
- Finally, at $8.2\,s$ the right foot has exited the irregularity and the robot can now switch to the rhythmic DMP again.

The response of the dynamical system on the *y*-axis is shown in Fig. 7.10 and the key moments marked with the black dashed lines correspond to the following changes:

- At $2.87\,s$, based on the information given by the perception system, the robot adjusts the step length to a value that will guarantee that the left foot will be placed on top of the first irregularity;

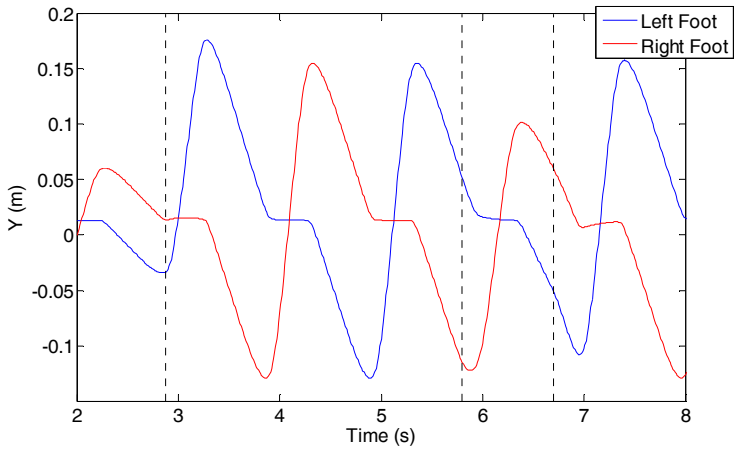

Fig. 7.10: Output of the dynamical system for both feet and the *y*-axis. For simplicity, the original DMP is not shown. Black dashed lines mark key events.

- This adjustment of the step length will not guarantee that the right foot will be correctly placed on the top of the second irregularity, so at $5.8\,s$ the robot adjusts the step length only for the right foot;
- Finally, at $6.7\,s$ the step length of the right foot is resumed to the previous value in order to guarantee that the right foot will clear the irregularity that is just leaving.

Fig. 7.7 showed on the detailed view of the feet that the right foot is not aligned with the irregularity that it is on its path. This requires a correction on the DMP related with the movement on the *x*-axis and the output of the dynamical system related with this foot and axis is shown in Fig. 7.11 and two events occur:

- At $5.8\,s$, the baseline of the DMP is changed. This will force the right foot to move to the right and in this way will be placed correctly on top of the irregularity right ahead of it. Notice that this change is performed exactly when the foot is leaving the ground;
- At $6.7\,s$, the baseline of the DMP is resumed to the previous value. At this instant, the right foot is on the ground and the left foot has just started to rise. This will then force the left foot to move to the right, getting closer to the right foot and avoiding the robot to walk with the legs spread.

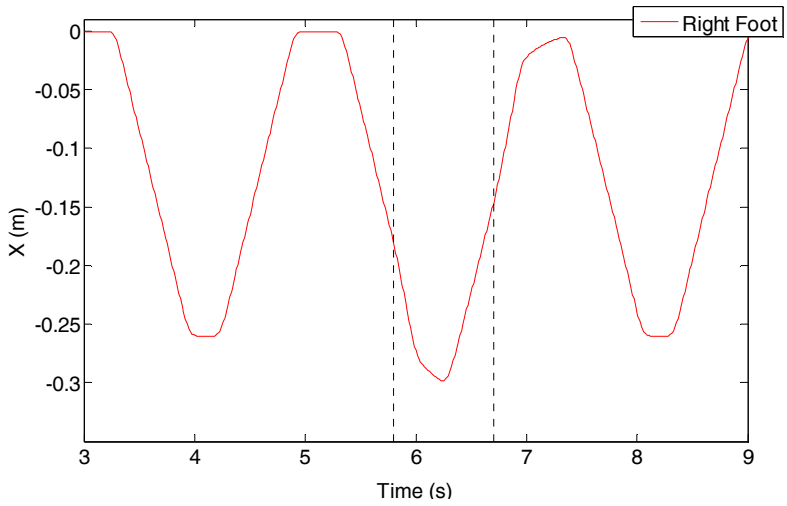

Fig. 7.11: Output of the dynamical system for the right feet *x*-axis. For simplicity, the original DMP is not shown. Black dashed lines mark key events.

Since one of the experiments performed in the VICON lab was similar to this scenario, some results from the kinematics analysis can be compared to human walking. For comparison purposes, Fig. 7.12 shows the heel markers position when seen from a referential placed on the hip. Some similarities are found, such as:

- The increase of the foot clearance near the $3.5\,s$;
- The hip height reduction at $3.6\,s$, when stepping on the first obstacle, followed by a rise when the right foot is rising
- The hip height reduction when stepping the second obstacle (height higher than the first) around $4.2\,s$.

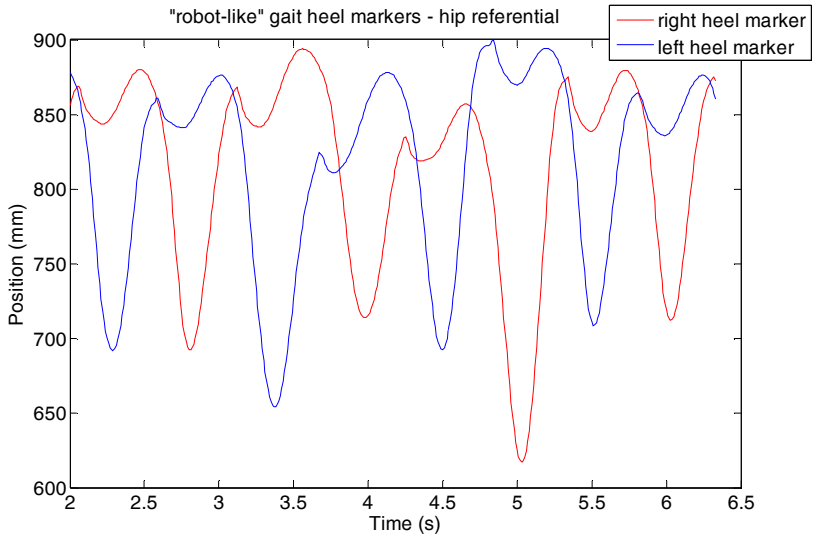

Fig. 7.12: Left and Right heel markers position seen from a referential placed on the hip, when walking on "robot-like" gait and stepping in two obstacles with different heights.

7.4 Anticipatory Adaptation for Obstacle Avoidance

This section will evaluate the performance of the proposed control system by examining anticipatory adaptation for three different kinds of obstacles found by the robot during walking: stepping over obstacles, overcoming a narrow path and turning to avoid an obstacle. In this context, the robot system is supposed to receive visual information regarding the obstacle location in order to modulate the basic gait pattern.

7.4.1 Stepping over Obstacles

Several computer simulations of varying heights and proximity were conducted. Fig. 7.13 shows a sequence of captured images of the robot stepping over a 5 cm obstacle height. The obstacle, placed at an arbitrary location, is cleared by the sequential modulation of the following parameters: the step length and the hip height when approaching the obstacle, and the trajectory of the swing foot (foot clearance) while stepping over the obstacle.

Fig. 7.14 depicts the response of the dynamical system during the anticipatory modulation, showing how the adaptation of the locomotion parameters is achieved when changing the DMP of the *y*- and *z*-coordinates of the left foot. The instants in which occurs the DMP modulation are marked with vertical dashed lines. First, at $t = 0.5\,s$ the hip height is reduced to promote increased stability. Notice that this change is performed when the robot is on the double support phase. At $t = 2.7\,s$, the step length is adjusted to allow the correct foot placement before the obstacle.

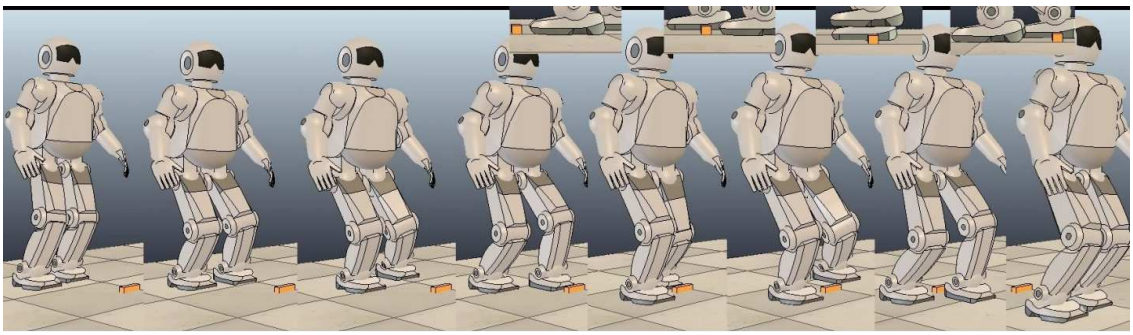

Fig. 7.13: Snapshots of the robot's response when avoiding an obstacle 5 cm high. During the motion, the robot system has available visual information to estimate the obstacle location and height. The top plots show close-ups of the interesting parts.

Once again, relying on the information provided by the perception system, the step length is chosen so that when the foot is passing over the obstacle, it will be at the maximum foot clearance. At the same time, the foot clearance is increased for the first time. Notice these changes occur only after the robot will have completely lowered its hip and is more stable. Later, at $t = 3.8\,s$, the foot clearance is re-adjusted to the obstacle height, based once again on the information provided by the perception system.

Finally, at $t = 6\,s$ the humanoid robot adopts the original step length and foot clearance as encoded in the originally learned DMP.

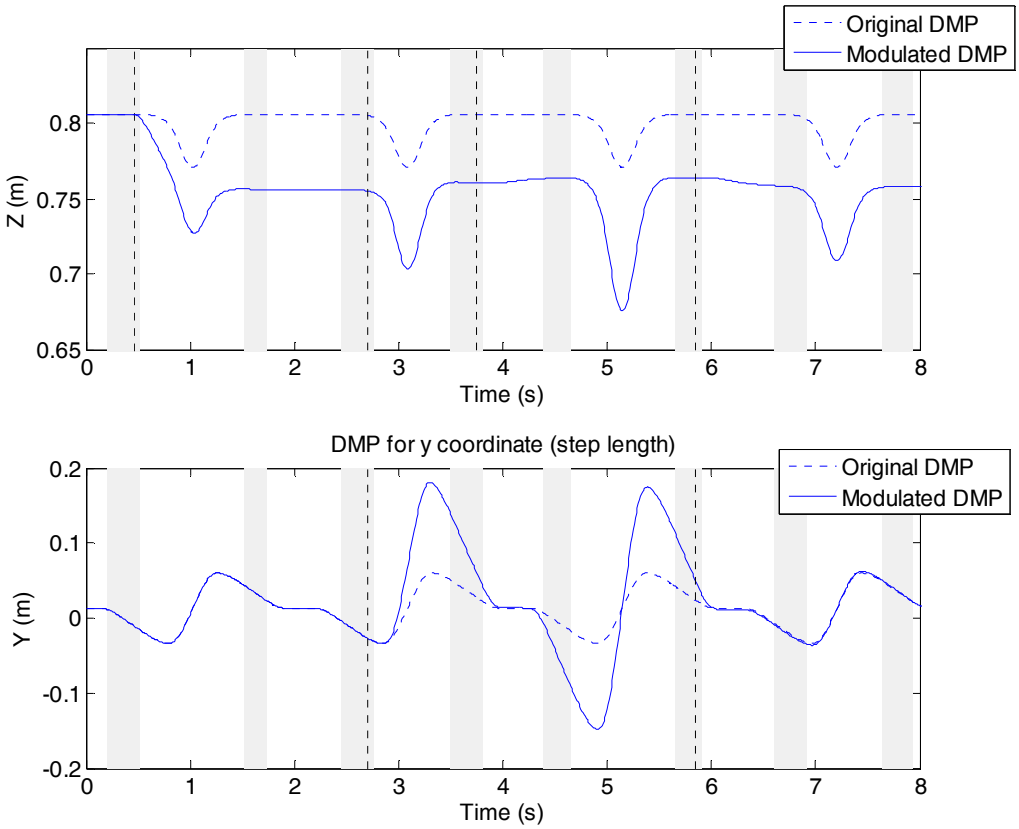

Fig. 7.14: The response of the dynamical system during anticipatory modulation of the DMP parameters: the top and bottom plots correspond to modulations associated with the *z*- and the *y*-coordinate, respectively. Vertical black dashed-lines mark the relevant instants and the gray shaded regions show phases of double-support. The blue dashed line represents the original DMP without modifications.

7.4.2 Overcoming a Narrow Path

A similar example of the use of DMP modulation to biped locomotion is shown in Fig. 7.15. Here a small wall is on the path of the robot and a narrow opening is available that allows the robot to go through. The strategy used is to stop the forward movement before reaching the wall, take a few steps to the side, so the robot is aligned with the opening on the wall and then resume the forward movement. As before, the robot is supposed to receive visual information regarding the obstacle and the opening placement.

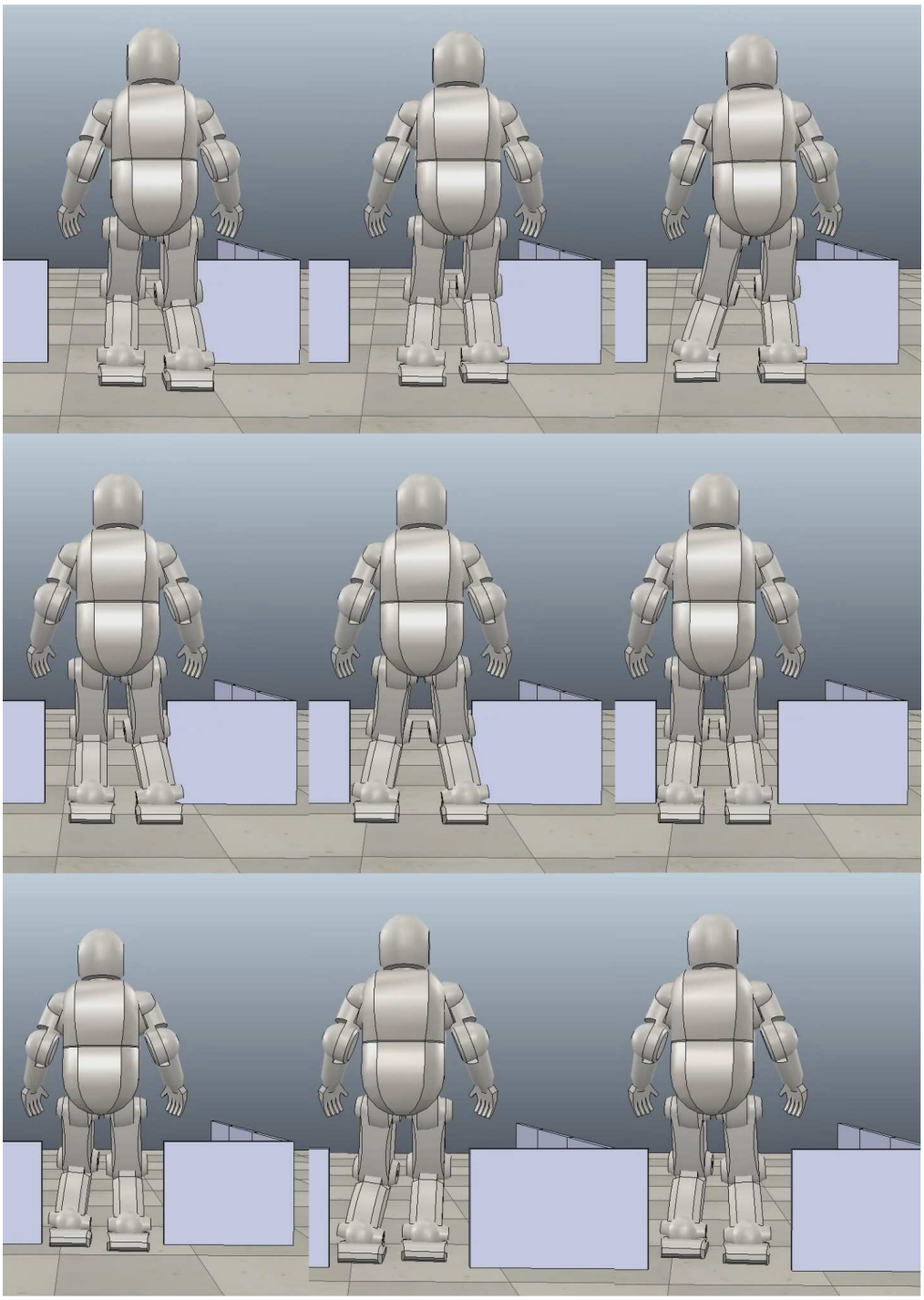

Fig. 7.15: Snapshots of the robot behaviour when overcoming a narrow path.

The response of the dynamical system is shown in Fig. 7.16, showing how the adaptation of the locomotion parameters is achieved when changing the DMP of the *x*-coordinates for the right foot and *y*-coordinates for both feet. As in previous examples the black dashed lines mark relevant moments. At $t = 2.9\,s$, the amplitude of DMP for the *y*-coordinate is set to zero, preventing the robot to proceed forward. Also, the

baseline of the *x*-coordinate is adjusted by -0.1 m. Since at this moment the right foot is on the ground, this action will leave to a shift to the left of the left foot.

The result of this action can be seen on the 3rd snapshot on the top row in Fig. 7.15, where the robot appears with the spread legs. At $t = 3.9\,s$ the baseline is resumed to the previous value. Since now it is the left foot that is on the ground, this procedure will make the right leg (and by consequence the body of the robot) shift to the left. These two procedures are repeated once again at $t = 4.93\,s$ and $t = 5.97\,s$, leaving to a second step on the left lateral direction (see the 2nd row in Fig. 7.15). Now, since the robot is aligned with the opening on the wall, the walking forward can be resumed by re-setting the amplitude of the *y*-coordinate of the DMP for both feet, which is done at $t = 7\,s$.

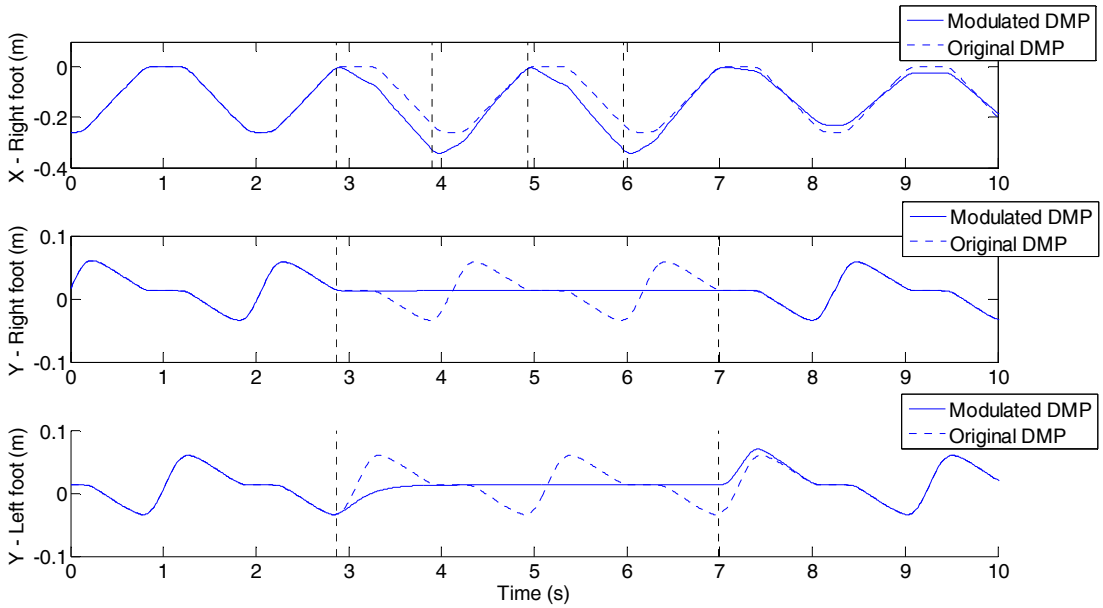

Fig. 7.16: The response of the dynamical system during anticipatory modulation of the DMP parameters: the top and center plots correspond to modulations associated with the *x*- and the *y*-coordinate for the right foot, respectively and the bottom plots correspond to the *y*-coordinate for the left foot. Vertical black dashed-lines mark the relevant instants. The blue dashed line represents the original DMP without modifications.

7.4.3 Turning to Avoid an Obstacle

Another example of the use of DMP modulation is shown in Fig. 7.17 and Fig. 7.18, where a transition from straight walk to curved walk allows obstacle avoidance. The turning motion is accomplished by modifying the relative step length of each leg, as

well as the corresponding foot clearances. This strategy differs from the human curved walking where the turning motion relies on the trunk rotations using the hips. Instead, the robot turns with a smooth curve using the rotational moments on the feet that lead to slipping to a new direction.

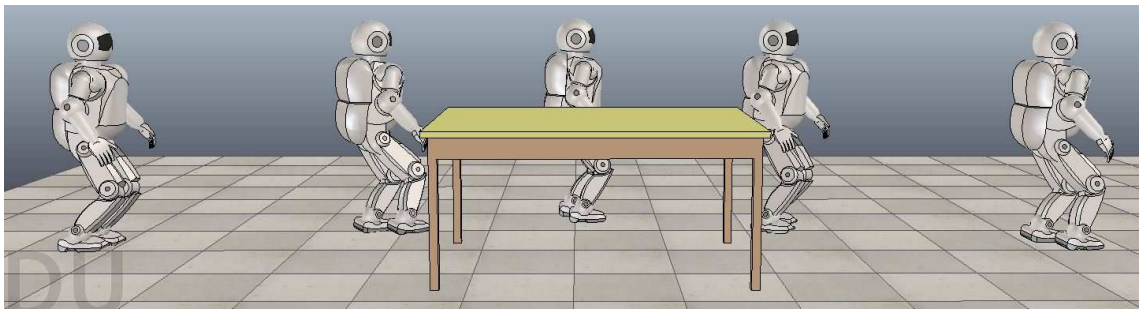

Fig. 7.17: Sequence of images showing the robot turning to avoid an obstacle.

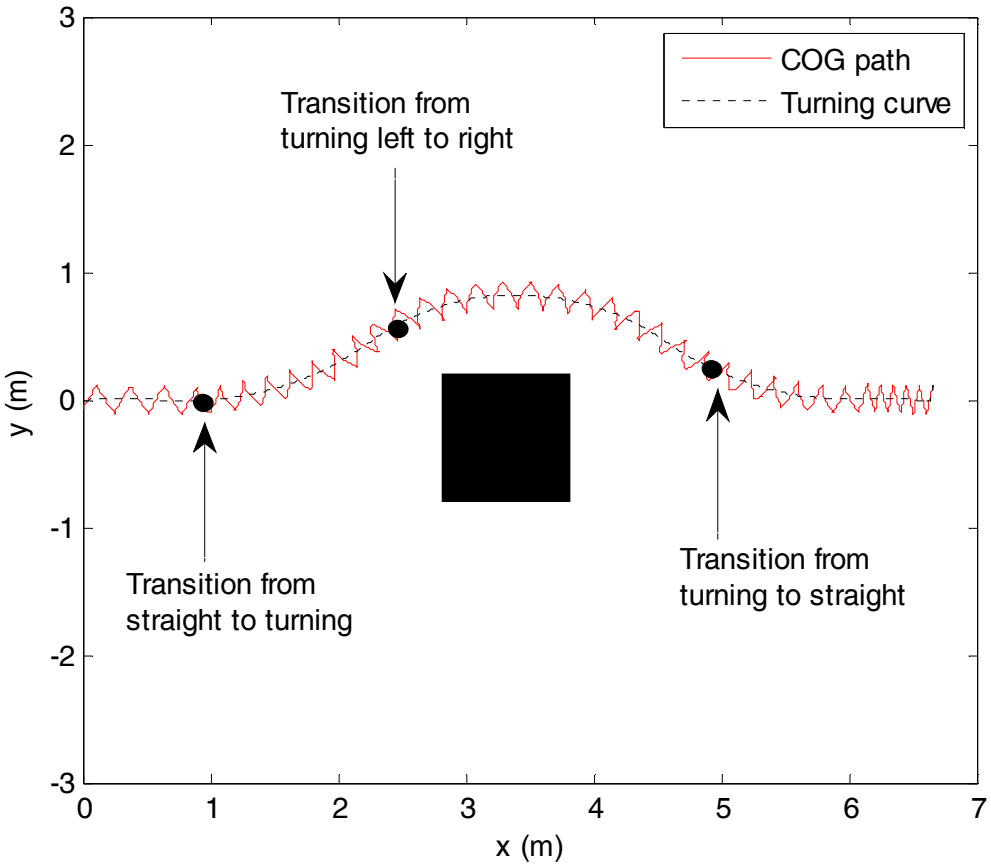

Fig. 7.18: View of the movement path of the robot's CoG projected on the ground with the corresponding turning curve. The black box represents an obstacle placed on the path.

7.5 Temporal Adaptation Using Phase Resetting

Closer to the concept of phase transition regulation in vertebrates, adaptability has been achieved through the regulation of the stance and swing phases by Righetti & Ijspeert, Maufroy and Matos & Santos (Righetti & Ijspeert, 2008; Maufroy et al., 2010; Matos & Santos, 2014). Many other researchers have explored the role of phase resetting for the generation of adaptive biped walking based on foot-contact information using theoretical models and physical robots (Nakanishi et al., 2004b; Aoi & Tsuchiya, 2006; Righetti & Ijspeert, 2006). Most of the reported advantages of phase shift and rhythm resetting are achieved or maximized when the robot is subject to external unpredictable perturbations.

Our study pursues this dimension of the problem by providing a deeper insight on the influence of the phase reset to increase robustness to environment changes and external forces. Furthermore, it is evaluated how much tolerance to external forces can be gained by using the phase shift in a system subject to delays present in all stages of the sensorimotor system, from the delay in receiving sensory information to the delay in the actuators responding to motor commands.

7.5.1 Robustness to Environment Changes

In this experiment, it is examined how the phase reset of the canonical oscillator provides changes on the DMP that allows the robot to overcome a set of irregularities that assemble like a set of steps of a small staircase. These consist of two consecutive steps up followed by two steps down, each one with 2 cm high. Beside this the robot system is also supposed to receive visual information regarding the stairs location and height in order to modify the basic gait pattern (foot clearance and step size). Fig. 7.19 shows the path the robot has to go through and the sequence of captured images of the robot stepping on the first step, followed by the second step, and after a few steps on this the first down step followed by the final down step takes the robot to the ground level. A phase reset is applied as soon the robot senses the foot has hit the ground sooner than expected.

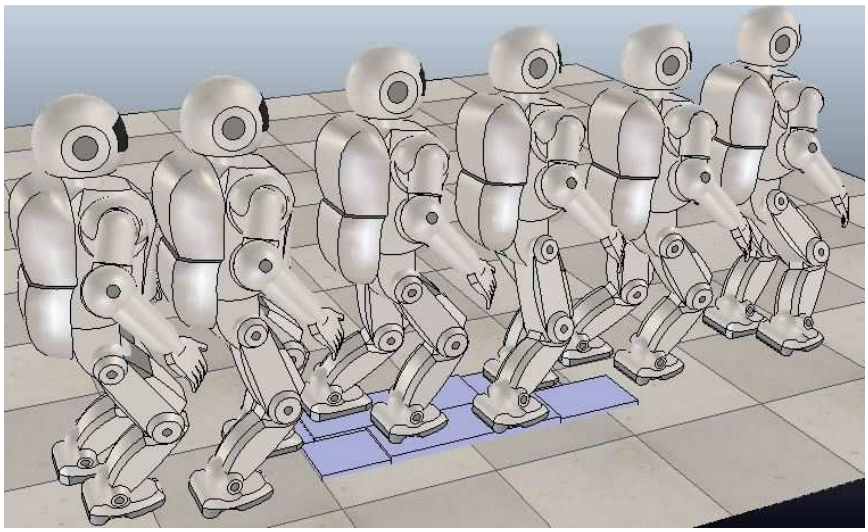

Fig. 7.19: Sequence of the robot walking through a path with small steps.

7.5.2 Robustness against External Forces

In this subsection, an external force is applied to the trunk section of the humanoid robot in two situations: a horizontal force is applied in the direction of the movement or, instead, in the backward direction. Specifically, after the robot has achieved steady-state walking, a horizontal force is applied at its CoG for $0.1\,s$. The instant in which this external force is applied varies from the moment the left foot leaves the ground to the instant when the same foot touches the ground in intervals of $50\,ms$. In both cases, the maximum force tolerated by the robot without falling was measured with and without phase resetting. Fig. 7.20 shows the increase on the tolerated forces with phase resetting.

The result of applying a force to the robot, with and without phase resetting, is observed on the variation of the CoG velocity on the direction of movement (see Fig. 7.21). Here a force of $500\,N$ was applied around the $11.6\,s$ and it can be seen that without phase resetting the robot lost the stability with a high increase on the CoG velocity leaving to the fall a few seconds after (blue curve). With phase resetting, the impact produces a moderate increase on the CoG velocity, but after a few seconds the normal cyclic pattern is recovered. At the same time, the coupling between the phase oscillators recovers the phase offset of 180° between each leg. In fact, the phase resetting produces an increase on the phase offset to around 205° degrees at the moment of the

force application and the coupling returns this offset to the 180° after a few seconds (black curve).

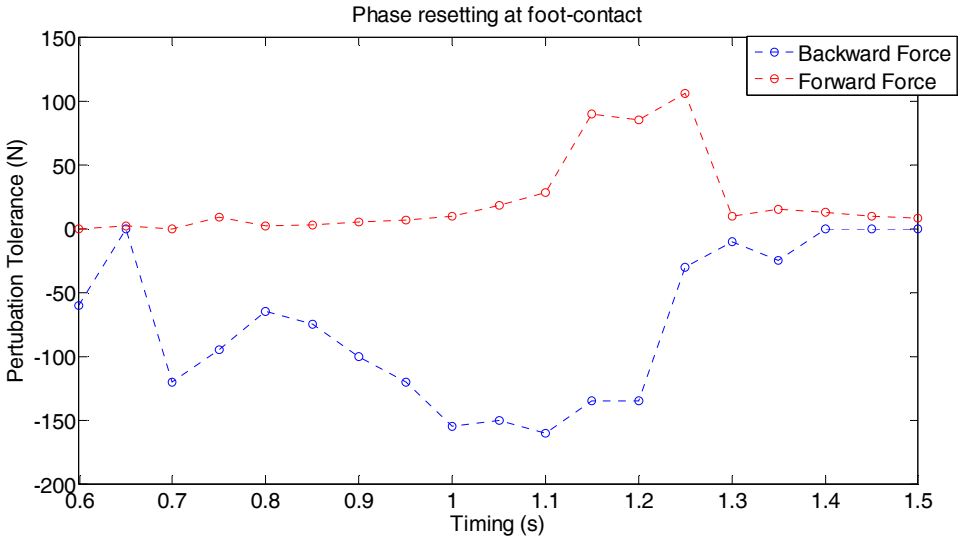

Fig. 7.20: Additional tolerance to perturbation forces applied at different instants of the movement cycle when using phase resetting.

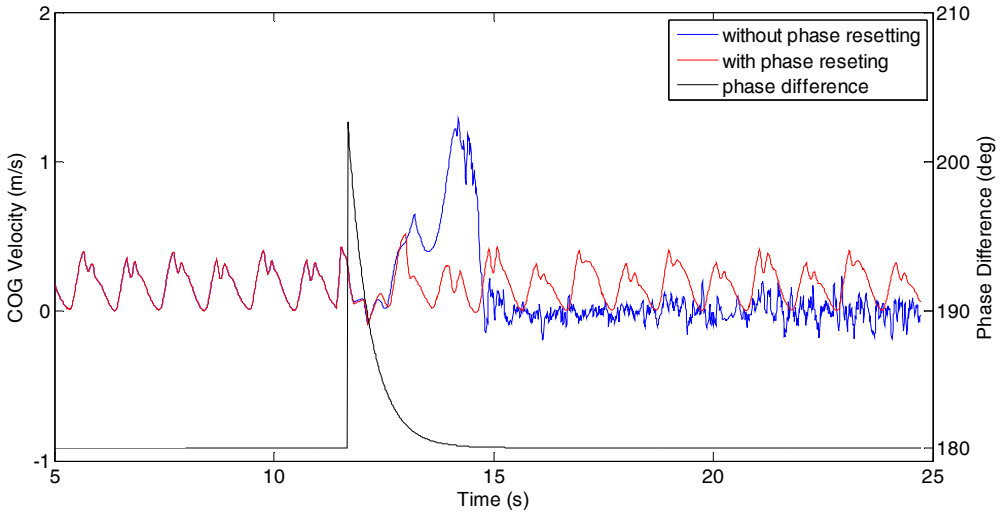

Fig. 7.21: Velocity of the CoG in the direction of the motion with a perturbation force applied at $11.6\,s$ without and with the use of phase resetting. The time course of the phase difference between the oscillators is represented in a different vertical axis.

7.6 Final Remarks

Humanoid robots intended to work in the real world need to quickly adapt their gait to new and unexpected situations. In this chapter, a locomotion control system that

combines dynamic movement primitives and coupled phase oscillators to generate adaptive biped walking was proposed. On the one hand, online modulation of the DMP parameters is used for providing spatial adaptation. The proposed approach is based on the assumption that DMP are learned in the task space from a single demonstration. Therefore, the humanoid robot is able to switch between different gait patterns by modifying DMP parameters that directly relate to the task variables, such as step length, hip height, foot clearance and forward velocity. Numerical simulations show that the proposed formulation is well-suited to achieve adaptive walking in terrains with irregularities and to provide anticipatory adaptation for stepping over obstacles.

On the other hand, the adjustment of rhythm and phase coordination under the DMP formulation helps to substantially increase the range of parameters and the tolerance to disturbances for which stable walking is possible. Adaptation of the inter-limb parameters by introducing phase coupling between limbs largely restores symmetry of the gait cycle with inherent advantages for stability. In line with this, increased robustness to changing environments and against external force perturbations in the direction of the robot's locomotion are obtained. Phase resetting is robust to perturbation as it can directly influence the centre of mass's velocity component in the same direction of the robot's locomotion.

From a control perspective, the need for adaptability and stability in biped robot systems can be accomplished by combining feedforward and feedback processes. These results are significant because they show that exploiting the generalization abilities of DMP and the phase coordination between legs can reduce the requirements of the feedback controller.

Chapter 8
Conclusions

The main goals proposed on the beginning of the work have been achieved: extraction and encoding of human demonstrations is performed using DMP and the development of a control framework that allows the robot to adapt to new situations departing only from a single demonstration. This chapter summarizes the main conclusions of this work, reporting the main developments and results achieved. In addition, some future work directions are also addressed.

8.1 Final Discussion

This work had, essentially, two main objectives: first, to encode a human demonstration and model locomotion tasks. Second, to develop a control framework that allows the robot to achieve adaptive locomotion from a single demonstration extracted from a "robot-like" human motion capture. In order to achieve the adaptive locomotion, the developed framework must be able to shape this signal in an automatic way by modifying high level parameters of the encoding tool used.

Being this a work related to the biped locomotion problem, Chapter 2 started by presenting a state of the art of the current research and work done in biped locomotion platforms. Talk about biped locomotion without considering the fundamental and most advanced biological organism present in nature would make this work less rich. Therefore, besides the state of the art in biped locomotion, the most relevant terms of

human anatomy, the dominant theories of biped locomotion and the methodologies used in control of biped locomotion are presented.

Transferring human demonstrations to be used on humanoid robots enters an area called learning from demonstration. Chapter 3 provides an overview of the main techniques used to robot learn, with particular focus on LfD and RL, as well as their application to biped locomotion. Besides transferring the demonstrations provided by the human teacher to the humanoid robot, these signals must also be encoded in an efficient and fast way. Some neurobiological studies have shown that in vertebrate animals the basic blocks for movement generation are generated at the spinal medulla and modulated by the cerebrum based on sensory information provided from vision, tact and other external stimulus. Based in these studies, many tools for encoding basic movements have appeared on the literature.

Chapter 4 provides an overview over these neurophysiological evidences and a specific tool created to encode these movements, known as Dynamic Movement Primitives. A study of the properties of this tool and their generalization capabilities was performed. These studies also show that when performing generalization tasks, the generalization error is lower if using the DMP in the task space instead of the joint space. This is justified by the following: first, DMP exhibit an invariance property, i.e., when changing the goal or the timing of the signal, the original shape is preserved; second, generalization of task (like the reaching task presented) is, in general, directly related to the Cartesian trajectory performed and not to the joint space. For example, by observing the signals representing a reaching task to two different points in space, it is more likely that these signal are more equal between them if looked at the Cartesian trajectories over time than if looked at the joint values over time.

Once the encoding task for the single demonstration is defined, there is the need to obtain the single demonstration. In Chapter 5, a relevant contribution of this work is described. Instead of trying to use direct human data, a new type of locomotion called “robot-like” was introduced. This locomotion process simplifies the task of human to humanoid transfer, since some of the restrictions usually found in biped locomotion tasks are already embedded in the demonstrator movements. A complete comparative study of this movement with the human natural gait was also performed in this

chapter. It is clear that when the human participant is subject to some restrictions found in humanoid robots, the locomotion pattern resembles that found in humanoid robots.

Chapter 6 presents the methodologies used for transferring the single demonstration from the human motion data to the humanoid robot. The proposed approach combines an off-line phase based on spatiotemporal scaling and an online phase that includes a reduced inverted pendulum and a CoG-Jacobian algorithm. Finally, Chapter 7 presents the control framework that combines all the elements from the previous chapters. First, generalization from a single demonstration was accomplished to create adaptive movements when the robot faces new situations. Second, rhythmic and discrete DMP were combined in order to adapt the robot's motion to a constant changing goal in an autonomous process. Third, the proposed pattern generator explores the transition between phases that emerged from events like foot contact or foot off, increasing the robustness against external perturbations.

8.2 Contributions and Publications

This work has contributed with the following novelty in the aspects related to the biped locomotion problem:

- Instead of extracting the human demonstrations from a normal human like, these one were extracted from a "robot-like" walking gait, resulting in less effort to transfer the motion to the robot and extract the CoP.
- A single demonstration signal has been used with the ability to adapt to new situations by simple changes on the high level parameters of the pattern generators based on dynamic movement primitives.
- The combination of rhythmic and discrete DMP, defined in task-space, increased the adaptability of the robot to new situations encountered on the environment, given the direct relationship with the locomotion parameters.
- The phase-reset under the DMP formulation allows moving from the classical time-based control into an event-based control. The proposed pattern generator

explores the transition between phases that emerge from interaction of the environment of the robot with the environment.

At the same time, this work led to the following publications sorted by date, including journals, book chapters and conference proceedings:

- Rosado, J., Silva, F., Santos, V., & Lu, Z. (2013). "Reproduction of human arm movements using Kinect-based motion capture data." In *Robotics and Biomimetics (ROBIO), 2013 IEEE International Conference on*(pp. 885-890). IEEE.
- Rosado, J., Silva, F., & Santos, V. (2014). "A Kinect-Based Motion Capture System for Robotic Gesture Imitation." In *ROBOT2013: First Iberian Robotics Conference* (pp. 585-595). Springer International Publishing.
- Rosado, José, Filipe Silva, & Vítor Santos (2014). "Using Kinect for Robot Gesture Imitation." *Procedia Technology* 17: 423–30.
- Rosado, José, Filipe Silva, & Vitor Santos. (2014). "Motion Generalization from a Single Demonstration Using Dynamic Primitives." In *2014 IEEE International Conference on Autonomous Robot Systems and Competitions (ICARSC)*, IEEE, 327–32.
- Rosado, J., Silva, F., & Santos, V. (2014). "Motion Generalization with Dynamic Primitives." *Mobile Service Robotics: CLAWAR 2014*, *12*, 215.
- Rosado, J., Silva, F., Santos, V. (2014). "Generalization of Biped Locomotion Tasks with Dynamic Motion Primitives.", *Proceedings of the Workshop on Policy Representations for Humanoids Robots,* IEEE-RAS International Conference on Humanoids Robots, Madrid, Spain, 2014.
- Rosado, J., Silva, F., Santos, V., & Lu, Z. (2015). "Modulation of Dynamic Movement Primitives for Biped Locomotion." In *Assistive Robotics: Proceedings of the 18th International Conference on CLAWAR 2015* (p. 389). World Scientific.
- Rosado, J., Silva, F., Santos, V. (2015). "Adaptive Behavior of a Biped Robot Using Dynamic Movement Primitives.", In *Proceedings of the 17th Portuguese Conference on Artificial Intelligence,* EPIA 2015, Coimbra, Portugal.

- Rosado, J., Silva, F., & Santos, V. (2015). "Biped Walking Learning from Imitation Using Dynamic Movement Primitives." In *Robot 2015: Second Iberian Robotics Conference* (pp. 185-196). Springer International Publishing.
- Rosado, J., Silva, F., & Santos, V. (2015, April). "Adaptation of Robot Locomotion Patterns with Dynamic Movement Primitives." In *Autonomous Robot Systems and Competitions (ICARSC), 2015 IEEE International Conference on* (pp. 23-28). IEEE.
- Rosado, José, Filipe Silva, Vítor Santos, and António Amaro (2016). "Adaptive Robot Biped Locomotion with Dynamic Motion Primitives and Coupled Phase Oscillators." *Journal of Intelligent & Robotic Systems*: 1–17.
- Rosado, J., Silva, F., & Santos, V. (2016, May). "Motion Primitives for Human-to-Humanoid Skill Transfer Under Balance Constraint" In *Autonomous Robot Systems and Competitions (ICARSC), 2016 IEEE International Conference on*.

8.3 Perspectives of Future Work

The perspectives of future work are related to improvements of the work currently developed and additions that can be performed. Having this in mind, a set of points can be enumerated:

- The combination of imitation (learning from a teacher) and trial-and-feedback (learning by practice) appears as a promising direction of research to deal with the limitations of existing approaches when taken separately. For example, using demonstrations to initialize reinforcement learning provides two obvious benefits. The first benefit is that it provides supervised training data of what actions to perform in states that are encountered, what may be helpful in terms of action selection. The second and perhaps most important benefit is that examples from a human demonstrator provide a powerful way for reducing the complexity of the search space by either starting the search from the observed example or by eliminating infeasible solutions.
- Adaptation to new situations can be extended to tasks such as stairs climbing and walk on slopes. However, it is important to note that adaptation in real

word requires a balancing algorithm. For example, a balancing controller based on the compensation of linear and angular momenta seems promising in order to control, independently, the desired ground reaction force and centre of pressure at each support foot

- Before the proposed methodology can be implemented and tested in the physical PHUA robot, it is required to assess its performance in a simulation environment. A full-body model of the PHUA was developed to the V-REP platform by Barros (Barros et al., 2015). The humanoid platform was designed with hybrid actuation for providing a more bio-inspired system.

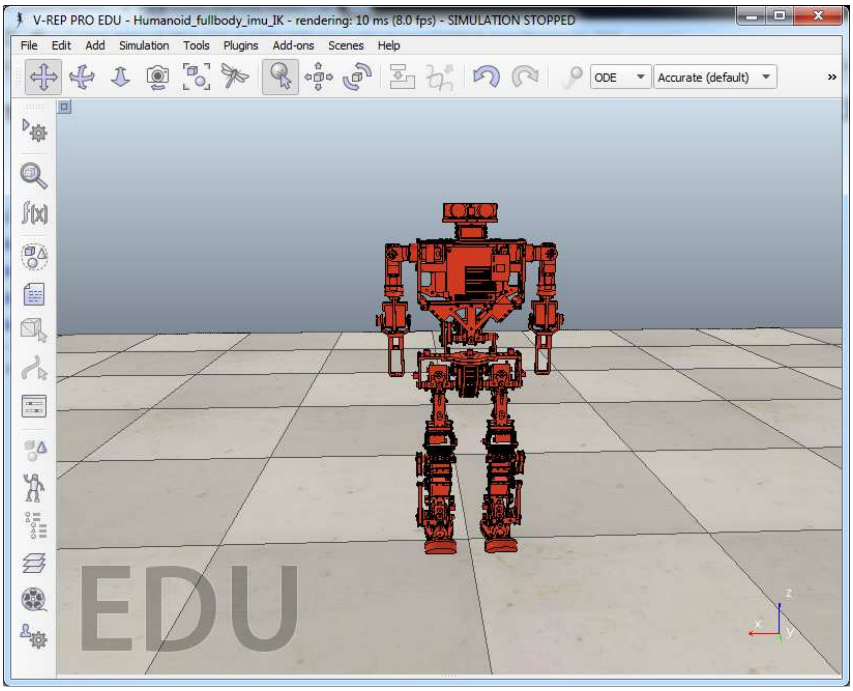

Fig. 8.1: The full-body PHUA robot model in the V-REP simulator (model and scene from Barros, 2014).

- In the same line of thought, it is worth noting that the human musculoskeletal system's ability to control force and position simultaneously is the key to versatile interactions with the environment. Although widely used in robot manipulators for stability and dexterity in contact tasks, the concept of impedance control (Hogan, 1985) has not been adapted widely in walking humanoid robots. In human walking and running, leg and ankle impedance is modulated for stable contact with the ground, impact absorption, and energy

efficiency (McMahon, 1984). These strategies have been suggested for humanoid walking through simulations (Park, 2001) and demonstrated for uneven surface walking with a biped robot (Kang et al., 2010).

Appendix A

V-REP: Virtual Robot Experimentation Platform

V-REP is probably the most versatile and complete simulation platform for robotics software and it is provided by coppelia robotics. It possesses an integrated development environment (Fig. A.1), based on a distributed control architecture, where each object/model can be individually controlled, be it via an embedded script, a plug in, a ROS node, a remote API client or a custom solution.

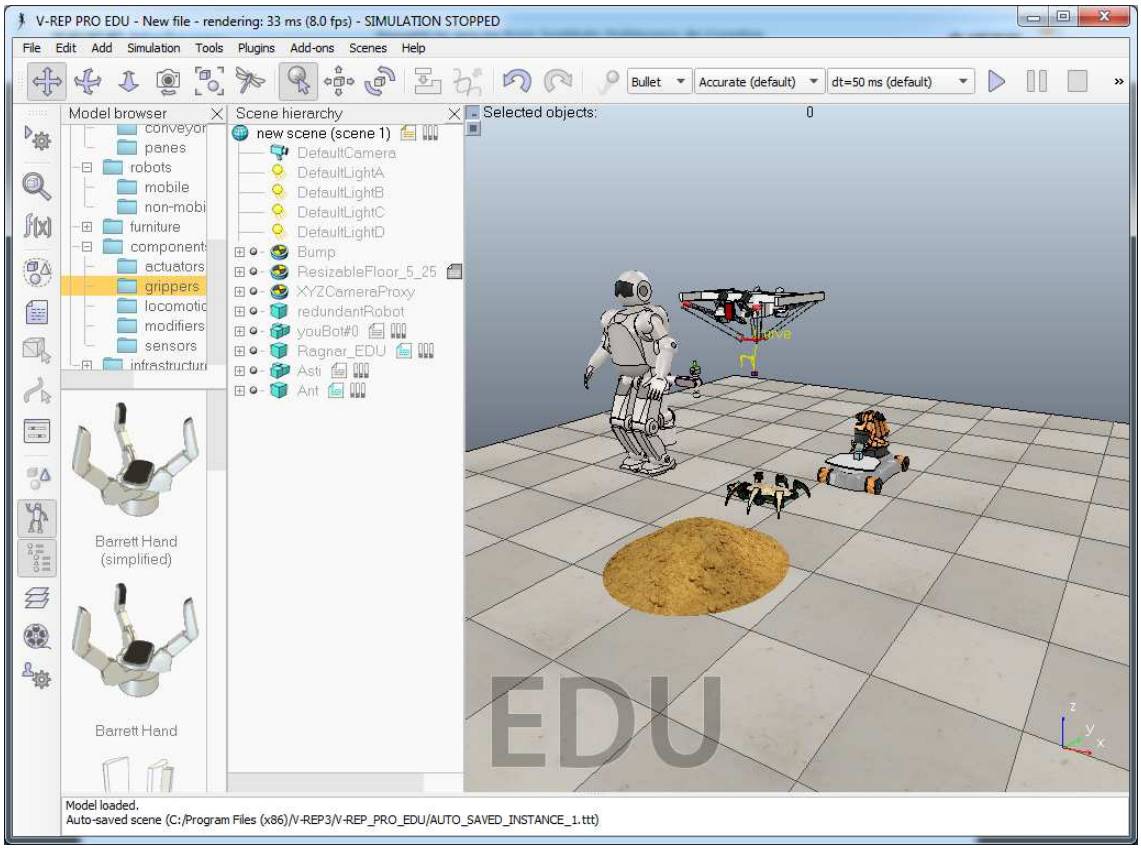

Fig. A.1: An example of a V-REP simulation scene combining showing the diversity of robot types that can be simulated simultaneously and the IDE.

V-REP can be used as a stand-alone application, or can easily be integrated into a main client application. Here are some of the main features provided by V-REP:

- Cross-Platform and portable: V-REP is cross-platform and allows the creation of portable, scalable and easy maintainable content – a single portable file can contain a fully functional model (or scene), including the control code.

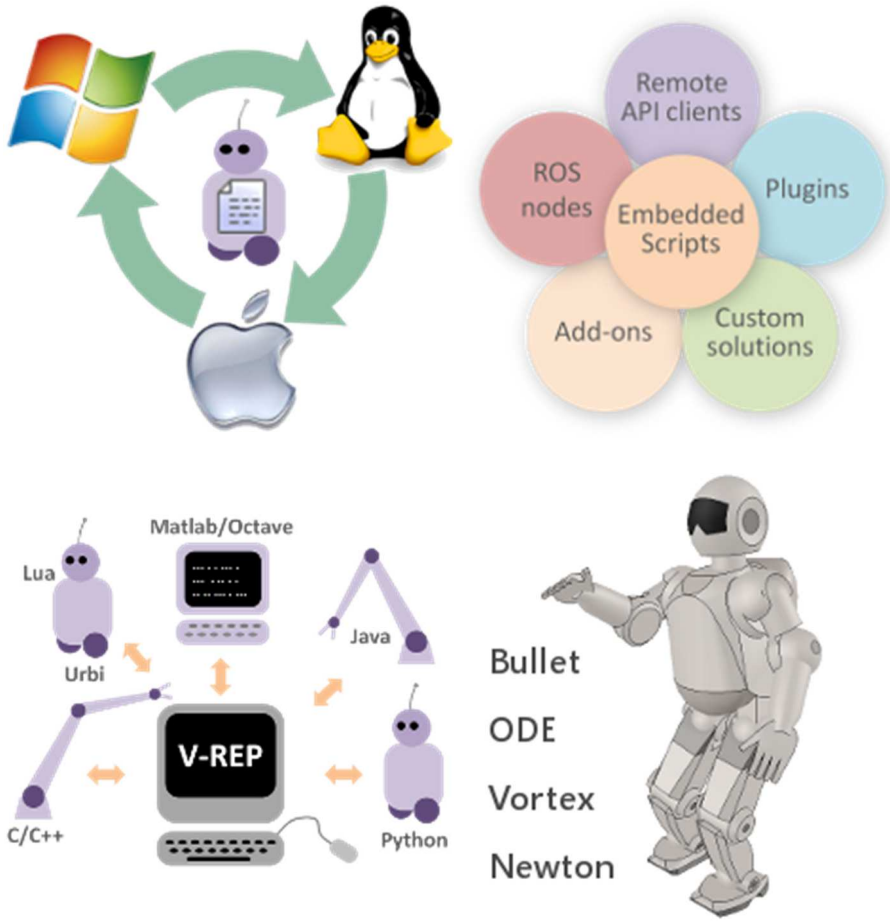

Fig. A.2: V-REP is multi-platform compatible, provides several programming approaches, remote APIs for multi-language programming and offers 4 physics engines (images adapted from coppelia robotics web page).

- Multi programming approaches: simulator and simulations are fully customizable, with 6 programming approaches that are mutually compatible.
- Powerfull APIs: the integrated API supports up to 500 functions available in Lua, C and C++. The remote API provides more than 100 functions that allow control the simulator and the simulation from external environments (other IDE, other PC or even a real robot), using C/C++, Python, Java, Matlab,

Octave, Lua and Urbi. An interface to ROS is also provided, with 100 services, 30 publisher types and 25 subscriber types.

- Dynamics/physics engines: 4 physics engines are provided: Bullet, ODE, Vortex and Newton for fast and customizable dynamics calculations that can simulate real world physics and object interactions
- Path/Motion Planning: holonomic path planning in 2-6 dimensions, non-holonomic path planning for car-like vehicles and motion planning for kinematic chains. Custom path/motion planning algorithms are also supported.
- Building Block Concept: anything – from sensors or actuators, to whole robotic systems – can be built within V-REP by combining basic objects and linking various functionalities via embedded scripts. Every scene object can have its own script.

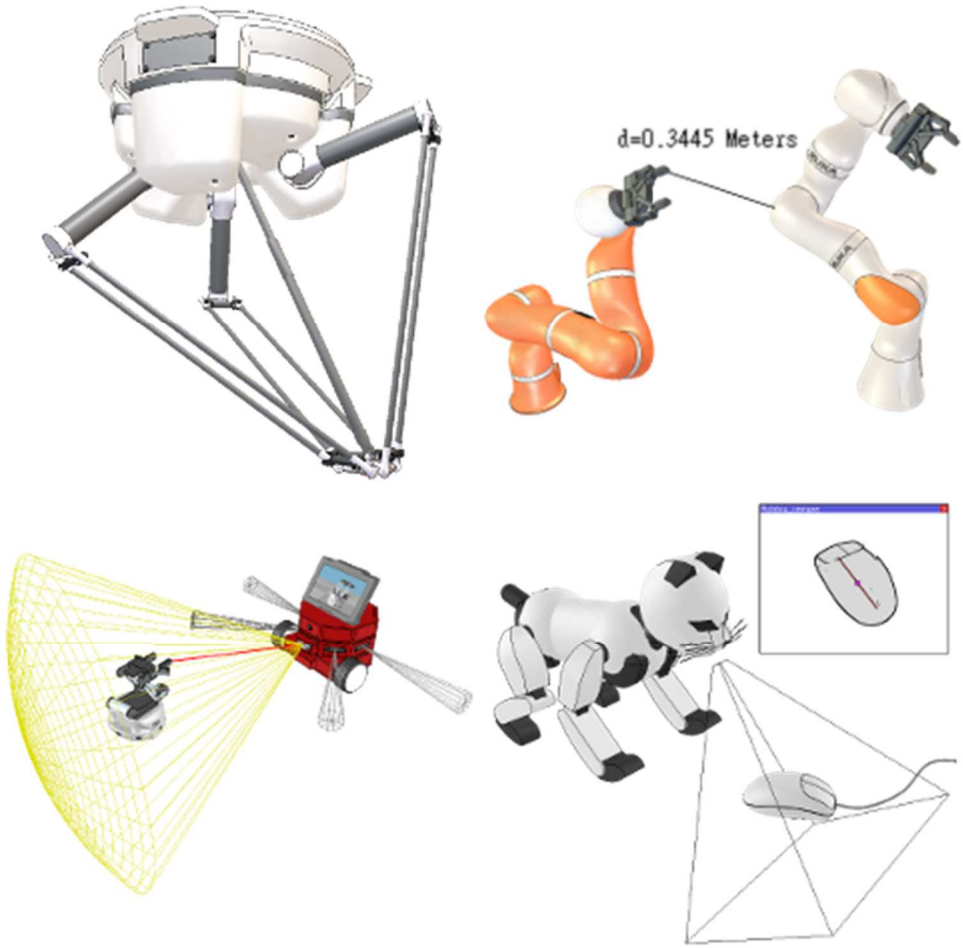

Fig. A.3: V-REP provides IK/FK calculations for any type o mechanism, precise minimum distance calculation, proximity and vision sensor simulation (images adapted from coppelia robotics web page).

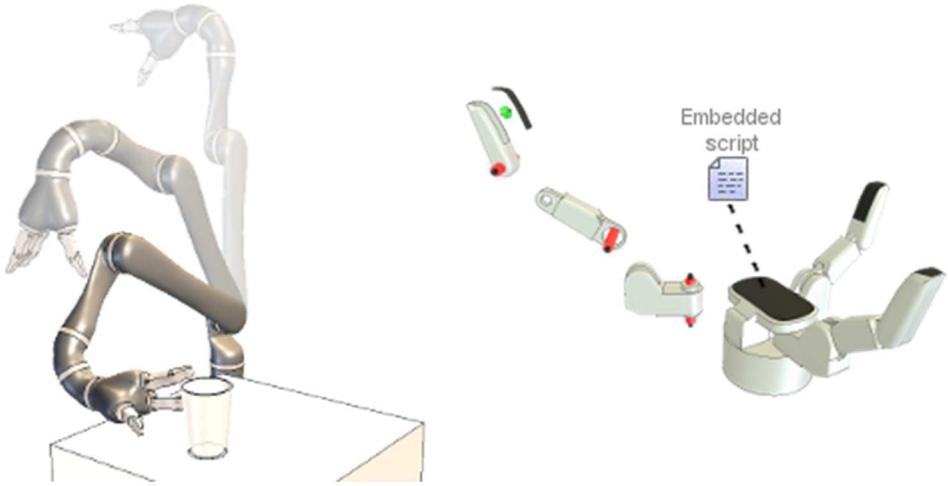

Fig. A.4: V-REP allows path/motion planning and building any kind of object each one with its own script (images adapted from coppelia robotics web page).

Over the course of this work, all the interaction with the V-REP was made through the Matlab API provided, except when the available API functions could not provide the necessary information in a direct form; in these situations, the built in script for the scene/object was modified and the necessary information was provided via signals, a functionality provided in V-REP that allows the communication of information between the remote application and the V-REP IDE. The communication between the Matlab script and V-REP is done via network interface. Prior to start the communication between Matlab and V-REP, a dynamic link library (DLL) provided by V-REP (remoteApi.dll) must be loaded using the command:

```
vrep=remApi('remoteApi');
```

where 'remApi' is a Matlab script provided by V-REP. Both the Matlab script and the DLL provided by V-REP must be in Matlab's path or in the some folder where our script is. From this point on, two methodologies exist to start the communication. Either the command is done on the Matlab script:

```
clientID=vrep.simxStart('127.0.0.1',19999,true,true,5000,5);
```

and in this case, the communication will be done with the localhost (127.0.0.1 is the computer where the script is running), using the port 19999. This however will require two extra steps. The first one is that on the main script on the V-REP scene, the following code must be added:

```
simExtRemoteApiStart(19999)
```

and then the simulation must be started in V-REP, prior to starting the Matlab script. This two extra steps are not very practical, since it requires manual start of the simulation in V-REP and there can be scenes where the external control should be ready to control or receive information from the V-REP right from the first simulation step. So, any extra delay, be it introduced by the time it takes the user to go from clicking to start of the simulation in V-REP until it clicks to run the Matlab script, or be it by the time the Matlab script can take to load some needed files or run extra code, could leave to unexpected outcomes.

Other option to start the communication is using the same command, but with a different destination port:

```
clientID=vrep.simxStart('127.0.0.1',19997,true,true,5000,5);
```

V-REP is always listening to contacts on the port 19997 (this port can be changed, if needed) and this does not require adding any extra code on the main script of the scene that is open in V-REP. This also allows the start of the simulation directly from the Matlab script, by issuing the command:

```
vrep.simxStartSimulation(clientID,vrep.simx_opmode_oneshot);
```

Optionally, there can be the need to synchronize the communication between the Matlab script and V-REP simulation, by issuing the commands:

```
vrep.simxSynchronous(clientID,true);
vrep.simxSynchronousTrigger(clientID);
```

The first command will force the V-REP to pause simulation until it receives the second command that will tell V-REP to move to the next step in the simulation. So each time it is needed to move to the next step in simulation, the second command should be issued. The time duration of each time step on the V-REP IDE can be adjusted on the top toolbar (Fig. A.5) and the default value is 50ms. It is possible to define any value for this time step, and the default options are: 200 ms, 100 ms, 50 ms, 25 ms, 10 ms and a custom option where the wanted the time step can be defined. Over the course of the simulations done on this work, the value chosen was 10 ms.

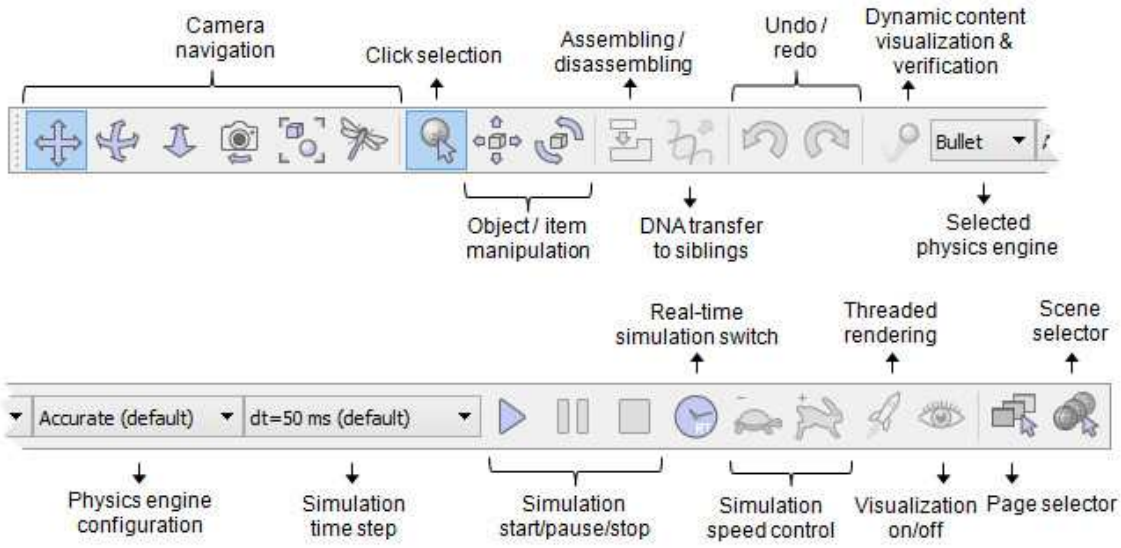

Fig. A.5: Top toolbar on the V-REP IDE (image adapted from the V-REP user manual).

Among the many robot models present on the V-REP is the Asti model (Fig. A.6, left), a humanoid robot with 1.28 m tall, 73 Kg of mass and a total of 20-DoF (Fig. A.6, right) distributed as follows:

- 2-DoF in each foot;
- 1-DoF in each knee;
- 3-DoF on the hips for each leg;
- 2-DoF in each shoulder;
- 1-DoF in each elbow;
- 2-DoF on the neck/head;

Unfortunately, the Asti model does not have force sensors, so there is necessity to know information like the time a foot contact with the ground happened or the evolution of the CoP, some tweaking has to be made. Two options are possible: either force sensors are added to the Asti model, either other functionalities provided by V-REP are used. Starting by the last option, V-REP API provides the following function:

```
simGetContactInfo(…)
```

this function returns a total of 8 values: the first 2 are the objects in contact, the next 3 are the position of contact and the other 3 are the forces generated by the contact in the 3 directions. So, with this function it is possible to know when the contact happened (the function only returns values, when a contact has happen), which objects

entered in contact (e.g., left foot and the ground), and the forces generated by these contacts. Since this command is only available on the V-REP API, in order to get the

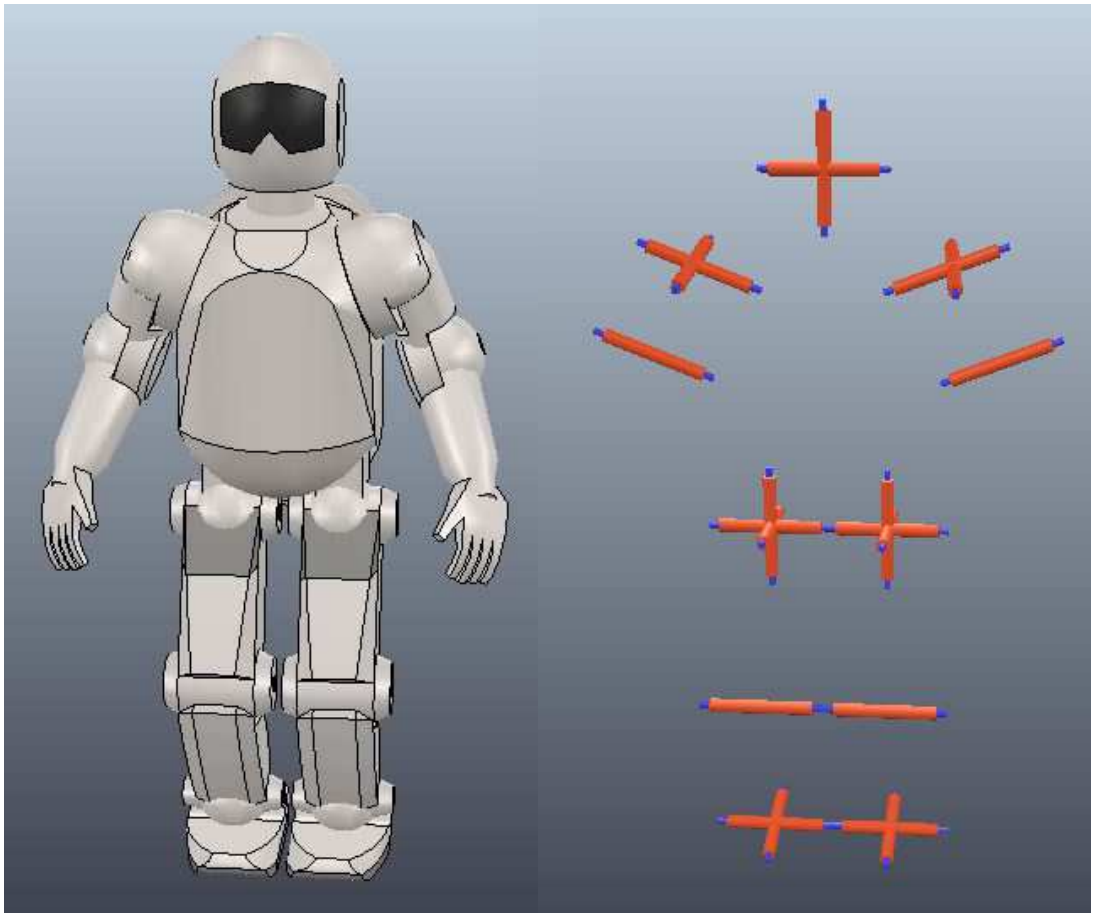

Fig. A.6: The Asti model present on the V-REP model library. Image on the right represents the joints of the Asti model.

information on the remote API, a process to send and receive that information must be created. The simple process is the use of signals, using the following commands:

```
vrep.simxGetFloatSignal(…)
vrep.simxSetFloatSignal(…)
vrep.simxGetIntegerSignal(…)
vrep.simxSetIntegerSignal(…)
simGetFloatSignal(…)
simSetFloatSignal(…)
simGetIntegerSignal(…)
simSetIntegerSignal(…)
```

The first four functions are used on the remote script and the last four are used on the V-REP scene scritps. The functions with the "Get" keyword on the command allow receiving values from a signal and the functions with the "Set" keyword allow send values using a signal. The same way, the functions with the "Integer" keyword work with only integer values and the functions with the "Float" keyword work with decimal values.

Another problem rises from the use of this function: in order to use the data provided by this function to compute the CoP, there is the necessity to know where the contact occurred, which objects where in contact (the Asti model returns a contact event on the neck/head joint). Also, each time a foot enters in contact with the ground, up to 4 points of contact are returned (one at each corner of the foot). Added to all of this, the call to the function referred above (simGetContactInfo) returns up to ten times at each simulation step (V-REP makes ten computations for each simulation step). Even though there's a parameter on the function that allows defining which computation cycle should be used to return the value[2], there's still a need to know which one of the four contacts occurred. This was solved using a rather complex algorithm.

Other possibility for getting info of the contact events and related forces is the addition of force sensors (Fig. A.7) to the Asti model. The force sensor provided by the V-REP library returns the forces and torques on the three dimensions, so a force sensor for each foot is sufficient. Force sensors need to connect two dynamic bodies in V-REP in order to work, so to add them, an element with the some dimensions of the foot was placed on the same place of the foot. To avoid collisions between this element and the already present foot, this element is made no respondable. Fig. A.8 shows the addition of those elements to the Asti feet. Since these new element are dynamic, the previous mass of the feet must now be distributed by the feet and these new element, so the dynamics of the robot are not affected. Despite this procedure has been done by the author and other corrections suggested by the V-REP team have been made, during the simulations done, a change of the dynamics of the robot was noticed.

[2] During the course of this work, the author found out there was a bug on this process, which was corrected on a new release (more info at http://www.coppeliarobotics.com/helpFiles/en/versionInfo.htm - version V3.1.3 - and at http://www.forum.coppeliarobotics.com/viewtopic.php?p=8775#p8775)

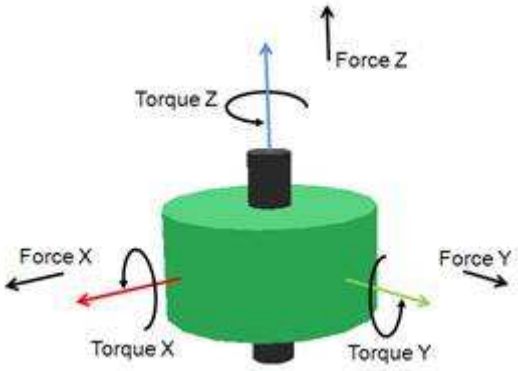

Fig. A.7: The force sensor element provided in the V-REP library.

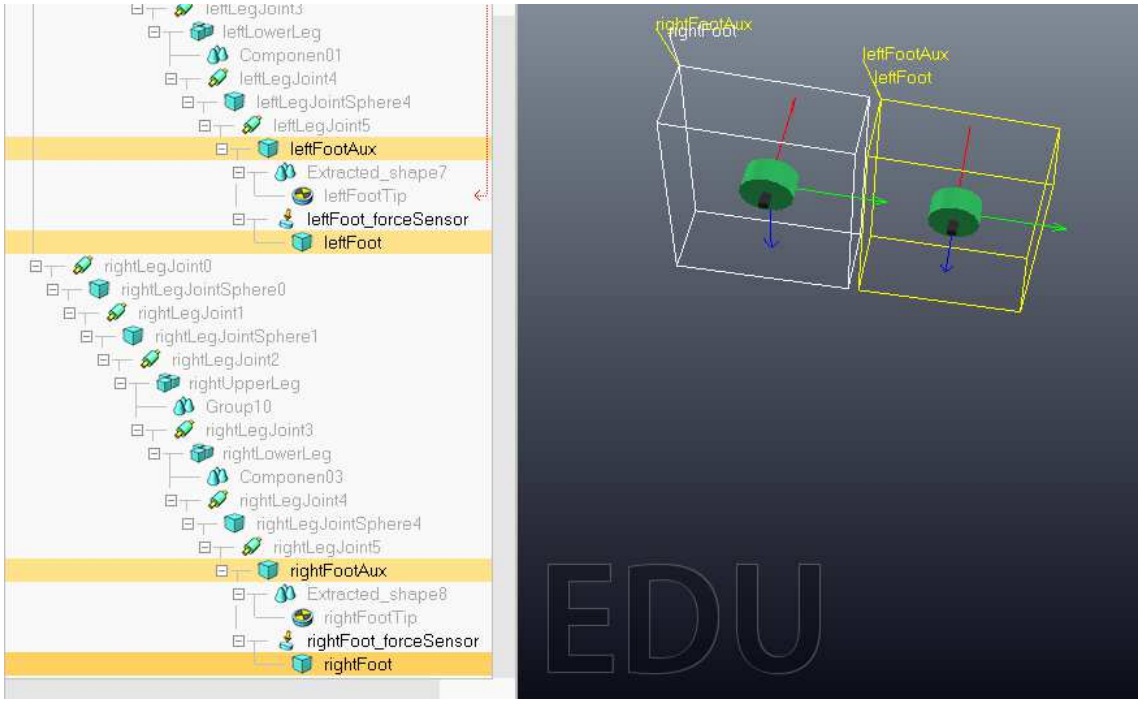

Fig. A.8: Adding force sensors to the Asti feet: the extra elements added (leftFootAux and rightFootAux), the force sensors, the existing feet elements and there location on the scene hierarchy tree.

Appendix B

VICON and Experimental Protocol

The motion capture experiments were performed at the motion lab available at the ESSUA installations (Fig. B.1). This lab is composed by a marker based system from VICON, 2 force platforms and a total of 30 non-invasive EMG sensors.

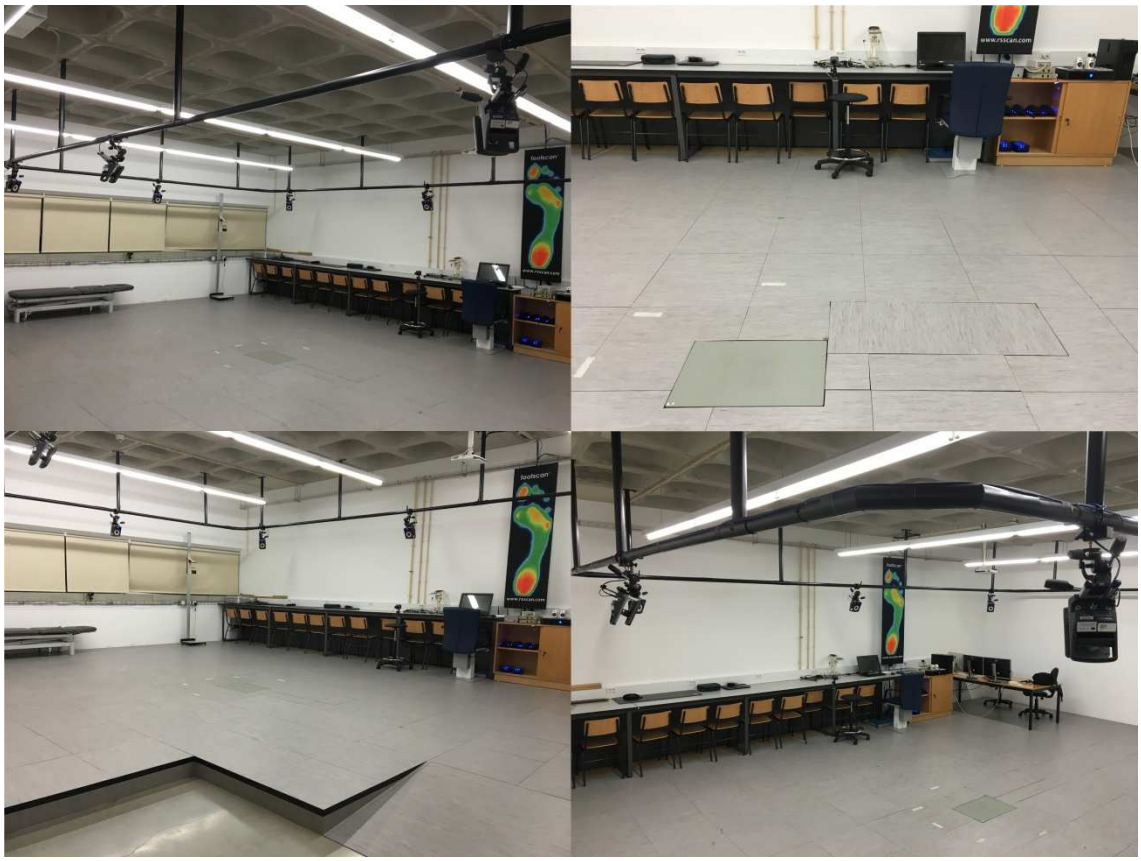

Fig. B.1: The motion lab at ESSUA installations.

VICON system compromises a complete motion capture system composed by the following elements:

- 35 reflective markers (spheres with approximately 1 cm in diameter) placed on the body of the subject according to the schema in Fig. B.2.

- 8 infrared cameras with 2.0 Mpixel, model MX T20-S resolution capable of capturing up to 690fps (Fig. B.3)
- 2 HD (1280×720) video cameras, model Bonita 720c, placed on the x and y axis, capable of capturing video up to 120fps.

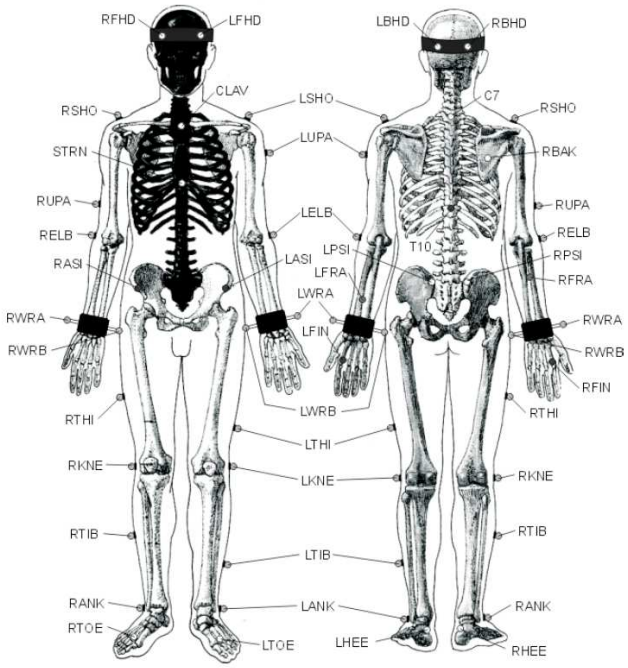

Fig. B.2: Markers placement and name convention on the VICON system.

Fig. B.3: Detailed view of one of the infrared cameras, model MX T-20S.

The force platforms (Fig. B.4), models AMTI BP4051040RS-2K-14162 and AMTI BP400600-2000, are placed on the centre of the capture area and have the following dimensions: 40 cm × 100 cm and 40 cm × 60 cm respectively and a capture rate up to 1000fps. The captured data is the reaction forces, the moments and the CoP, all on the 3 axis. All the captured data is kept synchronized with dedicated hardware and stored as a set of files that can be later processed.

Fig. B.4: Detailed view of the force platforms; left: with the leveling covers; right: without the leveling covers.

The processing is done with VICON Nexus software, version 1.8.5 (Fig. B.5). This software computes the 3D trajectory of each marker, and allows a later storing of this information, together with the force platforms information in a user format chosen (typically a CSV format file). It is also possible to export information like the markers velocity, acceleration and the joints values, velocities and acceleration. Although the software has the tools to automatically compute the markers positions for the entire motion capture (and recreate the skeleton figure seen in Fig. B.5), this rarely works 100% OK. Even when the subject stays inside the capture area all the time, when turning to do more steps on the opposite direction, some of the markers disappear from the scene, making it hard for the software to label them when they reappear latter on scene. Also, any reflecting object on the lab can create false positives reactions, confusing the software. Some of the tools provided by the software allow filling these gaps, but when they are big, the presented solution is not always the correct one and the process is typically manual, tedious and time consuming. The best solution is to do

the processing in sections that avoid these turnings, losing the data at those turnings, which does not represent any problem, since that data is rarely interesting.

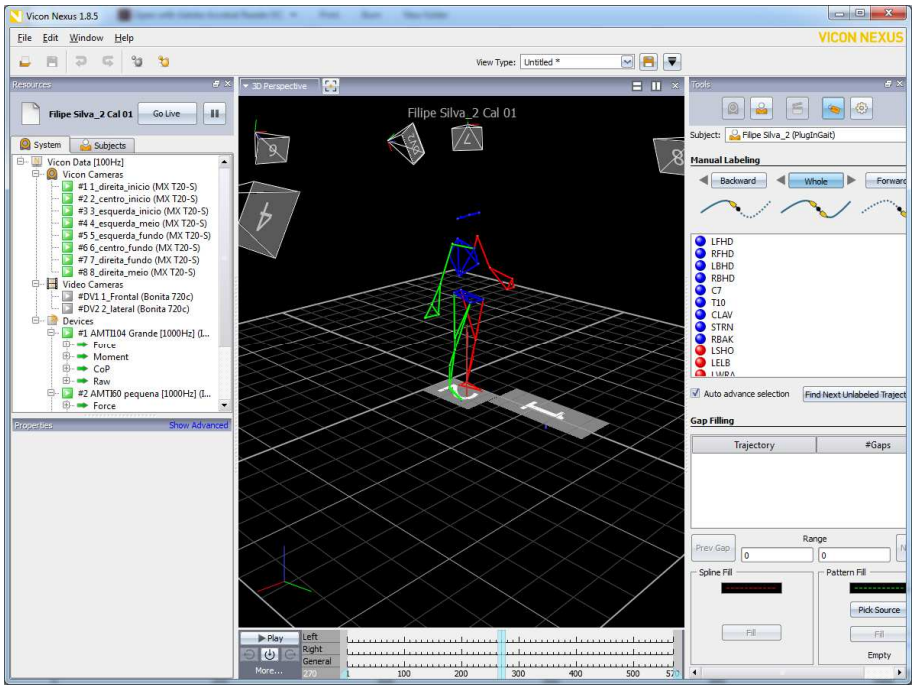

Fig. B.5: The VICON Nexus software used to process the captured data a get the relevant information.

Several experiments were conducted performed by four different subjects with heights varying between 1.71 m and 1.85m, weight varying between 70 Kg and 85 Kg and ages between 20 and 45 years. The experiments varied between walking on a plain surface, overcome an obstacle, pass over an obstacle with only one or both feet, stepping up/down some stairs and walking on a slope. Fig. B.6 shows some images of the experiments conducted.

All of these experiments were done walking on both modes: the human natural walking and the "robot-like" gait explained in section 5.2. In all experiments, the subject always walked without any restriction applied to his visual feedback, i.e., eyes always open and plain view of the entire path. For all the experiments, a series of protocol rules were defined, in order to assure that all the subjects would introduce the smallest variance possible in the same experiments. So, for the walking on plain surface, the following protocol was defined:

- When walking in human natural gait, walk the closest as possible in straight line, following a direction parallel to the *y*-axis of the VICON referential;
- Take a few steps, once reached near the capture area, stop, turn around and then take a few steps on the opposite direction. Repeat this for at least a total of 10 complete passages;
- Repeat the experiments using the same rules above, but with arms movement restriction, i.e., the subject should not move his arms;
- When walking in "robot-like" gait, repeat with the same rules mentioned above.

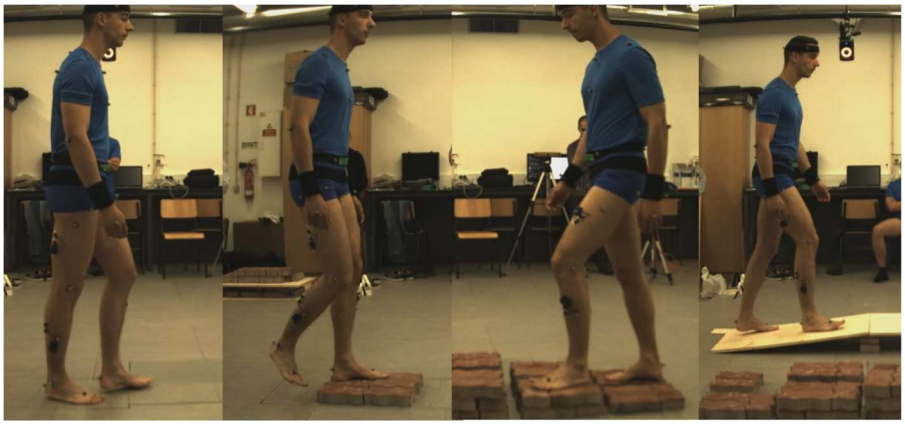

Fig. B.6: Sequence of images showing some of the experiments performed on the motion lab: walking on a plain surface, walking over an obstacle with only one foot, stepping up a group of steps on a small stairs, walking on a slope.

A series of other experiments walking in plain surface was made with the objective of collecting information from the force platforms. To these experiments, the following rules were defined:

- Either when walking in human natural gait or "robot-like" mode, obey the same rules defined above for walking in plain surface;
- On both modes, try to place one foot completely inside one of the platforms and the other completely inside the other platform;
- Each experiment had several passages performed.

As for the experiments with an obstacle on the path, three types of experiments were performed, with the following rules:

- On both walking modes (human natural gait and "robot-like" gait) pass with the foot over the obstacle without touching it and without put the foot over it;

- On both walking modes, walk and place only one foot on top of the obstacle (which had about 5 cm height) and the other foot stays on the ground level;
- On both walking modes, walk with both feet over the obstacle (step up the obstacle and step down);
- Each experiment had several passages performed.

In the experiments performed with the stairs (with 5cm step height), the following rules were given:

- When walking in human natural gait, step up and down the stairs, by placing each foot on a separate step of the stair, i.e., walk like usually a human without any gait pathologies does in stairs;
- When walking in human natural gait, place one foot on one of the steps and then place the other foot on the same step (gait typically performed by very young children when walking on stairs);
- When walking in "robot-like" gait, place one foot on one of stair's step and then place the other foot on the same step (a few experiments done previously confirmed that when using this locomotion mode, it is very hard to do like humans normally do, i.e., like the first rule defined for this experiment);
- On each experiment, the passage on the stairs was performed several times.

The last experiment, walking on slopes had no special rules defined. All the subjects should do, was walking in both modes. The scenario had a slope up, followed by a plain surface and then a slope down. Two different scenarios where built, where the only difference between them was the inclination of the slopes.

References

Adams, B., Breazeal, C., Brooks, R.A. & Scassellati, B. (2000). Humanoid robots: a new kind of tool. *Intelligent Systems and their Applications, IEEE*. 15 (4). p.pp. 25–31.

Akachi, K., Kaneko, K., Kanehira, N., Ota, S., Miyamori, G., Hirata, M., Kajita, S. & Kanehiro, F. (2005). Development of humanoid robot HRP-3P. In: *Humanoid Robots, 2005 5th IEEE-RAS International Conference on*. 2005, pp. 50–55.

Alexander, R. (1992). *Exploring Biomechanics: Animals in Motion*. Library series. Scientific American Library.

Alexander, R.M. & Vernon, A. (1975). The mechanics of hopping by kangaroos (Macropodidae). *Journal of Zoology*. 177 (2). p.pp. 265–303.

Anderson, M.L. (2003). Embodied Cognition: A field guide. *Artificial Intelligence*. 149 (1). p.pp. 91–130.

Anderson, S.O., Wisse, M., Atkeson, C.G., Hodgins, J.K., Zeglin, G.J. & Moyer, B. (2005). Powered bipeds based on passive dynamic principles. *Proceedings of 2005 5th IEEE-RAS International Conference on Humanoid Robots*. 2005. p.pp. 110–116.

Andrew Bagnell, J. (2014). Reinforcement Learning in Robotics: A Survey. *Springer Tracts in Advanced Robotics*. 97. p.pp. 9–67.

Aoi, S., Tsuchiya, K. & Tsujita, K. (2004a). Turning control of a biped locomotion robot using nonlinear oscillators. *Robotics and Automation, 2004. ....*

Aoi, S., Tsuchiya, K. & Tsujita, K. (2004b). Turning control of a biped locomotion robot using nonlinear oscillators. *Robotics and Automation, 2004.*

Aoi, S.A.S. & Tsuchiya, K. (2006). Stability analysis of a simple walking model driven by an oscillator with a phase reset using sensory feedback. *IEEE Transactions on Robotics*. 22 (2). p.pp. 391–397.

Arbib, M. a., Billard, A., Iacoboni, M. & Oztop, E. (2000). Synthetic brain imaging: Grasping, mirror neurons and imitation. *Neural Networks*. 13 (8-9). p.pp. 975–997.

Arena, P. (2000). The Central Pattern Generator: a paradigm for artificial locomotion. *Soft Computing*. 4 (4). p.pp. 251–266.

Argall, B.D., Argall, B.D., Chernova, S., Chernova, S., Veloso, M., Veloso, M., Browning, B. & Browning, B. (2009). A survey of robot learning from

demonstration. *Robotics and Autonomous Systems*. 57 (5). p.pp. 469–483.

Asfour, T., Azad, P., Gyarfas, F. & Dillmann, R. (2008). Imitation learning of dual-arm manipulation tasks in humanoid robots. *International Journal of Humanoid Robotics*. 5 (2). p.pp. 289–308.

Atkeson, C.G., Hale, J.G., Pollick, F., Riley, M., Kotosaka, S., Schaal, S., Shibata, T., Tevatia, G., Ude, A., Vijayakumar, S. & Kawato, M. (2000). Using humanoid robots to study human behavior. *Ieee Intelligent Systems & Their Applications*. 15 (4). p.pp. 46–55.

Baker, R., Kirtley, C. & Pandy, M. (2004). Minimizing the vertical excursion of the center of mass is not the primary aim of walking. In: *Eighth International Symposium on the 3-D Analysis of Human Movement*. 2004, Tampa, Florida, USA, pp. 101–103.

Barros, J. (2014). *LAR Projects*. [Online]. 2014. Available from: http://lars.mec.ua.pt/public/LAR Projects/Humanoid/2014_JoaoBarros/. [Accessed: 14 July 2016].

Barros, J., Santos, V. & Silva, F. (2015). *Cooperative Haptics for Humanoid Robot Teleoperation*. Aveiro.

Bauby, C.E. & Kuo, A.D. (2000). Active control of lateral balance in human walking. *Journal of Biomechanics*. 33 (11). p.pp. 1433–1440.

Bay, J.S. & Hemami, H. (1987). Modeling of a Neural Pattern Generator with Coupled nonlinear Oscillators. *IEEE Transactions on Biomedical Engineering*. BME-34 (4). p.pp. 297–306.

Behnke, S. & Stückler, J. (2008). Hierarchical reactive control for humanoid soccer robots. *International Journal of Humanoid Robotics*.

Bekey, G., Ambrose, R., Kumar, V., Lavery, D., Sanderson, A., Wilcox, B., Yuh, J. & Zheng, Y. (2008). *Robotics: State of the Art and Future Challenges*. Imperial College Press.

Billard, A., Calinon, S., Dillmann, R. & Schaal, S. (2008). Robot programming by demonstration. *Handbook of robotics*. p.pp. 1371–1394.

Billard, A.G. (2001). Learning motor skills by imitation: A biologically inspired robotic model. *Cybernetics and Systems*. 32. p.pp. 155–193.

Bizzi, E., Mussa-Ivaldi, F. a & Giszter, S. (1991). Computations underlying the execution of movement: a biological perspective. *Science (New York, N.Y.)*. 253 (5017). p.pp. 287–291.

Bizzi, E., Tresch, M.C., Saltiel, P. & D'Avella, A. (2000). New perspectives on spinal motor systems. *Nature reviews. Neuroscience*. 1 (2). p.pp. 101–8.

Borovac, B., Rakovic, M. & Nikolic, M. (2011). Biologicaly inspired on-line generation of complex movements using primitives. In: *Robotic Intelligence In Informationally Structured Space (RiiSS), 2011 IEEE Workshop on*. 2011, pp. 99–106.

Breazeal, C. & Scassellati, B. (2002). Challenges in building robots that imitate people. *Imitation in animals and artifacts*. (1998). p.pp. 363–390.

Brooks, R., Breazeal, C., Marjanović, M., Scassellati, B. & Williamson, M. (1999). The Cog Project: Building a Humanoid Robot. In: C. Nehaniv (ed.). *Computation for Metaphors, Analogy, and Agents*. Springer Berlin Heidelberg, pp. 52–87.

Bullock, D. & Grossberg, S. (1989). VITE and FLETE: Neural modules for trajectory formation and postural control. *Volitional action*.

Calinon, S., D'Halluin, F., Sauser, E.L., Caldwell, D.G. & Billard, A.G. (2010). Learning and reproduction of gestures by imitation. *IEEE Robotics and Automation Magazine*. 17 (2). p.pp. 44–54.

Calinon, S., Guenter, F. & Billard, A. (2007). On learning, representing, and generalizing a task in a humanoid robot. *IEEE Transactions on Systems, Man, and Cybernetics, Part B: Cybernetics*. 37 (2). p.pp. 286–298.

Cavagna, G.A. & Kaneko, M. (1977). Mechanical work and efficiency in level walking and running. *The Journal of physiology*. 268 (2). p.pp. 467–81.

Chalodhorn, R., Grimes, D.B., Grochow, K. & Rao, R.P.N. (2010). Learning to Walk by Imitation in Low-Dimensional Subspaces. *Advanced Robotics*. 24 (1-2). p.pp. 207–232.

Chalodhorn, R., Grimes, D.B., Maganis, G.Y. & Rao, R.P.N. (2005). Learning dynamic humanoid motion using predictive control in low dimensional subspaces. In: *2005 5th IEEE-RAS International Conference on Humanoid Robots*. 2005, pp. 214–219.

Chalodhorn, R. & Rao, R.P.N. (2010). Learning to Imitate Human Actions through Eigenposes. In: O. Sigaud & J. P. 0001 (eds.). *From Motor Learning to Interaction Learning in Robots*. Studies in Computational Intelligence. Springer, pp. 357–381.

Cheng, G., Fitzsimmons, N.A., Morimoto, J., Lebedev, M.A., Kawato, M. & Nicolelis, M. (2007a). Bipedal locomotion with a humanoid robot controlled by cortical ensemble activity. In: *Annual Meeting of the Society for Neuroscience*. 2007.

Cheng, G., Hyon, S., Morimoto, J. & Ude, A. (2007b). CB: A humanoid research

platform for exploring neuroscience. *Jouinal of Advanced Robotics*. 21 (10). p.pp. 1097–1114.

Chevallereau, C., Abba, G., Aoustin, Y., Plestan, F., Westervelt, E.R., Canudas-De-Wit, C. & Grizzle, J.W. (2003). RABBIT: a testbed for advanced control theory. *Control Systems, IEEE*. 23 (5). p.pp. 1–51.

Choi, J.T. & Bastian, A.J. (2007). Adaptation reveals independent control networks for human walking. *Nature neuroscience*. 10 (8). p.pp. 1055–1062.

Choi, Y., Kim, D., Oh, Y. & You, B.J. (2007). Posture/walking control for humanoid robot based on kinematic resolution of CoM Jacobian with embedded motion. *IEEE Transactions on Robotics*. 23 (6). p.pp. 1285–1293.

Cole, J.B., Grimes, D.B. & Rao, R.P.N. (2007). Learning full-body motions from monocular vision: Dynamic imitation in a humanoid robot. In: *IEEE International Conference on Intelligent Robots and Systems*. 2007, pp. 240–246.

Collins, S.H. & Ruina, A. (2005). A bipedal walking robot with efficient and human-like gait. *Proceedings - IEEE International Conference on Robotics and Automation*. 2005 (April). p.pp. 1983–1988.

Crespi, A., Ijspeert, A.J.A. & F, E.P. (2006). AmphiBot II : An Amphibious Snake Robot that Crawls and Swims using a Central Pattern Generator. *CLAWAR 2006: the 9th International Conference on Climbing and Walking Robots*. (September). p.pp. 19–27.

Della Croce, U., Riley, P.O., Lelas, J.L. & Kerrigan, D.C. (2001). A refined view of the determinants of gait. *Gait and Posture*. 14 (2). p.pp. 79–84.

Dariush, B., Gienger, M., Arumbakkam, A., Goerick, C., Zhu, Y. & Fujimura, K. (2008a). Online and markerless motion retargeting with kinematic constraints. In: *2008 IEEE/RSJ International Conference on Intelligent Robots and Systems, IROS*. 2008, pp. 191–198.

Dariush, B., Gienger, M., Arumbakkam, A., Zhu, Y., Jian, B., Fujimura, K. & Goerick, C. (2009). Online transfer of human motion to humanoids. *International Journal of Humanoid Robotics*. 6 (2). p.pp. 265–289.

Dariush, B., Gienger, M., Jian, B., Goerick, C. & Fujimura, K. (2008b). Whole body humanoid control from human motion descriptors. In: *Proceedings - IEEE International Conference on Robotics and Automation*. 2008, pp. 2677–2684.

Degallier, S. & Ijspeert, A. (2010). Modeling discrete and rhythmic movements through motor primitives: A review. *Biological Cybernetics*. 103 (4). p.pp. 319–338.

DeLisa, J. (1998). *Gait analysis in the science of rehabilitation*.

Denk, J. & Schmidt, G. (2003). Synthesis of walking primitive databases for biped robots in 3D-environments. ... *ICRA'03. IEEE International Conference on*.

Dickinson, M.H., Farley, C.T., Full, R.J., Koehl, M. a, Kram, R. & Lehman, S. (2000). How animals move: an integrative view. *Science*. 288. p.pp. 100–106.

Do, M., Azad, P., Asfour, T. & Dillmann, R. (2008). Imitation of human motion on a humanoid robot using non-linear optimization. *2008 8th IEEE-RAS International Conference on Humanoid Robots*. p.pp. 545–552.

Donkelaar, H. ten. (2001). Evolution of vertebrate motor systems. In: G. Roth & M. Wullimann (eds.). *Brain Evolution and Cognition*. Willey-Spectrum, pp. 77–112.

Doya, K. (2000). Complementary roles of basal ganglia and cerebellum in learning and motor control. *Current Opinion in Neurobiology*. 10. p.pp. 732–739.

Drumwright, E., Jenkins, O.C. & Matarić, M.J. (2004). Exemplar-based primitives for humanoid movement classification and control. In: *Proceedings - IEEE International Conference on Robotics and Automation*. 2004, pp. 140–145.

Dunn, E.R. & Howe, R.D. (1996). Foot placement and velocity control in smooth bipedal walking. *Proceedings of the 1996 Ieee International Conference on Robotics and Automation*. p.pp. 578–583 vol. 1.

Endo, G., Nakanishi, J., Morimoto, J. & Cheng, G. (2005). Experimental Studies of a Neural Oscillator for Biped Locomotion with QRIO. In: *Proceedings of the 2005 IEEE International Conference on Robotics and Automation*. 2005, pp. 596–602.

Flash, T. & Hochner, B. (2005). Motor primitives in vertebrates and invertebrates. *Current Opinion in Neurobiology*. 15 (6). p.pp. 660–666.

Fujitsu (2001). *Miyachi Systems Corporation. Miniature Humanoid Robots*. [Online]. 2001. Available from: https://pr.fujitsu.com/en/news/2001/09/10.html.

Furuta, T., Tawara, T., Okumura, Y., Shimizu, M. & Tomiyama, K. (2001). Design and construction of a series of compact humanoid robots and development of biped walk control strategies. *Robotics and Autonomous Systems*. 37 (2-3). p.pp. 81–100.

Gams, A., Ijspeert, A.J., Schaal, S. & Lenarčič, J. (2009). On-line learning and modulation of periodic movements with nonlinear dynamical systems. *Autonomous Robots*. 27 (1). p.pp. 3–23.

Gandevia, S.C. & Burke, D. (1994). Does the nervous system depend on kinesthetic

information to control natural limb movements? In: P. Cordo & S. Harnad (eds.). *Movement control*. Cambridge University Press, pp. 12–30.

Gard, S.A. & Childress, D.S. (1996). The effect of pelvic list on the vertical displacement of the trunk during normal walking. *Gait & Posture*. 4 (2) p.pp. 193–194.

Georgopoulos, A.P. (1996). On the translation of directional motor cortical commands to activation of muscles via spinal interneuronal systems. *Cognitive Brain Research*. 3. p.pp. 151–155.

Giszter, S.F., Mussa-Ivaldi, F.A. & Bizzi, E. (1993). Convergent force fields organized in the frog's spinal cord. *The Journal of Neuroscience*. 13 (2). p.pp. 467–491.

Golliday, C., J. & Hemami, H. (1977). An approach to analyzing biped locomotion dynamics and designing robot locomotion controls. *IEEE Transactions on Automatic Control*. 22.

Gouaillier, D., Hugel, V., Blazevic, P., Kilner, C., Monceaux, J., Lafourcade, P., Marnier, B., Serre, J. & Maisonnier, B. (2009). Mechatronic design of NAO humanoid. *2009 IEEE International Conference on Robotics and Automation*. p.pp. 769–774.

Grillner, S. (2006). Biological Pattern Generation: The Cellular and Computational Logic of Networks in Motion. *Neuron*. 52 (5). p.pp. 751–766.

Grillner, S. (1985). Neurobiological bases of rhythmic motor acts in vertebrates. *Science (New York, N.Y.)*. 228 (4696). p.pp. 143–149.

Grimes, D.B. & Rao, R.P.N. (2009). Learning actions through imitation and exploration: Towards humanoid robots that learn from humans. In: *Lecture Notes in Computer Science (including subseries Lecture Notes in Artificial Intelligence and Lecture Notes in Bioinformatics)*. 2009, pp. 103–138.

Grimes, D.B., Rashid, D.R. & Rao, R.P.N. (2007). Learning Nonparametric Models for Probabilistic Imitation. *Advances in Neural Information Processing Systems 19*. 19. p.pp. 521–528.

Gubina, F., Hemami, H. & McGhee, R.B. (1974). On the dynamic stability of biped locomotion. *IEEE transactions on bio-medical engineering*. 21 (2). p.pp. 102–8.

Hamilton, A.F.D.C. & Wolpert, D.M. (2002). Controlling the statistics of action: obstacle avoidance. *Journal of neurophysiology*. 87 (5). p.pp. 2434–2440.

Harcourt-Smith, W.E.H. (2007). The Origins of Bipedal Locomotion. *Handbook of Paleoanthropology*. Volume 3 (3). p.pp. 1483–1518.

Harris, C.M. & Wolpert, D.M. (1998). Signal-dependent noise determines motor planning. *Nature*. 394 (6695). p.pp. 780–4.

Herr, H. & Popovic, M. (2008). Angular momentum in human walking. *The Journal of experimental biology*. 211 (Pt 4). p.pp. 467–481.

Hersch, M., Guenter, F., Calinon, S. & Billard, A. (2008). Dynamical system modulation for robot learning via kinesthetic demonstrations. *IEEE Transactions on Robotics*. 24 (6). p.pp. 1463–1467.

Hirai, K., Hirose, M., Haikawa, Y. & Takenaka, T. (1998). The development of Honda humanoid robot. In: *Robotics and Automation, 1998. Proceedings. 1998 IEEE International Conference on*. 1998, pp. 1321–1326 vol.2.

Hirukawa, H., Kanehiro, F., Kaneko, K., Kajita, S., Fujiwara, K., Kawai, Y., Tomita, F., Hirai, S., Tanie, K., Isozumi, T., Akachi, K., Kawasaki, T., Ota, S., Yokoyama, K., Handa, H., Fukase, Y., Maeda, J., Nakamura, Y., Tachi, S. & Inoue, H. (2004). Humanoid robotics platforms developed in HRP. *Robotics and Autonomous Systems*. 48 (4). p.pp. 165–175.

Hobbelen, D.G.E. & Wisse, M. (2007). Limit cycle walking. *Humanoid Robotics*. (June). p.pp. 277–294.

Hodgins, J.K., Hodgins, J.K., Pollard, N.S. & Pollard, N.S. (1997). Adapting simulated behaviors for new characters. *Proceedings of the 24th annual conference on Computer graphics and interactive techniques - SIGGRAPH '97*. p.pp. 153–162.

Hoffmann, H., Pastor, P., Park, D.-H. & Schaal, S. (2009). Biologically-inspired dynamical systems for movement generation: Automatic real-time goal adaptation and obstacle avoidance. *2009 IEEE International Conference on Robotics and Automation*. p.pp. 2587–2592.

Hoffmann, M., Marques, H., Arieta, A., Sumioka, H., Lungarella, M. & Pfeifer, R. (2010). Body schema in robotics: A review. *IEEE Transactions on Autonomous Mental Development*. 2 (4) p.pp. 304–324.

Hogan, N. (1985). Impedance control - An approach to manipulation. I - Theory. II - Implementation. III - Applications. *Journal of Dynamic Systems, Measurement, and Control*. 107. p.pp. 1–24.

Hogan, N. & Sternad, D. (2007). On rhythmic and discrete movements: Reflections, definitions and implications for motor control. *Experimental Brain Research*. 181 (1). p.pp. 13–30.

Hong, H., Kim, S., Kim, C., Lee, S. & Park, S. (2013). Spring-like gait mechanics

observed during walking in both young and older adults. *Journal of Biomechanics*. 46 (1). p.pp. 77–82.

Houk, J.C. & Wise, S.P. (1995). Distributed modular architectures linking basal ganglia, cerebellum, and cerebral cortex: their role in planning and controlling action. *Cerebral cortex (New York, N.Y. : 1991)*. 5 (2). p.pp. 95–110.

Huang, Q. & Nakamura, Y. (2005). Sensory reflex control for humanoid walking. *IEEE Transactions on Robotics*. 21 (5). p.pp. 977–984.

Ibanez, A., Bidaud, P. & Padois, V. (2014). Automatic Optimal Biped Walking as a Mixed-Integer Quadratic Program. In: O. K. Jadran Lenarčič (ed.). *Advances in Robot Kinematics*. Springer International Publishing, pp. 505–516.

Iida, F. & Tedrake, R. (2010). Minimalistic control of biped walking in rough terrain. *Autonomous Robots*. 28 (3). p.pp. 355–368.

Ijspeert, A., Nakanishi, J. & Schaal, S. (2003). Learning attractor landscapes for learning motor primitives. In: *Advances in Neural Information Processing Systems 15*. 2003, cambridge, ma: mit press, pp. 1547–1554.

Ijspeert, A., Nakanishi, J. & Schaal, S. (2002a). Movement imitation with nonlinear dynamical systems in humanoid robots. In: *International Conference on Robotics and Automation*. 2002, pp. 1398–1403.

Ijspeert, A.J. (2008). Central pattern generators for locomotion control in animals and robots: A review. *Neural Networks*. 21 (4). p.pp. 642–653.

Ijspeert, A.J., Crespi, A., Ryczko, D. & Cabelguen, J.-M. (2007). From swimming to walking with a salamander robot driven by a spinal cord model. *Science (New York, N.Y.)*. 315 (5817). p.pp. 1416–1420.

Ijspeert, A.J., Hallam, J. & Willshaw, D. (1999). Evolving Swimming Controllers for a Simulated Lamprey with Inspiration from Neurobiology. *Adaptive Behavior*. 7 (2). p.pp. 151–172.

Ijspeert, A.J., Nakanishi, J., Hoffmann, H., Pastor, P. & Schaal, S. (2013). Dynamical movement primitives: learning attractor models for motor behaviors. *Neural computation*. 25 (2). p.pp. 328–73.

Ijspeert, A.J.I.A.J., Nakanishi, J.N.J. & Schaal, S. (2002b). Learning rhythmic movements by demonstration using nonlinear oscillators. *IEEE/RSJ International Conference on Intelligent Robots and Systems*. 1 (October). p.pp. 958–963.

Inamura, T., Toshima, I., Tanie, H. & Nakamura, Y. (2004). Embodied Symbol Emergence Based on Mimesis Theory. *The International Journal of Robotics*

Research. 23 (4). p.pp. 363–377.

Kaelbling, L., Littman, M. & Moore, A. (1996). Reinforcement learning: A survey. *Journal of Artificial Intelligence*. 4. p.pp. 237–285.

Kagami, S., Konno, A., Kageyama, R., Inaba, M. & Inoue, H. (2000). Development of a humanoid H4 with soft and distributed tactile sensor skin. In: *Experimental Robotics VI*. Springer London, pp. 499–507.

Kajita, S. & Kanehiro, F. (2003). Resolved momentum control: Humanoid motion planning based on the linear and angular momentum. ... *Robots and Systems ...*. 2 (October). p.pp. 1644–1650.

Kajita, S., Kanehiro, F., Kaneko, K., Fujiwara, K., Harada, K., Yokoi, K. & Hirukawa, H. (2003). Biped walking pattern generation by using preview control of zero-moment point. *Robotics and Automation, 2003. Proceedings. ICRA '03. IEEE International Conference on*. 2. p.pp. 1620–1626 vol.2.

Kajita, S. & Kobayashi, A. (1987). Dynamic walk control of a biped robot with potential energy conserving orbit. *Transactions of the Society of Instrument and Control Engineers*. 23. p.pp. 281–287.

Kaneko, K., Kanehiro, F., Kajita, S., Hirukawa, H., Kawasaki, T., Hirata, M., Akachi, K. & Isozumi, T. (2004). Humanoid robot HRP-2. In: *IEEE International Conference on Robotics and Automation, 2004. Proceedings. ICRA '04. 2004*. 2004, pp. 1083–1090 Vol.2.

Kang, H., Hashimoto, K., Kondo, H., Hattori, K., Nishikawa, K., Hama, Y., Lim, H., Takanishi, A., Suga, K. & Kato, K. (2010). Realization of Biped Walking on Uneven Terrain by New Foot. In: *2010 IEEE International Conference on Robotics and Automation*. 2010, pp. 5167–5172.

Kato, I., Ohteru, S., Kobayashi, H., Shirai, K. & Uchiyama, A. (1974). Information-Power Machine with Senses and Limbs. In: *On Theory and Practice of Robots and Manipulators*. Springer Vienna, pp. 11–24.

Kawamura, S. & Fukao, N. (1994). Interpolation for input torque patterns obtained through learning control. In: *third international conference on automation, robotics and computer vision*. 1994.

Kawato, M. (1996). *TRAJECTORY FORMATION IN ARM MOVEMENTS: MINIMIZATION PRINCIPLES AND PROCEDURES*.

Kerrigan, D.C. (2003). Discoveries from quantitative gait analysis. *Gait and Posture*. 18 (Suppl. I).

Khamassi, M. (2005). Actor-Critic Models of Reinforcement Learning in the Basal Ganglia: From Natural to Artificial Rats. *Adaptive Behavior*. 13 (2) p.pp. 131–148.

Khatib, O. (1986). Real-time Obstacle Avoidance for Manipulators and Mobile Robots. *Proceedings. 1985 IEEE International Conference on Robotics and Automation*. 2. p.pp. 90–98.

Khoshelham, K. & Elberink, S.O. (2012). Accuracy and resolution of Kinect depth data for indoor mapping applications. *Sensors (Basel, Switzerland)*. 12 (2). p.pp. 1437–54.

Kim, J.-H., Kim, D.-H., Kim, Y.-J., Park, K.-H., Park, J.-H., Moon, C.-K., Ryu, J.-H., Seow, K.T. & Koh, K.-C. (2004). *Humanoid Robot HanSaRam: Recent Progress and Developments*. 8. p.pp. 45–55.

Kim, S., Kim, C., You, B. & Oh, S. (2009). Stable whole-body motion generation for humanoid robots to imitate human motions. In: *2009 IEEE/RSJ International Conference on Intelligent Robots and Systems, IROS 2009*. 2009, pp. 2518–2524.

Kim, S. & Park, S. (2011). Leg stiffness increases with speed to modulate gait frequency and propulsion energy. *Journal of Biomechanics*. 44 (7). p.pp. 1253–1258.

Kimura, H., Akiyama, S. & Sakurama, K. (1999). Realization of dynamic walking and running of the quadruped using neural oscillator. *Autonomous Robots*. 258. p.pp. 247–258.

Kober, J. & Peters, J. (2013). *Learning Motor Skills: From Algorithms to Robot Experiments*.

Kober, J. & Peters, J. (2011a). Policy search for motor primitives in robotics. *Machine Learning*. 84 (1-2). p.pp. 171–203.

Kober, J. & Peters, J. (2011b). Policy search for motor primitives in robotics. *Machine Learning*. 84 (1-2). p.pp. 171–203.

Komatsu, T. & Usui, M. (2005). Dynamic walking and running of a bipedal robot using hybrid central pattern generator method. In: *IEEE International Conference on Mechatronics and Automation, ICMA 2005*. 2005, pp. 987–992.

Konczak, J. (2005). On the notion of motor primitives in humans and robots. In: *Proceedings of the Fifth International Workshop on Epigenetic Robotics: Modeling Cognitive Development in Robotic Systems*. pp. 47–53.

Kormushev, P., Nenchev, D.N., Calinon, S. & Caldwell, D.G. (2011). Upper-body kinesthetic teaching of a free-standing humanoid robot. *Proceedings - IEEE International Conference on Robotics and Automation*. p.pp. 3970–3975.

Koval, M. (2011). Policy Gradient Reinforcement Learning for Robotics. *Policy*. p.pp. 1–6.

Kubow, T. & Full, R. (1999). The role of the mechanical system in control: a hypothesis of self–stabilization in hexapedal runners. *Philosophical Transactions of* ….

Kulic, D., Ott, C., Lee, D., Ishikawa, J. & Nakamura, Y. (2012). Incremental learning of full body motion primitives and their sequencing through human motion observation. *The International Journal of Robotics Research*. 31 (3). p.pp. 330–345.

Lee, D., Ott, C. & Nakamura, Y. (2010). Mimetic Communication Model with Compliant Physical Contact in Human--Humanoid Interaction. *The International Journal of Robotics Research*. 29 (13). p.pp. 1684–1704.

Lewin, R. (2004). *Human Evolution: An Illustrated Introduction*. Wiley.

Lewis, M. (2002). Perception driven robot locomotion. *JOURNAL-ROBOTICS SOCIETY OF JAPAN*.

Li, P.Y. & Horowitz, R. (1999). Passive velocity field control of mechanical manipulators. *IEEE Transactions on Robotics and Automation*. 15 (4). p.pp. 751–763.

Li, T.-H.S., Su, Y.-T., Lai, S.-W. & Hu, J.-J. (2011). Walking Motion Generation, Synthesis, and Control for Biped Robot by Using PGRL, LPI, and Fuzzy Logic. *Systems, Man, and Cybernetics, Part B: Cybernetics, IEEE Transactions*. 41 (3). p.pp. 736 – 748.

Lohmeier, S., Loffler, K., Gienger, M., Ulbrich, H. & Pfeiffer, F. (2004). Computer System and Control of Biped 'Johnnie'. In: *Proceedings of the 2004 IEEE International Conference on Robotics and Automation*. 2004, pp. 4222–4227 vol. 4.

Lu, Z., Ma, S., Li, B. & Wang, Y. (2005). Serpentine locomotion of a snake-like robot controlled by musical theory. *2005 IEEE/RSJ International Conference on Intelligent Robots and Systems, IROS*. p.pp. 3025–3030.

Lungarella, M., Metta, G., Pfeifer, R. & Sandini, G. (2003). Developmental robotics: a survey. *Connection Science*. 15 (4). p.pp. 151–190.

Maass, W., Natschläger, T. & Markram, H. (2002). Real-time computing without stable states: a new framework for neural computation based on perturbations. *Neural computation*. 14 (11). p.pp. 2531–2560.

Matarić, M. (1998). Behavior-based robotics as a tool for synthesis of artificial behavior and analysis of natural behavior. *Trends in cognitive sciences*.

Mataric, M.J. (2002). Sensory-Motor Primitives as a Basis for Imitation: Linking Perception to Action and Biology to Robotics. *Imitation in animals and artifacts*. p.pp. 1–24.

Matos, V. & Santos, C. (2014). Towards goal-directed biped locomotion: Combining CPGs and motion primitives. *Robotics and Autonomous Systems*. 62 (12). p.pp. 1669–1690.

Matsubara, T., Morimoto, J., Nakanishi, J., Sato, M. & Doya, K. (2005a). Learning CPG-based biped locomotion with a policy gradient method. In: *Humanoid Robots, 2005 5th IEEE-RAS International Conference on*. 2005, pp. 208–213.

Matsubara, T., Morimoto, J., Nakanishi, J., Sato, M.-A. & Doya, K. (2006). Learning CPG-based biped locomotion with a policy gradient method. *Robotics and Autonomous Systems*. 54. p.pp. 911–920.

Matsubara, T., Sato, M. & Doya, K. (2005b). Learning Sensory Feedback to CPG with Policy Gradient for Biped Locomotion. In: *Proceedings of the 2005 IEEE International Conference on Robotics and Automation*. 2005, pp. 4164–4169.

Matsuoka, K. (1985). Sustained oscillations generated by mutually inhibiting neurons with adaptation. *Biological cybernetics*. 52 (6). p.pp. 367–376.

Matthews, P.C., Mirollo, R.E. & Strogatz, S.H. (1991). Dynamics of a large system of coupled nonlinear oscillators. *Physica D: Nonlinear Phenomena*. 52 (2-3). p.pp. 293–331.

Maufroy, C., Kimura, H. & Takase, K. (2010). Integration of posture and rhythmic motion controls in quadrupedal dynamic walking using phase modulations based on leg loading/unloading. *Autonomous Robots*. 28 (3). p.pp. 331–353.

McGeer, T. (1990). Passive Dynamic Walking. *The International Journal of Robotics Research*. 9 (2). p.pp. 62–82.

McGrath, M., Howard, D. & Baker, R. (2015). The strengths and weaknesses of inverted pendulum models of human walking. *Gait & Posture*. 41 (2). p.pp. 389–394.

McMahon, T.A. (1984). Muscles, reflexes, and locomotion BT - Reflexes and Motor Control. In: *Reflexes and Motor Control*. p. 331.

Medved, V. (2000). *Measurement of Human Locomotion*. CRC Press.

Mezger, J., Ilg, W. & Giese, M.A. (2005). Trajectory synthesis by hierarchical spatio-temporal correspondence. In: *Proceedings of the 2nd symposium on Appied perception in graphics and visualization - APGV '05*. 2005, p. 25.

Mita, T., Yamaguchi, T., Kashiwase, T. & Kawase, T. (1984). Realization of a high speed biped using modern control theory. *International Journal of Control*. 40 (1).

Miura, H. & Shimoyama, I. (1984). Dynamic Walk of a Biped. *The International Journal of Robotics Research*. 3 (2). p.pp. 60–74.

Miyamoto, H., Schaal, S., Gandolfo, F., Gomi, H., Koike, Y., Osu, R., Nakano, E., Wada, Y. & Kawato, M. (1996). A Kendama learning robot based on bi-directional theory. *Neural Networks*. 9 (8) p.pp. 1281–1302.

Montecillo, P., Sreenivasa, M. & Laumond, J.-P. (2010). On Real-Time Whole-Body Human to Humanoid Motion Transfer. *International Conference on Informatics in Control, Automation and Robotics*. (September 2015). p.pp. 22–31.

Morimoto, J., Cheng, G., Atkeson, C.G. & Zeglin, G. (2004). A Simple Reinforcement Learning Algorithm For Biped Walking. *International Conference on Robotics and Automation*. (April). p.pp. 3030–3035.

Morimoto, J., Endo, G., Nakanishi, J. & Cheng, G. (2008). A Biologically Inspired Biped Locomotion Strategy for Humanoid Robots: Modulation of Sinusoidal Patterns by a Coupled Oscillator Model. *IEEE Transactions on Robotics*. 24 (1). p.pp. 185–191.

Morimoto, J., Nakanishi, J., Endo, G., Cheng, G., Atkeson, C.G. & Zeglin, G. (2005). Poincare-map-based reinforcement learning for biped walking. *Robotics and Automation, 2005. ICRA 2005. Proceedings of the 2005 IEEE International Conference on*. p.pp. 2381–2386.

Muecke, K., Cox, P., Hong & W., D. (2006). DARwIn: Dynamic Anthropomorphic Robot with Intelligence, Part 1 – Concept & General Overview. *Servo Magazine, Vol. 4, No. 12*.

Muico, U., Lee, Y., Popović, J. & Popović, Z. (2009). Contact-aware nonlinear control of dynamic characters. *ACM Trans. Graph.* 28 (3). p.pp. 81:1–81:9.

Mussa-Ivaldi, F. a & Bizzi, E. (2000). Motor learning through the combination of primitives. *Philosophical transactions of the Royal Society of London. Series B, Biological sciences*. 355 (1404). p.pp. 1755–1769.

Mussa-Ivaldi, F.A. (1997). Nonlinear force fields: a distributed system of control primitives for representing and learning movements. *Proceedings 1997 IEEE International Symposium on Computational Intelligence in Robotics and Automation CIRA97 Towards New Computational Principles for Robotics and Automation*. 22 (4). p.pp. 84–90.

Nagasaka, K., Kuroki, Y., Suzuki, S., Itoh, Y. & Yamaguchi, J. (2004). Integrated motion control for walking, jumping and running on a small bipedal entertainment robot. In: *Robotics and Automation, 2004. Proceedings. ICRA '04. 2004 IEEE International Conference on*. 2004, pp. 3189–3194 Vol.4.

Nakamura, Y., Mori, T., Sato, M. & Ishii, S. (2007). Reinforcement learning for a biped robot based on a CPG-actor-critic method. *Neural Networks*. 20 (6). p.pp. 723–735.

Nakanishi, J. & Morimoto, J. (2004). An empirical exploration of phase resetting for robust biped locomotion with dynamical movement primitives. *Robots and Systems*. 47 (2-3). p.pp. 79–91.

Nakanishi, J., Morimoto, J., Endo, G., Cheng, G., Schaal, S. & Kawato, M. (2004a). Learning from demonstration and adaptation of biped locomotion. *Robotics and Autonomous Systems*. 47 (2-3). p.pp. 79–91.

Nakanishi, J.N.J., Morimoto, J.M.J., Endo, G., Cheng, G., Schaal, S. & Kawato, M. (2004b). A framework for learning biped locomotion with dynamical movement primitives. *4th IEEE/RAS International Conference on Humanoid Robots, 2004.* 2. p.pp. 925–940.

Nakaoka, S., Nakazawa, a., Yokoi, K., Hirukawa, H. & Ikeuchi, K. (2003). Generating whole body motions for a biped humanoid robot from captured human dances. *2003 IEEE International Conference on Robotics and Automation (Cat. No.03CH37422)*. 3. p.pp. 3905–3910.

Nakaoka, S., Nakazawa, A., Kanehiro, F., Kaneko, K., Morisawa, M. & Ikeuchi, K. (2005). Task model of lower body motion for a biped humanoid robot to imitate human dances. In: *2005 IEEE/RSJ International Conference on Intelligent Robots and Systems*. 2005, IEEE, pp. 3157–3162.

Narukawa, T., Yokoyama, K., Takahashi, M. & Yoshida, K. (2008). A simple 3D straight-legged passive walker with flat feet and ankle springs. In: *2008 IEEE/RSJ International Conference on Intelligent Robots and Systems, IROS*. 2008, pp. 2952–2957.

Nishii, J. (1998). A learning model for oscillatory networks. *Neural Networks*. 11 (2). p.pp. 249–257.

Nishiwaki, K., Kuga, M., Kagami, S., Inaba, M. & Inoue, H. (2005). Whole-body cooperative balanced motion generation for reaching. *International Journal of Humanoid Robotics*. 02 (04). p.pp. 437–457.

Obdrzálek, S., Kurillo, G., Ofli, F., Bajcsy, R., Seto, E., Jimison, H. & Pavel, M. (2012). Accuracy and robustness of Kinect pose estimation in the context of coaching of elderly population. *Conference proceedings : ... Annual International Conference of the IEEE Engineering in Medicine and Biology Society. IEEE Engineering in Medicine and Biology Society. Annual Conference*. 2012. p.pp. 1188–93.

Ogura, Y., Aikawa, H., Shimomura, K., Kondo, H., Morishima, A., Lim, H.O. & Takanishi, A. (2006). Development of a new humanoid robot WABIAN-2. *Proceedings - IEEE International Conference on Robotics and Automation*. 2006 (May). p.pp. 76–81.

Okada, M., Tatani, K. & Nakamura, Y. (2002). Polynomial design of the nonlinear dynamics for the brain-like information processing of whole body motion. In: *Proceedings of ICRA 2002*. 2002, pp. 1410–1415.

Orlovski, G.N., Deliagina, T.G. & Grillner, S. (1999). *Neuronal Control of Locomotion: From Mollusc to Man*. Oxford University Press.

Ott, C., Lee, D. & Nakamura, Y. (2008). Motion capture based human motion recognition and imitation by direct marker control. In: *2008 8th IEEE-RAS International Conference on Humanoid Robots, Humanoids 2008*. 2008, pp. 399–405.

Paine, R.W. & Tani, J. (2004). Motor primitive and sequence self-organization in a hierarchical recurrent neural network. In: *Neural Networks*. 2004, pp. 1291–1309.

Park, I.-W., Kim, J.-Y., Lee, J. & Oh, J.-H. (2007). Mechanical design of the humanoid robot platform, HUBO. *Advanced Robotics*. 21 (11). p.pp. 1305–1322.

Park, I.-W.P.I.-W., Kim, J.-Y.K.J.-Y., Park, S.-W.P.S.-W. & Oh, J.-H.O.J.-H. (2004). Development of humanoid robot platform KHR-2 (KAIST humanoid robot-2). *4th IEEERAS International Conference on Humanoid Robots 2004*. 1 (1) p.pp. 292–310.

Park, J.H. (2001). Impedance control for biped robot locomotion. *Robotics and Automation, IEEE Transactions on*. 17 (6). p.pp. 870–882.

Pastor, P., Hoffmann, H., Asfour, T. & Schaal, S. (2009). Learning and generalization of motor skills by learning from demonstration. *{IEEE} International Conference on Robotics and Automation, 2009. {ICRA} '09*. p.pp. 763–768.

Pearson, K.G. (1993). Common principles of motor control in vertebrates and invertebrates. *Annual review of neuroscience*. 16. p.pp. 265–297.

Perk, B.E. & Slotine, J.J.E. (2006). Motion Primitives for Robotic Flight Control.

Computing Research Repository, CORR. abs/cs/060. p.pp. 1–8.

Perry, J. (1992). *Gait Analysis: Normal and Pathological Function*.

Peters, J. & Schaal, S. (2006). Policy gradient methods for robotics. In: *IEEE International Conference on Intelligent Robots and Systems*. 2006, pp. 2219–2225.

Peters, J. & Schaal, S. (2008). Reinforcement learning of motor skills with policy gradients. *Neural Networks*. 21 (4). p.pp. 682–697.

Peters, J., Vijayakumar, S. & Schaal, S. (2003). Reinforcement Learning for Humanoid Robotics. *Proceedings of the third IEEERAS international conference on humanoid robots*. 18 (7). p.pp. 1–20.

Pfeiffer, F. (2007). The TUM walking machines. *Philos Trans A Math Phys Eng Sci*. 365 (1850). p.pp. 109–131.

Platz, T., Denzler, P., Kaden, B. & Mauritz, K.-H. (1994). Motor learning after recovery from hemiparesis. *Neuropsychologia*. 32 (10). p.pp. 1209–1223.

Pollard, N.S., Hodgins, J.K., Riley, M.J. & Atkenson, C.G. (2002). Adapting human motion for the control of a humanoid robot. *Proceedings - IEEE International Conference on Robotics and Automation*. 2. p.pp. 1390–1397.

Pongas, D., Billard, A. & Schaal, S. (2005). Rapid synchronization and accurate phase-locking of rhythmic motor primitives. In: *Intelligent Robots and Systems, 2005. (IROS 2005). 2005 IEEE/RSJ International Conference on*. 2005, pp. 2911–2916.

Pratt, J., Chee-Meng, C., Torres, A., Dilworth, P. & Prat, G. (2001). Virtual Model Control: An Intuitive Approach for Bipedal Locomotion. *The International Journal of Robotics Research*. 20 (2). p.pp. 129–143.

Pratt, J., Koolen, T., de Boer, T., Rebula, J., Cotton, S., Carff, J., Johnson, M. & Neuhaus, P. (2012). Capturability-based analysis and control of legged locomotion, Part 2: Application to M2V2, a lower-body humanoid. *The International Journal of Robotics Research*. 31 (10). p.pp. 1117–1133.

Righetti, L., Buchli, J. & Ijspeert, A.J. (2006). Dynamic Hebbian learning in adaptive frequency oscillators. *Physica D: Nonlinear Phenomena*. 216 (2). p.pp. 269–281.

Righetti, L. & Ijspeert, a J. (2006). Programmable central pattern generators: an application to biped locomotion control. *Robotics and Automation, 2006. ICRA 2006. Proceedings 2006 IEEE International Conference on*. (May). p.pp. 1585–1590.

Righetti, L. & Ijspeert, A.J. (2008). Pattern generators with sensory feedback for the control of quadruped locomotion. *Proceedings - IEEE International Conference on*

Robotics and Automation. (July 2015). p.pp. 819–824.

Riley, M., Ude, a., Wade, K. & Atkeson, C.G. (2003). Enabling real-time full-body imitation: a natural way of transferring human movement to humanoids. *2003 IEEE International Conference on Robotics and Automation (Cat. No.03CH37422)*. 2. p.pp. 2368–2374.

Robinovitch, S. (2007). *Clinical biomechanics of gait*. [Online]. 2007. Available from: http://www.sfu.ca/~stever/kin201/lecture_outlines/lecture_17_clinical_biomechanics_of_gait.pdf. [Accessed: 25 February 2016].

Rohmer, E., Singh, S.P.N. & Freese, M. (2013). V-REP: A versatile and scalable robot simulation framework. *IEEE International Conference on Intelligent Robots and Systems*. p.pp. 1321–1326.

Rohrer, B. & Hogan, N. (2003). Avoiding spurious submovement decompositions: a globally optimal algorithm. *Biological cybernetics*. 89 (3). p.pp. 190–9.

Ruchanurucks, M., Nakaoka, S., Kudoh, S. & Ikeuchi, K. (2006). Humanoid Robot Motion Generation with Sequential Physical Constraints. *IEEE International Conference on Robotics and Automation ICRA*. p.pp. 2649–2654.

Sakagami, Y., Watanabe, R., Aoyama, C., Matsunaga, S., Higaki, N. & Fujimura, K. (2002). The intelligent ASIMO: system overview and integration. In: *Intelligent Robots and Systems, 2002. IEEE/RSJ International Conference on*. 2002, pp. 2478–2483 vol.3.

Salatian, a. W., Yi, K.Y. & Zheng, Y.F. (1997). Reinforcement learning for a biped robot to climb sloping surfaces. *Journal of Robotic Systems*. 14 (4). p.pp. 283–296.

Saltiel, P., Tresch, M.C. & Bizzi, E. (1998). Spinal cord modular organization and rhythm generation: an NMDA iontophoretic study in the frog. *Journal of neurophysiology*. 80. p.pp. 2323–2339.

Sandini, G., Metta, G. & Vernon, D. (2004). RobotCub: an open framework for research in embodied cognition. In: *4th IEEE/RAS International Conference on Humanoid Robots, 2004.* 2004, pp. 13–32.

Sano, a. & Furusho, J. (1990). Realization of natural dynamic walking using the angular momentum information. *Proceedings., IEEE International Conference on Robotics and Automation*. p.pp. 1476–1481.

Santos, M.F. & Silva, M.T. (2006). Design and Low-Level Control of a Humanoid Robot Using a Distributed Architecture Approach,. In: *Journal of Vibration and Control,*. 2006, pp. 1431–1456.

Santos, V., Moreira, R. & Silva, F. (2012). Hybrid Actuation and Distributed Control for a Small-size Humanoid Robot. In: D. Chugo & S. Yokota (eds.). *Introduction to Modern Robotics*. CreateSpace Independent Publishing Platform (January 5, 2012), pp. 19–38.

Sato, M., Nakamura, Y. & Ishii, S. (2002). Reinforcement learning for biped locomotion. *Artificial Neural Networks—ICANN 2002*.

SAUNDERS, J.B., INMAN, V.T. & EBERHART, H.D. (1953). The major determinants in normal and pathological gait. *The Journal of Bone and Joint Surgery. American Volume*. 35-A (3). p.pp. 543–558.

Schaal, S. (1999). Is imitation learning the route to humanoid robots? *Trends in Cognitive Sciences*. 3. p.pp. 233–242.

Schaal, S. (2002). Learning robot control. *The handbook of brain theory and neural networks,*.

Schaal, S., Peters, J. & Nakanishi, J. (2005). Learning movement primitives. *Robotics Research*. p.pp. 1–10.

Schaal, S., Peters, J., Nakanishi, J. & Ijspeert, A. (2003). Control, Planning, Learning, and Imitation with Dynamic Movement Primitives. *Workshop on Bilateral Paradigms on Humans and Humanoids, 2003 IEEE International Conference on Intelligent Robots and Systems IROS*. p.pp. 1–21.

Schaal, S. & Schweighofer, N. (2005). Computational motor control in humans and robots. *Current opinion in neurobiology*. 15 (6). p.pp. 675–82.

Shon, A.P., Grochow, K. & Rao, R.P.N. (2005). Robotic Imitation for Human Motion Capture Using Gaussian Processes. In: *5th IEEE-RAS International Conference on Humanoid Robots*. 2005, pp. 129–134.

Siciliano, B. & Khatib, O. (2007). *Springer Handbook of Robotics*. Springer-Verlag New York, Inc.

Silva, F. & Santos, V. (2007). Multipurpose Low-Cost Humanoid Platform and Modular Control Software Development. In: *Humanoid Robots, Human-like Machines*. I-Tech Education and Publishing.

Simard, P. & Le Cun, Y. (1992). Reverse TDNN: An Architecture For Trajectory Generation. In: J. E. Moody, S. J. Hanson, & R. P. Lippmann (eds.). *Advances in Neural Information Processing Systems 4*. Morgan-Kaufmann, pp. 579–588.

Smisek, J., Jancosek, M. & Pajdla, T. (2011). 3D with Kinect. *Proceedings of the IEEE International Conference on Computer Vision*. p.pp. 1154–1160.

Solis, J. & Takanishi, A. (2010). Recent Trends in Humanoid Robotics Research: Scientific Background, Applications, and Implications. *Accountability in Research-Policies and Quality Assurance*. 17 (6). p.pp. 278–298.

Sophie Sakka, L., Penna-Poubel & Cehajic, D. (2014). Tasks prioritization for whole-body realtime imitation of human motion by humanoid robots. In: *Digital Intelligence*. 2014.

Srinivasan, M. (2011). Fifteen observations on the structure of energy-minimizing gaits in many simple biped models. *Journal of The Royal Society Interface*. 8 (54). p.pp. 74–98.

Stein, P.S.G. & Smith, J. (1997). *Neurons, Networks, and Motor Behavior*. MIT Press.

Stephens, B. (2007). Integral control of humanoid balance. *IEEE International Conference on Intelligent Robots and Systems*. p.pp. 4020–4027.

Sternad, D., Amazeen, E.L. & Turvey, M.T. (1996). Diffusive, synaptic, and synergetic coupling: An evaluation through in-phase and antiphase rhythmic movements. *J Mot Behav*. 28 (3). p.pp. 255–269.

Sugihar, T., Hiko Nakamur, Y., Inoue, H., Sugihara, T., Nakamura, Y., Inoue, H., Sugihar, T., Inoue, H., Hiko Nakamur, Y. & Inoue, H. (2002a). Realtime Humanoid Motion Generat ion through ZMP Manipulation based on Inverted Pendulum Control. In: *IEEE International Conference on Robotics & Automation*. 2002, pp. 1404–1409.

Sugihar, T., Hiko Nakamur, Y., Inoue, H., Sugihara, T., Nakamura, Y., Inoue, H., Sugihar, T., Inoue, H., Hiko Nakamur, Y. & Inoue, H. (2002b). Realtime Humanoid Motion Generat ion through ZMP Manipulation based on Inverted Pendulum Control. *IEEE International Conference on Robotics & Automation*. (May). p.pp. 1404–1409.

Sugihara, T. & Nakamura, Y. (2002). Whole-body cooperative balancing of humanoid robot using COG Jacobian. In: *Proc. IEEE/RSJ International Conference on Intelligent Robots and System*. 2002, pp. 2575–2580 vol.3.

Suleiman, W., Yoshida, E., Kanehiro, F., Laumond, J.P. & Monin, A. (2008). On human motion imitation by humanoid robot. In: *Proceedings - IEEE International Conference on Robotics and Automation*. 2008, pp. 2697–2704.

Sutton, R.S. & Barto, A.G. (1998). Reinforcement learning: an introduction. In: *MIT Press*.

Taga, G. (1995a). A model of the neuro-musculo-skeletal system for human locomotion

- II. Real-time adaptability under various constraints. *Biological Cybernetics*. 73 (2). p.pp. 113–121.

Taga, G. (1995b). A model of the neuro-musculo-skeletal system for human locomotion. I. Emergence of basic gait. *Biological Cybernetics*. 73 (2). p.pp. 97–111.

Taga, G., Yamaguchi, Y., Shimizu, H. & Yamaguehi, Y. (1991). Self-organized control of bipedal locomotion by neural oscillators in unpredictable environment. *Biological Cybernetics*. 65 (3). p.pp. 147–159.

Tani, J. & Ito, M. (2003). Self-organization of behavioral primitives as multiple attractor dynamics: A robot experiment. *IEEE Transactions on Systems, Man, and Cybernetics Part A:Systems and Humans.* 33 (4). p.pp. 481–488.

Thomas, L. (1949). *Elliptic Problems in Linear Differential Equations over a Network*.

Thoroughman, K. & Shadmehr, R. (2000). Learning of action through adaptive combination of motor primitives. *Nature*. 407 (6805). p.pp. 742–747.

Todorov, E. (2004). Optimality principles in sensorimotor control. *Nature neuroscience*. 7 (9). p.pp. 907–915.

Todorov, E., Li, W. & Pan, X. (2005). From task parameters to motor synergies: A hierarchical framework for approximately optimal control of redundant manipulators. *Journal of Robotic Systems*. 22 (11). p.pp. 691–710.

Tomoyuki, T., Azuma, Y. & Shibata, T. (2009). Acquisition of energy-efficient bipedal walking using CPG-based reinforcement learning. *Intelligent Robots and* ….

Townsend, M.A. (1985). Biped gait stabilization via foot placement. *Journal of Biomechanics*. 18 (1). p.pp. 21–38.

Tresch, M.C., Saltiel, P. & Bizzi, E. (1999). The construction of movement by the spinal cord. *Nature neuroscience*. 2 (2). p.pp. 162–167.

Tresch, M.C., Saltiel, P., D'Avella, A. & Bizzi, E. (2002). Coordination and localization in spinal motor systems. *Brain Res Brain Res Rev*. 40 (1-3). p.pp. 66–79.

Tsagarakis, N.G., Vanderborght, B., Laffranchi, M. & Caldwell, D.G. (2009). The mechanical design of the new lower body for the child humanoid robot 'iCub'. In: *2009 IEEE/RSJ International Conference on Intelligent Robots and Systems*. October 2009, pp. 4962–4968.

Tsuji, T., Tanaka, Y., Morasso, P.G., Sanguineti, V. & Kaneko, M. (2002). Bio-mimetic trajectory generation of robots via artificial potential field with time base

generator. *IEEE Transactions on Systems, Man and Cybernetics Part C: Applications and Reviews*. 32 (4). p.pp. 426–439.

Tuan, T.M., Souères, P., Taïx, M., Sreenivasa, M.N. & Halgand, C. (2010). Humanoid human-like reaching control based on movement primitives. *Proceedings - IEEE International Workshop on Robot and Human Interactive Communication*. p.pp. 546–551.

Ude, A., Gams, A., Asfour, T. & Morimoto, J. (2010). Task-specific generalization of discrete and periodic dynamic movement primitives. *IEEE Transactions on Robotics*. 26 (5). p.pp. 800–815.

Ude, A., Riley, M., Nemec, B., Kos, A., Asfour, T. & Cheng, G. (2008). Synthesizing goal-directed actions from a library of example movements. In: *Proceedings of the 2007 7th IEEE-RAS International Conference on Humanoid Robots, HUMANOIDS 2007*. 2008, pp. 115–121.

Vicon Systems (2015). *Motion Capture*. [Online]. 2015. Available from: http://www.vicon.com/what-is-motion-capture.

Vukobratović, M. & Borovac, B. (2004). Zero-Moment Point — Thirty Five Years of Its Life. *International Journal of Humanoid Robotics*. 01 (01). p.pp. 157–173.

Vukobratovic, M. & Juricic, D. (1969). Contribution to the Synthesis of Biped Gait. *Biomedical Engineering, IEEE Transactions on*. BME-16 (1). p.pp. 1–6.

Wang, Q., Wang, L., Huang, Y., Zhu, J. & Chen, W. (2009). Three-dimensional quasi-passive dynamic bipedal walking with flat feet and compliant ankles. *Proceedings of the IEEE Conference on Decision and Control*. p.pp. 8200–8205.

Westervelt, E., Grizzle, J. & Chevallereau, C. (2007). *Feedback control of dynamic bipedal robot locomotion*.

Whelan, P. (1996). Control of Locomotion in the Decerebrate Cat. *Progress in Neurobiology*. 49 (5). p.pp. 481–515.

Whittle, M. (2007a). *Gait analysis: an introduction*. Fourth Ed. Butterworth Heineman Elsevier.

Whittle, M. (2007b). *Gait analysis: an introduction*. Fourth. Butterworth Heineman Elsevier.

Williamson, M.M. (1998). Neural control of rhythmic arm movements. *Neural Networks*. 11 (7-8). p.pp. 1379–1394.

Winter, D. a (1990). *Biomechanics and Motor Control of Human Movement*.

Wisse, M., Feliksadal, G., van Frankenhyyzen, J. & Moyer, B. (2007). Passive-based walking robot. *IEEE Robotics and Automation Magazine*. 14 (2). p.pp. 52–62.

Wolpert, D.M. & Kawato, M. (1998). Multiple paired forward and inverse models for motor control. *Neural Networks*. 11 (7-8). p.pp. 1317–1329.

Yamane, K. & Hodgins, J. (2009). Simultaneous tracking and balancing of humanoid robots for imitating human motion capture data. In: *2009 IEEE/RSJ International Conference on Intelligent Robots and Systems, IROS 2009*. 2009, pp. 2510–2517.

Yamasaki, F., Matsui, T., Miyashita, T. & Kitano, H. (2001). PINO The Humanoid: A Basic Architecture. *RoboCup 2000*. p.pp. 269–278.

Zegers, P. & Sundareshan, M.K. (2003). Trajectory generation and modulation using dynamic neural networks. *IEEE Transactions on Neural Networks*. 14 (3). p.pp. 520–533.

Zhou, C. & Meng, Q. (2003). Dynamic balance of a biped robot using fuzzy reinforcement learning agents. *Fuzzy Sets and Systems*. 134 (1). p.pp. 169–187.